

Effective Depth of Soil Compaction in Relation to Applied Compactive Energy

Dante Fratta and Kyu-Sun Kim

University of Wisconsin-Madison

WisDOT ID no. 0092-08-11

February 2015



RESEARCH & LIBRARY UNIT



WISCONSIN HIGHWAY RESEARCH PROGRAM

WISCONSIN DOT
PUTTING RESEARCH TO WORK

Disclaimer

This research was funded through the Wisconsin Highway Research Program by the Wisconsin Department of Transportation and the Federal Highway Administration under Project 0092-08-11. The contents of this report reflect the views of the authors who are responsible for the facts and accuracy of the data presented herein. The contents do not necessarily reflect the official views of the Wisconsin Department of Transportation or the Federal Highway Administration at the time of publication.

This document is disseminated under the sponsorship of the Department of Transportation in the interest of information exchange. The United States Government assumes no liability for its contents or use thereof. This report does not constitute a standard, specification or regulation.

The United States Government does not endorse products or manufacturers. Trade and manufacturers' names appear in this report only because they are considered essential to the object of the document.

Technical Report Documentation Page

1. Report No. 0092-08-11		2. Government Accession No		3. Recipient's Catalog No	
4. Title and Subtitle Effective Depth of Soil Compaction in Relation to Applied Compactive Energy			5. Report Date February 2015		
			6. Performing Organization Code		
7. Authors Dante Fratta and Kyu-Sun Kim			8. Performing Organization Report No.		
9. Performing Organization Name and Address University of Wisconsin-Madison Madison, WI 53706			10. Work Unit No. (TRAIS)		
			11. Contract or Grant No. WHRP No. 0092-08-11		
12. Sponsoring Agency Name and Address Wisconsin Department of Transportation Research & Library Unit 4802 Sheboygan Ave. Rm 104 Madison, WI 53707			13. Type of Report and Period Covered Technical Report		
			14. Sponsoring Agency Code		
15. Supplementary Notes					
<p>16. Abstract</p> <p>The determination of appropriate lift thickness used in the embankment construction has important economic and engineering implications in the design, construction, and performance of transportation systems. Department of Transportations (DOTs) across the United States require lift thicknesses ranging from 0.2 to 0.3 m (8 to 12 in.) depending on soil types, regardless of compaction equipment used. However, modern earthmoving and compaction equipment with much larger footprints and weight could potentially compact thicker soil layers without sacrificing the mechanical performance of embankments while reducing construction costs.</p> <p>This research program presents a series of field monitoring, testing, and numerical studies used to evaluate the response of coarse and fine-grained soils during compaction operations at various soil depths under the action of the smooth-drum vibratory roller, rubber-tired roller, padfoot roller, and scraper. Different soil property profiles were used to assess the effectiveness of different compaction methods, including shear-induced displacement and rotation monitoring, dynamic cone penetrometer (DCP), soil stiffness gauge (SSG), pressure plate, sand cone, nuclear density gauge (NDG), and P-wave propagation. Numerical modeling using a hardening soil model was used to expand the results of the compaction effectiveness in depth. The experimental and numerical results provided ranges to evaluate the compaction effectiveness of increasing lift thickness for different compactive energies. The results provide a better understanding of the compaction effectiveness as a function of depth and showed an evidence of the potential for an increase in the Wisconsin Department of Transportation (WisDOT)'s lift thickness specification. The results indicate that 0.3-m (12-in) loose lifts for coarse-grained and fine-grained soils could be implemented when using Quality Management Program (QMP). If standard compaction is used, 0.2-m (8-in) loose lifts for coarse-grained and fine-grained soils should remain the state of practice for WisDOT. These recommendations should be further studied by WisDOT officials before they are implemented in embankment construction projects.</p>					
17. Key Words Compaction, embankment, lift thickness, coarse-grained soils, fine-grained soils, compaction equipment, field testing, numerical modelling			18. Distribution Statement No restriction. This document is available to the public through the National Technical Information Service 5285 Port Royal Road Springfield VA 22161		
18. Security Classif.(of this report) Unclassified		19. Security Classif. (of this page) Unclassified		20. No. of Pages 234	21. Price

WISCONSIN HIGHWAY RESEARCH PROGRAM #0092-08-11

**EFFECTIVE DEPTH OF SOIL COMPACTION IN
RELATION TO APPLIED COMPACTIVE ENERGY**

Final Report

By

Dante Fratta and Kyu-Sun Kim

**Department of Civil and Environmental Engineering
University of Wisconsin-Madison**

**Submitted to the
Wisconsin Department of Transportation**

February 2015

EXECUTIVE SUMMARY

The determination of appropriate lift thickness used in the embankment construction has important economic and engineering implications in the design, construction, and performance of transportation systems. Department of Transportations (DOTs) across the United States require lift thicknesses ranging from 0.2 to 0.3 m (8 to 12 in.) depending on soil types, regardless of compaction equipment used. However, modern earthmoving and compaction equipment with much larger footprints and weight could potentially compact thicker soil layers without sacrificing the mechanical performance of embankments while reducing construction costs.

This research program presents a series of field monitoring, testing, and numerical studies used to evaluate the response of coarse and fine-grained soils during compaction operations at various soil depths under the action of the smooth-drum vibratory roller, rubber-tired roller, padfoot roller, and scraper. Different soil property profiles were used to assess the effectiveness of different compaction methods, including shear-induced displacement and rotation monitoring, dynamic cone penetrometer (DCP), soil stiffness gauge (SSG), pressure plate, sand cone, nuclear density gauge (NDG), and P-wave propagation. Numerical modeling using a hardening soil model was used to expand the results of the compaction effectiveness in depth. The experimental and numerical results provided ranges to evaluate the compaction effectiveness of increasing lift thickness for different compactive energies. The results provide a better understanding of the compaction effectiveness as a function of depth and showed an evidence of the potential

for an increase in the Wisconsin Department of Transportation (WisDOT)'s lift thickness specification. The results indicate that 0.3-m (12-in) loose lifts for coarse-grained and fine-grained soils could be implemented when using Quality Management Program (QMP). If standard compaction is used, 0.2-m (8-in) loose lifts for coarse-grained and fine-grained soils should remain the state of practice for WisDOT. These recommendations should be further studied by WisDOT officials before they are implemented in embankment construction projects.

TABLE OF CONTENT

Title page	
Disclaimer	2
EXECUTIVE SUMMARY	5
TABLE OF CONTENT	7
Chapter 1 - INTRODUCTION	10
1.1 Introduction.....	10
1.2 Research Background and Objectives	10
1.3 Report Organization.....	12
Chapter 2 - FIELD SOIL COMPACTION	13
2.1 Compaction Characteristics	13
2.2 Compaction Energy Propagation in Soils	17
2.3 Compaction Equipment and Techniques	19
2.3.1 Smooth-drum Vibratory Roller.....	19
2.3.2 Rubber-tired Roller	21
2.3.3 Padfoot Roller	21
2.4 Controlling Parameters in Field Compaction Operations	23
2.5 Specifications on Lift Thickness in the United States	26
Chapter 3 - MATERIALS AND LABORATORY TESTING	30
3.1 Testing Site Locations.....	30
3.2 Geomaterial Samples	32
3.3 Engineering Properties of the Tested Soils.....	32
3.3.2 Grain Size Distribution (ASTM D422-63, ASTM D421-85, and ASTM D2487-00)	33
3.3.1 Specific Gravity (ASTM D854-02)	34
3.3.3 Standard Proctor Compaction Test (ASTM D698-07)	35
Chapter 4 - FIELD MONITORING AND TESTING	37
4.1 Introduction.....	37
4.2 Field Measurement Methods.....	37
4.2.1 Soil Stiffness Gauge.....	38
4.2.2 Dynamic Cone Penetrometer	39
4.2.3 Time Domain Reflectometry	42
4.2.4 MEMS Accelerometers.....	43
4.2.5 Hydraulic Pressure Plate	45
4.2.6 Sand Cone and Nuclear Density Gauge.....	47
4.3 Coarse-Grained Soils: Junction City Field Testing	48

4.3.1 Compaction and Earthmoving Equipment.....	49
4.3.2 Field Testing Program.....	50
4.3.3 Test Results and Data Interpretation.....	56
Pressure Plate Responses	57
Shear-induced Rotation Measurements using MEMS Accelerometers.....	58
Shear-induced Displacements Measurements using MEMS Accelerometers	62
Soil Stiffness using SSG and P-wave Propagation.....	67
Shear Resistance – DPI Profile.....	69
Correlations of Volumetric and Gravimetric Water Contents	72
Relative Compaction: Density & Water Content Measurements	74
4.4 Fine-Grained Soil: Town of Sylvania Field Testing.....	76
4.4.1 Compaction and Earthmoving Equipment.....	77
4.4.2 Field Testing Program.....	78
4.4.3 Test Results and Data Interpretation.....	79
Pressure Plate Responses	80
Shear-induced Rotation Measurements using MEMS Accelerometers.....	82
Unit Weight & Water Content Measurements.....	85
Soil Stiffness using the Soil Stiffness Gauge.....	88
Shear Resistance – DPI Profile.....	91
Chapter 5 - NUMERICAL MODELING AND ANALYSES	94
5.1 Introduction.....	94
5.2 Numerical Analysis.....	94
5.2.1 Soil Compaction under Wheel Loading.....	94
5.2.2 Computer Code: PLAXIS	96
5.2.3 Soil Model.....	96
5.3 Modeling results and interpretations.....	99
5.3.1 Maximum Displacement.....	99
5.3.2 Volumetric Strain.....	101
5.2.3 Failure Zone Distribution.....	102
Chapter 6 – SUMMARY, ENGINEERING RECOMMENDATIONS AND	
CONCLUSIONS.....	104
REFERENCES	108
APPENDIX A: MEMS ACCELEROMETER RESPONSES	113
APPENDIX B: MEMS ACCELEROMENTER ROTATION MEASUREMENTS	136
APPENDIX C: MEMS ACCELEROMETERS TIME SERIES	146
APPENDIX D: P-WAVE PROPAGATION – TRAVEL TIME EVALUATION	206

APPENDIX E: GEOMETRY OF TESTING SETUP AT THE TOWN OF SYLVANIA

SITE 226

Chapter 1 - INTRODUCTION

1.1 Introduction

The determination of appropriate lift thicknesses used in embankment construction operations has important engineering and economic implications in the design, construction, and performance of roads, levees and earth dams. Small lift thickness cause excessive construction costs, while large lift thickness may compromise the stability and performance of embankments due to a reduction of the compaction homogeneity and therefore the effectiveness of compaction operations.

This research program used field experimental results and numerical analyses to evaluate the compaction effective depth for optimal embankment construction operations. Field testing included the monitoring of the engineering performance of compacted soils and the quality evaluation of compacted lifts. These field measurements along with numerical analyses provide a more robust engineering understanding of the compaction problem and seem to justify an increase in maximum lift thickness, for certain soil types and earthmoving and compaction equipment used in this testing program, to be recommended to Wisconsin Department of Transportation (WisDOT) for embankment construction projects.

1.2 Research Background and Objectives

During embankment and road construction, compaction operations are designed to create stable structures that are able to transmit traffic loads to the foundation soil with acceptable total and differential deformation levels and thus contribute to the overall health of pavement systems or embankment structures. To achieve stable embankment

structures, WisDOT has developed specifications for the compaction density and water content. Commonly acceptable specifications for embankment lift thickness during construction processes range from 0.20 m (8 in) for most soil types and, in some cases, to 0.30 m (12 in) for granular soils (Hoppe 1999; Lenke 2006). These lift thickness limits were established based on field experiences for contractors' methods and field compaction equipment (Holtz and Kovacs 1981; Holtz 1990). This practice has engineering implications as it contributes to adequate embankment compaction with minimizing the need detailed inspection operations by WisDOT personnel. However, the blanket use of 0.20-m (8-in) lift thickness may no longer be justified and may be unnecessarily increasing embankment construction costs. This concern is based on the fact that modern compaction equipment has increased in size and weight and new compactors are capable of delivering greater energy levels (Bowels 1979; Rollings and Rollings 1996). For these reasons, there is a strong interest from both earthmoving contractors and WisDOT officials in investigating the technical feasibility of increasing the current compacting lift thickness practice. The engineering challenge to changes in specifications is that small lift thickness may cause excessive construction costs while large lift thickness may reduce the compaction effectiveness and may compromise the mechanical performance of embankments.

The objective of this research program was to evaluate the effect of commonly used Wisconsin compactors and earthmoving equipment on different lift thickness and propose recommendations about the possibility of increasing lift thickness for road construction operations. To accomplish this objective, field data were collected and analyzed to

evaluate optimum lift thickness during an embankment construction. The results helped establishing a relationship between the applied compaction energy (types of compactors) and the level of compaction achieved at increasing depths for different soil conditions (soil types). The data, analyses, and correlations may be useful for WisDOT officials to decide if a revision of the current construction specification, including the need to change current 0.20-m (8-in) loose lift thickness in the construction of compacted embankments, is necessary such that stable and economical subgrade/subbase structures can be built.

1.3 Report Organization

The field experimental and numerical research program provides the needed information for the justification of construction requirement changes. The research program includes:

- 1) Development of a field monitoring system to evaluate applied compaction energy and the degree of compaction at various depths under field conditions and different compactor geometries.
- 2) Numerical analyses to relate the degree of soil compaction at various depths as a function of energy applied to the surface (e.g., compactor type and operating weight), and footprint (contact width).
- 3) Determination of the influence of soil parameters (e.g., soil texture, plasticity, and water content) on the compactive energy dissipation and compaction achieved.
- 4) Recommendations to optimize lift thickness as a function of Wisconsin construction experiences: typical compaction equipment (delivered compaction energy) and soil types.

Chapter 2 - FIELD SOIL COMPACTION

2.1 Compaction Characteristics

Soil compaction is the process by which the volume of air voids in soils is reduced by means of applied external mechanical energy. Compaction processes are performed to densify soils, improve engineering properties, to stabilize the behavior of soils (Holtz and Kovacs 1981; Holtz 1990). Traditionally, soil compaction operations have been based on the relationship and procedure developed by R. Proctor in the 1930's and further described by Olson (1963). The classic relationship of dry densities plotted as a function of water contents at a single compactive energy as shown in Figure 2.1. This figure also shows the zero-air-voids line (i.e., the line that corresponds to saturated soils) and the common compaction specification of 90% relative compaction.

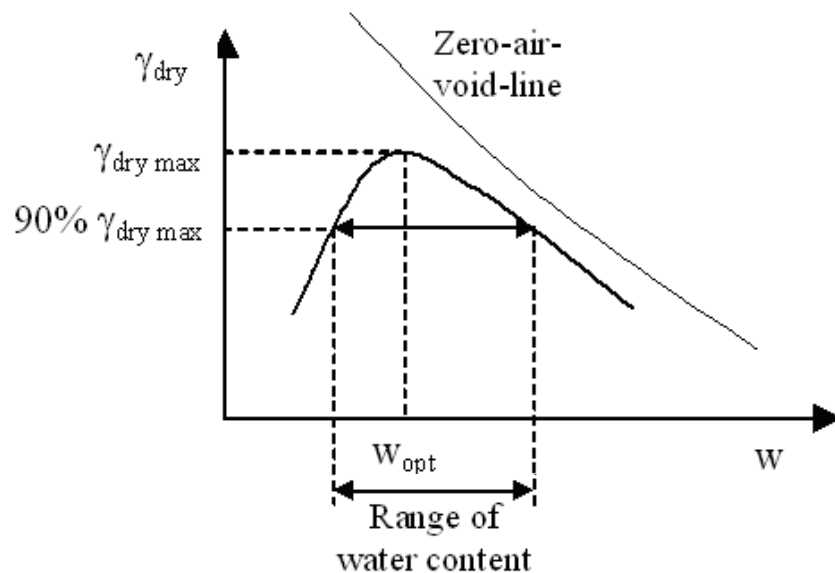


Figure 2.1: Typical Proctor results and the effect of water content changes on the soil modulus (w_{opt} is the optimum water content and $\gamma_{dry\ max}$ and is the maximum dry unit weight).

Several factors influence the compaction process (i.e., maximum density or unit weight and optimum water content):

- compaction method (i.e., pounding, kneading, pressure, vibration, etc.)
- molding water content (i.e., the water content of the soil when compacted)
- compactive effort (i.e., the amount of applied external energy)
- type of soil

Furthermore, variations of the soil structure during compaction influence engineering properties, including hydraulic conductivity, compressibility, and shear strength. Figure 2.2 illustrates how the soil structure can be affected by compactive effort and water content. For example, textures of soils compacted on the dry side of optimum water content tend to be flocculated, whereas soils compacted on the wet side of optimum water content tend to be dispersed due to the expansion of the diffused double layer (Lambe 1958).

Seed and Chan (1959) reported that different water contents and compaction methods yield very different shear strengths and volumetric stabilities (i.e., axial shrinkage). Figure 2.3 summarizes the very different behavior response of soils even when they belong to the same compaction curve. These results indicate that different compaction methods may yield very different internal structures in soils. That is, a range of soil properties was obtained by different compaction operations, energies, and water contents. These observations have led researchers to propose different degree of compactions depending on the intended engineering use of soils.

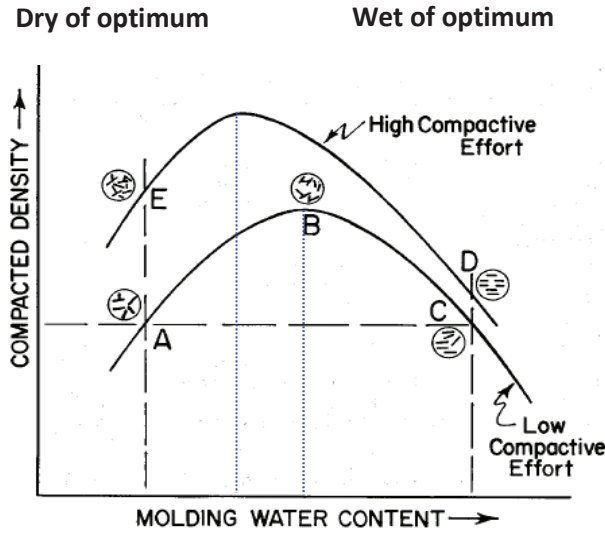


Figure 2.2: Effect compaction energy and optimal water content on the final density and structure of compacted soils (Lambe 1958).

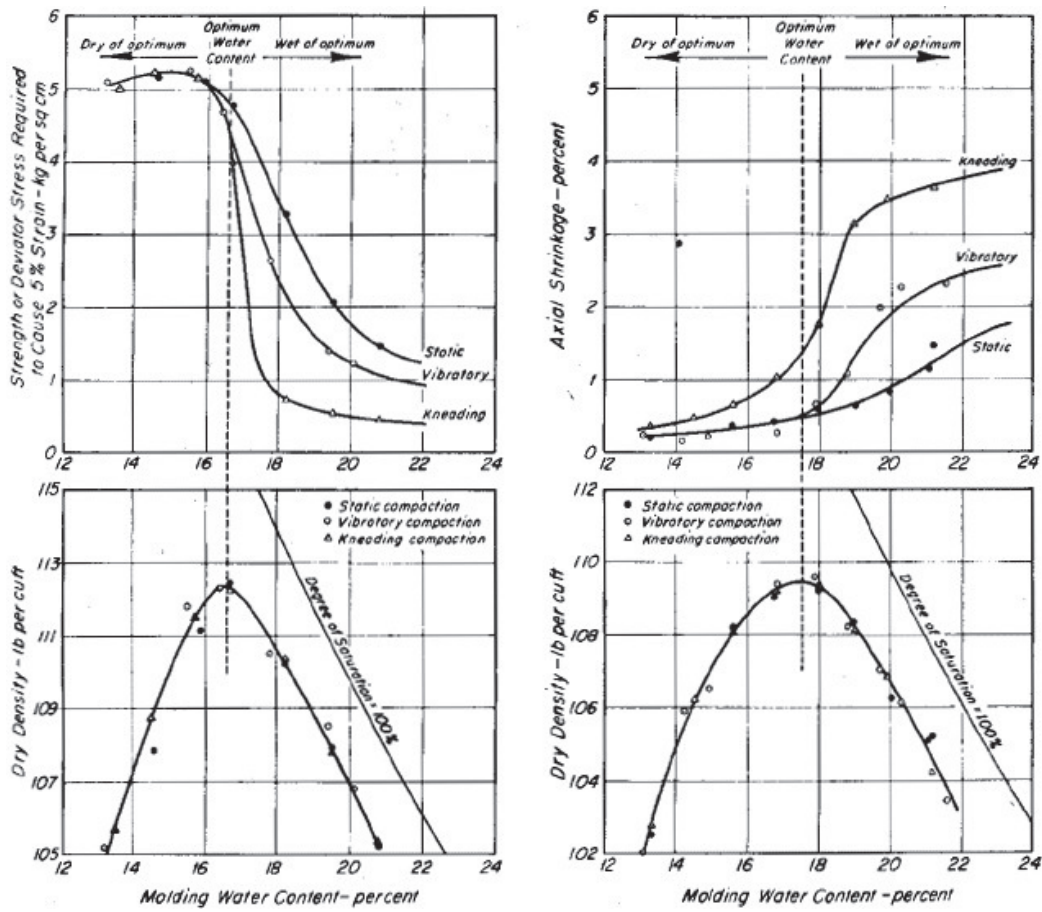


Figure 2.3: Influence of the compaction method on the strength and volumetric stability of soils (Seed and Chan 1959).

For example, Daniel and Benson (1990) have suggested levels of compaction for soils to be used either for embankments (high shear strength and low compressibility) or as impervious barriers or liners (low hydraulic conductivity). These optimal ranges are presented in Figure 2.4 and expanded in Figure 2.5. Figure 2.5 presents the qualitative effect of water content and strain level on the low-strain modulus. The low-strain stiffness is an important parameter that is related to the modulus used in the mechanistic-empirical design method for pavement systems (Schuettpelez et al. 2009). Finally, under normal highway use, the compacted materials in the base/subbase may increase their water content or be exposed to higher strain levels due to traffic loads; both conditions cause a decrease of the stiffness and loading capacity of embankments.

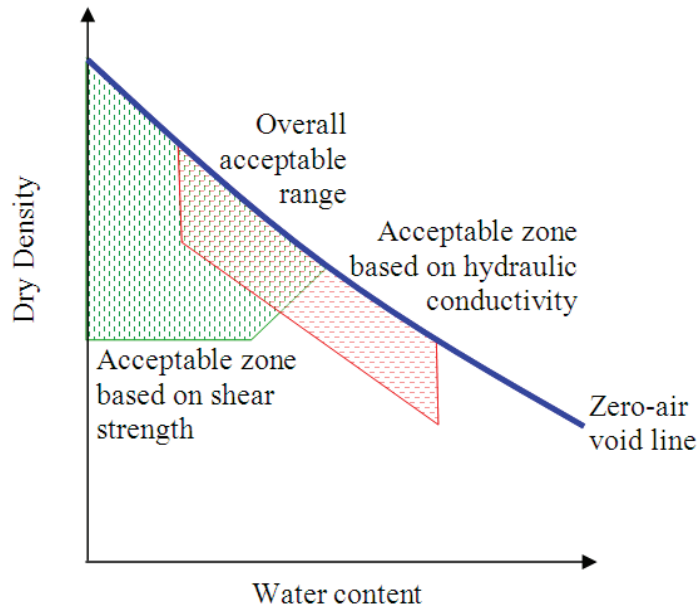


Figure 2.4: Schematic of acceptable ranges for compacted soils in terms of properties and applications (after Daniel and Benson 1990).

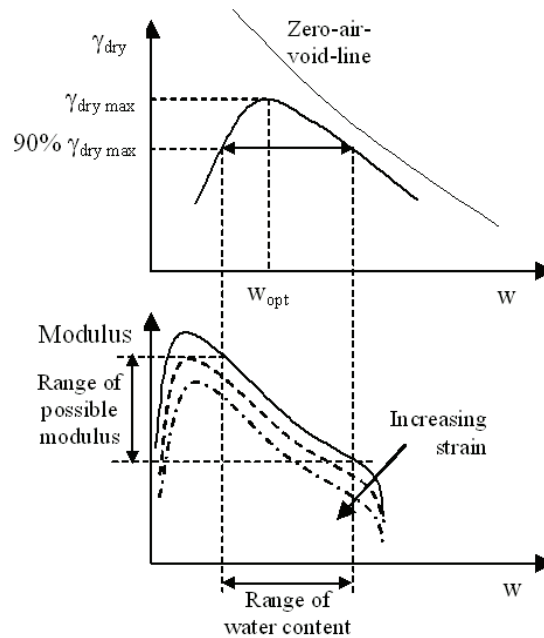


Figure 2.5: Typical Proctor results and the effect of water content changes on the soil modulus.

2.2 Compaction Energy Propagation in Soils

During compaction operations, the static and dynamic energy generated by compaction equipment is transmitted to the ground by large amplitude P, S, and R-waves. Figure 2.6 shows how the wave energy is transmitted from the source of dynamic loading in radial and vertical directions (Richart et al. 1970). These waves interact with the soil producing compressions and distortions while increasing the soil density. Figure 2.7 presents the dynamic stress and acceleration distribution induced by the vibratory roller in during compaction processes (D'Appolonia et al. 1969). The deformation field induced by passing compaction equipment forces soil particles to move and rotated past each other. During this process the soil tends to reduce the air void space. A large deformation created by the compaction equipment rapidly attenuates (non-linear strain regime) so the depth of compaction is constrained by this rapid attenuation.

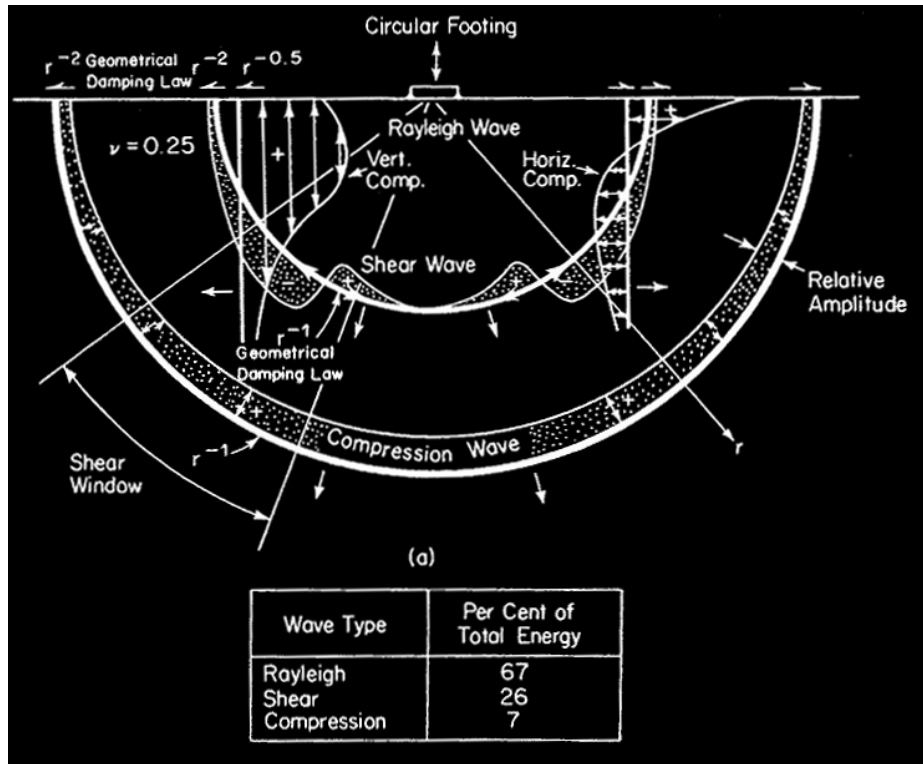


Figure 2.6: Distribution of displacement waves from a footing (Richart et al. 1970).

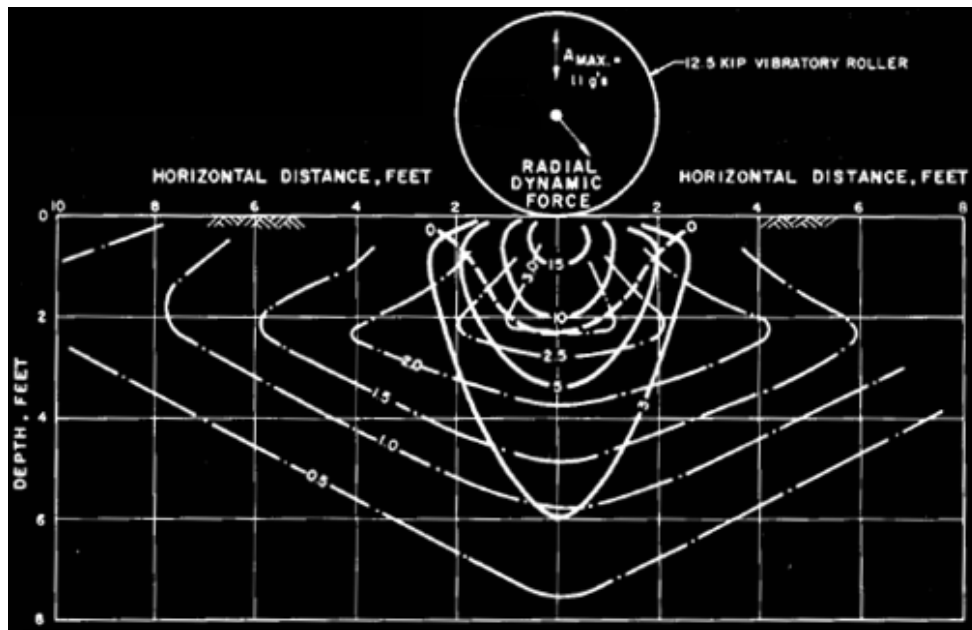


Figure 2.7: Distribution of dynamic stresses and soil acceleration as a function of the distance from a vibratory roller (5700 kg-12,500 lbs roller - D'Appolonia et al. 1969). Continuous lines correspond to vertical stresses.

2.3 Compaction Equipment and Techniques

There are two main variables controlling the field densification of soils. One is the selection of the field compacting equipment, and the other is the soil type and moisture at compaction. The compactor weight, drum and tire size (physical parameters), and operating frequency of the vibratory roller (dynamic parameters) are main equipment parameters used to control field soil compaction operations (Holtz and Kovacs 1981; Soane et al. 1981). The demand for increasing and more efficient compaction operations as applied to the construction and rehabilitation of civil infrastructure has led to the development of larger and heavier compaction and earthmoving equipment (Bowels 1979; Rollings and Rollings 1996). These more powerful compaction and earthmoving equipment may potentially improve compaction operations. However, soil parameters (i.e., initial dry density, grain size and shape, and water content) are still important material properties in controlling how well a soil can be compacted (Holtz and Kovacs 1981; Holtz 1990; Rollings and Rollings 1996). That is, the interaction of modern compaction equipment with different soils and soil conditions will ultimately control how these compaction operations may be optimized.

2.3.1 Smooth-drum Vibratory Roller

The smooth-drum vibratory roller consists of a single drum and two rubber-tired wheels (Rollings and Rollings 1996 - Figure 2.8). Rotating eccentric weights inside of the drum generate the vibration for additional dynamic loads. This dynamic action helps overcome the interparticle friction between soil particles and facilitate the densification of soils. Thus, this equipment is most efficiently used in the compaction of coarse-grained soils. The effects of vibratory rollers can be analyzed using nonlinear analytical models of the

soil-machine system as shown in Figure 2.9 in which both the compaction equipment and the soil are treated as coupled single degree of freedom systems (Yoo and Selig 1979; Anderegg and Kaufmann 2004).



Figure 2.8: Caterpillar™ CS563 smooth-drum vibratory roller (Operating equipment mass is 11,120 kg - 24,520 lb. Operating drum mass at drum is 5,840 kg - 12,877 lb – Source: Caterpillar 2009).

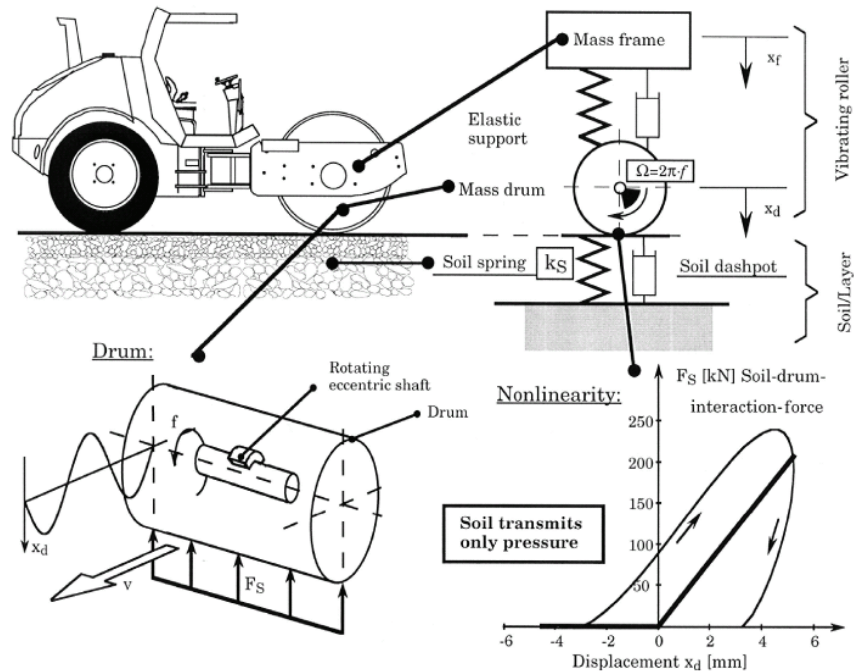


Figure 2.9: Schematic representation of soil-machine interactions during compaction operations (Anderegg and Kaufmann 2004).

2.3.2 Rubber-tired Roller

The wheel dozer or rubber-tired roller for earthwork is a two-axle roller with 4 rubber tires (Figure 2.10). The rubber-tired roller has about 80% coverage with 700 kPa (100 psi) contact pressure comparing 100% coverage under the wheel with 380 kPa (55 psi) of the smooth-drum vibratory roller. This equipment is mainly used for filling in highway and earth dam constructions.



Figure 2.10: Caterpillar™ 824C rubber-tired roller (Operating equipment mass is 28,724 kg - 63,325 lb – Source: Caterpillar 2009).

2.3.3 Padfoot Roller

The padfoot roller contains a drum with protruding feet. There are different types of feet thus these types of compactor often also called pad-foot, club-foot, or tamping-foot compactor (Rollings and Rollings 1996). These types of roller are widely used in the fine-grained soils. The padfoot roller has 8 to 12% coverage under the wheel with 1400 to 7000 kPa (200 to 1000 psi) contact pressure due to its small coverage area by each of the feet (Holtz and Kovacs 1981).



(a)



(b)



(c)

Figure 2.11: (a) Caterpillar™ CP563 padfoot roller (Operating equipment mass is 11,555 kg - 25,479 lb. Operating drum mass at drum is 6,075 kg - 13,395 lb - Source: Caterpillar 2009); (b) Dyanpac™ CT262 padfoot roller (Operating equipment mass is 21600 kg - 47620 lb - Source: Ritchie Specs 2014); and (c) Dyanpac™ CA251PD padfoot roller (Operating equipment mass is 11,177 kg – 25,590 lb - Source: Ritchie Specs 2014).

2.4 Controlling Parameters in Field Compaction Operations

During construction operations, the compactor geometry and weight, soil type, moisture content, number of passes of compactor, lift thickness, and speed of roller control the final quality of compaction operations. Figure 2.12 summarizes results of the compaction effectiveness as a function of the weight of compactor for different types of soils and lift thickness. Trends indicate that as the normalized weight of compactors increases the compaction density, as a function of the modified maximum compaction, increases as well. However, other factors such as lift thickness and frequency of the compaction equipment also control the quality of compaction operations. These parameters are poorly documented.

Figure 2.12: Effect of static weight on the vibratory roller (Rollings and Rollings 1996).

Turnbull and Foster (1956) describes that the dry density of the embankment is controlled by the roller passes, roller tire pressure, and lift thickness. Figure 2.13 shows the effect of

the tire pressure and coverage on the compacted dry density. These observations imply that there is a correlation between the contact pressure (weight of compactor), compactor passes, and water content of soils. This correlation is also optimized to obtain a specific dry density. D'Appolonia et al. (1969) discusses the relationship between the number of roller passes and dry density versus for compaction of coarse-grained soils using the vibratory compactor. Using experimental results, it provides guidelines for lift thickness and the number of roller passes (Figure 2.14). D'Appolonia et al. (1969) also suggests that not more than five roller passes are needed during compaction operations.

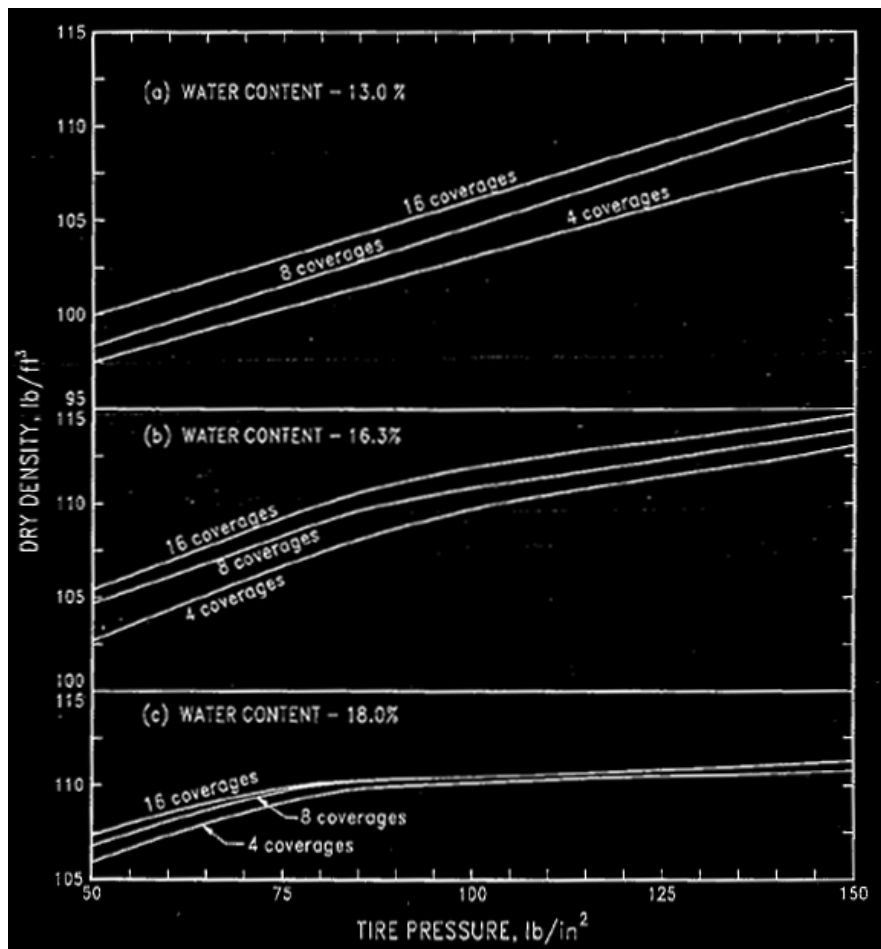


Figure 2.13: Effect of the tire pressure, number of passes and water content (after Turnbull and Foster 1956).

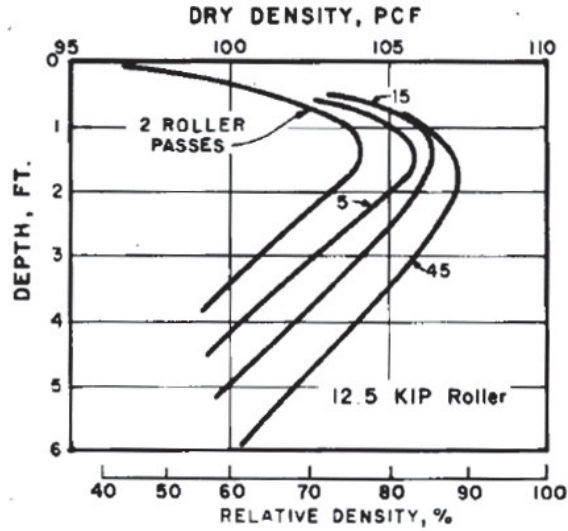


Figure 2.14: Density-depth relationship by the cumulative number of compaction equipment passes (D'Appolonia et al. 1969).

Lift thickness of embankments is dependent on the size and type of compactors and on the size and type of fill materials. A conventional range of lift thickness varies between 0.15 and 0.45 m (6 and 18 in - Holtz and Kovacs 1981). Turnbull and Foster (1956) evaluate the effect of lift thickness on the dry density gradient versus depth. Figure 2.15 summarizes the results. The presented data do not allow the comparison between 0.15 and 0.30 m (6 and 12 in) lift thickness but they show that the dry density gradient is steeper for 0.3 m (12 in) than for 0.6 m (24 in) lift thicknesses for soils compacted at and the wet side of optimum.

Figure 2.15: Effect of lift thicknesses on the dry density of compacted soils (after Turnbull and Foster 1956).

2.5 Specifications on Lift Thickness in the United States

Table 2.1 summarizes the recommended combinations of the compaction equipment and lift thickness for several soils (Bowles 1979). Table 2.2 summarizes the currently used specification of lift thickness at each State's DOT (0.15 to 0.30 m - 6 to 12 in). Most states specify a 0.20-m (8-in) lift thickness before compaction. New Hampshire, Louisiana, New Jersey, and Texas require a 0.30-m (12-in) lift thickness before compaction. Maryland, Massachusetts, Montana, North Dakota, Ohio, and Oklahoma require a 0.15-m (6 in) lift thickness after compaction. This variation is most likely

caused by the experience on different base/subbases soils available within each state. Although New York DOT specifies lift thickness as a function of soil and compaction equipment (State of New York 2008), most DOT specifications still provide just lift thickness and the percentage of compaction as a quality controlling parameters (Hoppe 1999).

Table 2.1: Compaction equipment and compaction applications of fills (Bowels 1979).

Soil group	Soil type	Compaction condition	Degree of compaction	Compaction equipment	No. of passes	Lift thickness	Moisture control	Unit weight	Field control	
Pervious	GW GP	Compacted	95 to 105% of standard compaction test or 70 to 85% of relative density	Vibratory roller	As required	As required	Saturate by flooding	17-21 kN/m ³ (108-134 pcf)	Field density test at random locations	
				Rubber-tired roller Crawler-type tractor	2 to 5 2 to 5	0.30 m (12 in) 0.20 m (8 in)				
	SW SP	Semi-compacted	90 to 95% of standard compaction test or 60 to 70% of relative density	Rubber-tired roller	2 to 5	0.35 m (14 in)	Saturate by flooding	16-20 kN/m ³ (102-127 pcf)	Field density test at random locations	
				Crawler-type tractor	1 to 2	0.25 m (10 in)				
Semi-imperious to imperious	GM GC SM	Compacted	95 to 105% of standard compaction test	Rubber-tired roller	2 to 5	0.20 m (8 in)	OMC based on lab compaction test	16-20 kN/m ³ (102-127 pcf)	Field density test at random locations to determine relative compaction	
				Padfoot roller	4 to 8	0.15 m (6 in)				
	SC ML CL MH CH	Semi-compacted	90 to 95% of standard compaction test	Rubber-tired roller	2 to 4	0.25 m (10 in)			14-19 kN/m ³ (89-121 pcf)	
				Padfoot roller	4 to 8	0.20 m (8 in)				
				Crawler-type tractor	2 to 4	0.15 m (6 in)				

Table 2.2: State compaction specifications (Hoppe 1999; Lenke 2006).

State	Loose lift thickness cm (in)	% compaction	Remark
Alabama	0.20 (8)	95	
Arizona	0.20 (8)	100	
California	0.20 (8)	95	For top 0.75 m (30-inch)
Connecticut	0.15 (6)	100	Compacted lift indicated
Delaware	0.20 (8)	95	
Florida	0.20 (8)	100	
Georgia		100	
Idaho	0.20 (8)	95	
Illinois	0.20 (8)	95	For top; remainder varies with embankment depth
Indiana	0.20 (8)	95	
Iowa	0.20 (8)	None	One roller pass per inch thickness
Kansas	0.20 (8)	90	
Kentucky	0.15 (6)	95	Compacted lift indicated; water +2% / -4% of optimum
Louisiana	0.30 (12)	95	
Maine	0.20 (8)	-	At or near optimum water
Maryland	0.15 (6)	97	For top 0.30 m (12 in); remainder is 92%
Massachusetts	0.15 (6)	95	
Michigan	0.23 (9)	95	
Minnesota	0.20 (8)	95	
Mississippi	0.20 (8)	-	
Missouri	0.20 (8)	95	
Montana	0.15 (6)	95	At or near optimum water
Nebraska		95	
Nevada		95	
New Hampshire	0.30 (12)	98	
New Jersey	0.30 (12)	95	
North Dakota	0.15 (6)	-	
Ohio	0.15 (6)	-	
Oklahoma	0.15 (6)	95	
Oregon	0.20 (8)	95	For top 0.90 m (36 in); remainder is 90%
South Carolina	0.20 (8)	95	
South Dakota	0.20-0.30 (8-12)	97	0.20 m (8 in) for embankment; 0.30 m (12-in) for bridge end backfill
Texas	0.30 (12)	-	
Vermont	0.20 (8)	90	
Virginia	0.20 (8)	95	+ or - 20% of optimum water
Washington	0.10 (4)	95	Top 24-in are 0.10 m (4-in) lifts; remainder are 0.20 m (8 in) lifts
Wisconsin	0.20 (8)	95	Top 1.8 m (6 ft), within 30 m (200 ft) of abutment; remainder is 90%
Wyoming	0.30 (12)	-	Use of reinforced geotextile layers

Note: New York DOT specifies lift thickness as function of soil and compaction equipment (State of New York 2008).

Chapter 3 - MATERIALS AND LABORATORY TESTING

3.1 Testing Site Locations

Two different sites were used to evaluate the effect of energy of compaction on different lift thicknesses. The first field was located approximately 10 miles northwest of Stevens Point in Central Wisconsin (Figure 3.1). The site was an embankment construction area on the approach to a new bridge on US Highway 10 (old County Road H) over State Highway 34. Hoffman Construction Company was contracted by the Wisconsin Department of Transportation (WisDOT) to build the embankments for the new County Road H. Hoffman Construction Company gave this research team access to the site construction and provided the compaction equipment and support for the field testing. Two coarse grained soils were tested: poorly graded sand and silty sand at natural water and wet conditions.



Figure 3.1: The testing field site was located about 10 miles Northwest of Stevens Point in Central Wisconsin (after Google Maps 2014).



Figure 3.2: The testing field site was located at Town of Sylvania west of Racine in South East Wisconsin (after Google Maps 2014).

The second field was located in the Town of Sylvania west of Racine in South East Wisconsin (Figure 3.2). The testing site was placed on the area where the new W. Frontage Road was being built west of Interstate 94. WisDOT contractors built the tested area, gave this research team access to the construction site, and provided the compaction equipment and support for the field testing. A fine-grained plastic soil was tested at three different moisture contents and at three different lift thicknesses.

3.2 Geomaterial Samples

Representative soil samples were collected from both field sites. The samples were selected considering the construction job schedule and expected borrowed materials to be used at the embankment construction during field testing. The soil samples represent typical Wisconsin soils used in road construction practice. Three different soils were tested. Two coarse-grained soils at the Junction City, WI site and one plastic, fine-grained soil at the Town of Sylvania, WI site were tested. At the Junction City, WI site, the soil samples were collected by Hoffman Construction Company personnel from the borrow site used during construction site. At the Town of Sylvania, WI site, the soil samples were collected by the research team.

3.3 Engineering Properties of the Tested Soils

Collected soil samples were characterized using American Standard Test Methods (ASTM) test procedures. These tests included:

- ASTM D854-02: Standard Test Methods for Specific Gravity of Soil Solids by Water Pycnometer
- ASTM D422-63: Standard Test Method for Particle-Size Analysis of Soils
- ASTM D421-85: Standard Practice for Dry Preparation of Soil Samples for Particle-Size Analysis and Determination of Soil Constants
- ASTM D2487-00: Standard Practice for Classification of Soils for Engineering Purpose (Unified Soil Classification System)
- ASTM D698-07: Standard Test Methods for Laboratory Compaction Characteristics of Soil Using Standard Effort (12 400 ft-lbf/ft³ - 600 kN-m/m³).

3.3.2 Grain Size Distribution (ASTM D422-63, ASTM D421-85, and ASTM D2487-00)

Hydrometer and sieve analyses were conducted to determine the grain size distribution curve and related grain size parameters on fine- and coarse-grained soil specimens. Particle size distributions for the soils are shown in Figure 3.3. Two parameters can be determined from the grain size distribution curves of coarse-grained soils: the coefficient of uniformity (C_u) and the coefficient of gradation or coefficient of curvature (C_c):

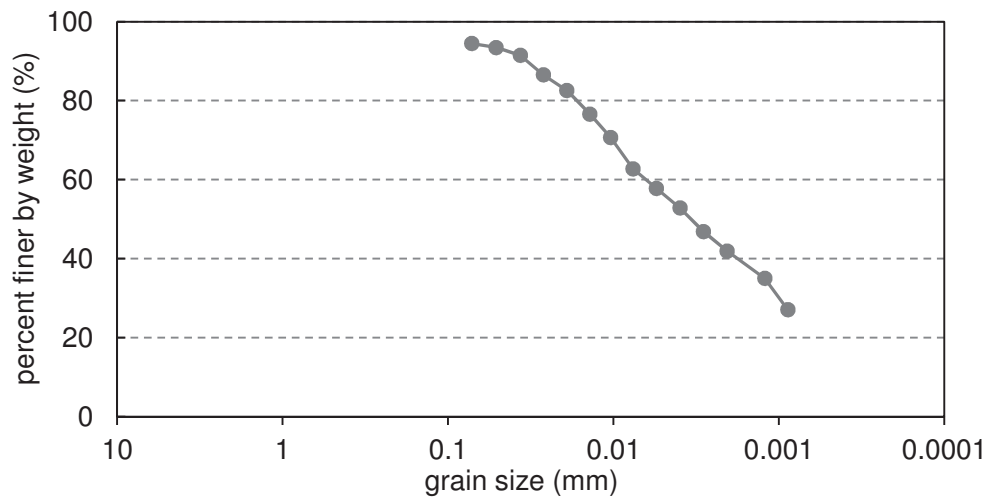


Figure 3.3: Grain size distributions of tested soils: (a) coarse-grained soils (Junction City site) and (b) fine grained soils (Town of Sylvania site).

$$C_u = \frac{D_{60}}{D_{10}} \quad (3.1)$$

$$C_c = \frac{D_{30}^2}{(D_{60})(D_{10})} \quad (3.2)$$

where D_{10} is the grain diameter corresponding to 10% passing, D_{30} is the grain diameter that corresponds to 30% passing, and D_{60} is the grain diameter that corresponds to 60% passing, by weight. The uniform coefficient, coefficient of curvature (gradation), and soil type as determined by the Unified Soil Classification System (USCS - ASTM D2487-00) of each soil are summarized in Table 3.1.

Table 3.1: Summary of particle size distribution and soil type.

Soil type	Mean particle size (mm)	Coefficient of uniformity (C_u)	Coefficient of curvature (C_c)	USCS Soil Type
Coarse-grained soil 1 – Junction City	~0.3	2.37	1.00	SP
Coarse-grained soil 2 – Junction City	~0.4	31.95	1.72	SM
Fine-grained soil 1 – Town of Sylvania	~0.004	N/A	N/A	CL

3.3.1 Specific Gravity (ASTM D854-02)

Two coarse-grained soils and one fine-grained soil were characterized in the laboratory. The measured specific gravity values, based on the ASTM D854 standard, are summarized in Table 3.2.

Table 3.2: Summary of specific gravity test results.

property	coarse-grained soil Junction City - SP	coarse-grained soil Junction City - SM	fine-grained soil Town of Sylvania- CL
specific gravity	2.83	2.66	2.69

3.3.3 Standard Proctor Compaction Test (ASTM D698-07)

Standard Proctor compaction tests were conducted to evaluate the compaction response of the coarse-grained soils. Compaction curves corresponding to standard Proctor effort were determined for each soil type and the results are shown in Figure 3.4. The maximum dry unit weights and optimum water contents are summarized in Table 3.3.

Figure 3.4: Compaction curves for tested soils coarse grained soils (Junction City, WI).

Table 3.3: Summary of maximum dry unit weights and the optimum water contents for all tested soils.

Soil type	Maximum dry unit weight kN/m³ (pcf)	Optimum water content %
Coarse-grained soil SP – Junction City	18.1 (115.5)	16.7
Coarse-grained soil SM – Junction City	17.1 (108.6)	9.5
Fine-grained soil CL – Town of Sylvania	17.6 (112)	16

Chapter 4 - FIELD MONITORING AND TESTING

4.1 Introduction

This chapter describes the field monitoring program used to evaluate the response of the soil during field compaction processes directly or indirectly. To directly evaluate soil responses during compaction, field measurements using MEMS accelerometers were used. These MEMS accelerometers captured the soil vibration when compaction and earthmoving equipment pass over the instrumented soil lift. Then, physical and performance data collected with sand cone, nuclear density gauge, dynamic cone penetrometer, soil stiffness gauge, and P-wave propagation were used to evaluate the compaction effectiveness of the different lift thicknesses with depth. The objective of the field testing program was to determine how different compactors and earthmoving equipment interacted with different soil types and lift thicknesses and how soil lift thickness influences the final compaction quality on different embankment soils.

4.2 Field Measurement Methods

To evaluate soil properties before, during and after compaction, field tests such as stiffness gauge (SSG), dynamic cone penetrometer (DCP), time domain reflectometry (TDR), shear-induced displacement and rotation using MEMS accelerometers, P-wave propagation using MEMS accelerometers, sand cone density, and nuclear density gauge (NDG) tests were conducted in each test section for different lift thicknesses. A brief description of all of these tests is presented next.

4.2.1 Soil Stiffness Gauge

The soil stiffness gauge (SSG), which is also known as GeoGauge, is a portable instrument that is designed for measuring near surface soil stiffness (Figure 4.1 - ASTM D6758-08). The SSG is a 0.28-m (11-in) diameter and 0.25-m (10 in) high cylinder that evaluates near surface soil stiffness by generating vibration and monitoring the response of the soil surface to the vibration. The stiffness is evaluated by the average force per unit displacement over a range of measured frequencies (Sawanguriya et al. 2003; Edil and Sawanguriya 2006). The SSG measures the impedance at the surface of soils. Soil stiffness can be calculated by the impedance:

$$K = \frac{P}{\delta} \approx \frac{1.77 \cdot R \cdot E}{1 - \nu^2} \quad (4.1)$$

where P is the load generated by vibration, δ is the vertical displacement of the soil surface, R is the outer radius of the ring foot of the GeoGauge, E is the Young's modulus of the soil, and ν is the Poisson's ratio of the soil.

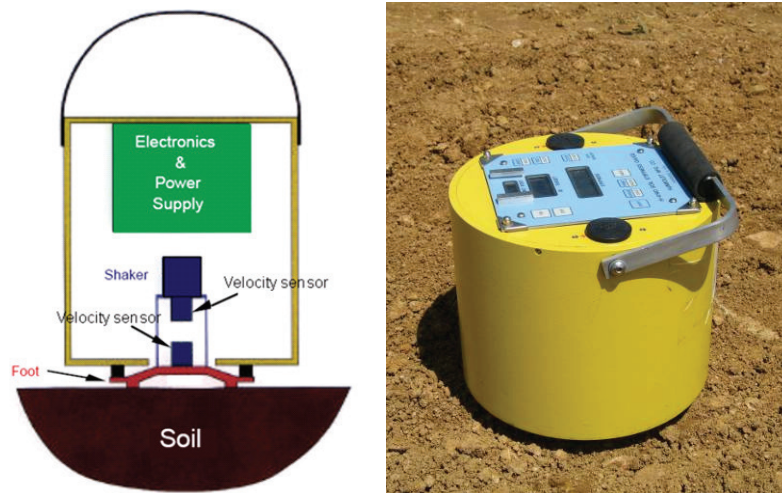


Figure 4.1: Schematic view of soil stiffness gauge (Source: Humboldt Mfg. Co. 2009).

4.2.2 Dynamic Cone Penetrometer

The dynamic cone penetrometer (DCP) has been used for quality control and quality assurance (QC-QA) tests for subgrade compaction due to its effectiveness on evaluating the in situ strength and stiffness (Abu-Farsakh et al. 2005; Gas Technology Institute 2005; Edil and Sawangsuriya 2006). The DCP cone with an apex angle of 60° and 0.02-m (0.79-in) diameter penetrates into the soil when it is driven by an 8-kg (17.6-lb) falling mass (Figures 4.2 and 4.3). These properties are summarized in Table 4.1.

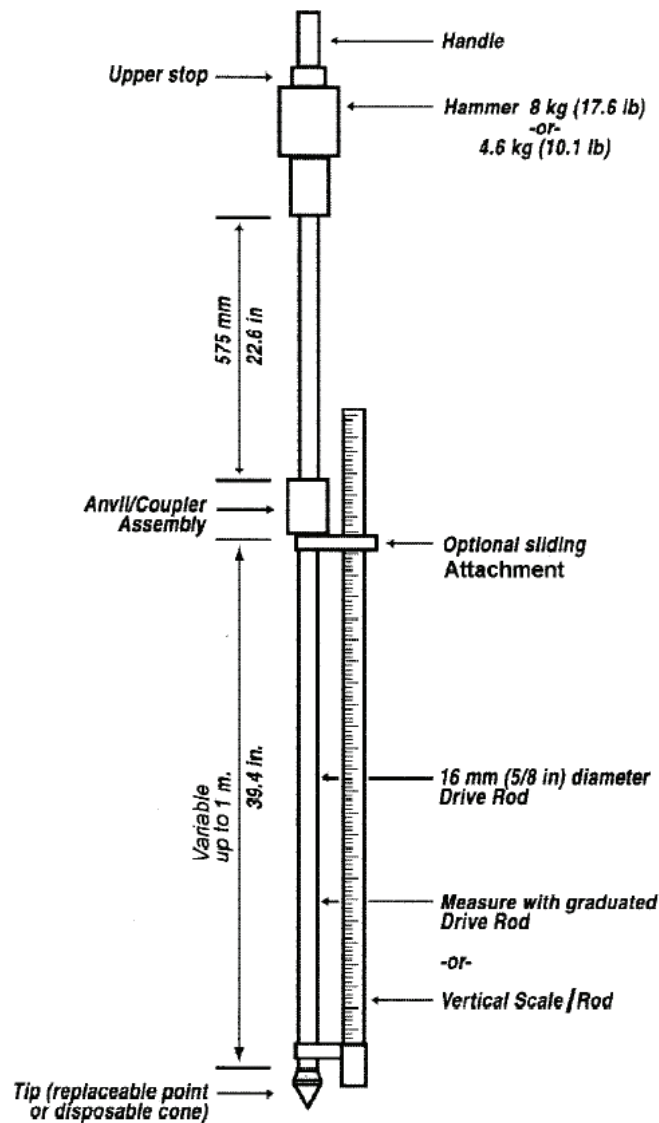


Figure 4.2: Schematic of DCP device (ASTM 6951-03 standard).



Figure 4.3: Testing using the dynamic cone penetrometer (DCP).

Table 4.1: DCP equipment specification.

Drop hammer mass	8 kg (17.6 lb)
Falling height	0.57 m (22.6 in)
Mass of anvil and accessories	6 kg (13.2 lb)
Cone angle	60°
Cone diameter	2 cm (0.79 in)

DCP testing applications include: preliminary soils survey, construction control, and structural evaluation of existing pavements. Engineers assess high strength layers in pavement structures, identify the presence of weak spots in constructed embankments, measure the uniformity of in situ base materials, supplement foundation testing for design purposes, and test the compaction of backfills around edges of drain trenches.

The penetration rate is expressed DCP index (DPI) and defined as the penetration depth per mass blow. The DPI provides an indication of the uniformity of soil layers and a measure of shear strength as a function of dry density and effective stress (Table 4.2). DPI profiles also give an indirect measure of the effect of compaction in soils. The DCP values have been correlated to soil density, CBR, shear strength, resilient modulus, elastic modulus, and soil classification (Burnham and Johnson 1993; Gas Technology Institute 2005).

The DPI is expressed by:

$$DPI = \frac{P_{i+1} - P_i}{B_{i+1} - B_i} \quad (4.2)$$

where P is the penetration (mm) and B is the blow count. The penetration is measured by dropping of a weight:

$$P_i = \sum_{i=1}^{i=n} RR_i - RR_0 \quad (4.3)$$

where RR_0 is the rod reading after seating, RR_i is the rod reading at i-th hammer drop, and n is the total number of hammer drops.

DCP index profiles show the effectiveness of compaction processes, that is, the homogeneity of the compacted soil strength both at different locations and depths at one location. DCP index profiles are able to detect increments in the strength and stiffness of the soil because of compaction. DCP index profiles also yield thicknesses of compacted layers. A sudden change in the DCP index is an indication of significant changes in the shear strength of the tested materials.

Table 4.2: Suggested DPI values for sounding (after Mohammadi et al. 2008).

DPI (mm/blow)	Dr (%)	Description
>42	<25	Very loose
42 – 23	25 – 35	Loose
23 – 12	35 – 50	Medium
12 – 5	50 – 75	Dense
<5	>75	Very dense

4.2.3 Time Domain Reflectometry

The time domain reflectometry (TDR) is an electromagnetic wave-based technique used to measure water content and electrical conductivity in soils (Benson and Bosscher 1999; Jones et al. 2001; Schneider and Fratta 2009). A probe measures the electromagnetic wave velocity of soils surrounding the probe. The electromagnetic wave velocity in soils is mainly controlled by the volume of water in the pores (Topp et al. 1980; Santamarina et al. 2005). That is, the TDR technique is used in geotechnical and agricultural engineering practice to monitor the volumetric water content. The TDR probe can be placed in the soil lift before compaction to monitor changes in the water content and to help in the estimation of changes in the strength and stiffness of soils (Figure 4.4).

$$\theta = -0.053 + 2.92 \cdot 10^{-2} K_a - 5.5 \cdot 10^{-4} K_a^2 + 4.3 \cdot 10^{-6} K_a^3 \quad (4.4)$$

where, θ is the volumetric water content, $K_a = (c/V)^2$ is the apparent dielectric constant, V is the measured electromagnetic wave velocity with the TDR probe, and c is the electromagnetic wave velocity in free space.

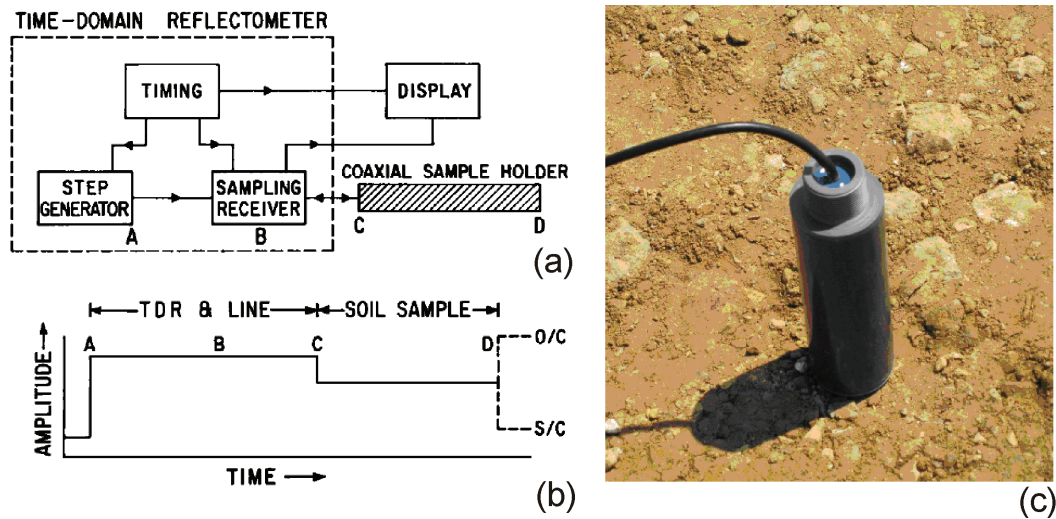


Figure 4.4: Time domain reflectometry: (a) block diagram; (b) example of the TDR output (time interval of C-D indicates the travel time in the soil, and O/C and S/C indicate open circuit and short circuit - after Topp et al. 1980).

4.2.4 MEMS Accelerometers

Miniature Electro-Mechanical Systems (MEMS) accelerometers are inexpensive sensors that can be embedded in compacted soils to help monitoring soil acceleration and displacement and stiffness over time. Due to the robustness of the measurement circuit and the low cost of these sensors, MEMS accelerometers provide large amount of information at low cost. For example, MEMS accelerometers can be used to monitor shear-induced rotation by evaluating voltage differences during compaction processes and then establishing an influence depth of compacted soils (Schuettpelez et al. 2009a - Figure 4.5). The same accelerometers can be used to estimate displacement and also to capture wave propagation to determine low-strain moduli. This can be done because MEMS accelerometers sense accelerations from 0 Hz to about 1 kHz.

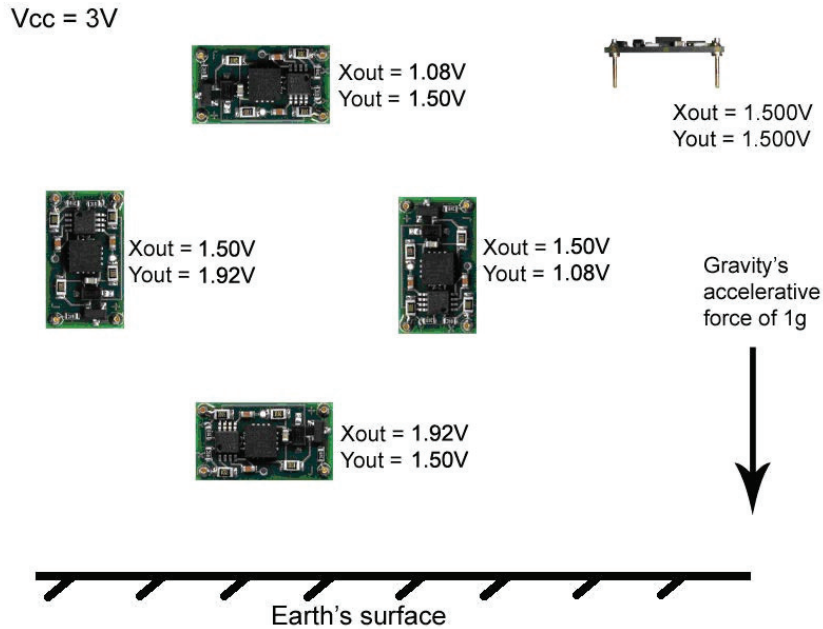


Figure 4.5: Rotation and calibration measurements with MEMS accelerometers
(Excitation: 3 V_{DC}- Source: Dimension Engineering 2009).

The ADXL322™ MEMS accelerometers were selected in this study. They are small, thin, low power, analog, dual-axis accelerometer with signal conditioned voltage outputs. MEMS devices measure acceleration with a full-scale range of $\pm 19.01 \text{ m/sec}^2$. These devices can measure both dynamic acceleration (vibration) and static acceleration (i.e., acceleration of gravity). The ADXL322™ sensor is available in a 4 mm × 4 mm × 1.45 mm, 16-lead, printed circuit board. The response voltage of the 2D-MEMS corresponds to acceleration in the x and y directions. The sensitivity of output voltage is dependent on the input voltage. The sensitivity is $0.765 \text{ V}/(\text{cm/s}^2)$ when an excitation of 5.0 V is applied. The MEMS device is available on an integrated circuit. This circuit provides protective functions such as reverse voltage, over-voltage, short circuit (Dimension Engineering 2009). To endure the high pressure induced by the heavy field soil

compaction operations, plastic epoxy was employed as plastic housing of MEMS accelerometer.

4.2.5 Hydraulic Pressure Plate

A main function of the pressure plate is to monitor pressure changes caused by compactors at the bottom of soil layer. To monitor transferred stress changes in subsoils, a pressure plate installed in the bottom of layer. The pressure plate used in this study was developed at the University of Wisconsin-Madison by late professor Peter Bosscher (Figure 4.6). Hydraulic changes of the pressure plate are converted to electrical signals for measuring pressure changes. Figure 4.7 shows the calibration curve of the pressure plate. In the field, there are several issues and concerns related to the response of the pressure plate. For example, small hard particles may puncture the rubber membrane while a large bolder sitting on top of the pressure plate may mask average vertical stresses. In spite of these problems, the pressure plate is capable of sensing, at least qualitatively, the pressure generated by compactors, when they pass over the sensor.

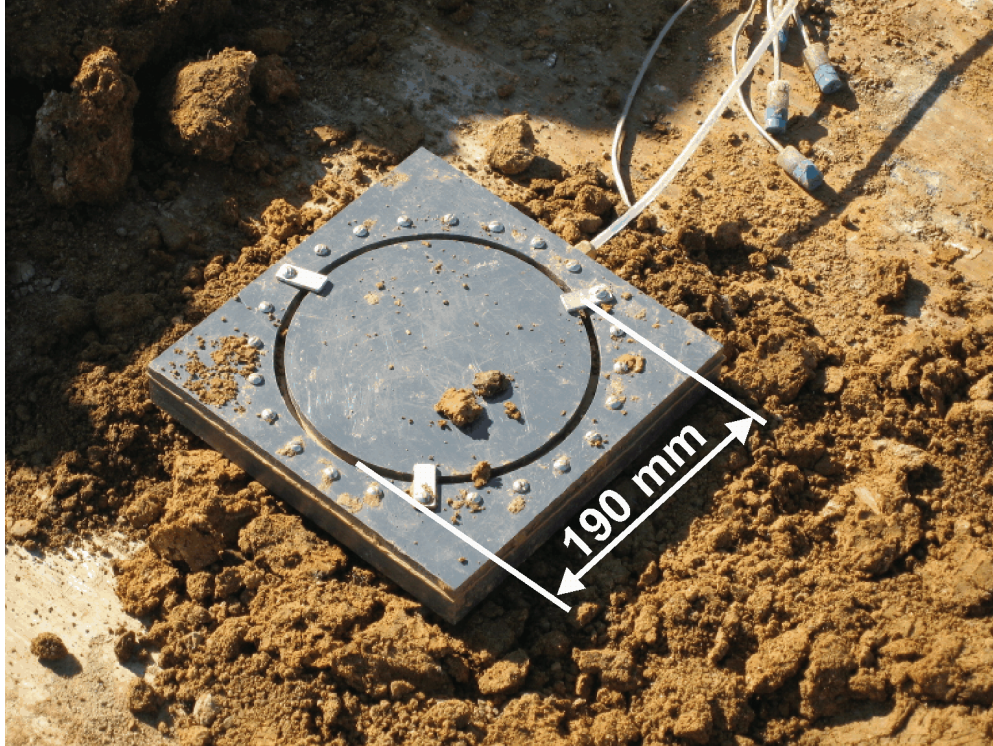


Figure 4.6: Hydraulic pressure plate and MEMS accelerometers.

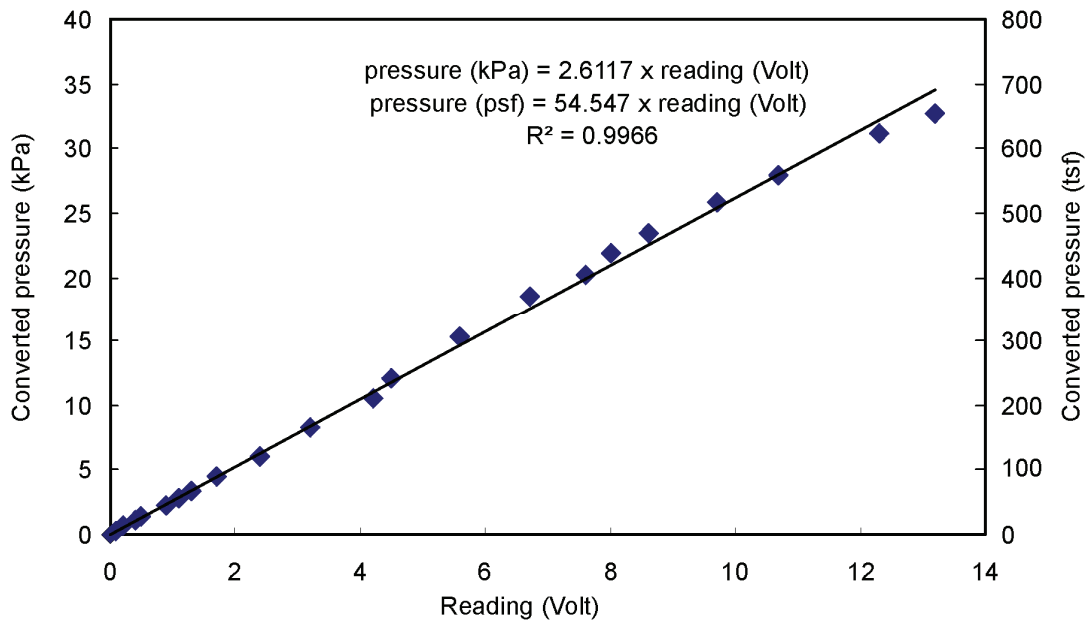


Figure 4.7: Calibration of the pressure plate.

4.2.6 Sand Cone and Nuclear Density Gauge

Soil density and water content are measured using the traditional sand cone method and with the nuclear density gauges (NDG) with gamma and neutron sources. Sand cone method was conducted by ASTM standard (ASTM D1556-07). NDG (ASTM D6938-08a) is often used in evaluating the density profile of compacted layers by the direct transmission mode and water content profile by backscatter mode (Winter and Clarke 2002 – Figure 4.8).

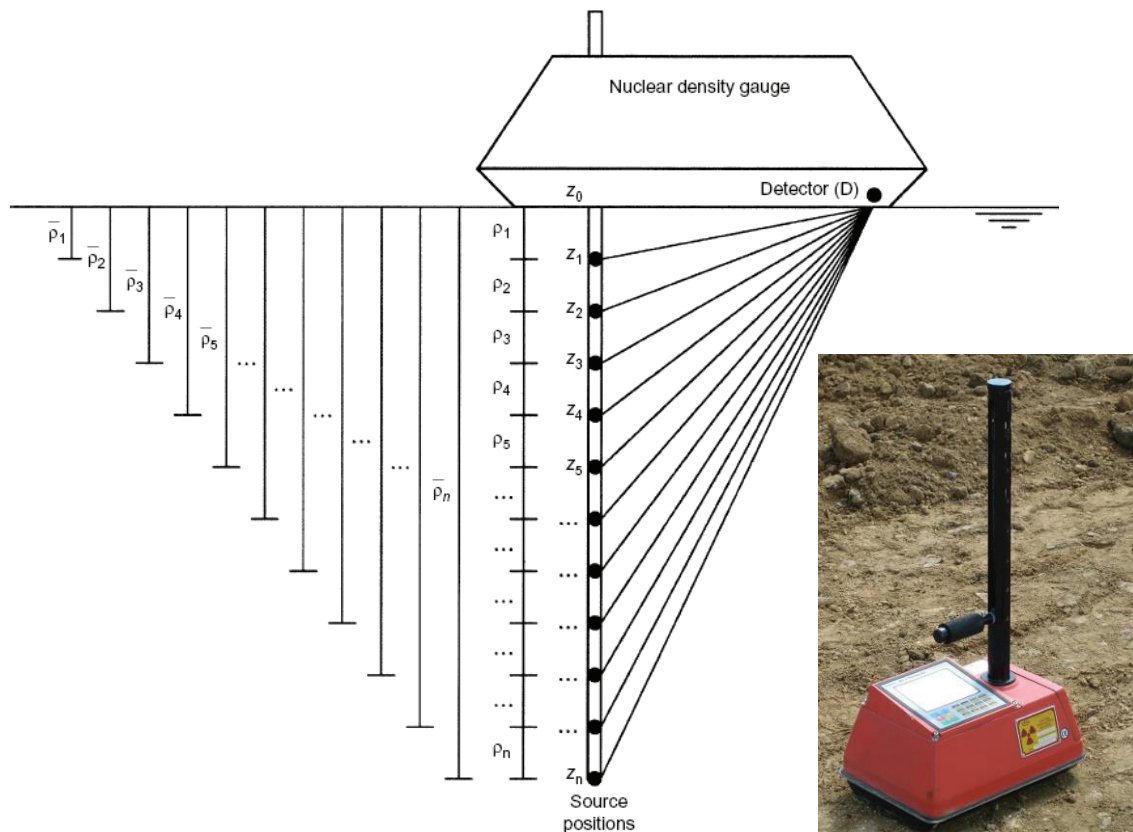


Figure 4.8: Nuclear density gauge (Winter and Clarke 2002) and the measurement profile versus depth.

4.3 Coarse-Grained Soils: Junction City Field Testing

As presented in Section 3.1, the selected site for the field testing is located approximately 10 miles northwest of Stevens Point in Central Wisconsin. The site was a road construction zone where a road expansion and a new bridge were built on US highway 10 (old County Road H) over State Highway 34 (Figure 3.1). The evaluation of the compaction operations was performed on the embankment just East of the bridge over State Highway 34 (Figure 4.9). Hoffman Construction Company facilitated the access to the site, provided personnel support, and compaction and earthmoving equipment.

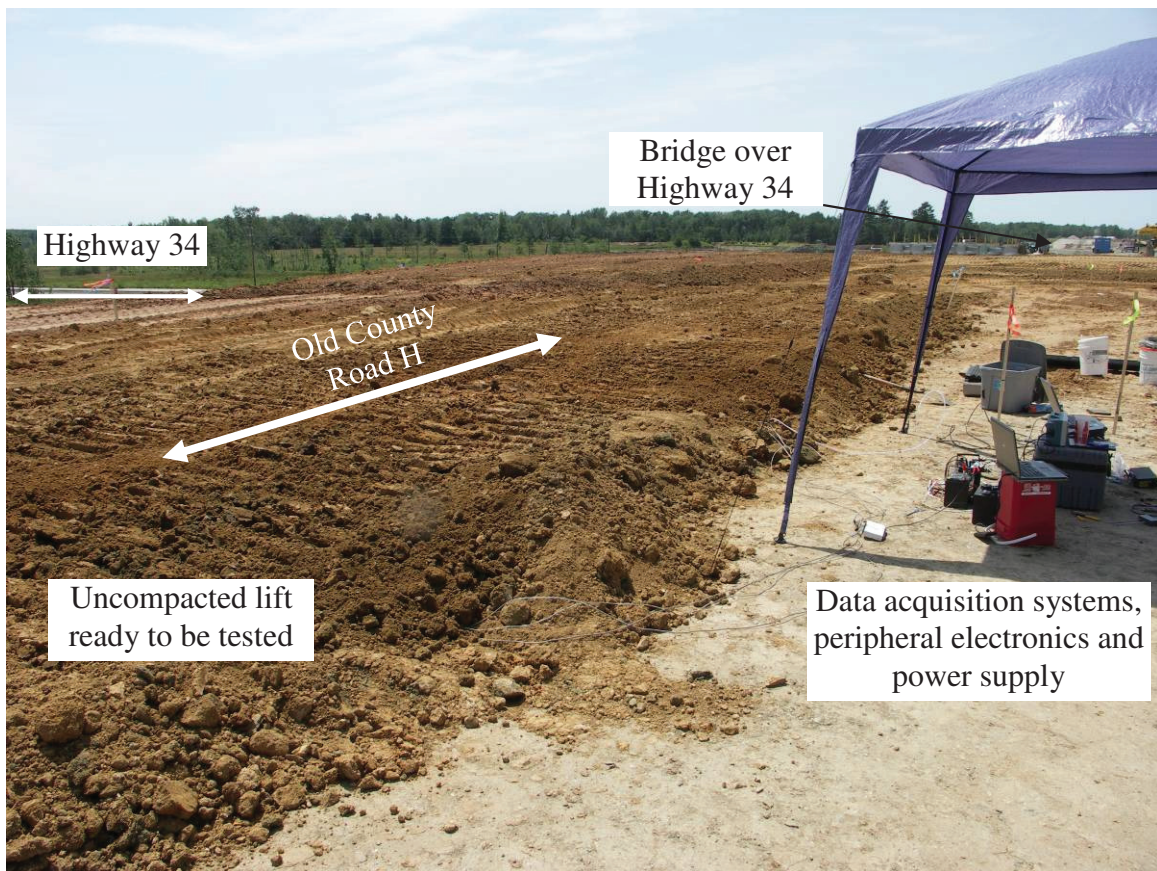


Figure 4.9: View of the testing site on County Road H just east of Highway 34 in Junction City, WI.

4.3.1 Compaction and Earthmoving Equipment

The compaction and earthmoving equipment used for the Junction City work were selected mainly based on the soil type at the site and equipment provided by Hoffman Construction Company. The operating weight and wheel contact area of the compaction equipment directly affect the compaction energy propagation through the soil mass. To evaluate different compaction energy levels, test sections were compacted using four types of Caterpillar™ equipment: Model 563E smooth-drum vibratory roller, Model 824C rubber-tired roller, Model 825C padfoot roller, and Model 631G scraper (Figure 4.10). The operating weights of compaction and earthmoving equipment along with wheels and drums sizes are summarized in Table 4.3.

Figure 4.10: Field soil compactors used during field testing (Junction City site).

Table 4.3: Operating weight of compaction and earthmoving equipment (Junction City Site - Source: Caterpillar 2009).

Compactor Type	Model Number	Operating weight of equipment (tsf)	Tire Type or Drum Dimension
Wheel dozer (Rubber-tired roller)	824	31.7	29.5RR25 XHA MX L3
Smooth-drum vibratory roller	CS-563	12.3	Width: 44.3 in Diameter: 51.1 in
Padfoot vibratory roller	825	36.1	Width: 83.9 in Diameter: 60.0 in
Scraper	631	92.3	37.50-R35 Radial

4.3.2 Field Testing Program

During the compaction study using different types of compactors, soil and lift thicknesses, the shear-induced rotation and pressure response in the instrumented soil layer were measured by monitoring MEMS accelerations and pressure responses (Figure 4.11). After the compaction process was concluded, different types of field testing techniques were applied to evaluate engineering properties of soils after compaction. These tests included: dynamic cone penetration (DCP), P-wave propagation, soil stiffness gauge (SSG), time domain reflectometry (TDR), sand cone, and nuclear density gauge (NDG). The matrix of different soil compactors, lift thickness of soil layers, and conducted measurements is summarized in Tables 4.4 through 4.6. The measurement techniques for evaluating the water content, compaction effectiveness and compactive energy versus depth are complemented with traditional surface measurements to evaluate the quality of compaction operations. These traditional measurements include sand cone,

nuclear density gauge (NDG), soil stiffness gauge (SSG), and dynamic cone penetration (DCP).

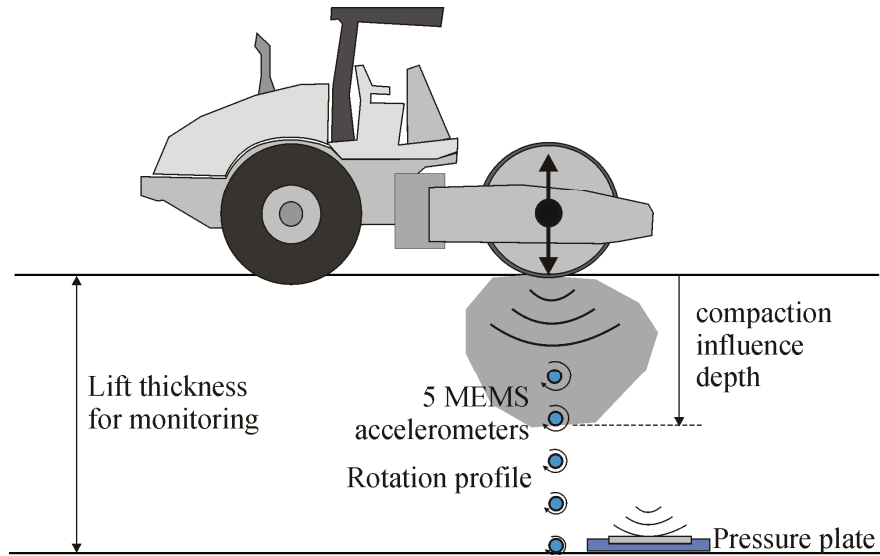


Figure 4.11: Instrumented soil layer by MEMS accelerometers.

Table 4.4: Testing program: coarse-grained soil SP (natural water content – Junction City Site).

Compactor	Lift thickness	Measured parameters
Smooth-drum vibratory roller	0.30 m (12 in)	<ul style="list-style-type: none"> • MEMS particle acceleration and rotation (1 spot) • DCP (3 spots) • Pressure plate (1 spot) • TDR (3 spots) • SSG (8 spots) • Sand cone density(2 spots)
	0.43 m (17 in)	<ul style="list-style-type: none"> • MEMS particle acceleration and rotation (1 spot) • DCP (3 spots) • Pressure plate (1 spot) • TDR (3 spots) • SSG (13 spots) • Sand cone density (2 spots)
	0.61 m (24 in)	<ul style="list-style-type: none"> • MEMS particle acceleration and rotation (1 spot) • DCP (1 spot) • Pressure plate (1 spot) • TDR (4 spots) • SSG (9 spots) • Nuclear density gauge (1 spot)
Rubber-tired Roller (Wheel dozer)	0.20-0.28 m (8-11 in)	<ul style="list-style-type: none"> • MEMS particle acceleration and rotation (2 spots) • DCP (4 spots) • Pressure plate (1 spot) • TDR (7 spots) • SSG (11 spots) • Sand cone density (2 spots)
	0.51 m (20 in)	<ul style="list-style-type: none"> • MEMS particle acceleration and rotation (1 spot) • DCP (3 spots) • Pressure plate (1 spot) • TDR (3 spots) • SSG (4 spots) • Sand cone density (2 spots)
Padfoot vibratory roller	0.25-0.41 m (10-16 in)	<ul style="list-style-type: none"> • MEMS particle acceleration and rotation (2 spots) • DCP (6 spots) • Pressure plate (1 spot) • TDR (8 spots) • SSG (8 spots) • Sand cone density (3 spots)
	0.51 m (20 in)	<ul style="list-style-type: none"> • MEMS particle acceleration and rotation (1 spot) • DCP (1 spot) • Pressure plate (1 spot) • TDR (3 spots) • SSG (3 spots) • Nuclear density gauge (1 spot)
Scraper	0.61 m (24 in)	<ul style="list-style-type: none"> • MEMS particle acceleration and rotation (1 spot) • DCP (3 spots) • Pressure plate (1 spot) • TDR (3 spots) • SSG (8 spots) • Nuclear density gauge (1 spot)

Table 4.5: Testing program: coarse-grained soil SM (natural water content - Junction City Site).

Compactor	Lift thickness	Measured parameters
Smooth-drum vibratory roller	0.20 m (8 in)	<ul style="list-style-type: none"> • MEMS particle acceleration and rotation (2 spots) • DCP (1 spot) • Pressure plate (1 spot) • TDR (8 spots) • SSG (6 spots) • Sand cone density (1 spot)
	0.33 m (13 in)	<ul style="list-style-type: none"> • MEMS particle acceleration and rotation (2 spots) • DCP (1 spot) • Pressure plate (1 spot) • TDR (9 spots) • SSG (6 spots) • Sand cone density (2 spots)
	0.61 m (24 in)	<ul style="list-style-type: none"> • MEMS particle acceleration and rotation (2 spots) • DCP (1 spot) • Pressure plate (1 spot) • TDR (10 spots) • SSG (10 spots) • Sand cone density (3 spots)
Rubber-tired Roller (Wheel dozer)	0.20 m (8 in)	<ul style="list-style-type: none"> • MEMS particle acceleration and rotation (2 spots) • DCP (1 spot) • Pressure plate (1 spot) • TDR (6 spots) • SSG (8 spots) • Sand cone density (1 spot)
	0.33 m (13 in)	<ul style="list-style-type: none"> • MEMS particle acceleration and rotation (2 spots) • DCP (1 spot) • Pressure plate (1 spot) • TDR (6 spots) • SSG (8 spots) • Sand cone density (2 spots)
	0.51 m (20 in)	<ul style="list-style-type: none"> • MEMS particle acceleration and rotation (2 spots) • DCP (1 spot) • Pressure plate (1 spot) • TDR (8 spots) • SSG (8 spots) • Sand cone density (3 spots)
Scraper	0.33 m (13 in)	<ul style="list-style-type: none"> • MEMS particle acceleration and rotation (2 spots) • DCP (1 spot) • Pressure plate (1 spot) • TDR (8 spots) • SSG (8 spots) • Sand cone density (2 spots)
	0.58 m (23 in)	<ul style="list-style-type: none"> • MEMS particle acceleration and rotation (2 spots) • DCP (3 spots) • Pressure plate (1 spot) • TDR (8 spots) • SSG (8 spots) • Sand cone density (2 spots)

Table 4.6: Testing program: coarse-grained soil SM (wet condition - Junction City Site).

Compactor	Lift thickness	Measured parameters
Smooth-drum vibratory roller	0.20 m (8 in)	<ul style="list-style-type: none"> • MEMS particle acceleration and rotation (2 spots) • DCP (1 spot) • Pressure plate (1 spot) • TDR (8 spots) • SSG (8 spots) • Sand cone density (1 spot)
	0.33 m (13 in)	<ul style="list-style-type: none"> • MEMS particle acceleration and rotation (2 spots) • DCP (1 spot) • Pressure plate (1 spot) • TDR (8 spots) • SSG (8 spots) • Sand cone density (1 spot)
	0.58 m (23 in)	<ul style="list-style-type: none"> • MEMS particle acceleration and rotation (2 spots) • DCP (1 spot) • Pressure plate (1 spot) • TDR (8 spots) • SSG (8 spots) • Sand cone density (2 spots)
Rubber-tired Roller (Wheel dozer)	0.33 m (13 in)	<ul style="list-style-type: none"> • MEMS particle acceleration and rotation (2 spots) • DCP (1 spot) • Pressure plate (1 spot) • TDR (8 spots) • SSG (8 spots) • Sand cone density (2 spots)
	0.58 m (23 in)	<ul style="list-style-type: none"> • MEMS particle acceleration and rotation (2 spots) • DCP (1 spot) • Pressure plate (1 spot) • TDR (8 spots) • SSG (8 spots) • Sand cone density (2 spots)

4.3.3 Test Results and Data Interpretation

The presentation of test results is organized in two parts. The first part documents the results of monitoring soil responses during compaction operations (e.g., pressure plate responses and MEMS vibration and displacement monitoring). The second part discusses the results from tests that evaluated conditions of the soil after compaction operations were completed (e.g., stiffness gauge, P-wave propagation, dynamic cone penetration, time domain reflectometry, sand cone and nuclear density gauge). These results are then

analyzed to evaluate soil responses and the influence of different lift thicknesses and compaction equipment on the quality of compacted layers.

Pressure Plate Responses

The hydraulic pressure plate was installed at the bottom of lifts to monitor maximum pressure responses as compaction and earthmoving equipment passed over the testing section (Figure 4.11). Figure 4.12 shows the results of maximum pressure responses. Even though the data are noisy, they provide insight about the interaction between the compaction equipment and lift thickness. On one hand, the results show that the maximum pressure for the vibratory roller remains approximately same regardless of the tested soil. The maximum pressure also shows a decrease with increasing lift thickness. On the other hand, the maximum vertical pressure measured under the rubber-tired roller and the rubber-tired scraper shows a wide range of values that depends both on soil and equipment types. (The scraper is the heaviest of compaction equipment used in the study and it consistently yields the highest vertical pressures.) Some observations of these results are explained by the misalignment between the location of the wheel path of the rubber-tired compactors and scraper and the location of the pressure plate. When the compactor missed the exact location of the pressure plate, pressure responses are lowered. This implies that the importance of the area coverage in the compacted plane using tire-based soil compactors.

Figure 4.12: Maximum pressure responses at the bottom of soil layers by lift thickness and compaction equipment (Junction City Site): (a) coarse-grained soil SP; (b) natural moisture coarse-grained soil SM; and (c) wet coarse-grained soil SM.

Shear-induced Rotation Measurements using MEMS Accelerometers

The internal soil distortion caused by the action of the compaction equipment was monitored with MEMS accelerometers. MEMS accelerometers capture the misalignment between the sensing axis and the acceleration of gravity. That is, the angle with respect to the acceleration of gravity is calculated by measuring the MEMS accelerometer voltage values before and after the compactor passes over the testing lift (Schuettpelz et al. 2009a). Large shear-induced rotation angles indicate the larger soil distortion and greater densification action on the lift. Therefore, the rotation monitoring provides an estimation of the compaction effectiveness.

Five two-dimensional Analog Devices ADXL322™ MEMS accelerometers were installed at each section to monitor x and y shear-induced rotations during compaction

(Figure 4.11). The assessment of shear-induced rotations is used in the evaluation of the compaction effectiveness versus depth; thus, the reduction of the rotation angle versus depth indicates the increase of the soil stiffness and the reduction of the compaction action on tested lifts. The collected rotation data are quite noisy for mainly three reasons. The first reason is that the distortion and shear deformations produced by compaction and earthmoving equipment in loose soil are not uniform; that is, the density and stiffness are not homogeneous and in some cases large boulders interfere with the soil response. The second reason is that compaction or earthmoving equipment pass the test section in the different direction (i.e., forward moving or backward moving). The third reason is that the rubber-tired roller, padfoot roller, and scraper do not necessarily compact the soil along the same path creating further heterogeneity in rotation results. These limitations should be considered when analyzing the data.

Figures 4.13 through 4.15 show the shear-induced rotation profiles measured with MEMS accelerometers. All data with different lifts for the same soil and the compactor were combined for evaluating the influencing depth of compaction operations. The rotation angles in the coarse-grained SP soil are all very small except first two passes of the rubber-tired roller. Mostly, all measurements are less than 5 degrees from the surface to 0.30-m (12-in) depth (Figure 4.13). However, the measured rotations at natural moisture in the coarse-grained SM soil are much larger than those of SP soil. Rotations from 10 to 20 degrees are detected from the surface to about 0.30-m (12-in) depth (Figure 4.14). Rotations in the wet SM soil are presented in Figure 4.15. These rotations are shallower than those of the SM soil at natural moisture (around 0.20-m – 8-in depth) with

the smooth-drum vibratory roller (Figure 4.15). All rotations decrease with increasing the number of passes. After about 4 passes, the measured rotations are very small.

Figure 4.13: Rotation angles during compaction in the coarse-grained SP soil during compaction (Junction City Site) with (a) smooth-drum vibratory roller; (b) rubber-tired roller; (c) padfoot roller; and (d) scraper.

Figure 4.14: Rotation angle during compaction in the coarse-grained SM soil at natural moisture content (Junction City Site) with: (a) smooth-drum vibratory roller; (b) rubber-tired roller; and (c) scraper.

Figure 4.15: Rotation angle during compaction of the coarse-grained SM soils at wet condition (Junction City Site) with: (a) smooth-drum vibratory roller; (b) rubber-tired roller.

Shear-induced Displacements Measurements using MEMS Accelerometers

Measured electrical voltages from MEMS accelerometers can be converted into the gravity acceleration scales (cm/s^2) using the sensor sensitivity. After single integrating and double integrating gravity accelerations, velocity and displacement histories of sensors are obtained, respectively. To minimize numerical distortions during the numerical integrations, a baseline correction is required to estimate the velocity and displacement histories:

$$v(t) = v_0 + \int_0^t a(\tau) d\tau \quad (4.5)$$

$$x(t) = x_0 + \int_0^t v(\tau) d\tau = x_0 + v_0 t + \int_0^t \int_0^t a(\tau) d\tau dt \quad (4.6)$$

where $a(\tau)$ is acceleration at time τ , $v(t)$ is velocity at t , $x(t)$ is displacement at t , v_0 and x_0 are initial velocity and displacement as zero. Figure 4.16 illustrates the examples of accelerations and velocities versus depths.

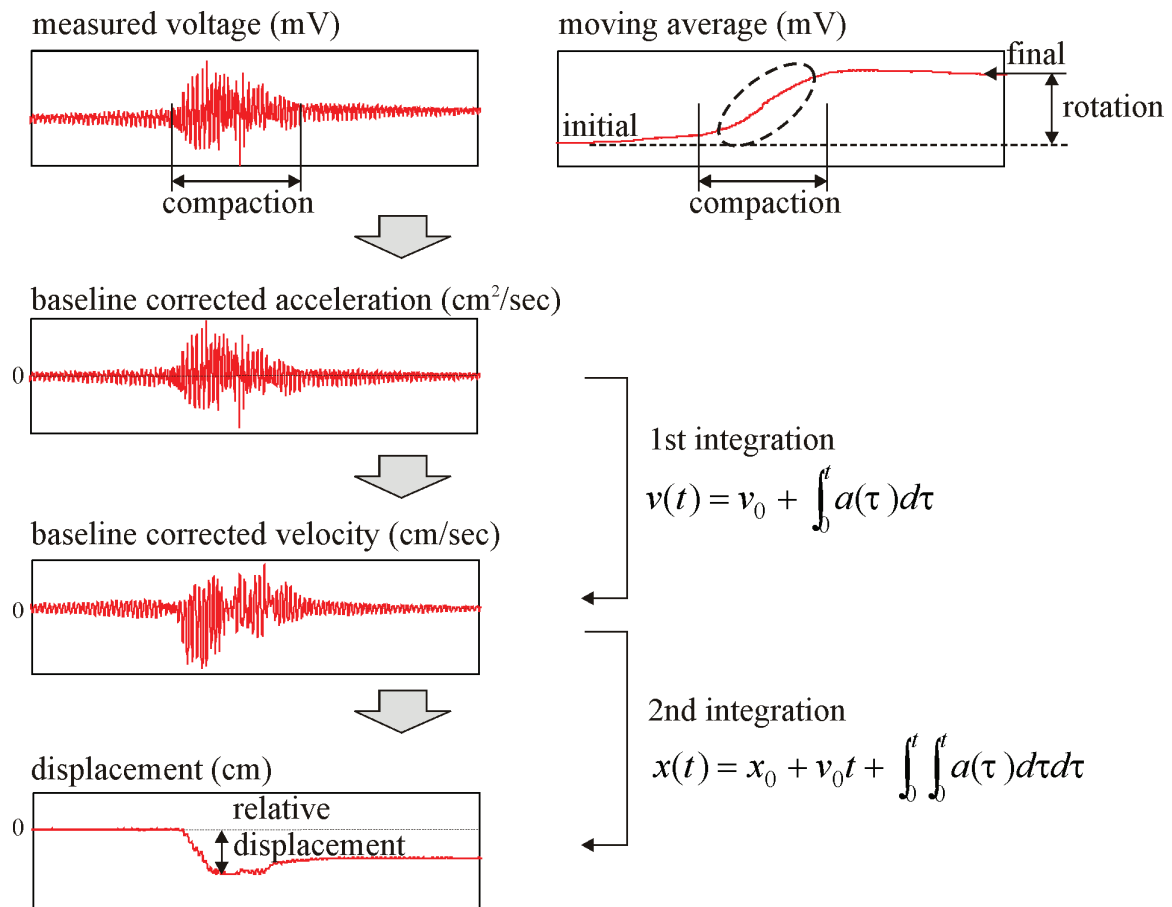


Figure 4.15: MEMS acceleration data interpretation procedures – conversion to displacement of sensor.

The amplitude of vibratory motions at a specific distance is dependent on the magnitude of energy at the source. These simple expressions can be correlated with the distance from the applied energy source (Figures 4.16 and 4.17). The degree of perturbation in the SM soil is higher than that of the SP soils. Then, the SP soil layers may have under-

compacted region at the bottom of thick lifts. All data profiles including peak acceleration, peak velocity, and relative displacement of both soils indicate that the compaction effective depth up to about 40 cm (16 in.) depth as shown in Figure 4.16 and 4.17.

Figure 4.16: Peak particle acceleration, velocity, relative displacement in the horizontal and vertical axes for the SP soil (Junction City Site).

Figure 4.17: Peak particle acceleration, velocity, relative displacement in the horizontal and vertical axes for the SM soils (Junction City Site).

Soil Stiffness using SSG and P-wave Propagation

The stiffness of compacted soils was measured on the surface with the soil stiffness gauge (SSG) measurement or within the lift by interpreting P-wave propagation from MEMS accelerometer data (Figure 4.18). The SSG stiffness reflects on the surface modulus and the embedded MEMS in the bottom of soil layers can provide the stiffness of the lower part of lifts. Figure 4.19 presents the correlation between the SSG modulus and the P-wave velocity. It can be seen that the P-wave velocity increases with the increase of the SSG modulus. Figure 4.20 compares the elastic modulus obtained from the SSG and P-wave propagation. Data points include all different soils and compactors and are divided by lift thickness.

Less than 0.33-m (13-in) thick lifts are represented with filled diamonds while more than 0.41-m (16-in) thick lifts are represented with open circles. The values by each technique are correlated by a linear relationship; however, some data points seem to have achieved the large stiffness on the surface as indicated by the SSG data but the low stiffness at depth as determined from P-wave propagation. These data, marked by the dashed circle in Figure 4.20 and corresponding to fine-grained soils compacted by the smooth-drum vibratory roller, seem to indicate that thick lifts are not properly compacted. This is indicated as undercompacted on the figure. More details are presented in Kim et al. (2014).

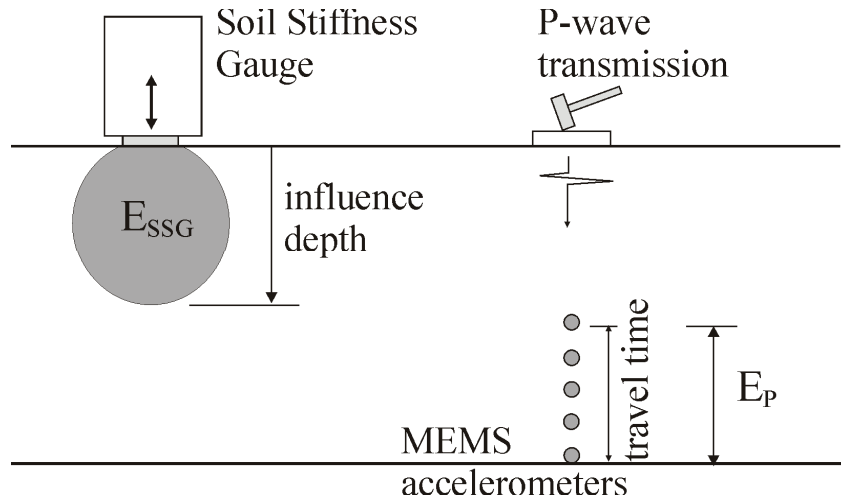


Figure 4.18: Setups for stiffness measurements using the soil stiffness gauge and the interpretation of P-wave propagation.

Figure 4.19: Relationship between SSG modulus vs. P-wave velocity for the soils at the Junction City Site.

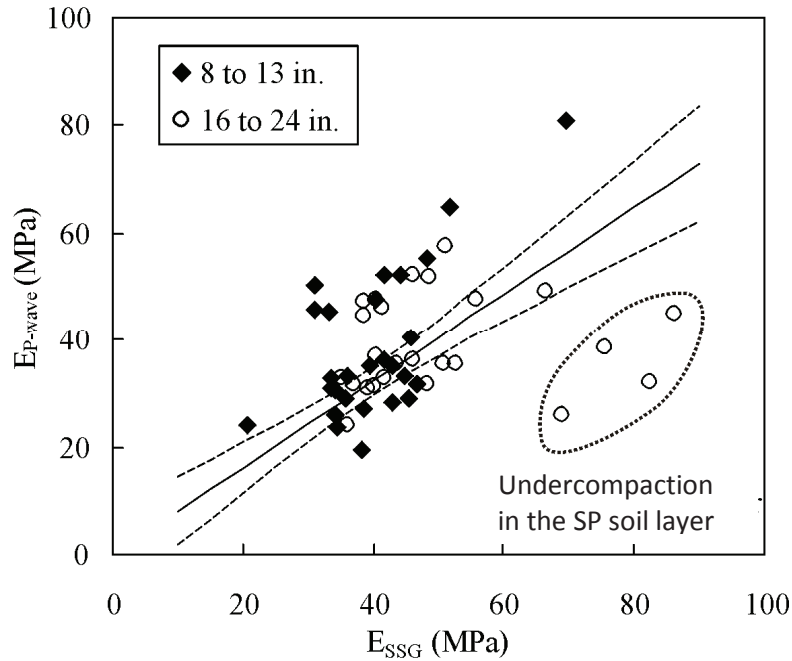


Figure 4.20: Comparison of SSG modulus against P-wave propagation modulus for the compacted soil at the Junction City Site.

Shear Resistance – DPI Profile

Figure 4.21 shows the DCP index profile obtained for fine-grained soils using different compactors. The top 20 cm (8 in) of compacted soils shows constant DCP index values. However, the data in thick lifts tend to increase with the increase of the depth deeper than 20-cm (8-in) depth. These results appear to imply a heterogeneous compaction distribution region across the lift because the shear resistance decreases with increasing depth. Figure 4.22 and 4.23 show the DCP index profiles for natural and wet moisture for the SM soil. DCP index values linearly decrease up to 20-in depth. This observation indicates that the quality of compaction is quite homogeneous without under-compaction regions at the bottom of thick layers, the higher shear strength is expected with depth as

the effective stress increases with depth. That is, the overburden pressure is only factor of decreasing the DCP index of coarse-grained soils in depth increasing.

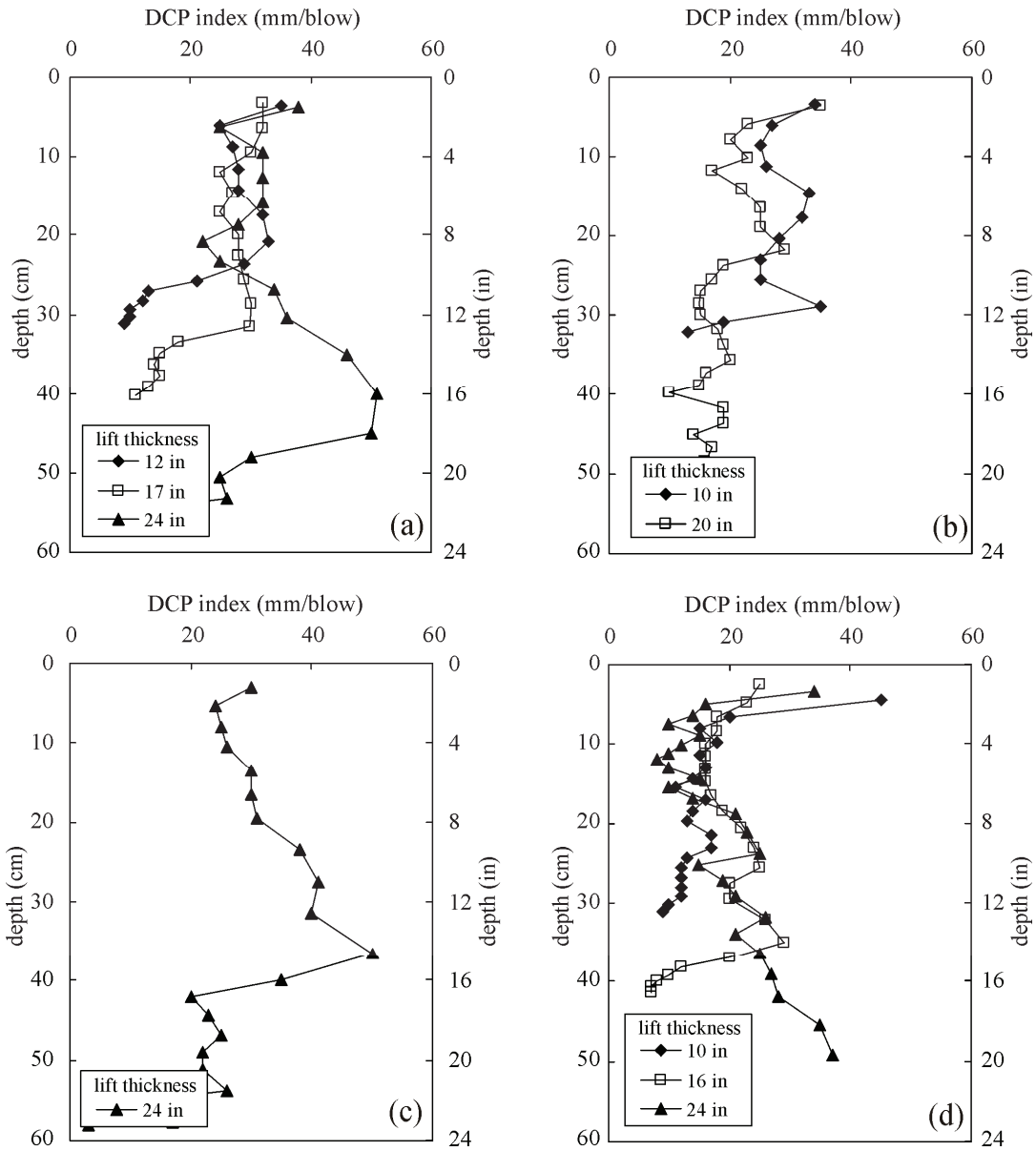


Figure 4.21: DCP index profile for the SP soil compacted (Junction City Site) with: (a) smooth-drum vibratory roller; (b) rubber-tired roller; (c) padfoot roller; and (d) scraper.

Figure 4.22: DCP index profile for the SM soil at natural moisture compacted (Junction City Site) with: (a) smooth-drum vibratory roller; (b) rubber-tired roller; and (c) scraper.

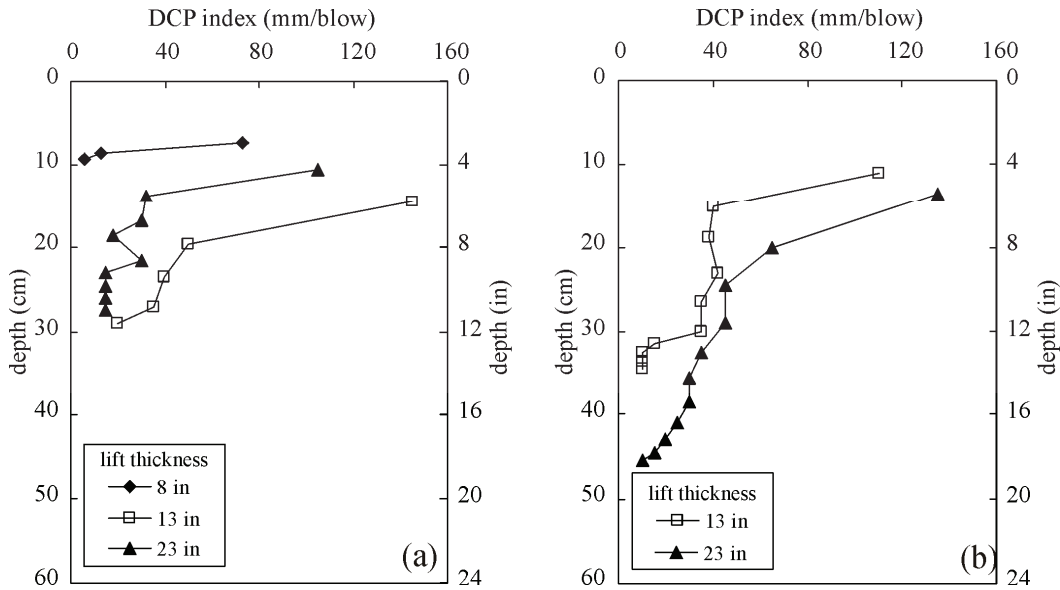


Figure 4.23: DCP index profile for SM soils at wet moisture compacted (Junction City Site) with: (a) smooth-drum vibratory roller; (b) rubber-tired roller.

Correlations of Volumetric and Gravimetric Water Contents

The time domain reflectometry (TDR) has been used to estimate the volumetric water content. Topp et al. (1980) proposed a universal relationship between the volumetric water content and the apparent dielectric constant. To correlate the measured volumetric water content to the gravimetric water, volumetric water contents need to be converted (Yu and Drnevich 2004). The gravimetric water content is related to the volumetric water content by the dry density of soil (ρ_d) and the density of pore water (ρ_w):

$$\theta = \frac{V_w}{V} = \frac{\rho_d}{\rho_w} w \quad (4.7)$$

where θ is the volumetric water content, V_w is the volume of water, V is the total volume, and w is the gravimetric water content. That is, the volumetric water content is a measure of both gravimetric water content and dry unit weight.

Figure 4.24 show the relationship between measured volumetric and gravimetric water contents. As the volumetric water content increases, the gravimetric water content increases as well. However, this relationship is not identical among the soils. There is relative little variations within the measured gravimetric water content for the two soil types tested at this site. However, there is a large variation in the measured volumetric water content due to different types of compaction equipment used in this study. This observation is directly related to the final dry unit weight achieved by the soil.



Figure 4.24: Relationship between volumetric water content and gravimetric water content for the soils at the Junction City Site.

Relative Compaction: Density & Water Content Measurements

The sand cone method and nuclear density gauge are widely used techniques for the evaluation of achieved compaction. Measured values are typically presented as relative compaction:

$$RC = \frac{\gamma_{d \text{ field}}}{\gamma_{d \text{ max}}} \times 100(\%) \quad (4.8)$$

where $\gamma_{d \text{ field}}$ is the measured field dry unit weight and $\gamma_{d \text{ max}}$ is the maximum dry unit weight determined by the Proctor test. The typical values of relative compaction range from 90 to 105%. Figures 4.25 and 4.26 present relative compaction profiles obtained using the nuclear density gauge and the sand cone method. The relative compaction data in fine-grained soils show stable compaction profiles with depth for the smooth vibratory roller. However, relative density profiles show a sudden drop in the relative compaction close to the surface for the padfoot compaction and the scraper. These data may be explained by the interaction of the equipment with the soil. Both the padfoot compactor and the scraper tend to greatly disturb the soil close to the surface. They both apply very large pressures in small areas. These large pressures bring the surface soil to failure at the surface preventing homogeneous compaction.

Figure 4.26 shows relative compaction profiles obtained with the sand cone method in SM soil. The data show that that compaction energy is transferred up to 30-cm (12-in) depth. However, the results also indicate that the smooth-drum vibratory roller (a light weight compactor) may not be suitable for wet coarse-grained soils.

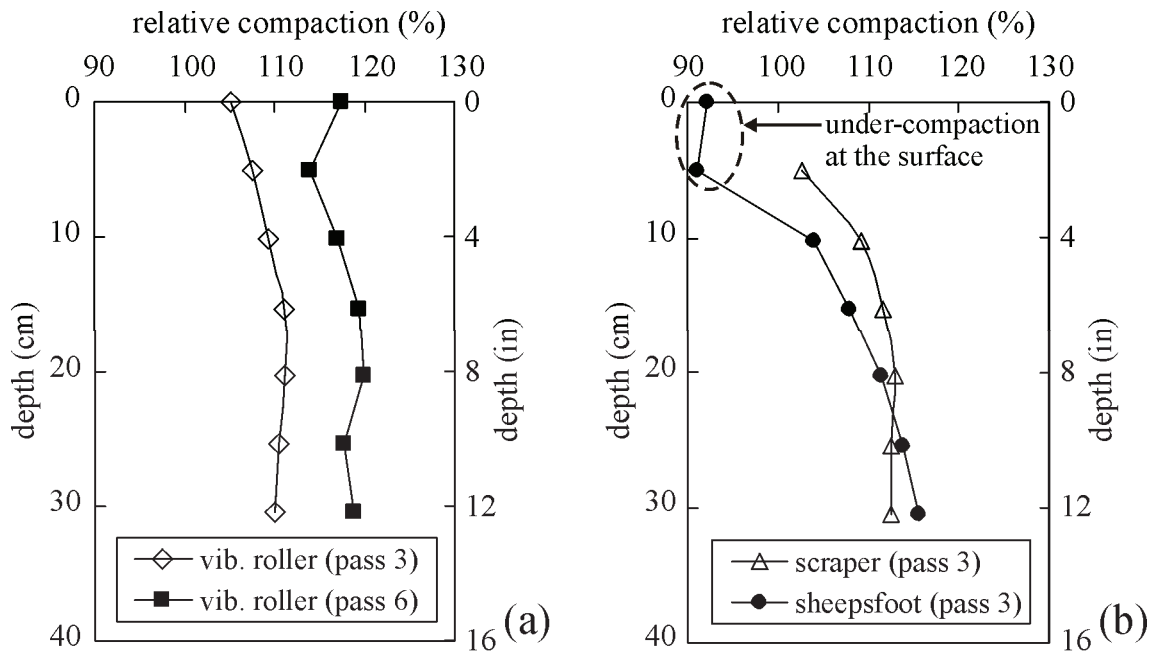


Figure 4.25: Relative compaction results for the SM soils using nuclear density gauge (Junction City Site): (a) smooth-drum vibratory roller; (b) scraper and padfoot roller.

Figure 4.26: Relative compaction results using the sand cone method Junction City Site: (a) natural moisture SM soils; (b) wet moisture SM soils.

4.4 Fine-Grained Soil: Town of Sylvania Field Testing

As presented in Section 3.1, the selected site for the testing of fine-grained soils is located in the Town of Sylvania, just west of Racine in South East Wisconsin. The site was a construction zone where a new Frontage Road was being built (Figure 3.2). The evaluation of compaction operations was performed on a testing site specially prepared for this field study (Figure 4.27). In this site, the WisDOT contractor dug out a trench where different lift thickness of fine grained soils at different water contents were placed and compacted with different compaction equipment.



Figure 4.27: View of the testing site in the town of Sylvania west of Interstate 94 near Racine, WI. At the site, the WisDOT contractor dug out a trench where the different soil lifts thicknesses were tested.

4.4.1 Compaction and Earthmoving Equipment

The compaction and earthmoving equipment used for at this site were selected mainly based on the soil type and equipment provided by the WisDOT contractor. To evaluate the effect of the different compaction energy levels, the test section was compacted using two types of Dynapac equipment: padfoot rollers Model CT262 and Model CA251PD (Figure 4.28). The specification of the compaction equipment along is summarized in Table 4.3.



Figure 4.28: Field soil compactors used during field testing at the Town of Sylvania site.

Table 4.3: Operating weight of compaction and earthmoving equipment (Town of Sylvania site - Sources: www.ritchiespecs.com; www.equipmentwatch.com)

Compactor Type	Model Number	Operating Mass of Equipment	Tire Type or Drum Dimension
Large Padfoot Roller	Dynapac CT262	21600 kg (47619.9 lbs)	Drum width: 4.41 m (173.6 in) – Padfoot
Small Padfoot Roller - Dynamic	Dynapac CA251PD	11177 kg (24590 lbs)	Drum width: 2.13 m (84 in) – Padfoot

4.4.2 Field Testing Program

During the compaction study at the Town of Sylvania site, the effect of different types of compactors, lift thicknesses, and moisture content were monitored with MEMS accelerations, pressure gauge, dynamic cone penetration (DCP), soil stiffness gauge (SSG), and nuclear density gauge (NDG). Table 4.6 summarizes the testing program. The testing program included different compactors, lift thickness of soil layers, and the conducted measurements. The measurement techniques for evaluating the water content, compaction effectiveness and compactive energy versus depth are complemented with traditional surface measurements to evaluate the quality of compaction operations. These traditional measurement techniques include sand cone, nuclear density gauge (NDG), soil stiffness gauge (SSG), and dynamic cone penetration (DCP). Figure 4.29 sketches the measurement methodology used in to assess the response of fine-grained soils.

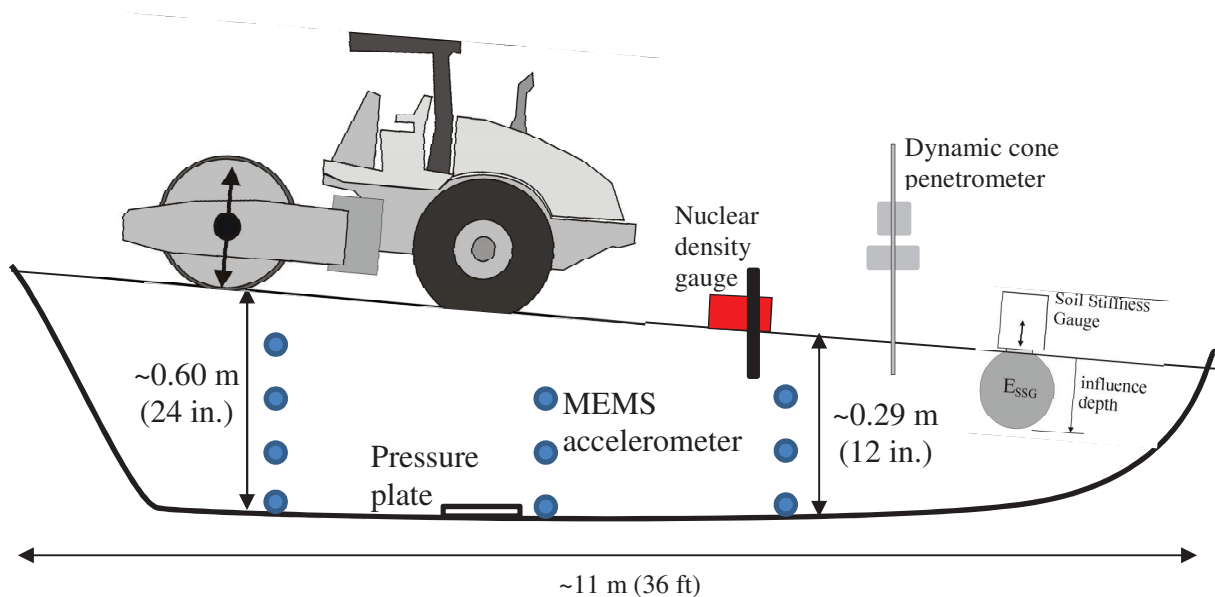


Figure 4.29: Instrumented soil layer at the Town of Sylvania site. Different lift thicknesses were tested by gradually varying the depth of the soil in the testing trench. Details of the location of sensor in the lifts are presented in the appendices.

Table 4.4: Testing program: fine-grained soil (all moisture contents - Town of Sylvania site).

Compactor	Approx. lift thickness	Measured parameters
Padfoot vibratory roller	0.30 m (12 in)	<ul style="list-style-type: none"> • 3 MEMS particle acceleration and rotation (1 spot) • DCP (1 spot) • Pressure plate (1 spot) • SSG (1 spots) • Nuclear density gauge (2 spots)
	0.43 m (18 in)	<ul style="list-style-type: none"> • 3 MEMS particle acceleration and rotation (1 spot) • DCP (1 spot) • Pressure plate (1 spot) • SSG (1 spots) • Nuclear density gauge (2 spots)
	0.61 m (24 in)	<ul style="list-style-type: none"> • 3 MEMS particle acceleration and rotation (1 spot) • DCP (1 spot) • Pressure plate (1 spot) • SSG (1 spots) • Nuclear density gauge (2 spots)
Padfoot roller (no vibration)	0.30 m (12 in)	<ul style="list-style-type: none"> • 3 MEMS particle acceleration and rotation (1 spot) • DCP (1 spot) • Pressure plate (1 spot) • SSG (1 spots) • Nuclear density gauge (2 spots)
	0.43 m (18 in)	<ul style="list-style-type: none"> • 3 MEMS particle acceleration and rotation (1 spot) • DCP (1 spot) • Pressure plate (1 spot) • SSG (1 spots) • Nuclear density gauge (2 spots)
	0.61 m (24 in)	<ul style="list-style-type: none"> • 3 MEMS particle acceleration and rotation (1 spot) • DCP (1 spot) • Pressure plate (1 spot) • SSG (1 spots) • Nuclear density gauge (2 spots)

4.4.3 Test Results and Data Interpretation

The presentation of test results is organized in two parts. The first part documents the results of monitoring soil responses during compaction operations (e.g., pressure plate responses and MEMS vibration). The second part of this section discusses the results from tests that evaluated conditions of the soil after compaction operations were completed (i.e., stiffness gauge; dynamic cone penetration, and nuclear density gauge).

These results are then interpreted to assess soil responses and the influence of different lift thicknesses and compaction equipment on the quality of compacted layers.

Pressure Plate Responses

The hydraulic pressure plate was installed at the bottom of the ~0.45 cm (18 in.) lift to monitor the maximum pressure at the bottom as the compactor passed over the testing section (Figure 4.29). On one hand, the results show that the maximum pressure for the vibratory roller remains approximately same regardless of the moisture content of the soils and the compaction equipment however there are two distinct trends: in the case of the large (static) padfoot roller there is a tendency of the pressure to increase with moisture content and number of passes. These trends are much less obvious in the case of the small (dynamic) padfoot roller. In spite of these differences and the weight of the compactor, the average pressure of the two compactors is almost the same.

These observations can be better explained by the mass per unit length of the roller than by the weight of the compactors themselves. That is, the mass per unit length of the roller is 4900 kg/m in the large padfoot roller and 5250 kg/m in the small padfoot roller. The effect of the dynamic vibration in the small padfoot roller is not documented by the maximum response of the pressure plate even though the pressure transducer in pressure plate sensed the vibration as shown in Figure 4.31.

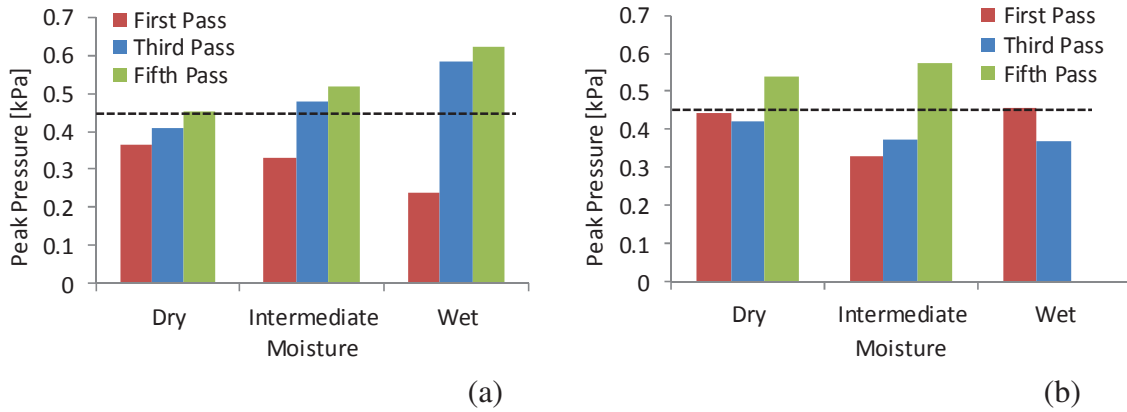


Figure 4.30: Maximum pressure responses at the bottom of the medium thick lift as the number of passes and moisture increases (Town of Sylvania site): (a) Large Padfoot Roller and (b) Small Padfoot Roller.

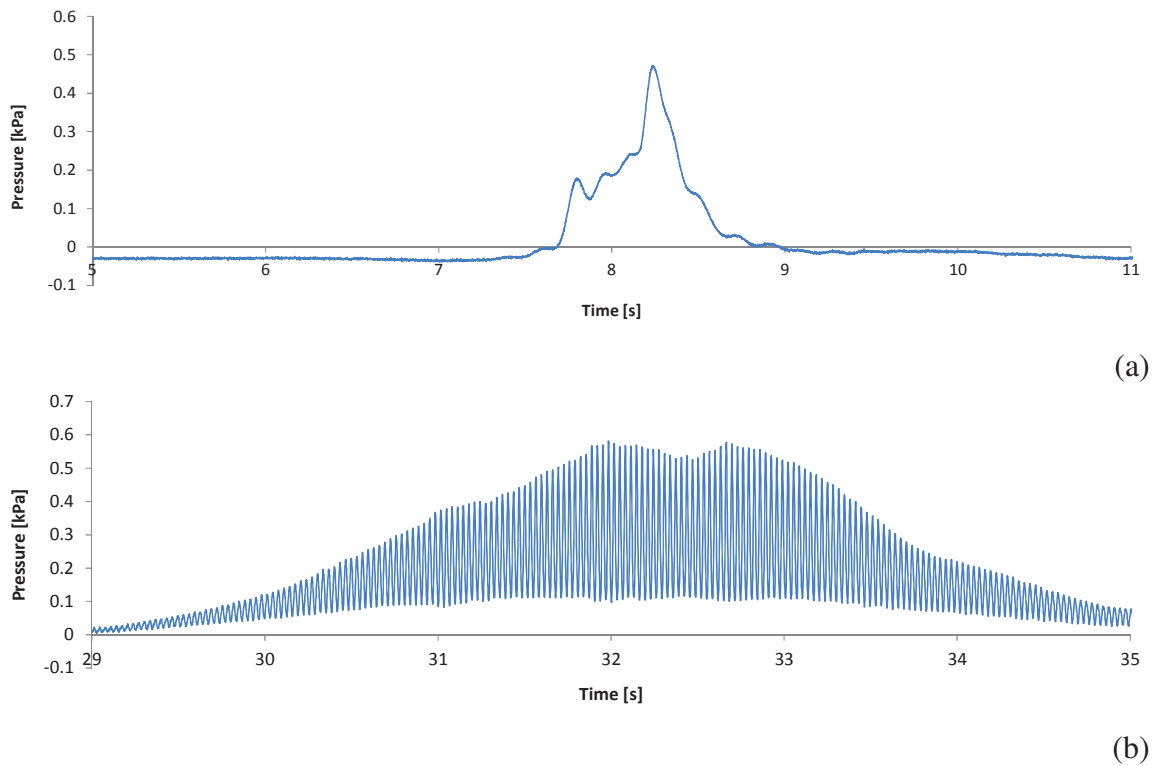


Figure 4.31: Responses of the pressure plate under: (a) the large (static) padfoot compactor and (b) the small (dynamic) padfoot compactor (Town of Sylvania site).

Shear-induced Rotation Measurements using MEMS Accelerometers

The internal soil movement caused by the action of the compactors was monitored with MEMS accelerometers. The intent of these measurements was to capture the soil distortion needed for the densification process. That is, the internal distortion measured with the MEMS accelerometers provides an estimation of the compaction effectiveness.

Ten two-dimensional MEMS accelerometers were installed at each section to monitor x and y shear-induced rotations during compaction (Figure 4.11). The assessment of shear-induced rotations is used in the evaluation of the compaction effectiveness versus depth; thus, the reduction of the rotation angle versus depth indicates the increase of the soil stiffness and the reduction of the compaction action on tested lifts. Even though the rotation data are quite noisy, they yield some important information. The MEMS accelerometer response capture both rotation and displacement of the soils caused by the compaction and earthmoving equipment in loose soils. These effects are not uniform, mainly for two reasons. First, the effect of the compactor: the padfoot roller does not necessarily compact the soil along the same paths and the relative location of the pads with respect to the position of the MEMS will control the response. Second, the soil in the lift is not uniform and it could create a distortion on the sensor response.

Even though, the results appear to show a decrease in the MEMS response with depth, the noise in the data prevents drawing definite conclusion. Figures 4.32 and 4.33 present typical results. Note the noise level in the data.

Lift Thickness:

60 cm (24 in.)

45 cm (18 in.)

30 cm (12 in.)

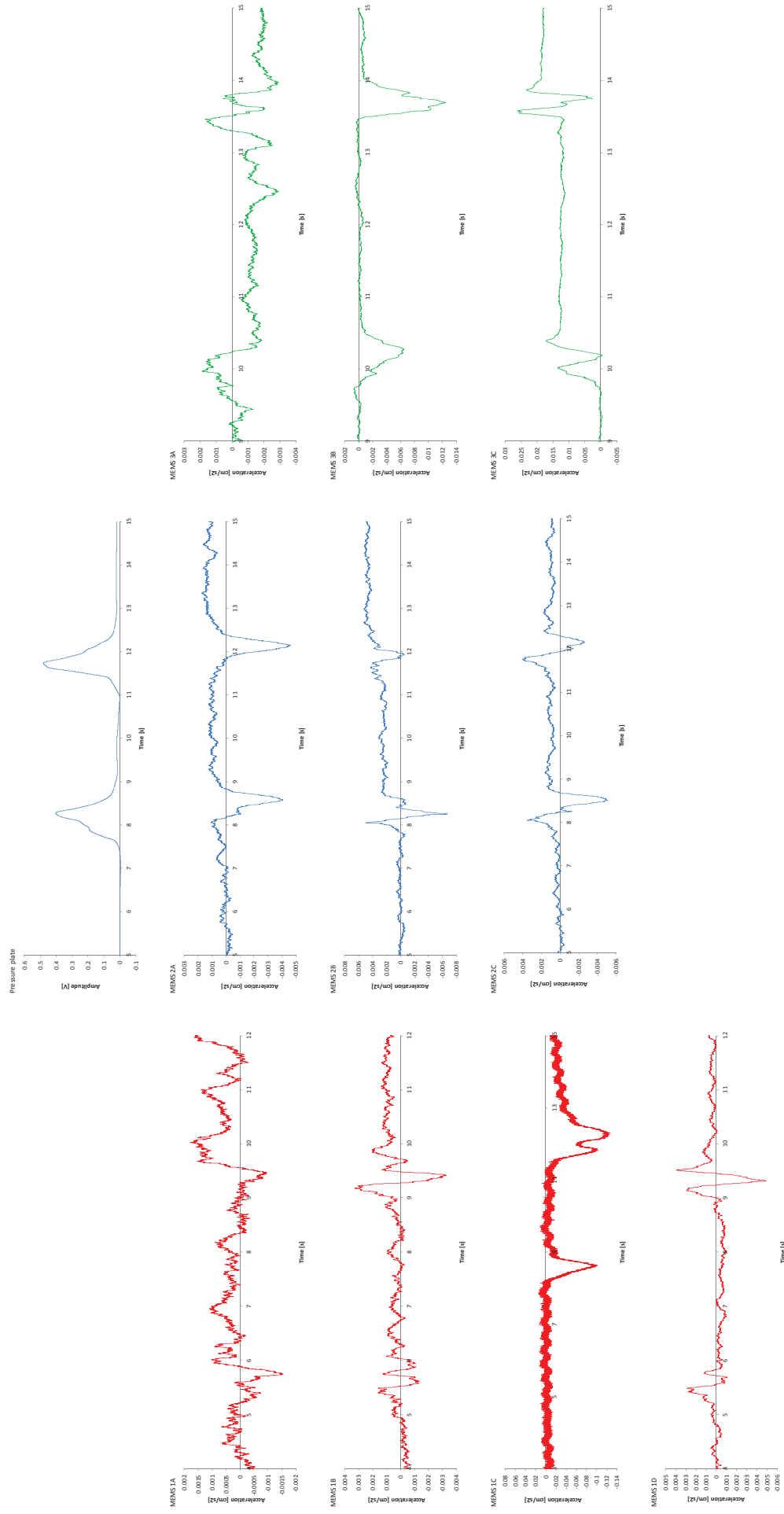


Figure 4.32: Particle acceleration response at the fifth pass at the intermediate water content for fine grained soils during compaction with the large (non-vibratory) compactor (Town of Sylvania site).

Lift Thickness:

60 cm (24 in.)

45 cm (18 in.)

30 cm (12 in.)

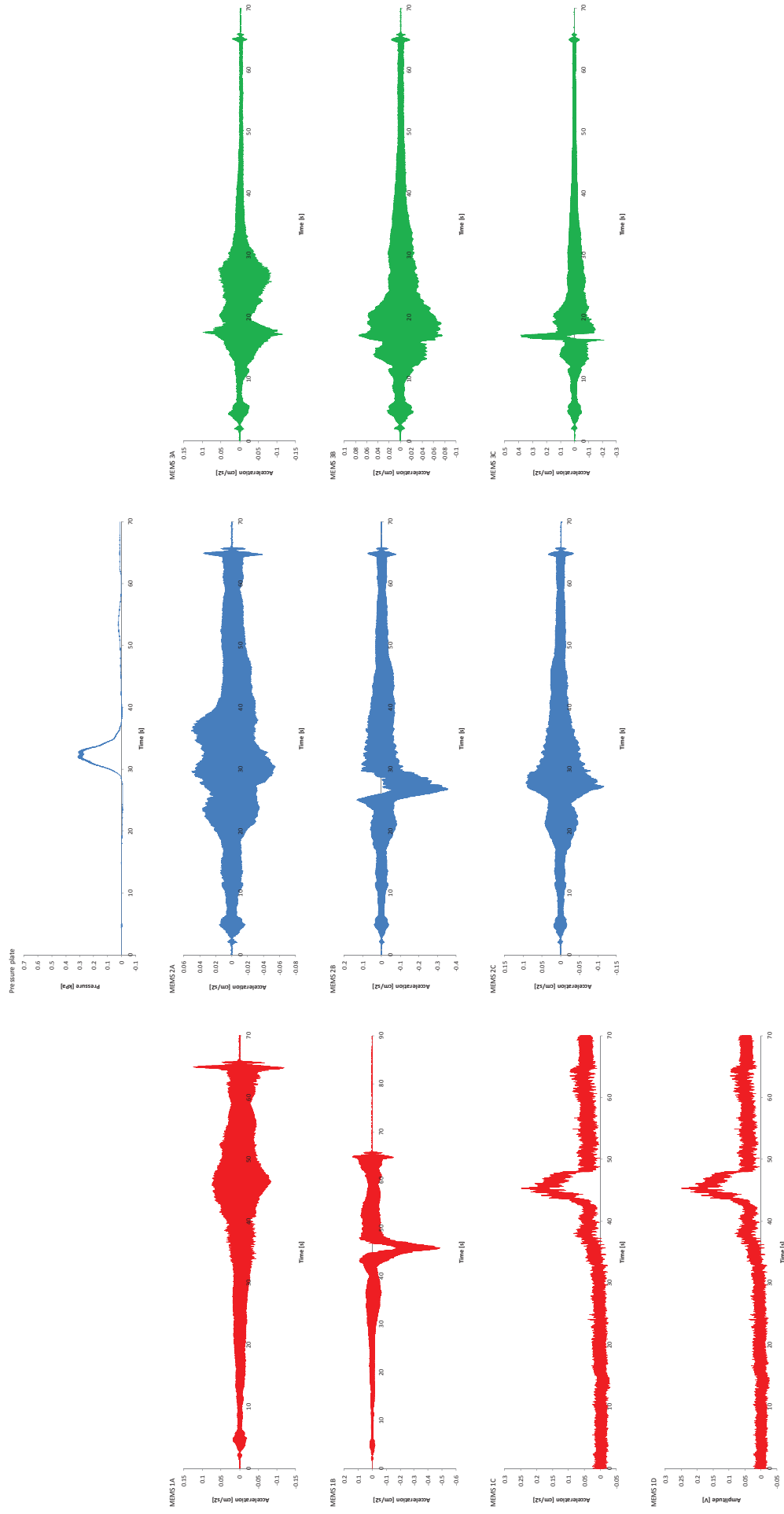


Figure 4.33: Particle acceleration response at the fifth pass at the intermediate water content for fine grained soils during compaction with the small (vibratory) compactor (Town of Sylvania site).

Unit Weight & Water Content Measurements

Figures 4.34 and 4.35 present profiles of dry unit weight and moisture content obtained using the nuclear density gauge for the tested fine-grained soils with different lift thickness and compaction equipment. Results show that in general there is modest increase in the dry unit weight with decrease in lift thickness (Location 1 to Location 3). These results are followed by moisture content measurements. Moisture content measurements do not appear to show a clear increase between test in spite of the efforts in the field by the contractor and the research team to change the water content in the different lifts. For all the different sequences, the soil was either aired or sprayed with water to change the moisture content from the natural moisture content of the soil. Furthermore, the data show that that the final dry density appears to be independent of the compaction equipment: once again is not the weight of the equipment that appear to be responsible but the mass per unit length of the drum and that the vibration of the compaction has no influence on the final compaction. The results do not show a clear tendency of the reduction of density versus depth.

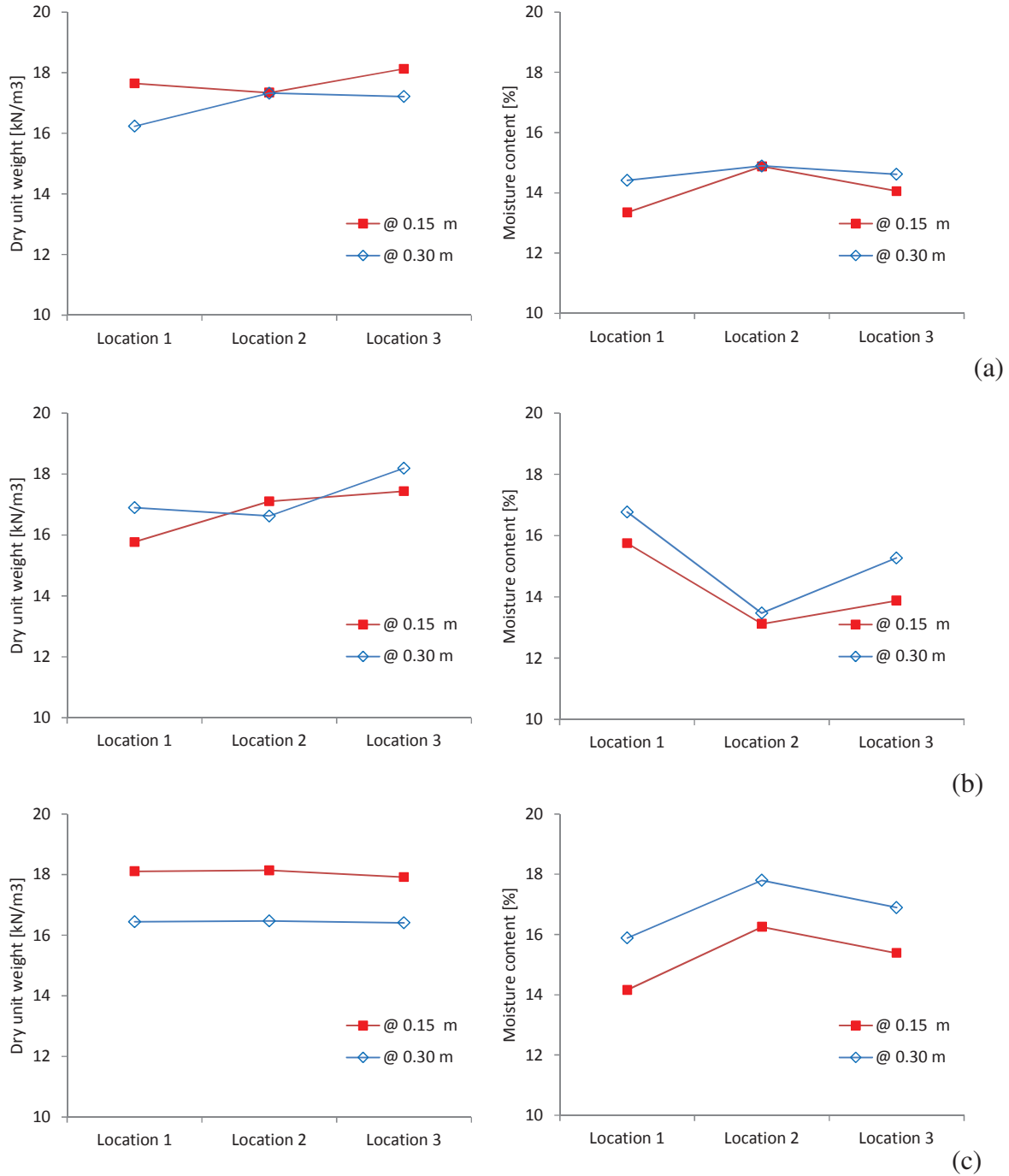


Figure 4.34: Dry density and moisture content for the large (non-vibratory) compactor (Town of Sylvania site): Mominal moisture content (a) dry of optimum; (b) around optimum; (c) wet of optimum. Note: Locations 1, 2, and 3 correspond to lift thicknesses of approximately 60 cm (24 in.), 45 cm (18 in.) and 30 cm (12 in.), respectively.

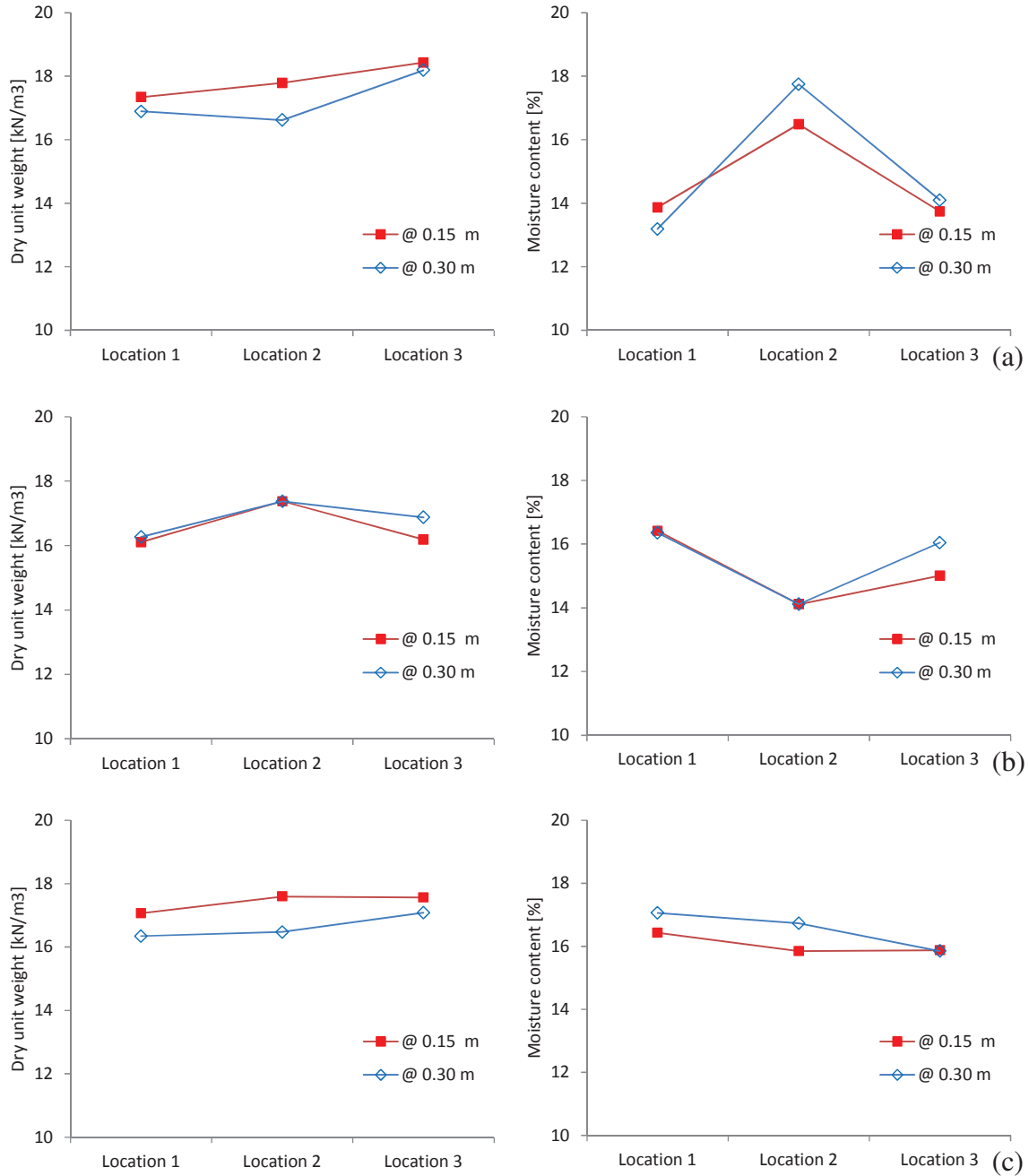
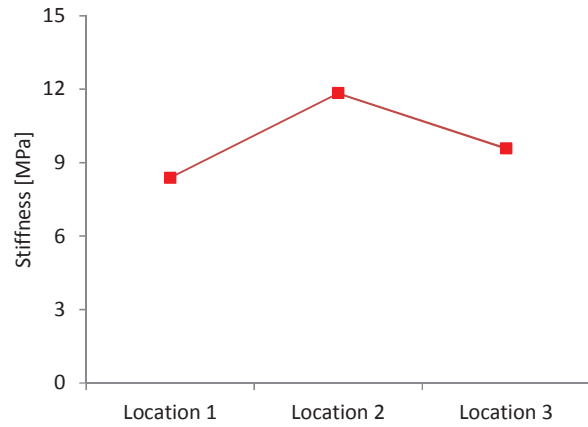


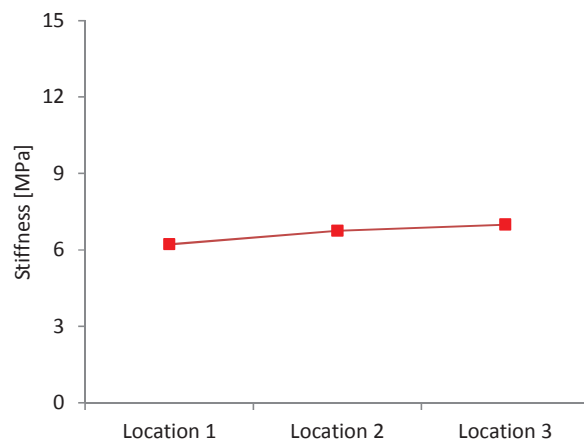
Figure 4.35: Dry density and moisture content for the small (vibratory) compactor (Town of Sylvania site): Nominal moisture content (a) dry of optimum; (b) around optimum; (c) wet of optimum. Note: Locations 1, 2, and 3 correspond to lift thicknesses of approximately 60 cm (24 in.), 45 cm (18 in.) and 30 cm (12 in.), respectively.

Soil Stiffness using the Soil Stiffness Gauge

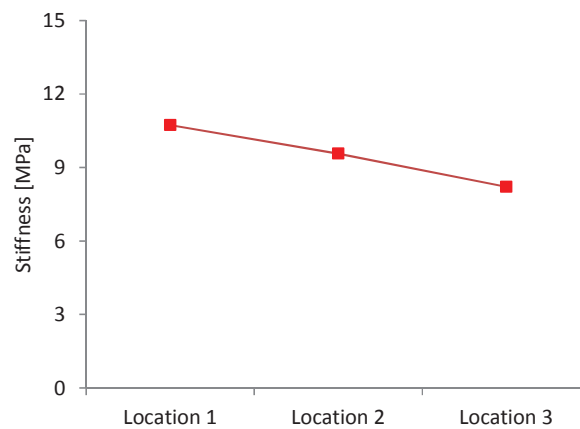
Similar to the results obtained with the nuclear density gauge, there is not a clear trend on the results of stiffness with the Soil Stiffness Gauge. The measurements do not seem to be controlled by the lift thickness, moisture content or compaction equipment. If any small trends seems to appear, it is that the stiffness increases with moisture content, those results do not appear to be meaningful as for a constant dry unit weight the soil stiffness should decrease with increasing water content because there is a decrease in matric suction (i.e., capillary forces).



(a)



(b)



(c)

Figure 4.36: SSG modulus for the large (non-vibratory) compactor (Town of Sylvania site): Nominal moisture content (a) wet of optimum; (b) around optimum; (c) wet of optimum. Note: Locations 1, 2, and 3 correspond to lift thicknesses of approximately 60 cm (24 in.), 45 cm (18 in.) and 30 cm (12 in.), respectively.

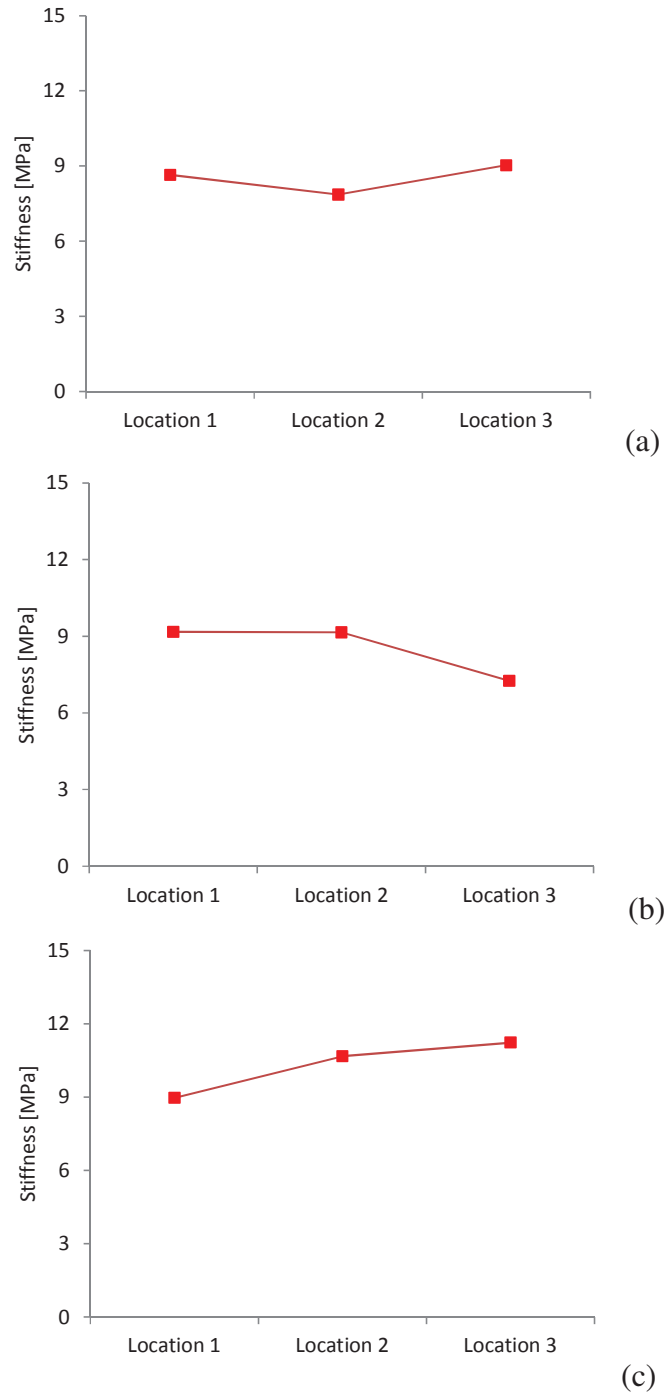


Figure 4.37: SSG modulus for the small (vibratory) compactor (Town of Sylvania site): Nominal moisture content (a) wet of optimum; (b) around optimum; (c) wet of optimum. Note: Locations 1, 2, and 3 correspond to lift thicknesses of approximately 60 cm (24 in.), 45 cm (18 in.) and 30 cm (12 in.), respectively.

Shear Resistance – DPI Profile

Figures 4.38 and 4.39 show the DCP index profiles obtained for the two compactors for the compacted soil under different moisture content and lift thickness. The results are quite interesting for most profiles: from top to bottom most of the results show drop in the DCP index just below the surface (an indication of the increase in the shear strength of the compacted soil) to then increase in then DPI index about 10 to 15 cm (4 to 6 in.) below the compacted surface (an indication of a decrease of shear strength versus depth). In general, the smallest lift thicknesses tested (30 cm - 12 in.) yielded more uniform DCP index profiles (with smaller values). This observation appears to indicate maller lift thicknesses work better at least for the tested compactors and soils. That is, the quality of compaction is mostly more homogeneous without under-compaction regions for the thin lift layers while for the thicker layers the swing in shear strength is quite large (see data in Figure 4.38b and 4.38c for prime examples of this observation).

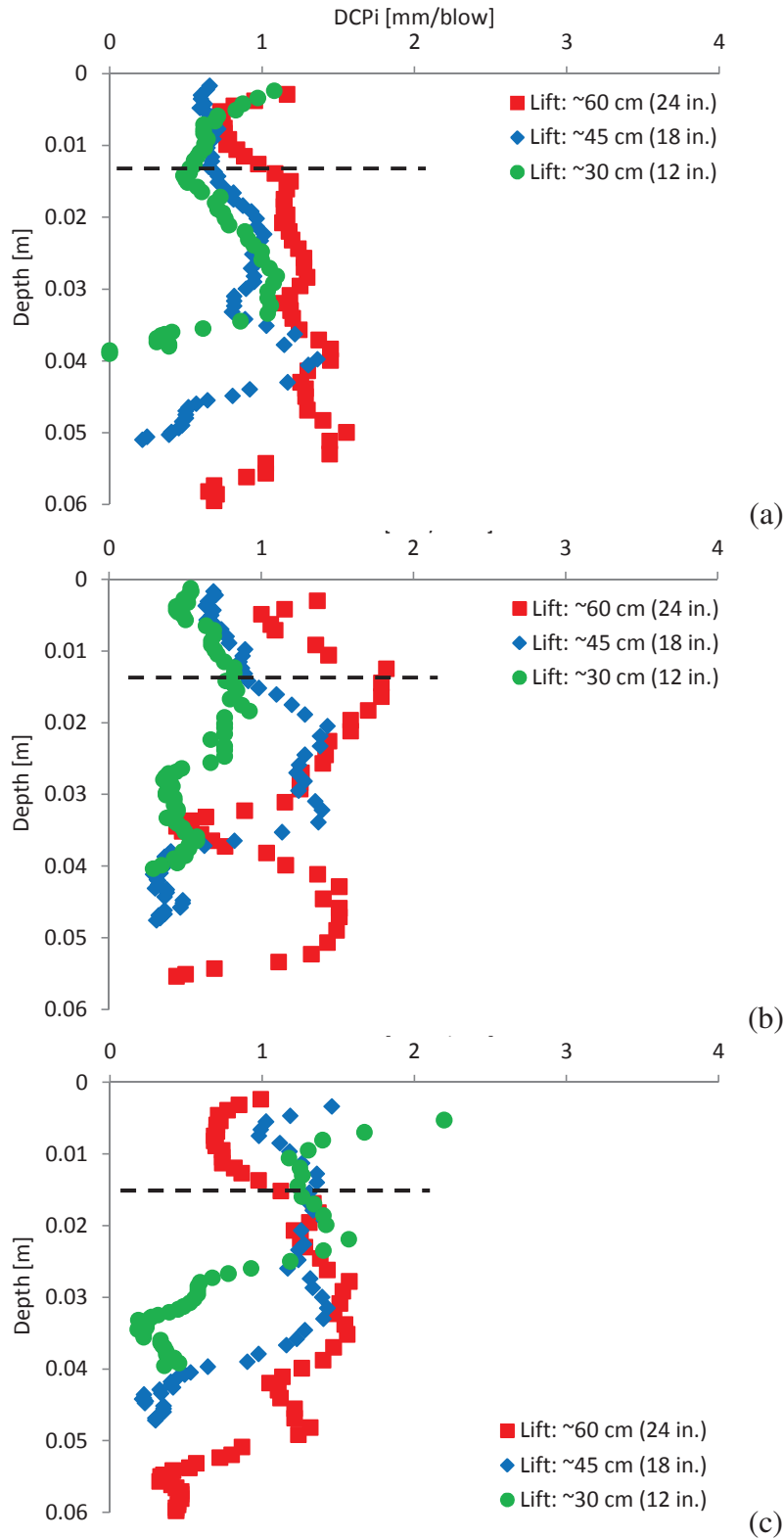


Figure 4.38: DCP index profile for the large (non-vibratory) compactor (Town of Sylvania site): Nominal moisture content (a) wet; (b) optimum; (c) dry of optimum.

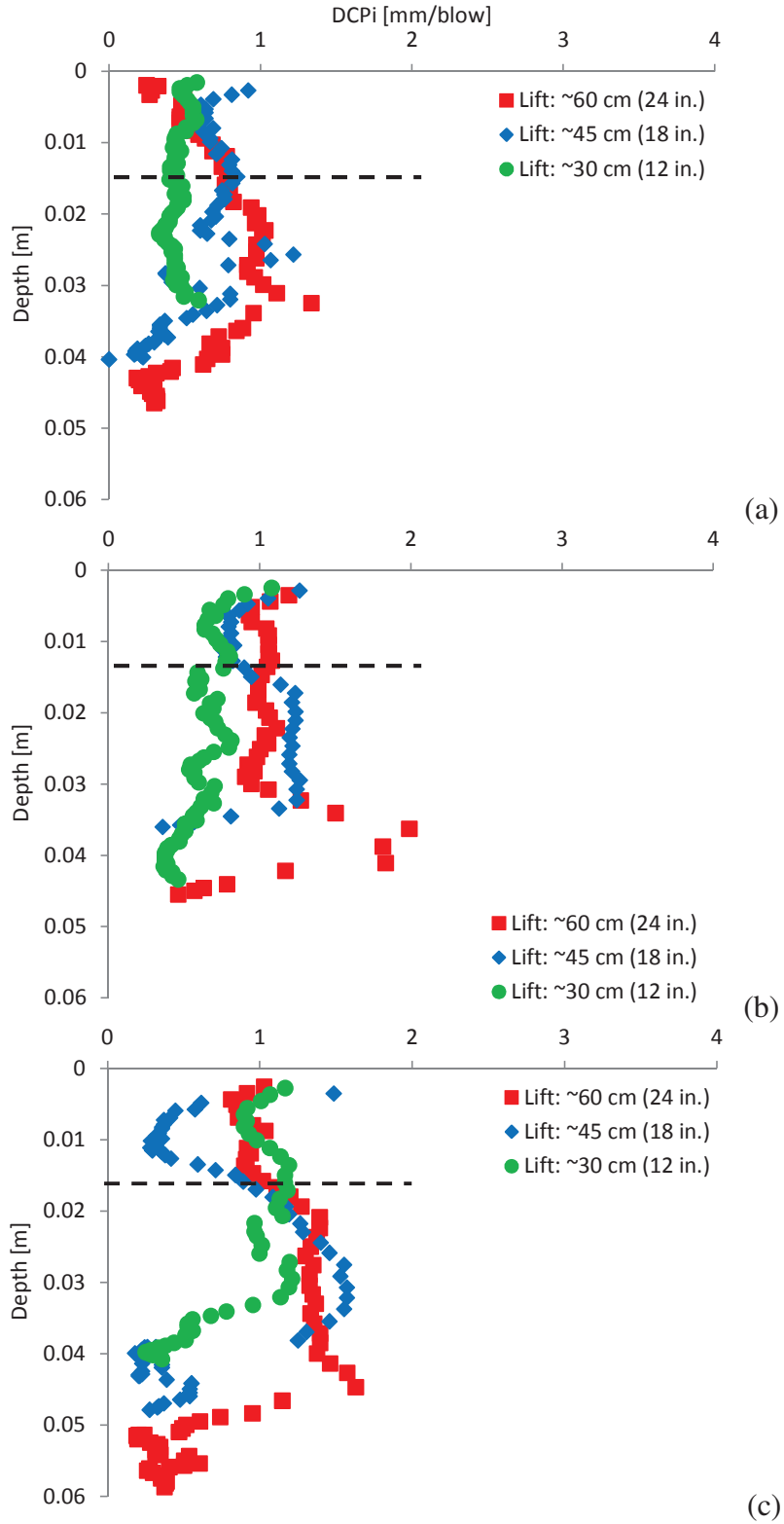


Figure 4.39: DCP index profile for the small (vibratory) compactor (Town of Sylvania site): Nominal moisture content (a) wet; (b) optimum; (c) dry of optimum.

Chapter 5 - NUMERICAL MODELING AND ANALYSES

5.1 Introduction

Numerical simulations using finite elements were conducted to evaluate the interaction of different compaction and earthmoving equipment with embankment soils. The studied parameters included the effect of the compactor geometry versus lift thickness, applied compactor energy, and soil properties. The numerical studies provided the base for the better understanding of the interaction of different compaction operation parameters.

The finite element method (FEM) has been successfully used to simulate wheel loadings on soils. The FEM was used to locate the zones of maximum compaction stresses and to illustrate the propagation of compaction energy during compaction operations. In the static analysis modeling, the location of maximum volumetric strain and the plastic state depends on the contact area, contact pressure, and soil type (Pollack et al. 1986).

5.2 Numerical Analysis

5.2.1 Soil Compaction under Wheel Loading

A stress-strain relationship under wheel load compaction is a complex process due to high strain rates, large deformations, and moving loading mechanisms. Compaction under conventional pneumatic wheels is related to the weight of equipment, contact pressure, wheel dimension, wheel stiffness, equipment speed, and the number of passes (Soane et al. 1981). To simplify the complex wheel loading mechanism, the loading process is commonly modeled assuming a static foundation loading condition.

In the simplified static analysis of wheel loading, the determination of distributed weight of equipment and contact areas is most important for estimating the influence depth of compaction. Depending on types of compactors, the contact area is categorized as: the strip footing with the specific foundation width (contact area, B) and the circular footing with the specific foundation diameter (contact area diameters, D) that correspond to drum type roller or rubber-tired roller respectively (Figure 5.1). Based on the contact area type assumption, the load can be estimated for different types of compactors. The estimated load values for each type of compactor are summarized in Table 5.1.

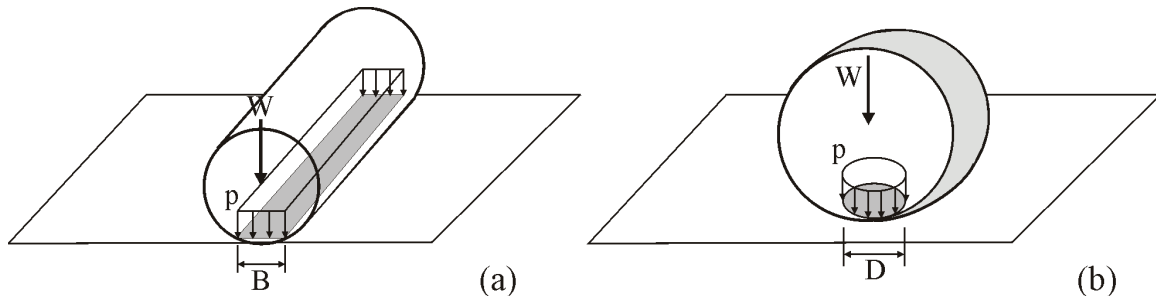


Figure 5.1: Assumed contact area and contact pressure distribution: (a) strip footing – drum-type roller and (b) circular footing - tire-based compactor (W is the equipment load per roller or wheel and p is the contact pressure).

Table 5.1: Estimated applied compaction pressure at surface.

Compactor Type	weight of equipment (kN)	Weight at each tire or drum (kN)	Estimated contact area (m ²)	Applied compaction pressure (kPa)
Tire-based roller: Rubber-tired roller	282	70	$\pi D^2/4$	D=0.2 m; 2,242 kPa D=0.4 m; 561 kPa D=0.6 m; 249 kPa D=0.8 m; 140 kPa
Drum-based roller: Smooth drum vibratory roller	110	55	L D	B=0.2 m; 131 kPa B=0.4 m; 65 kPa B=0.6 m; 44 kPa B=0.8 m; 33 kPa

Note: It is assumed that the overall weight of compaction equipment is equally distributed to each tire and roller. The contact area of tire-based compactor is assumed to be circular. The drum width L is 2.1 m.

5.2.2 Computer Code: PLAXIS

PLAXIS, which is a two-dimensional finite element code, was used in this numerical study. Mohr-Coulomb, hardening, and soft soil models are included in this software package. To simulate the compaction process, the soil hardening model (advanced hyperbolic model) was selected for the numerical modeling.

5.2.3 Soil Model

The stress-strain relationship during soil compaction is highly non-linear and stress dependent. The hardening soil model enables to estimate non-linear soil behavior with approximate hyperbolic relationships (Figure 5.2):

$$E_{50} = E_{50}^{\text{ref}} \left(\frac{\sigma_3 + c \cdot \cot\phi}{\sigma^{\text{ref}} + c \cdot \cot\phi} \right)^m \quad (5.1)$$

$$E_{ur} = E_{ur}^{ref} \left(\frac{\sigma_3 + c \cdot \cot\phi}{\sigma^{ref} + c \cdot \cot\phi} \right)^m \quad (5.2)$$

where σ_3 is smallest principal stress, c and ϕ are the strength parameters, E_{50}^{ref} is the secant modulus at 50% of the failure stress and at effective reference pressure of σ^{ref} , E_{ur}^{ref} is the unloading and reloading modulus at effective reference pressure of σ^{ref} , and m is the power coefficient (a function of soil type).

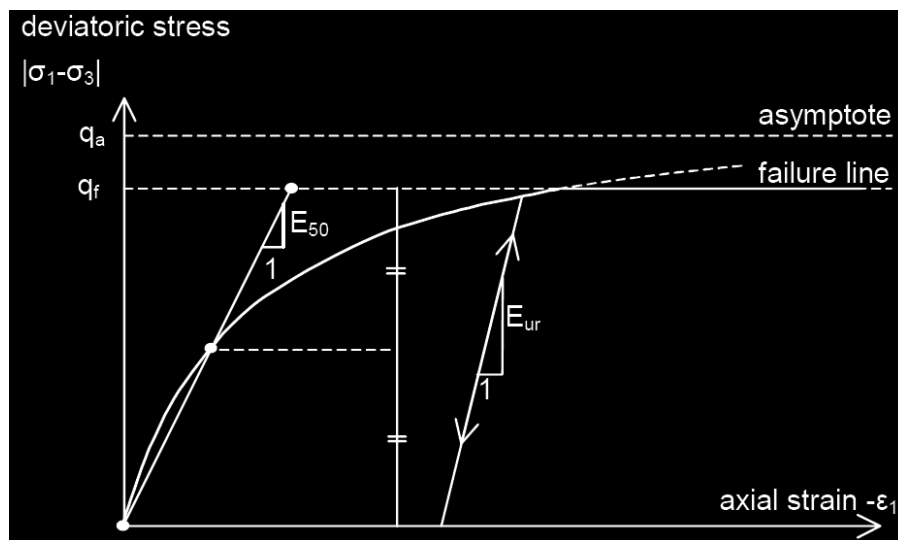


Figure 5.2: Hyperbolic stress-strain relation in primary loading.

As the soil is loaded, the soil undergoes plastic deformations, hardens, and increases its elastic limit. Therefore, the yield surface of the soils is determined by following its stress history; that is, the yield surface is expanded by the plastic strain. During deviatoric loading, the stiffness of soils decreases and irreversible plastic strains are developed. The hardening soil model is implemented in the compaction analysis using PLAXIS. This hardening soil model allows for volumetric hardening (cap hardening) and deviatoric

hardening (shear hardening - Figure 5.3). This model uses the Coulomb failure criterion and a stress-dependent non-linear stress-strain formulation.

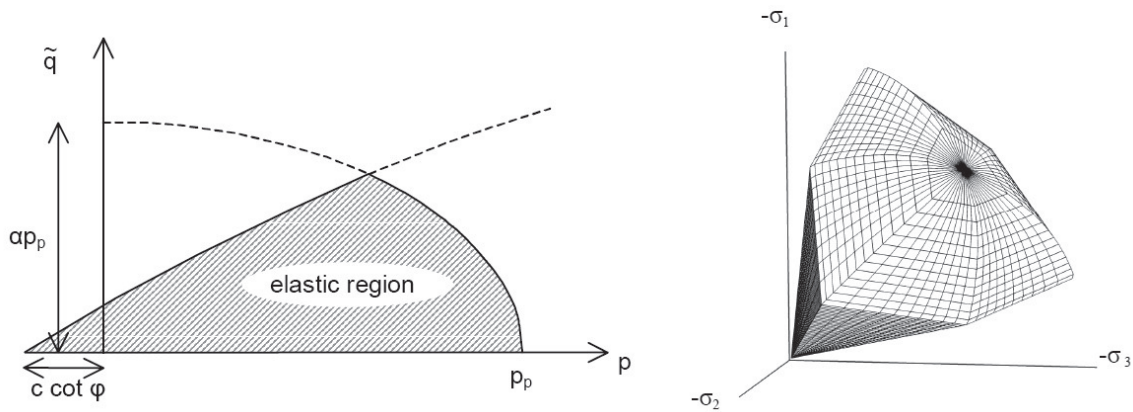


Figure 5.3: Yield surface of hardening soil model in p-q plane and hardening cap in principal stress space (Brinkgreve 2002).

The hardening soil model requires ten input parameters, including three stiffness parameters (i.e., triaxial loading stiffness E_{50} , triaxial unloading stiffness E_{ur} , and oedometer loading stiffness E_{oed}), a power coefficient (m) for the stress-dependent stiffness relationship, the Poisson's ratio (ν), the Mohr-Coulomb criteria parameters (c and ϕ), the dilatancy angle (ψ), the K_0 -value, and failure ratio (R_f). The used input parameters are summarized in Table 5.2. To represent the two types of soils (i.e., fine-grained and coarse-grained soils), typical soil parameters were selected from a published value database (Hunt 1986).

Table 5.2: Soil parameters of hardening model.

Parameters		Soil type	
		Fine-grained soil	coarse-grained soil
Density	γ_{unsat} (kN/m ³)	15.5	14.5
	γ_{sat} (kN/m ³)	17	16
Stiffness	E_{50}^{ref} (kPa)	2,100	4,000
	$E_{\text{oed}}^{\text{ref}}$ (kPa)	2,100	4,000
	$E_{\text{ur}}^{\text{ref}}$ (kPa)	8,400	15,640
	coefficient, m	0.7	0.5
	ν	0.3	0.3
Strength	c_{ref} (kPa)	10.0	1.0*
	Φ (deg)	31	37
	failure ratio, R_f	0.9	0.9

Note: Density values are determined by maximum dry density in standard Proctor test. Stiffness parameters are determined by correlations by soil type and compactness (Hunt 1986). Strength parameters are determined by correlations by soil types (NAVFAC DM 7.02). * is used to numerical stability as a small value.

5.3 Modeling results and interpretations

As the compaction equipment moves, the stiffness of soils and contact width of compactor wheels get smaller. This behavior is represented by the numerical modeling. To simplify the complex wheel moving and soil foundation interactions, the drum-based roller is represented as a strip footing under plane strain conditions, while the tire-based roller is represented as a circular footing in the axisymmetric condition.

5.3.1 Maximum Displacement

Figures 5.4 and 5.5 show the calculated maximum displacement under the two different compactors. The contact width is the most important controlling parameter in the

calculation of the displacement field in fine-grained soils. Typically, the contact width decreases as the compaction process progresses. However, the maximum displacement results contain both elastic and plastic displacements. Thus, the maximum displacement does not completely explain the compaction effectiveness.

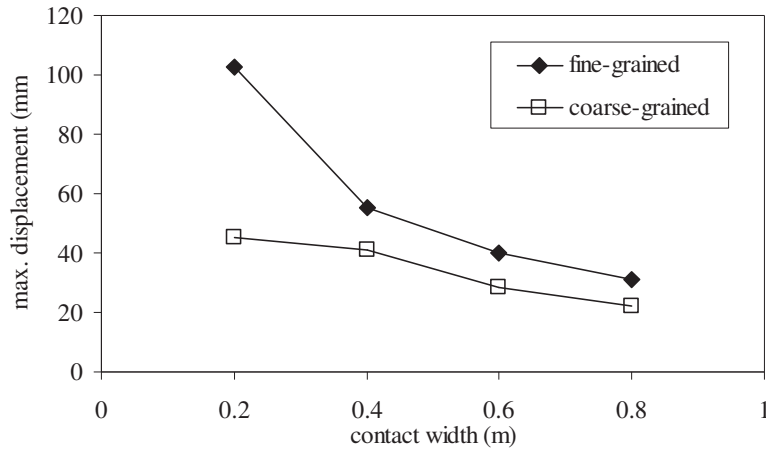


Figure 5.4: Maximum displacement of under the drum-based compactor.

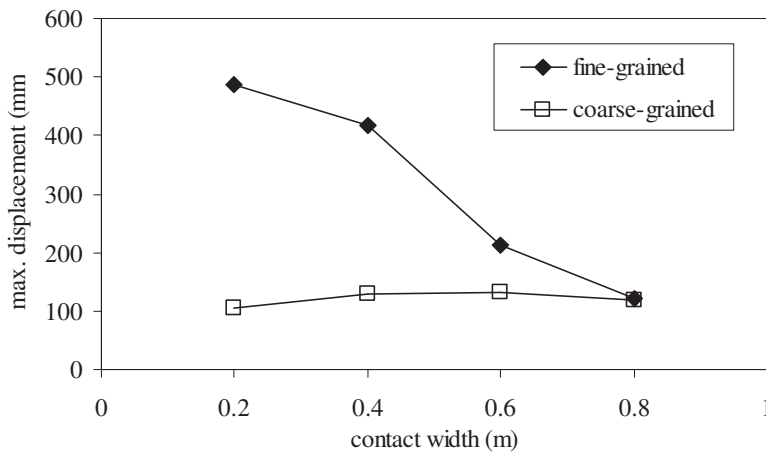


Figure 5.5: Maximum displacement of under tire-based compactor.

5.3.2 Volumetric Strain

Volumetric strains in the soil element can be used for evaluating the effectiveness of soil compaction. The total volumetric strain ε_v at the stress point is computed as:

$$\varepsilon_v = \varepsilon_z + \varepsilon_r + \varepsilon_\theta \quad (5.3)$$

where ε_z , ε_r , and ε_θ , are volumetric strains in vertical, radial, and tangential directions.

As the volumetric strain distribution is directly connected to the stress distribution, the bulk unit weight of soil after compaction is calculated from the stress and volumetric strain distributions:

$$\gamma_f = \gamma_i + (\Delta\varepsilon_v \cdot \gamma_i) \quad (5.4)$$

where γ_i and γ_f are the initial and final bulk unit weights of soils, and $\Delta\varepsilon_v$ is the change in volumetric strain. Using the maximum dry unit weight of soil, the degree of compaction can be evaluated.

The wheel load movement is simulated by changing the contact width (from large contact width to small contact width). Figure 5.6 summarizes the combination results for the two types of soils and two types of compactors. For tire-based compactor, the required 95% of relative compaction condition is reached up to 0.60 m (24 in) depth. However, as the compactor moves over the embankment, under-compaction is also occurred outside to the narrow wheel footprint. For drum-based compactor, the compaction effectiveness is improved as the compaction process progresses. The compaction effective depth reaches a depth of about 0.30 m (12 in). The contours show that there is no under-compaction region in the drum-based roller.

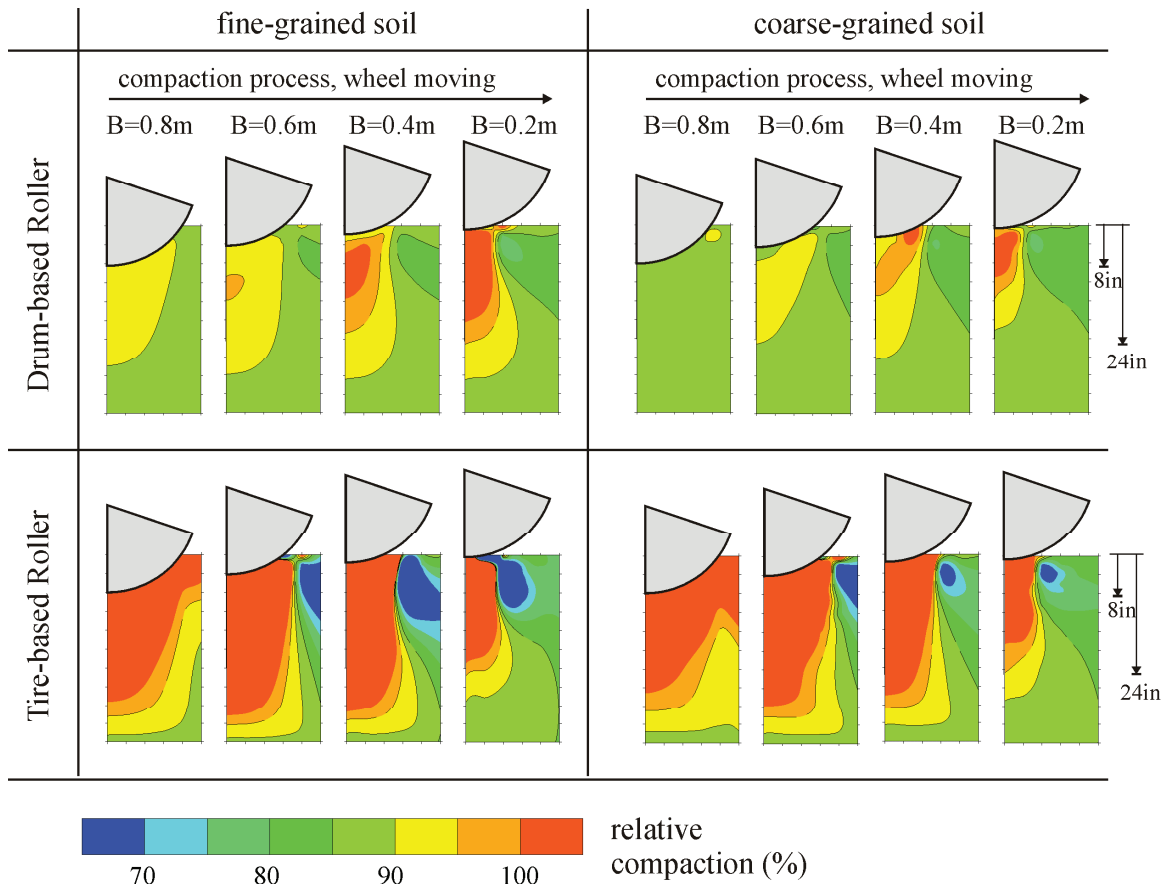
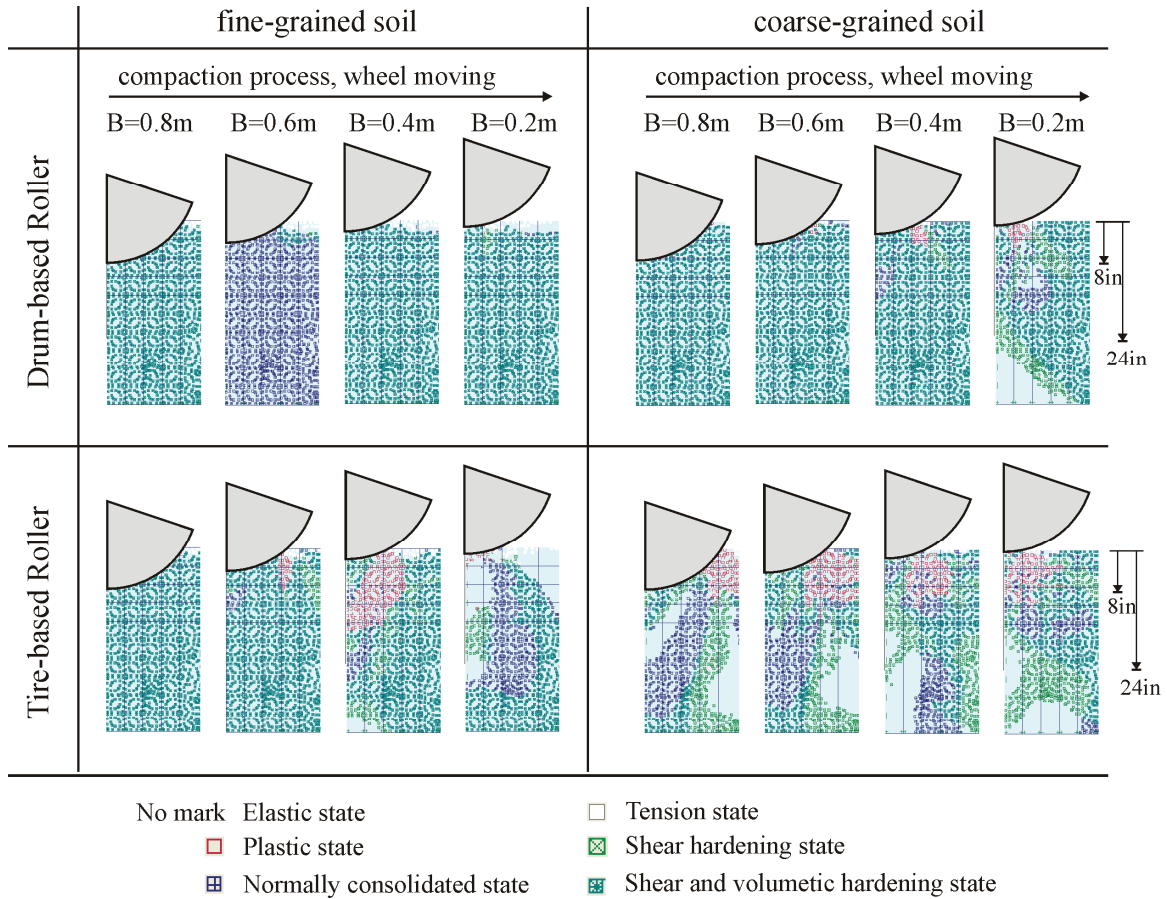


Figure 5.6: Distribution of relative compaction as a function of the number passes (represented by footprint width), soil type, and compactor type.

5.2.3 Failure Zone Distribution

The failure zone is defined as the region of soil elements where the compactor induced stresses cause the local failure. In this failure zone, the soil undergoes large plastic deformation, and compaction effects dominate. However, these local deformations also cause the heterogeneous compaction quality. Figure 5.7 summarizes the failure zone distribution for each numerical simulation case. For drum-based compactor, the plastic state is barely generated due to the light weight of compactors and the larger contact area.

However, the failure is generated at the edge of wheel load in the tire-based compactor up to depths of 30 cm (12 in). These regions closely match the results using the volumetric strain approach.



Chapter 6 – SUMMARY, ENGINEERING RECOMMENDATIONS AND CONCLUSIONS

This report summarizes the results of two experimental studies designed to evaluate the effective depth of soil compaction. The studies aimed at quantifying the effect of applied compaction energy, compactor types and different soils to assess optimal lift thicknesses in road construction. The research team performed field monitoring tests by

- Instrumented soil layers to evaluate shear-induced rotations and displacements and pressure responses during compaction processes
- conducting field tests to evaluate stiffness and shear strength, and to measure water content and density after compaction operations were completed

Field experimental testing was conducted using six different types of soil compactors and earthmoving equipment on three different soil types. The evaluation of the compaction effectiveness was evaluated using soil stiffness gauge, pressure plate, dynamic cone penetrometer, sand cone, nuclear density gauge, and P-wave propagation analysis. For different subgrade lift thicknesses, the evaluation of soil responses during field compaction was performed using three different type soils (i.e., poorly graded sand, silty sand and low plasticity clays) at different water contents, increasing loose lift thickness (i.e., between 20 cm -8 in- and 60 cm -24 in.) and compaction and earth moving equipment (included rollers, vibrating rollers, padded rollers, tire-based rollers, dozers, and scrapers). The experimental studies were complemented with a numerical simulation designed to evaluate the compaction-soil interaction to support the experimental studies.

The field testing results have shown that:

- For the coarse grained soils (Junction City site), loose lift thickness up to 40 cm (16 in.) performed well in all tested parameters (including soil particle rotation, dynamic cone penetration and nuclear density gauge). However, the interpretation of the SSG modulus at the near surface and P-wave-based modulus at the bottom of thick lift layers provided evidence of under-compaction regions at the bottom of lifts in coarse and fine-grained soils. These data justify setting maximum limits of 40 cm (16 in.) on loose lift thickness even though for most coarse grained soils the use of large equipment appears to be effective in compacting thick lifts.
- For fine grained soils (Town of Sylvania site), the data are not as definitive, however nuclear density gauge results from two different sampling depths do not appear to show a detrimental effect for the tested loose lift thickness at different water contents and for different compaction equipment. These results are also confirmed with the results from the dynamic cone penetration testing where for all condition the 30 cm (12 in.) showed overall the maximum shear strength along the compaction profiles in all but one of the tested cases.

Overall results and interpretations of the field monitoring, field testing, and numerical modeling of wheel loading compaction suggest that 0.3-m (12-in) loose lifts for coarse-grained and fine-grained soils could be implemented when using Quality Management Program (QMP). Due to the limited nature of the student, it is recommended that if standard compaction is used, 0.2-m (8-in) loose lifts for coarse-grained and fine-grained soils should remain the state of practice for WisDOT.

However it must be emphasized that, the collected data are limited since these studies were conducted at two specific construction locations using just three different soil types. Therefore, the collection of more data for different soils types and compaction equipment is recommended to establish and confirm general conclusions for revising the Wisconsin Department of Transportation's specifications.

Other observations and recommendations include:

- Tire-based roller and earthmoving equipment (e.g., scraper) provided higher contact pressures. These high pressures propagate deep into the soil mass and allow the compaction of thick layers (as for the coarse-grained soils at the Junction City site). However, this type of roller may produce uneven compaction regions (i.e., zones that were under-compacted). When the compactor missed the path above the pressure plate, pressure responses were lowered. This implies that the importance of the area coverage in the compacted plane using tire-based soil compactors. Therefore, WisDOT officials and contractors need to be careful offsetting passes to equally compact all of the compaction area and effectively compact lifts even when the evaluated compaction performance appears to acceptable for thick lift thicknesses.
- Dynamic cone penetration index (DPI) profiles in fine-grained soils detected the areas of low shear strength at the bottom of thick lifts (i.e., greater than 0.30 m - 12 in).
- Shear-induced rotation measurements provide indication of soil particle movements. Rotation movements are dependent on the type of soil and compaction equipment

used. These observations imply that the current conservative lift thickness specification in coarse-grained soils may be increased by well controlled compaction equipment and water contents of soils.

Numerical simulations were used to further evaluate a possible effective compaction depth for drum-based and the tire-based compactors. Results of numerical modeling have shown that:

- The compaction process is a function of compactor's weight, soil type, and contact width of the wheel loading. Using various contact widths, the research team simulated the effect of the wheel load moving during compaction processes.
- A hardening soil model was implemented to simulate the compaction process using volumetric hardening (cap hardening) and deviatoric hardening (shear hardening). Volumetric strain and failure zones in numerical simulations can be indicators of depths of the compaction effectiveness.
- The evaluation of the relative compaction using volumetric strain analyses indicate that the compaction effectiveness ($RC > 95\%$) is observed at 0.30-m (12-in) depth regardless of soil types and soil compactor types. However, the tire-based roller may leave areas that are under-compacted regions due to highly localized and high pressure footprints

REFERENCES

- Abu-Farsakh, M. Y., Nazzal, M. D., Alshibli, K., and Seyman, E. (2005). "Application of dynamic cone penetrometer in pavement construction control." *Journal of the Transportation Research Board*, No. 1913, pp. 53–61.
- Anderegg, R., and Kaufmann, K. (2004). "Intelligent compaction with vibratory rollers." *Transportation Research Record. 1868*, Transportation Research Board, Washington, D.C., 124–134.
- Benson, C. and Bosscher, P. (1999), Time-domain reflectometry in geotechnics: A review, *Nondestructive and Automated Testing for Soil and Rock Properties*, STP 1350, ASTM, W. Marr and C. Fairhurst, Eds., 113-136.
- Bowels, J. E. (1979). *Physical and Geotechnical Properties of Soils*, McGraw Hill, New York.
- Burnham, T., and Johnson, D. (1993). *In situ Foundation Characterization using the Dynamic Cone Penetrometer*, Minnesota Department of Transportation Final Report, MN/RD-93/05.
- Caterpillar (2009). Company Web Site. URL: <http://www.cat.com> (Accessed on January 15, 2009)
- Daniel, D. and Benson, C. (1990). "Water content-density criteria for compacted soil liners." *Journal of Geotechnical Engineering*, 116(12), 1811-1830.
- D'Appolonia, D. J., Whitman, R. V., and D'Appolonia, E. D. (1969) "Sand compaction with vibratory compaction equipment." *Journal of the Soil Mechanics and Foundations Division*, 95(SM1), 263-284.
- Brinkgreve, R. B. J. (2002). *PLAXIS 2D – version 8*, Balkema Publishers, AN DELFT, Netherlands.
- Dimension Engineering (2009). Company Web Site. URL: <http://www.dimensionengineering.com> (Accessed on June 20, 2008).

- Edil, T. B., and Sawangsuriya, A. (2006). "Use of stiffness and strength for earthwork quality evaluation." *ASCE Geotechnical Special Publication (GSP): Site and Geomaterial Characterization*, GeoShanghai Conference, Shanghai, China.
- Gas Technology Institute (2005). "Evaluation of Soil Compaction Measuring Devices". FINAL REPORT GRI-04/0067. 1700 South Mount Prospect Road. Des Plaines, IL 60018. 132 pages.
- Holtz, R.D., and Kovacs, W.D. (1981). *An Introduction to Geotechnical Engineering*, Prentice-Hall, 733 pages.
- Holtz, R. D., editor (1990). *Guide to Earthwork Construction*, State of the Art Report 8, Transportation Research Board, Washington, D.C., 107 pages.
- Hoppe, E.J. *Guidelines for the Use, Design, and Construction of Bridge Approach Slabs*. Report VTRC 00-R4, Virginia Transportation Research Council, Charlottesville, VA, 1999.
- Humboldt Mfg. Co. (2009). *User Guide – Model H-4140 Soil Stiffness / Modulus Gauge*. 7300 West Agatite Avenue. Norridge, IL 60706. USA. 17 pages.
- Jones, S. B., Wairth, J. M. and Or, D. (2001). "Time domain reflectometry measurement principles and applications". *Hydrological Processes*. Vol. 16. pp. 141-153.
- Kim, K.-S., Fratta, D., and Wen, H. (2014). "Field Measurements of Compaction Energy in Thick Lifts of Coarse-Grained Soils". *Korean Journal of Civil Engineering*. Vol. 8, No. 2, pp. 497-504. DOI:10.1007/s12205-014-0144-8.
- Lambe, T.W. (1958) "The structure of compacted clay". *Journal of Soil Mechanics and Foundation Engineering Division*, 84(2), 1-35.
- Mohammadi, S. D., Nikoudel, M.R., Rahimi, H., and Khamehchiyan, M. (2008). "Application of the dynamic cone penetrometer (DCP) for determination of the engineering parameters of sandy soils." *Engineering Geology*, 101, 195-203.
- Olson, R. E. (1963). "Effective stress theory of soil compaction." *Journal of the Soil Mechanics and Foundations Division*, 89(SM2), 27-45.

- Pollock, D., Perumpral, J.V., and Kuppusamy, T. (1986). "Finite element analysis of multipass effects of vehicles on soil compaction." *Transactions of the ASAE*, 29(1), 45-50.
- Ritchie Specs (2014). Dynapac CT262 Compactor. URL: <http://www.ritchiespecs.com/specification?type=construction+equipment&category=Compactor&make=Dynapac&model=CT262&modelid=93372#ixzz3E2frA4nA> [Accessed on September 20, 2014]
- Rollings, M. P., and Rollings, R. S. (1996). *Geotechnical materials in construction*, McGraw-Hill, New York.
- Santamarina, J. C., Rinaldi, V. A., Fratta, D., Klein, K. A., Wang, Y.-H., Cho, G.-C., and Cascante, G. (2005). "A Survey of Elastic and Electromagnetic Properties of Near-Surface Soils". *Near-Surface Geophysics*. Ed. D. Buttler, SEG. Tulsa, OK. pp. 71-87.
- Sawanguriya, A., Edil, T. B., and Bosscher, P. J. (2003), "Relationship between soil stiffness gauge modulus and other test moduli for granular soils." *Transportation Research Record* 1849, Paper No. 03-4089, 3-10.
- Schneider, J. M. and Fratta, D. (2009). "Time Domain Reflectometry: Parametric Study for the Evaluation of Physical Properties in Soils". *Canadian Geotechnical Journal* (In print).
- Schuettpelz, C. C., Fratta, D., and Edil, T. B. (2009a). "Evaluation of the Influence of Geogrid Reinforcement on soil Rotation and Stiffness in Compacted Based Course Soil". *Journal of the Transportation Research Board* (In print).
- Schuettpelz, C. C., Fratta, D., and Edil, T. B. (2009b). "Mechanistic method for determining the resilient modulus of base course materials based on elastic wave measurements". *Journal of Geotechnical and Geoenvironmental Engineering* (Submitted for publication).
- Seed, H. B., and Chan, C. K. (1959) "Structure and strength characteristics of compacted clays." *Journal of Soil Mechanics and Foundation Division*, 85(SM5), 87-128.

- Soane, B. D., Blackwell, P. S. Dickson, J. W., and Painter, D. J. (1981). "Compaction by agricultural vehicles: A review I. Soil and wheel characteristics." *Soil and Tillage Research*, 1, 207–237.
- Topp, G. C., Davis, J. L., and Annan, A. P. (1980). "Electromagnetic determination of soil water content: Measurements in coaxial transmission lines." *Water Resources Research*, 16(3), 574-582.
- Turnbull, W. J., and Foster, C. R. (1956). "Stabilization of materials by compaction." *Journal of the Soil Mechanics and Foundations Division*, 82(SM), 934-1-934-23.
- Winter M.G. and Clarke, B. G. (2002). "Methods for determining representative density-depth profiles using nuclear density gauges". *Geotechnique*, 52(7), 519-525.
- Yoo, T.-S., and Selig, E. T. (1979). "Dynamic of vibratory-roller compaction." *Journal of the Geotechnical Engineering Division*, 105(GT10), 1211-1231.

APPENDIX A: MEMS ACCELEROMETER RESPONSES

A.1. MEMS voltage measurement (natural moisture)

A.1.1. Smooth-drum vibratory roller

a) 12 in lift thickness

Channel	Pass #1			Pass #2			Remarks
	voltage (before)	voltage (after)	rotation (degree)	voltage (before)	voltage (after)	rotation (degree)	
0	2.99276	2.98642	-0.82	2.98529	2.97478	-1.35	sensor #1 - x direction
1	2.41305	2.41001	-0.39	2.40919	2.41362	0.57	sensor #1 - y direction
2	2.82737	2.83260	0.67	2.83141	2.81655	-1.91	sensor #2 - x direction
3	2.51046	2.50484	-0.72	2.50417	2.49866	-0.71	sensor #2 - y direction
4	3.13573	3.13053	-0.67	3.12985	3.13562	0.74	sensor #3 - x direction
5	2.47355	2.46872	-0.62	2.46785	2.46136	-0.83	sensor #3 - y direction
6	3.03257	3.02799	-0.59	3.02739	3.03932	1.53	sensor #4 - x direction
7	2.44799	2.44250	-0.71	2.44183	2.43881	-0.39	sensor #4 - y direction
8	3.06094	3.05448	-0.83	3.05378	3.06692	1.69	sensor #5 - x direction
9	2.64403	2.64376	-0.03	2.64314	2.63459	-1.10	sensor #5 - y direction

Channel	Pass #3			Pass #4			Remarks
	voltage (before)	voltage (after)	rotation (degree)	voltage (before)	voltage (after)	rotation (degree)	
0	2.97531	2.97621	0.12	2.97429	2.97204	-0.29	sensor #1 - x direction
1	2.41498	2.41509	0.01	2.41403	2.41397	-0.01	sensor #1 - y direction
2	2.81708	2.81795	0.11	2.81646	2.81322	-0.42	sensor #2 - x direction
3	2.49972	2.50015	0.06	2.49875	2.49426	-0.58	sensor #2 - y direction
4	3.13641	3.13659	0.02	3.13474	3.13355	-0.15	sensor #3 - x direction
5	2.46238	2.46315	0.10	2.46175	2.45208	-1.24	sensor #3 - y direction
6	3.04014	3.04031	0.02	3.03835	3.03618	-0.28	sensor #4 - x direction
7	2.43977	2.44004	0.03	2.43891	2.43694	-0.25	sensor #4 - y direction
8	3.06748	3.06768	0.03	3.06571	3.06398	-0.22	sensor #5 - x direction
9	2.63498	2.63578	0.10	2.63455	2.63819	0.47	sensor #5 - y direction

Channel	Pass #5			Pass #6			Remarks
	voltage (before)	voltage (after)	rotation (degree)	voltage (before)	voltage (after)	rotation (degree)	
0	2.97449	2.98335	1.14	2.98237	2.96535	-2.19	sensor #1 - x direction
1	2.41587	2.41148	-0.56	2.41121	2.41468	0.45	sensor #1 - y direction
2	2.81525	2.84109	3.32	2.84047	2.81667	-3.06	sensor #2 - x direction
3	2.49637	2.49649	0.02	2.49594	2.49418	-0.23	sensor #2 - y direction
4	3.13678	3.12671	-1.29	3.12600	3.13707	1.42	sensor #3 - x direction
5	2.45398	2.46340	1.21	2.46297	2.46468	0.22	sensor #3 - y direction
6	3.03933	3.01973	-2.52	3.01924	3.04705	3.58	sensor #4 - x direction
7	2.43856	2.43656	-0.26	2.43611	2.43511	-0.13	sensor #4 - y direction
8	3.06706	3.05024	-2.16	3.04958	3.07585	3.38	sensor #5 - x direction
9	2.64004	2.64913	1.17	2.64869	2.62906	-2.52	sensor #5 - y direction

b) 17 in lift thickness

Channel	Pass #1			Pass #2			Remarks
	voltage (before)	voltage (after)	rotation (degree)	voltage (before)	voltage (after)	rotation (degree)	
0	3.10764	3.10750	-0.02	3.10833	3.10790	-0.05	sensor #1 - x direction
1	2.45330	2.46074	0.96	2.46132	2.47226	1.41	sensor #1 - y direction
2	3.05182	3.05067	-0.15	3.05134	3.04183	-1.22	sensor #2 - x direction
3	2.49664	2.50210	0.70	2.50270	2.50951	0.87	sensor #2 - y direction
4	3.14483	3.14364	-0.15	3.14432	3.14483	0.07	sensor #3 - x direction
5	2.34077	2.33717	-0.46	2.33788	2.33594	-0.25	sensor #3 - y direction
6	3.14914	3.14942	0.04	3.15017	3.14977	-0.05	sensor #4 - x direction
7	2.47039	2.46106	-1.20	2.46163	2.45501	-0.85	sensor #4 - y direction
8	3.14763	3.14565	-0.25	3.14661	3.14737	0.10	sensor #5 - x direction
9	2.40340	2.40373	0.04	2.40427	2.40496	0.09	sensor #5 - y direction

Channel	Pass #3			Pass #4			Remarks
	voltage (before)	voltage (after)	rotation (degree)	voltage (before)	voltage (after)	rotation (degree)	
0	3.11128	3.10838	-0.37	3.10892	3.10838	-0.07	sensor #1 - x direction
1	2.47283	2.47329	0.06	2.47372	2.47956	0.75	sensor #1 - y direction
2	3.04428	3.04331	-0.12	3.04383	3.03831	-0.71	sensor #2 - x direction
3	2.51061	2.50637	-0.54	2.50743	2.51146	0.52	sensor #2 - y direction
4	3.14837	3.14392	-0.57	3.14460	3.14541	0.10	sensor #3 - x direction
5	2.33615	2.33196	-0.54	2.33263	2.33637	0.48	sensor #3 - y direction
6	3.15330	3.15012	-0.41	3.15100	3.14970	-0.17	sensor #4 - x direction
7	2.45626	2.44713	-1.17	2.44756	2.45148	0.50	sensor #4 - y direction
8	3.15122	3.14686	-0.56	3.14810	3.14862	0.07	sensor #5 - x direction
9	2.40592	2.39025	-2.01	2.39096	2.40808	2.20	sensor #5 - y direction

Channel	Pass #5			Pass #6			Remarks
	voltage (before)	voltage (after)	rotation (degree)	voltage (before)	voltage (after)	rotation (degree)	
0	3.10819	3.10953	0.17	3.11086	3.11039	-0.06	sensor #1 - x direction
1	2.47925	2.48022	0.13	2.48087	2.48143	0.07	sensor #1 - y direction
2	3.03808	3.03981	0.22	3.04086	3.04006	-0.10	sensor #2 - x direction
3	2.51096	2.51294	0.25	2.51381	2.51428	0.06	sensor #2 - y direction
4	3.14527	3.14654	0.16	3.14768	3.14774	0.01	sensor #3 - x direction
5	2.33612	2.33701	0.11	2.33777	2.33853	0.10	sensor #3 - y direction
6	3.14956	3.15103	0.19	3.15230	3.15190	-0.05	sensor #4 - x direction
7	2.45152	2.45311	0.20	2.45391	2.45520	0.17	sensor #4 - y direction
8	3.14881	3.14986	0.14	3.15104	3.15089	-0.02	sensor #5 - x direction
9	2.40758	2.40803	0.06	2.40877	2.40894	0.02	sensor #5 - y direction

c) 24 in lift thickness

Channel	Pass #1			Pass #2			Remarks
	voltage (before)	voltage (after)	rotation (degree)	voltage (before)	voltage (after)	rotation (degree)	
0	3.09567	3.09555	-0.02	3.09568	3.09624	0.07	sensor #1 - x direction
1	2.47937	2.47934	0.00	2.47933	2.48165	0.30	sensor #1 - y direction
2	3.11257	3.11306	0.06	3.11327	3.11437	0.14	sensor #2 - x direction
3	2.57503	2.57496	-0.01	2.57489	2.57555	0.08	sensor #2 - y direction
4	2.64994	2.65058	0.08	2.65054	2.64956	-0.13	sensor #3 - x direction
5	2.49532	2.49536	0.00	2.49540	2.49292	-0.32	sensor #3 - y direction
6	1.93519	1.93390	-0.17	1.93356	1.93287	-0.09	sensor #4 - x direction
7	2.54769	2.55060	0.37	2.55081	2.55189	0.14	sensor #4 - y direction
8	2.53618	2.53447	-0.22	2.53483	2.53496	0.02	sensor #5 - x direction
9	2.44398	2.44357	-0.05	2.44354	2.44375	0.03	sensor #5 - y direction

Channel	Pass #3			Pass #4			Remarks
	voltage (before)	voltage (after)	rotation (degree)	voltage (before)	voltage (after)	rotation (degree)	
0	3.09600	3.09708	0.14	3.10029	3.09890	-0.18	sensor #1 - x direction
1	2.48191	2.48259	0.09	2.48546	2.48610	0.08	sensor #1 - y direction
2	3.11405	3.11562	0.20	3.11938	3.11769	-0.22	sensor #2 - x direction
3	2.57580	2.57584	0.00	2.57906	2.57900	-0.01	sensor #2 - y direction
4	2.64953	2.65232	0.36	2.65521	2.65251	-0.35	sensor #3 - x direction
5	2.49303	2.49350	0.06	2.49605	2.49533	-0.09	sensor #3 - y direction
6	1.93309	1.93361	0.07	1.93560	1.93454	-0.14	sensor #4 - x direction
7	2.55166	2.55574	0.52	2.55843	2.55726	-0.15	sensor #4 - y direction
8	2.53507	2.53719	0.27	2.53218	2.53024	-0.25	sensor #5 - x direction
9	2.44343	2.44339	-0.01	2.45292	2.45311	0.03	sensor #5 - y direction

Channel	Pass #5			Pass #6			Remarks
	voltage (before)	voltage (after)	rotation (degree)	voltage (before)	voltage (after)	rotation (degree)	
0	3.09939	3.10019	0.10	3.10015	3.09889	-0.16	sensor #1 - x direction
1	2.48657	2.48719	0.08	2.48700	2.48756	0.07	sensor #1 - y direction
2	3.11811	3.11948	0.18	3.11935	3.11798	-0.18	sensor #2 - x direction
3	2.57944	2.57930	-0.02	2.57932	2.57963	0.04	sensor #2 - y direction
4	2.65284	2.65416	0.17	2.65454	2.65150	-0.39	sensor #3 - x direction
5	2.49559	2.49532	-0.03	2.49532	2.49492	-0.05	sensor #3 - y direction
6	1.93478	1.93491	0.02	1.93506	1.93387	-0.15	sensor #4 - x direction
7	2.55748	2.55794	0.06	2.55797	2.55763	-0.04	sensor #4 - y direction
8	2.53062	2.53078	0.02	2.53085	2.52878	-0.27	sensor #5 - x direction
9	2.45328	2.45343	0.02	2.45346	2.45203	-0.18	sensor #5 - y direction

A.1.2. Rubber-tired roller

a) 11 in lift thickness

Channel	Pass #1			Pass #2			Remarks
	voltage (before)	voltage (after)	rotation (degree)	voltage (before)	voltage (after)	rotation (degree)	
0	3.10718	3.08581	-2.75	3.10360	3.10496	0.17	sensor #1 - x direction
1	2.44469	2.42509	-2.52	2.43833	2.44090	0.33	sensor #1 - y direction
2	3.16579	3.16963	0.49	3.16633	3.16703	0.09	sensor #2 - x direction
3	2.54842	2.53526	-1.69	2.53246	2.53371	0.16	sensor #2 - y direction
4	3.15966	3.16091	0.16	3.15719	3.15781	0.08	sensor #3 - x direction
5	2.57924	2.56832	-1.40	2.56541	2.56765	0.29	sensor #3 - y direction
6	3.12575	3.12450	-0.16	3.12096	3.12149	0.07	sensor #4 - x direction
7	2.49450	2.46608	-3.65	2.46354	2.46640	0.37	sensor #4 - y direction

Channel	Pass #3			Pass #4			Remarks
	voltage (before)	voltage (after)	rotation (degree)	voltage (before)	voltage (after)	rotation (degree)	
0	3.10416	3.10167	-0.32	3.10304	3.10121	-0.24	sensor #1 - x direction
1	2.44045	2.43185	-1.11	2.43281	2.43694	0.53	sensor #1 - y direction
2	3.16650	3.16613	-0.05	3.16635	3.16612	-0.03	sensor #2 - x direction
3	2.53372	2.54018	0.83	2.54035	2.54324	0.37	sensor #2 - y direction
4	3.15745	3.15574	-0.22	3.15602	3.15599	0.00	sensor #3 - x direction
5	2.56738	2.57556	1.05	2.57567	2.57752	0.24	sensor #3 - y direction
6	3.12136	3.12049	-0.11	3.12036	3.11974	-0.08	sensor #4 - x direction
7	2.46602	2.47947	1.73	2.47957	2.48115	0.20	sensor #4 - y direction

Channel	Pass #5			Pass #6			Remarks
	voltage (before)	voltage (after)	rotation (degree)	voltage (before)	voltage (after)	rotation (degree)	
0	3.10062	3.10229	0.21	3.06017	3.05946	-0.09	sensor #1 - x direction
1	2.43656	2.43444	-0.27	2.40321	2.40324	0.00	sensor #1 - y direction
2	3.16514	3.16701	0.24	3.16614	3.16756	0.18	sensor #2 - x direction
3	2.54259	2.53278	-1.26	2.53201	2.53342	0.18	sensor #2 - y direction
4	3.15514	3.15671	0.20	3.15575	3.15699	0.16	sensor #3 - x direction
5	2.57692	2.56444	-1.60	2.56379	2.56543	0.21	sensor #3 - y direction
6	3.11898	3.11859	-0.05	3.11771	3.11915	0.18	sensor #4 - x direction
7	2.48058	2.45790	-2.92	2.45741	2.45896	0.20	sensor #4 - y direction

b) 20 in lift thickness

Channel	Pass #1			Pass #2			Remarks
	voltage (before)	voltage (after)	rotation (degree)	voltage (before)	voltage (after)	rotation (degree)	
0	1.72224	1.72177	-0.06	1.72164	1.72093	-0.09	sensor #1 - x direction
1	2.50959	2.50820	-0.18	2.50779	2.51539	0.98	sensor #1 - y direction
2	3.16852	3.16902	0.06	3.16906	3.16932	0.03	sensor #2 - x direction
3	2.46769	2.48357	2.04	2.48332	2.47016	-1.69	sensor #2 - y direction
4	3.13174	3.13561	0.50	3.13561	3.13987	0.55	sensor #3 - x direction
5	2.54958	2.55657	0.90	2.55622	2.51996	-4.66	sensor #3 - y direction
6	3.01777	3.01199	-0.74	3.01194	3.01132	-0.08	sensor #4 - x direction
7	2.50415	2.57113	8.61	2.57101	2.50204	-8.87	sensor #4 - y direction

Channel	Pass #3			Pass #4			Remarks
	voltage (before)	voltage (after)	rotation (degree)	voltage (before)	voltage (after)	rotation (degree)	
0	1.71998	1.72105	0.14	1.72114	1.72104	-0.01	sensor #1 - x direction
1	2.51352	2.51527	0.23	2.51527	2.51552	0.03	sensor #1 - y direction
2	3.16731	3.16943	0.27	3.16922	3.16903	-0.02	sensor #2 - x direction
3	2.46855	2.47024	0.22	2.47036	2.46545	-0.63	sensor #2 - y direction
4	3.13766	3.13999	0.30	3.13985	3.13977	-0.01	sensor #3 - x direction
5	2.51856	2.52030	0.22	2.52052	2.51382	-0.86	sensor #3 - y direction
6	3.00958	3.01140	0.23	3.01167	3.01295	0.16	sensor #4 - x direction
7	2.50052	2.50233	0.23	2.50238	2.49740	-0.64	sensor #4 - y direction

Channel	Pass #5			Pass #6			Remarks
	voltage (before)	voltage (after)	rotation (degree)	voltage (before)	voltage (after)	rotation (degree)	
0	1.72114	1.72092	-0.03	1.72131	1.72086	-0.06	sensor #1 - x direction
1	2.51626	2.51569	-0.07	2.51619	2.51492	-0.16	sensor #1 - y direction
2	3.16962	3.16893	-0.09	3.16978	3.16866	-0.14	sensor #2 - x direction
3	2.46596	2.46533	-0.08	2.46586	2.46604	0.02	sensor #2 - y direction
4	3.14025	3.13961	-0.08	3.14032	3.13936	-0.12	sensor #3 - x direction
5	2.51424	2.51377	-0.06	2.51442	2.51151	-0.37	sensor #3 - y direction
6	3.01350	3.01267	-0.11	3.01333	3.00989	-0.44	sensor #4 - x direction
7	2.49795	2.49747	-0.06	2.49816	2.49645	-0.22	sensor #4 - y direction

A.1.3. Padfoot roller

a) 16 in lift thickness

Channel	Pass #1			Pass #2			Remarks
	voltage (before)	voltage (after)	rotation (degree)	voltage (before)	voltage (after)	rotation (degree)	
0	2.45870	2.45839	-0.04	2.45791	2.45790	0.00	sensor #1 - x direction
1	2.76840	2.76797	-0.05	2.76746	2.76990	0.31	sensor #1 - y direction
2	2.37884	2.37839	-0.06	2.37794	2.37726	-0.09	sensor #2 - x direction
3	2.90889	2.90835	-0.07	2.90771	2.90711	-0.08	sensor #2 - y direction
4	2.44726	2.44706	-0.03	2.44647	2.44891	0.31	sensor #3 - x direction
5	3.16266	3.16188	-0.10	3.16156	3.16176	0.03	sensor #3 - y direction
6	2.60331	2.60307	-0.03	2.60247	2.60522	0.35	sensor #4 - x direction
7	2.55587	2.55541	-0.06	2.55490	2.55581	0.12	sensor #4 - y direction
8	2.56882	2.56849	-0.04	2.56805	2.57007	0.26	sensor #5 - x direction
9	2.99011	2.98945	-0.09	2.98883	2.98915	0.04	sensor #5 - y direction

Channel	Pass #3			Pass #4			Remarks
	voltage (before)	voltage (after)	rotation (degree)	voltage (before)	voltage (after)	rotation (degree)	
0	2.45856	2.45850	-0.01	2.45848	2.45275	-0.74	sensor #1 - x direction
1	2.77047	2.77043	-0.01	2.77041	2.77028	-0.02	sensor #1 - y direction
2	2.37792	2.37799	0.01	2.37808	2.37620	-0.24	sensor #2 - x direction
3	2.90768	2.90758	-0.01	2.90759	2.90548	-0.27	sensor #2 - y direction
4	2.44967	2.44962	-0.01	2.44976	2.45039	0.08	sensor #3 - x direction
5	3.16244	3.16260	0.02	3.16262	3.16126	-0.17	sensor #3 - y direction
6	2.60564	2.60578	0.02	2.60591	2.60512	-0.10	sensor #4 - x direction
7	2.55635	2.55646	0.01	2.55642	2.55567	-0.10	sensor #4 - y direction
8	2.57069	2.57078	0.01	2.57065	2.56985	-0.10	sensor #5 - x direction
9	2.98985	2.98976	-0.01	2.98978	2.98902	-0.10	sensor #5 - y direction

Channel	Pass #5			Pass #6			Remarks
	voltage (before)	voltage (after)	rotation (degree)	voltage (before)	voltage (after)	rotation (degree)	
0	2.45312	2.45529	0.28	2.45320	2.36285	-11.62	sensor #1 - x direction
1	2.77072	2.77230	0.20	2.77016	2.77803	1.01	sensor #1 - y direction
2	2.37667	2.37852	0.24	2.37658	2.37569	-0.11	sensor #2 - x direction
3	2.90580	2.90823	0.31	2.90569	2.90780	0.27	sensor #2 - y direction
4	2.45049	2.45293	0.31	2.45096	2.46160	1.37	sensor #3 - x direction
5	3.16184	3.16414	0.30	3.16156	3.16152	-0.01	sensor #3 - y direction
6	2.60507	2.60711	0.26	2.60516	2.60031	-0.62	sensor #4 - x direction
7	2.55577	2.55785	0.27	2.55582	2.55337	-0.32	sensor #4 - y direction
8	2.56967	2.57198	0.30	2.57009	2.56386	-0.80	sensor #5 - x direction
9	2.98937	2.99152	0.28	2.98898	2.98812	-0.11	sensor #5 - y direction

b) 24 in lift thickness

Channel	Pass #1			Pass #2			Remarks
	voltage (before)	voltage (after)	rotation (degree)	voltage (before)	voltage (after)	rotation (degree)	
0	2.46554	2.46915	0.46	2.46602	2.46558	-0.06	sensor #1 - x direction
1	2.94008	2.93944	-0.08	2.93231	2.93007	-0.29	sensor #1 - y direction
2	2.25649	2.25753	0.13	2.26600	2.27043	0.57	sensor #2 - x direction
3	3.05250	3.05438	0.24	3.05425	3.05700	0.35	sensor #2 - y direction
4	2.67921	2.68182	0.33	2.66947	2.66788	-0.20	sensor #3 - x direction
5	3.04735	3.04872	0.18	3.04952	3.05117	0.21	sensor #3 - y direction
6	2.60694	2.60845	0.19	2.59807	2.59584	-0.29	sensor #4 - x direction
7	3.13456	3.13596	0.18	3.13569	3.13761	0.25	sensor #4 - y direction
8	2.51903	2.51917	0.02	2.52255	2.52588	0.43	sensor #5 - x direction
9	3.07564	3.07716	0.20	3.07567	3.07638	0.09	sensor #5 - y direction

Channel	Pass #3			Pass #4			Remarks
	voltage (before)	voltage (after)	rotation (degree)	voltage (before)	voltage (after)	rotation (degree)	
0	2.46534	2.46570	0.05	2.46360	2.46534	0.22	sensor #1 - x direction
1	2.92988	2.92985	0.00	2.92819	2.92835	0.02	sensor #1 - y direction
2	2.27023	2.26961	-0.08	2.26784	2.26941	0.20	sensor #2 - x direction
3	3.05704	3.05684	-0.03	3.05490	3.05505	0.02	sensor #2 - y direction
4	2.66782	2.66850	0.09	2.66646	2.66745	0.13	sensor #3 - x direction
5	3.05088	3.05099	0.01	3.04908	3.04877	-0.04	sensor #3 - y direction
6	2.59562	2.59655	0.12	2.59445	2.59520	0.10	sensor #4 - x direction
7	3.13732	3.13721	-0.01	3.13536	3.13539	0.00	sensor #4 - y direction
8	2.52567	2.52551	-0.02	2.52400	2.52400	0.00	sensor #5 - x direction
9	3.07629	3.07649	0.03	3.07450	3.07436	-0.02	sensor #5 - y direction

Channel	Pass #5			Pass #6			Remarks
	voltage (before)	voltage (after)	rotation (degree)	voltage (before)	voltage (after)	rotation (degree)	
0	2.46518	2.46419	-0.13	2.46534	2.46565	0.04	sensor #1 - x direction
1	2.92843	2.92460	-0.49	2.92617	2.92687	0.09	sensor #1 - y direction
2	2.26917	2.27314	0.51	2.27427	2.27364	-0.08	sensor #2 - x direction
3	3.05518	3.05792	0.35	3.05956	3.05913	-0.06	sensor #2 - y direction
4	2.66754	2.66455	-0.39	2.66594	2.66668	0.09	sensor #3 - x direction
5	3.04881	3.05080	0.26	3.05238	3.05212	-0.03	sensor #3 - y direction
6	2.59511	2.59257	-0.33	2.59405	2.59447	0.05	sensor #4 - x direction
7	3.13543	3.13616	0.09	3.13775	3.13753	-0.03	sensor #4 - y direction
8	2.52380	2.52462	0.11	2.52598	2.52593	-0.01	sensor #5 - x direction
9	3.07446	3.07441	-0.01	3.07603	3.07597	-0.01	sensor #5 - y direction

A.1.4. Scraper

a) 20 in lift thickness

Channel	Pass #1			Pass #2			Remarks
	voltage (before)	voltage (after)	rotation (degree)	voltage (before)	voltage (after)	rotation (degree)	
0	1.71956	1.71710	-0.32	1.71711	1.71775	0.08	sensor #1 - x direction
1	2.51404	2.50982	-0.54	2.51113	2.51152	0.05	sensor #1 - y direction
2	3.16616	3.16584	-0.04	3.16590	3.16681	0.12	sensor #2 - x direction
3	2.46402	2.47485	1.39	2.47960	2.47262	-0.90	sensor #2 - y direction
4	3.13779	3.13450	-0.42	3.13451	3.13559	0.14	sensor #3 - x direction
5	2.50985	2.51194	0.27	2.51358	2.51212	-0.19	sensor #3 - y direction
6	3.00832	3.00082	-0.96	3.00028	3.00174	0.19	sensor #4 - x direction
7	2.49529	2.51423	2.44	2.51942	2.51726	-0.28	sensor #4 - y direction

Channel	Pass #3			Pass #4			Remarks
	voltage (before)	voltage (after)	rotation (degree)	voltage (before)	voltage (after)	rotation (degree)	
0	1.71902	1.71763	-0.18	1.71760	1.71736	-0.03	sensor #1 - x direction
1	2.51376	2.51232	-0.18	2.51195	2.51276	0.10	sensor #1 - y direction
2	3.16989	3.16703	-0.37	3.16658	3.16683	0.03	sensor #2 - x direction
3	2.47490	2.47315	-0.22	2.47280	2.46831	-0.58	sensor #2 - y direction
4	3.13851	3.13553	-0.38	3.13535	3.13446	-0.11	sensor #3 - x direction
5	2.51464	2.51295	-0.22	2.51259	2.49911	-1.73	sensor #3 - y direction
6	3.00461	3.00180	-0.36	3.00128	2.99675	-0.58	sensor #4 - x direction
7	2.51968	2.51796	-0.22	2.51777	2.50641	-1.46	sensor #4 - y direction

b) 24 in lift thickness

Channel	Pass #1			Pass #2			Remarks
	voltage (before)	voltage (after)	rotation (degree)	voltage (before)	voltage (after)	rotation (degree)	
0	3.10538	3.10114	-0.54	3.09830	3.10065	0.30	sensor #1 - x direction
1	2.49222	2.50428	1.55	2.50391	2.50710	0.41	sensor #1 - y direction
2	3.12451	3.11983	-0.60	3.11673	3.11953	0.36	sensor #2 - x direction
3	2.58437	2.59322	1.14	2.59264	2.59652	0.50	sensor #2 - y direction
4	2.65676	2.63029	-3.40	2.63094	2.63264	0.22	sensor #3 - x direction
5	2.49935	2.47532	-3.09	2.47613	2.47795	0.23	sensor #3 - y direction
6	1.93664	1.91708	-2.51	1.91882	1.91886	0.01	sensor #4 - x direction
7	2.56226	2.56022	-0.26	2.56068	2.56310	0.31	sensor #4 - y direction
8	2.53407	2.52196	-1.56	2.52243	2.52082	-0.21	sensor #5 - x direction
9	2.45359	2.44659	-0.90	2.44858	2.45319	0.59	sensor #5 - y direction

Channel	Pass #3						Remarks
	voltage (before)	voltage (after)	rotation (degree)				
0	3.10008	3.09577	-0.55				sensor #1 - x direction
1	2.50614	2.50285	-0.42				sensor #1 - y direction
2	3.11904	3.11350	-0.71				sensor #2 - x direction
3	2.59586	2.59470	-0.15				sensor #2 - y direction
4	2.63215	2.61762	-1.87				sensor #3 - x direction
5	2.47737	2.47916	0.23				sensor #3 - y direction
6	1.91856	1.90519	-1.72				sensor #4 - x direction
7	2.56263	2.56818	0.71				sensor #4 - y direction
8	2.52015	2.51563	-0.58				sensor #5 - x direction
9	2.45284	2.44041	-1.60				sensor #5 - y direction

A.2. MEMS voltage measurement (natural moisture)

A.2.1. Smooth-drum vibratory roller

a) 8 in lift thickness

Channel	Pass #1			Pass #2			Remarks
	voltage (before)	voltage (after)	rotation (degree)	voltage (before)	voltage (after)	rotation (degree)	
0	2.85348	2.87007	2.13	2.86972	2.85206	-2.27	sensor #1 - x direction
1	2.41643	2.41685	0.05	2.41682	2.41732	0.06	sensor #1 - y direction
2	2.32215	2.33566	1.74	2.33582	2.38301	6.07	sensor #2 - x direction
3	2.63019	2.63892	1.12	2.63859	2.63719	-0.18	sensor #2 - y direction
4	2.76849	2.74110	-3.52	2.74089	2.70630	-4.45	sensor #3 - x direction
5	2.60809	2.61608	1.03	2.61515	2.60193	-1.70	sensor #3 - y direction
6	3.12553	3.12375	-0.23	3.12332	3.11572	-0.98	sensor #4 - x direction
7	2.35662	2.35427	-0.30	2.35132	2.34990	-0.18	sensor #4 - y direction
8	2.39782	2.29777	-12.86	2.29751	2.30054	0.39	sensor #5 - x direction
9	2.36382	2.37470	1.40	2.37340	2.46624	11.94	sensor #5 - y direction

Channel	Pass #3			Pass #4			Remarks
	voltage (before)	voltage (after)	rotation (degree)	voltage (before)	voltage (after)	rotation (degree)	
0	2.85077	2.88093	3.88	3.11725	3.12076	0.45	sensor #1 - x direction
1	2.41801	2.41920	0.15	2.34880	2.33684	-1.54	sensor #1 - y direction
2	2.38908	2.31733	-9.22	2.29184	2.29815	0.81	sensor #2 - x direction
3	2.63776	2.62763	-1.30	2.46877	2.37532	-12.01	sensor #2 - y direction
4	2.70107	2.76570	8.31	2.56046	2.62764	8.64	sensor #3 - x direction
5	2.60238	2.58921	-1.69	2.34522	2.34795	0.35	sensor #3 - y direction
6	3.11725	3.12076	0.45	1.82365	1.75325	-9.05	sensor #4 - x direction
7	2.34880	2.33684	-1.54	2.67326	2.68477	1.48	sensor #4 - y direction
8	2.29184	2.29815	0.81	2.29981	2.30973	1.28	sensor #5 - x direction
9	2.46877	2.37532	-12.01	2.48853	2.50640	2.30	sensor #5 - y direction

Channel	Pass #5			Pass #6			Remarks
	voltage (before)	voltage (after)	rotation (degree)	voltage (before)	voltage (after)	rotation (degree)	
0	2.86465	2.88162	2.18	2.88134	2.86240	-2.43	sensor #1 - x direction
1	2.41849	2.41568	-0.36	2.41549	2.41509	-0.05	sensor #1 - y direction
2	2.35669	2.33006	-3.42	2.32996	2.36889	5.01	sensor #2 - x direction
3	2.62880	2.63315	0.56	2.63292	2.62999	-0.38	sensor #2 - y direction
4	2.72624	2.76213	4.61	2.76169	2.71582	-5.90	sensor #3 - x direction
5	2.58588	2.58597	0.01	2.58561	2.57726	-1.07	sensor #3 - y direction
6	3.11433	3.11746	0.40	3.11712	3.11504	-0.27	sensor #4 - x direction
7	2.33606	2.32472	-1.46	2.32458	2.32286	-0.22	sensor #4 - y direction
8	2.27678	2.28851	1.51	2.28838	2.44072	19.59	sensor #5 - x direction
9	2.45746	2.46806	1.36	2.46787	2.54924	10.46	sensor #5 - y direction

b) 13 in lift thickness

Channel	Pass #1			Pass #2			Remarks
	voltage (before)	voltage (after)	rotation (degree)	voltage (before)	voltage (after)	rotation (degree)	
0	2.53099	2.51150	-2.50	2.51145	2.56607	7.02	sensor #1 - x direction
1	2.47040	2.47474	0.56	2.47434	2.48307	1.12	sensor #1 - y direction
2	1.76150	1.76045	-0.13	1.76033	1.75603	-0.55	sensor #2 - x direction
3	2.38567	2.42787	5.43	2.42729	2.43891	1.49	sensor #2 - y direction
4	2.38316	2.41696	4.35	2.41667	2.37899	-4.84	sensor #3 - x direction
5	2.39117	2.41415	2.95	2.41378	2.42103	0.93	sensor #3 - y direction
6	1.76362	1.77247	1.14	1.77228	1.76091	-1.46	sensor #4 - x direction
7	2.47578	2.47871	0.38	2.47830	2.48003	0.22	sensor #4 - y direction
8	2.64575	2.63736	-1.08	2.63688	2.59559	-5.31	sensor #5 - x direction
9	2.29709	2.33682	5.11	2.33672	2.34258	0.75	sensor #5 - y direction

Channel	Pass #3			Pass #4			Remarks
	voltage (before)	voltage (after)	rotation (degree)	voltage (before)	voltage (after)	rotation (degree)	
0	2.56586	2.52271	-5.55	1.76214	1.77165	1.22	sensor #1 - x direction
1	2.48314	2.49103	1.02	2.47978	2.46925	-1.35	sensor #1 - y direction
2	1.75722	1.75830	0.14	2.59508	2.62779	4.21	sensor #2 - x direction
3	2.43915	2.44142	0.29	2.34271	2.32849	-1.83	sensor #2 - y direction
4	2.37888	2.41410	4.53	3.11650	3.12820	1.50	sensor #3 - x direction
5	2.42099	2.41330	-0.99	2.38305	2.37485	-1.05	sensor #3 - y direction
6	1.76214	1.77165	1.22	1.76780	1.78412	2.10	sensor #4 - x direction
7	2.47978	2.46925	-1.35	2.59752	2.60036	0.37	sensor #4 - y direction
8	2.59508	2.62779	4.21	2.75096	2.78504	4.38	sensor #5 - x direction
9	2.34271	2.32849	-1.83	2.54556	2.54946	0.50	sensor #5 - y direction

Channel	Pass #5			Pass #6			Remarks
	voltage (before)	voltage (after)	rotation (degree)	voltage (before)	voltage (after)	rotation (degree)	
0	2.54090	2.51577	-3.23	2.51543	2.54803	4.19	sensor #1 - x direction
1	2.49349	2.49571	0.29	2.49518	2.49609	0.12	sensor #1 - y direction
2	1.75850	1.76007	0.20	1.76001	1.75862	-0.18	sensor #2 - x direction
3	2.44632	2.44723	0.12	2.44684	2.44930	0.32	sensor #2 - y direction
4	2.40193	2.42324	2.74	2.42338	2.39175	-4.07	sensor #3 - x direction
5	2.41721	2.41802	0.10	2.41756	2.41946	0.24	sensor #3 - y direction
6	1.76791	1.77380	0.76	1.77388	1.76453	-1.20	sensor #4 - x direction
7	2.47349	2.47271	-0.10	2.47227	2.47268	0.05	sensor #4 - y direction
8	2.61169	2.63065	2.44	2.63072	2.59018	-5.21	sensor #5 - x direction
9	2.33932	2.34136	0.26	2.34105	2.33890	-0.28	sensor #5 - y direction

c) 24 in lift thickness

Channel	Pass #1			Pass #2			Remarks
	voltage (before)	voltage (after)	rotation (degree)	voltage (before)	voltage (after)	rotation (degree)	
0	2.05381	2.05366	-0.02	2.05254	2.04345	-1.17	sensor #1 - x direction
1	2.43252	2.43326	0.10	2.44341	2.44448	0.14	sensor #1 - y direction
2	2.62672	2.62498	-0.22	2.62031	2.60512	-1.95	sensor #2 - x direction
3	2.44585	2.44740	0.20	2.45569	2.45954	0.49	sensor #2 - y direction
4	2.29909	2.29978	0.09	2.29737	2.31430	2.18	sensor #3 - x direction
5	2.37825	2.37735	-0.12	2.36358	2.36811	0.58	sensor #3 - y direction
6	1.81576	1.81584	0.01	1.82064	1.81502	-0.72	sensor #4 - x direction
7	2.12937	2.12955	0.02	2.12594	2.12925	0.42	sensor #4 - y direction
8	2.63385	2.63433	0.06	2.61794	2.64354	3.29	sensor #5 - x direction
9	2.34412	2.34471	0.07	2.34089	2.34317	0.29	sensor #5 - y direction

Channel	Pass #3			Pass #4			Remarks
	voltage (before)	voltage (after)	rotation (degree)	voltage (before)	voltage (after)	rotation (degree)	
0	2.04351	2.05423	1.38	2.05404	2.04657	-0.96	sensor #1 - x direction
1	2.44529	2.44370	-0.20	2.44376	2.44372	0.00	sensor #1 - y direction
2	2.60547	2.61917	1.76	2.61841	2.60827	-1.30	sensor #2 - x direction
3	2.46035	2.45871	-0.21	2.45905	2.45948	0.05	sensor #2 - y direction
4	2.31482	2.30030	-1.87	2.30151	2.31102	1.22	sensor #3 - x direction
5	2.36879	2.36563	-0.41	2.36618	2.36766	0.19	sensor #3 - y direction
6	1.81522	1.81709	0.24	1.81713	1.81439	-0.35	sensor #4 - x direction
7	2.12935	2.12878	-0.07	2.12894	2.13068	0.22	sensor #4 - y direction
8	2.64478	2.62808	-2.15	2.62932	2.64189	1.62	sensor #5 - x direction
9	2.34388	2.34328	-0.08	2.34343	2.34399	0.07	sensor #5 - y direction

Channel	Pass #5			Pass #6			Remarks
	voltage (before)	voltage (after)	rotation (degree)	voltage (before)	voltage (after)	rotation (degree)	
0	2.04678	2.05689	1.30	2.05675	2.04728	-1.22	sensor #1 - x direction
1	2.44364	2.44400	0.05	2.44386	2.44423	0.05	sensor #1 - y direction
2	2.60866	2.62110	1.60	2.62085	2.60906	-1.52	sensor #2 - x direction
3	2.45927	2.45998	0.09	2.45969	2.46057	0.11	sensor #2 - y direction
4	2.31064	2.30047	-1.31	2.30008	2.31121	1.43	sensor #3 - x direction
5	2.36736	2.36734	0.00	2.36718	2.36952	0.30	sensor #3 - y direction
6	1.81429	1.81695	0.34	1.81693	1.81386	-0.39	sensor #4 - x direction
7	2.13084	2.13154	0.09	2.13109	2.13313	0.26	sensor #4 - y direction
8	2.64162	2.63000	-1.49	2.62970	2.64392	1.83	sensor #5 - x direction
9	2.34368	2.34508	0.18	2.34498	2.34544	0.06	sensor #5 - y direction

A.2.2. Rubber-tired roller

a) 8 in lift thickness

Channel	Pass #1			Pass #2			Remarks
	voltage (before)	voltage (after)	rotation (degree)	voltage (before)	voltage (after)	rotation (degree)	
0	2.16163	2.16522	0.46	2.16653	2.14449	-2.83	sensor #1 - x direction
1	2.45489	2.45520	0.04	2.45601	2.46273	0.86	sensor #1 - y direction
2	3.09461	3.09026	-0.56	3.08994	3.09726	0.94	sensor #2 - x direction
3	2.49406	2.48711	-0.89	2.48653	2.48721	0.09	sensor #2 - y direction
4	2.79894	2.78685	-1.55	2.78630	2.77872	-0.98	sensor #3 - x direction
5	2.65176	2.66444	1.63	2.66763	2.66651	-0.14	sensor #3 - y direction
6	1.75029	1.75174	0.19	1.75232	1.75385	0.20	sensor #4 - x direction
7	2.57112	2.55898	-1.56	2.55883	2.46609	-11.92	sensor #4 - y direction
8	2.22360	2.23052	0.89	2.23629	2.32710	11.67	sensor #5 - x direction
9	2.75388	2.75259	-0.17	2.75273	2.73266	-2.58	sensor #5 - y direction

Channel	Pass #3			Pass #4			Remarks
	voltage (before)	voltage (after)	rotation (degree)	voltage (before)	voltage (after)	rotation (degree)	
0	2.14453	2.14383	-0.09	2.14443	2.14883	0.57	sensor #1 - x direction
1	2.46297	2.46336	0.05	2.46357	2.47107	0.96	sensor #1 - y direction
2	3.09733	3.09749	0.02	3.09785	3.09291	-0.63	sensor #2 - x direction
3	2.48749	2.48756	0.01	2.48776	2.52461	4.74	sensor #2 - y direction
4	2.77883	2.77878	-0.01	2.77909	2.76480	-1.84	sensor #3 - x direction
5	2.66673	2.66705	0.04	2.66724	2.68508	2.29	sensor #3 - y direction
6	1.75389	1.75391	0.00	1.75446	1.76227	1.00	sensor #4 - x direction
7	2.46631	2.46651	0.03	2.46669	2.52203	7.12	sensor #4 - y direction
8	2.32727	2.32800	0.09	2.32814	2.32348	-0.60	sensor #5 - x direction
9	2.73291	2.73446	0.20	2.73516	2.66168	-9.45	sensor #5 - y direction

Channel	Pass #5			Pass #6			Remarks
	voltage (before)	voltage (after)	rotation (degree)	voltage (before)	voltage (after)	rotation (degree)	
0	2.14880	2.14766	-0.15	2.14524	2.13232	-1.66	sensor #1 - x direction
1	2.47115	2.47078	-0.05	2.47422	2.47329	-0.12	sensor #1 - y direction
2	3.09308	3.09309	0.00	3.09361	3.10213	1.10	sensor #2 - x direction
3	2.52476	2.52337	-0.18	2.53060	2.52790	-0.35	sensor #2 - y direction
4	2.76500	2.76487	-0.02	2.76201	2.78346	2.76	sensor #3 - x direction
5	2.68534	2.68443	-0.12	2.68275	2.68591	0.41	sensor #3 - y direction
6	1.76248	1.76232	-0.02	1.76386	1.76227	-0.20	sensor #4 - x direction
7	2.52193	2.51875	-0.41	2.51925	2.53053	1.45	sensor #4 - y direction
8	2.32355	2.32057	-0.38	2.37097	2.35384	-2.20	sensor #5 - x direction
9	2.66203	2.66018	-0.24	2.64947	2.67841	3.72	sensor #5 - y direction

b) 13 in lift thickness

Channel	Pass #1			Pass #2			Remarks
	voltage (before)	voltage (after)	rotation (degree)	voltage (before)	voltage (after)	rotation (degree)	
0	2.36181	2.36177	0.00	2.37643	2.39574	2.48	sensor #1 - x direction
1	2.37932	2.37880	-0.07	2.41259	2.41186	-0.09	sensor #1 - y direction
2	1.87599	1.87584	-0.02	1.87583	1.86319	-1.62	sensor #2 - x direction
3	2.35255	2.35252	0.00	2.40064	2.40606	0.70	sensor #2 - y direction
4	2.94258	2.94218	-0.05	2.93452	2.94787	1.72	sensor #3 - x direction
5	2.43160	2.43146	-0.02	2.51098	2.52450	1.74	sensor #3 - y direction
6	1.81317	1.81273	-0.06	1.80547	1.79800	-0.96	sensor #4 - x direction
7	2.33467	2.33445	-0.03	2.44829	2.47011	2.81	sensor #4 - y direction
8	2.94988	2.94960	-0.04	2.93212	2.91312	-2.44	sensor #5 - x direction
9	2.55803	2.55750	-0.07	2.64424	2.67704	4.22	sensor #5 - y direction

Channel	Pass #3			Pass #4			Remarks
	voltage (before)	voltage (after)	rotation (degree)	voltage (before)	voltage (after)	rotation (degree)	
0	2.39547	2.33763	-7.44	2.33848	2.35828	2.55	sensor #1 - x direction
1	2.41192	2.41989	1.03	2.42069	2.43057	1.27	sensor #1 - y direction
2	1.86295	1.88888	3.33	1.88936	1.87643	-1.66	sensor #2 - x direction
3	2.40596	2.37828	-3.56	2.37914	2.37474	-0.57	sensor #2 - y direction
4	2.94770	2.90554	-5.42	2.90621	2.92251	2.10	sensor #3 - x direction
5	2.52420	2.45481	-8.92	2.45546	2.44006	-1.98	sensor #3 - y direction
6	1.79801	1.81581	2.29	1.81625	1.81115	-0.66	sensor #4 - x direction
7	2.46994	2.40072	-8.90	2.40158	2.36612	-4.56	sensor #4 - y direction
8	2.91296	2.95262	5.10	2.95350	2.94546	-1.03	sensor #5 - x direction
9	2.67710	2.55540	-15.65	2.55603	2.50738	-6.26	sensor #5 - y direction

Channel	Pass #5			Pass #6			Remarks
	voltage (before)	voltage (after)	rotation (degree)	voltage (before)	voltage (after)	rotation (degree)	
0	2.35785	2.35536	-0.32	2.35554	2.38262	3.48	sensor #1 - x direction
1	2.43039	2.43317	0.36	2.43324	2.43836	0.66	sensor #1 - y direction
2	1.87631	1.87779	0.19	1.87786	1.86835	-1.22	sensor #2 - x direction
3	2.37451	2.37351	-0.13	2.37369	2.39296	2.48	sensor #2 - y direction
4	2.92191	2.92218	0.03	2.92242	2.93784	1.98	sensor #3 - x direction
5	2.43998	2.44790	1.02	2.44814	2.47331	3.24	sensor #3 - y direction
6	1.81105	1.80934	-0.22	1.80934	1.79548	-1.78	sensor #4 - x direction
7	2.36578	2.38282	2.19	2.38314	2.40848	3.26	sensor #4 - y direction
8	2.94509	2.94240	-0.35	2.94254	2.92076	-2.80	sensor #5 - x direction
9	2.50718	2.53537	3.62	2.53548	2.55126	2.03	sensor #5 - y direction

c) 20 in lift thickness

Channel	Pass #1			Pass #2			Remarks
	voltage (before)	voltage (after)	rotation (degree)	voltage (before)	voltage (after)	rotation (degree)	
0	3.06883	3.04836	-2.63	3.04774	3.04419	-0.46	sensor #1 - x direction
1	2.47879	2.48599	0.93	2.48563	2.50039	1.90	sensor #1 - y direction
2	2.72061	2.66275	-7.44	2.66233	2.68046	2.33	sensor #2 - x direction
3	2.51018	2.51268	0.32	2.51237	2.52823	2.04	sensor #2 - y direction
4	2.86887	2.85731	-1.49	2.85706	2.83906	-2.32	sensor #3 - x direction
5	2.58852	2.60622	2.27	2.60569	2.61196	0.81	sensor #3 - y direction
6	1.75592	1.75448	-0.18	1.75450	1.76206	0.97	sensor #4 - x direction
7	2.29897	2.32265	3.04	2.32235	2.30601	-2.10	sensor #4 - y direction
8	1.93592	1.94557	1.24	1.94518	1.96399	2.42	sensor #5 - x direction
9	2.43319	2.48786	7.03	2.48742	2.42846	-7.58	sensor #5 - y direction

Channel	Pass #3			Pass #4			Remarks
	voltage (before)	voltage (after)	rotation (degree)	voltage (before)	voltage (after)	rotation (degree)	
0	3.04369	3.04671	0.39	3.04720	3.04434	-0.37	sensor #1 - x direction
1	2.50057	2.50191	0.17	2.50205	2.50455	0.32	sensor #1 - y direction
2	2.68005	2.68525	0.67	2.68569	2.68308	-0.34	sensor #2 - x direction
3	2.52821	2.52875	0.07	2.52907	2.53359	0.58	sensor #2 - y direction
4	2.83888	2.84223	0.43	2.84255	2.83583	-0.86	sensor #3 - x direction
5	2.61160	2.61590	0.55	2.61624	2.61420	-0.26	sensor #3 - y direction
6	1.76185	1.76161	-0.03	1.76198	1.76443	0.32	sensor #4 - x direction
7	2.30564	2.30578	0.02	2.30627	2.30467	-0.21	sensor #4 - y direction
8	1.96389	1.96057	-0.43	1.96087	1.97086	1.28	sensor #5 - x direction
9	2.42844	2.43628	1.01	2.43648	2.42138	-1.94	sensor #5 - y direction

Channel	Pass #5			Pass #6			Remarks
	voltage (before)	voltage (after)	rotation (degree)	voltage (before)	voltage (after)	rotation (degree)	
0	3.04412	3.05251	1.08	3.05149	3.04814	-0.43	sensor #1 - x direction
1	2.50464	2.49880	-0.75	2.49821	2.50352	0.68	sensor #1 - y direction
2	2.68299	2.70017	2.21	2.69930	2.69508	-0.54	sensor #2 - x direction
3	2.53345	2.53075	-0.35	2.53017	2.53281	0.34	sensor #2 - y direction
4	2.83568	2.85989	3.11	2.85895	2.84815	-1.39	sensor #3 - x direction
5	2.61428	2.60703	-0.93	2.60635	2.61333	0.90	sensor #3 - y direction
6	1.76434	1.75746	-0.88	1.75733	1.75992	0.33	sensor #4 - x direction
7	2.30466	2.30812	0.44	2.30757	2.30864	0.14	sensor #4 - y direction
8	1.97064	1.94706	-3.03	1.94684	1.95614	1.20	sensor #5 - x direction
9	2.42136	2.42118	-0.02	2.42074	2.42268	0.25	sensor #5 - y direction

A.2.3. Scraper

a) 13 in lift thickness

Channel	Pass #1			Pass #2			Remarks
	voltage (before)	voltage (after)	rotation (degree)	voltage (before)	voltage (after)	rotation (degree)	
0	2.85256	2.92927	9.86	2.92926	2.92764	-0.21	sensor #1 - x direction
1	2.45991	2.44209	-2.29	2.44278	2.44468	0.24	sensor #1 - y direction
2	2.07310	2.02843	-5.74	2.02842	2.02999	0.20	sensor #2 - x direction
3	2.54247	2.56423	2.80	2.56444	2.56721	0.36	sensor #2 - y direction
4	2.42574	2.38898	-4.73	2.38894	2.39016	0.16	sensor #3 - x direction
5	2.46597	2.46471	-0.16	2.46500	2.46754	0.33	sensor #3 - y direction
6	1.82399	1.80923	-1.90	1.80882	1.80910	0.04	sensor #4 - x direction
7	2.40053	2.33631	-8.26	2.33670	2.33883	0.27	sensor #4 - y direction
8	2.04600	2.05107	0.65	2.05085	2.05003	-0.11	sensor #5 - x direction
9	2.36787	2.29524	-9.34	2.29576	2.29823	0.32	sensor #5 - y direction

Channel	Pass #3			Pass #4			Remarks
	voltage (before)	voltage (after)	rotation (degree)	voltage (before)	voltage (after)	rotation (degree)	
0	missing	-	-	2.92396	2.92991	0.77	sensor #1 - x direction
1	-	-	-	2.44934	2.47238	2.96	sensor #1 - y direction
2	-	-	-	2.03353	2.02860	-0.63	sensor #2 - x direction
3	-	-	-	2.58655	2.61205	3.28	sensor #2 - y direction
4	-	-	-	2.39111	2.37441	-2.15	sensor #3 - x direction
5	-	-	-	2.48351	2.47263	-1.40	sensor #3 - y direction
6	-	-	-	1.80890	1.90257	12.04	sensor #4 - x direction
7	-	-	-	2.35581	2.03240	-41.58	sensor #4 - y direction
8	-	-	-	2.04841	2.11615	8.71	sensor #5 - x direction
9	-	-	-	2.31315	2.35174	4.96	sensor #5 - y direction

Channel	Pass #5			Pass #6			Remarks
	voltage (before)	voltage (after)	rotation (degree)	voltage (before)	voltage (after)	rotation (degree)	
0	2.92958	2.90052	-3.74	2.90086	2.92323	2.88	sensor #1 - x direction
1	2.47167	2.43114	-5.21	2.43139	2.45001	2.39	sensor #1 - y direction
2	2.02820	2.03701	1.13	2.03747	1.99388	-5.61	sensor #2 - x direction
3	2.61062	2.55437	-7.23	2.55444	2.55510	0.09	sensor #2 - y direction
4	2.37450	2.39260	2.33	2.39266	2.32122	-9.19	sensor #3 - x direction
5	2.47151	2.41873	-6.79	2.41913	2.45068	4.06	sensor #3 - y direction
6	1.90327	1.90436	0.14	1.90421	1.82697	-9.93	sensor #4 - x direction
7	2.03133	2.04397	1.63	2.04410	2.19136	18.93	sensor #4 - y direction
8	2.11585	2.19364	10.00	2.19375	2.17864	-1.94	sensor #5 - x direction
9	2.34979	2.08413	-34.16	2.08457	2.32318	30.68	sensor #5 - y direction

b) 23 in lift thickness

Channel	Pass #1			Pass #2			Remarks
	voltage (before)	voltage (after)	rotation (degree)	voltage (before)	voltage (after)	rotation (degree)	
0	1.87017	1.87937	1.18	1.87917	1.87350	-0.73	sensor #1 - x direction
1	2.50524	2.50812	0.37	2.50798	2.52169	1.76	sensor #1 - y direction
2	2.53432	2.51137	-2.95	2.51106	2.51445	0.44	sensor #2 - x direction
3	2.66487	2.63056	-4.41	2.63040	2.64218	1.52	sensor #2 - y direction
4	2.74886	2.69086	-7.46	2.69064	2.68452	-0.79	sensor #3 - x direction
5	2.73028	2.70122	-3.74	2.70073	2.72339	2.91	sensor #3 - y direction
6	1.86656	1.82109	-5.85	1.82095	1.82552	0.59	sensor #4 - x direction
7	2.44072	2.46673	3.34	2.46665	2.48838	2.79	sensor #4 - y direction
8	3.10100	3.13189	3.97	3.13159	3.12554	-0.78	sensor #5 - x direction
9	2.53535	2.49745	-4.87	2.49731	2.52550	3.62	sensor #5 - y direction

Channel	Pass #3			Pass #4			Remarks
	voltage (before)	voltage (after)	rotation (degree)	voltage (before)	voltage (after)	rotation (degree)	
0	1.87344	1.87509	0.21	missing	-	-	sensor #1 - x direction
1	2.52194	2.50927	-1.63	-	-	-	sensor #1 - y direction
2	2.51441	2.50817	-0.80	-	-	-	sensor #2 - x direction
3	2.64245	2.61975	-2.92	-	-	-	sensor #2 - y direction
4	2.68464	2.67697	-0.99	-	-	-	sensor #3 - x direction
5	2.72351	2.69871	-3.19	-	-	-	sensor #3 - y direction
6	1.82547	1.81756	-1.02	-	-	-	sensor #4 - x direction
7	2.48862	2.46104	-3.55	-	-	-	sensor #4 - y direction
8	3.12570	3.13642	1.38	-	-	-	sensor #5 - x direction
9	2.52558	2.49149	-4.38	-	-	-	sensor #5 - y direction

Channel	Pass #5			Pass #6			Remarks
	voltage (before)	voltage (after)	rotation (degree)	voltage (before)	voltage (after)	rotation (degree)	
0	1.87529	1.87467	-0.08	1.87478	1.87287	-0.25	sensor #1 - x direction
1	2.50929	2.51698	0.99	2.51703	2.52375	0.86	sensor #1 - y direction
2	2.50832	2.50828	0.00	2.50833	2.50551	-0.36	sensor #2 - x direction
3	2.61982	2.62765	1.01	2.62792	2.63495	0.90	sensor #2 - y direction
4	2.67693	2.67470	-0.29	2.67477	2.67015	-0.59	sensor #3 - x direction
5	2.69886	2.70650	0.98	2.70637	2.71680	1.34	sensor #3 - y direction
6	1.81740	1.81822	0.11	1.81826	1.81871	0.06	sensor #4 - x direction
7	2.46130	2.46954	1.06	2.46970	2.48072	1.42	sensor #4 - y direction
8	3.13625	3.13506	-0.15	3.13504	3.13261	-0.31	sensor #5 - x direction
9	2.49167	2.50052	1.14	2.50071	2.51467	1.79	sensor #5 - y direction

A.3. MEMS voltage measurement (wet condition moisture)

A.3.1. Smooth-drum vibratory roller

a) 8 in lift thickness

Channel	Pass #1			Pass #2			Remarks
	voltage (before)	voltage (after)	rotation (degree)	voltage (before)	voltage (after)	rotation (degree)	
0	2.00436	2.01038	0.77	2.01038	2.07544	8.36	sensor #1 - x direction
1	2.48845	2.50981	2.75	2.50981	2.50173	-1.04	sensor #1 - y direction
2	2.98968	2.87005	-15.38	2.87005	2.90519	4.52	sensor #2 - x direction
3	2.55740	2.57549	2.33	2.57549	2.55945	-2.06	sensor #2 - y direction
4	2.61684	2.64370	3.45	2.64370	2.81018	21.41	sensor #3 - x direction
5	2.39674	2.42723	3.92	2.42723	2.42327	-0.51	sensor #3 - y direction
6	2.60579	2.73027	16.00	2.73027	2.89581	21.28	sensor #4 - x direction
7	2.13931	2.22285	10.74	2.22285	2.28973	8.60	sensor #4 - y direction
8	2.26017	2.27627	2.07	2.27627	2.30625	3.85	sensor #5 - x direction
9	3.24792	2.43042	-105.11	2.43042	2.41257	-2.29	sensor #5 - y direction

Channel	Pass #3			Pass #4			Remarks
	voltage (before)	voltage (after)	rotation (degree)	voltage (before)	voltage (after)	rotation (degree)	
0	2.07566	2.05405	-2.78	2.05405	2.14545	11.75	sensor #1 - x direction
1	2.50242	2.49722	-0.67	2.49722	2.50148	0.55	sensor #1 - y direction
2	2.90570	2.94639	5.23	2.94639	2.91898	-3.52	sensor #2 - x direction
3	2.56015	2.57324	1.68	2.57324	2.57155	-0.22	sensor #2 - y direction
4	2.81115	2.76003	-6.57	2.76003	2.83239	9.30	sensor #3 - x direction
5	2.42411	2.41068	-1.73	2.41068	2.43916	3.66	sensor #3 - y direction
6	2.89731	2.87970	-2.26	2.87970	2.88608	0.82	sensor #4 - x direction
7	2.29028	2.29207	0.23	2.29207	2.31399	2.82	sensor #4 - y direction
8	2.30639	2.30147	-0.63	2.30147	2.31383	1.59	sensor #5 - x direction
9	2.40785	2.46114	6.85	2.46114	2.45129	-1.27	sensor #5 - y direction

Channel	Pass #5			Pass #6			Remarks
	voltage (before)	voltage (after)	rotation (degree)	voltage (before)	voltage (after)	rotation (degree)	
0	2.14579	2.15947	1.76	2.15947	2.23338	9.50	sensor #1 - x direction
1	2.50097	2.49888	-0.27	2.49888	2.49468	-0.54	sensor #1 - y direction
2	2.91851	2.95215	4.33	2.95215	2.92105	-4.00	sensor #2 - x direction
3	2.57122	2.57728	0.78	2.57728	2.56728	-1.29	sensor #2 - y direction
4	2.83236	2.80193	-3.91	2.80193	2.84537	5.59	sensor #3 - x direction
5	2.43934	2.41904	-2.61	2.41904	2.40505	-1.80	sensor #3 - y direction
6	2.88628	2.86362	-2.91	2.86362	2.88618	2.90	sensor #4 - x direction
7	2.31422	2.29162	-2.91	2.29162	2.30175	1.30	sensor #4 - y direction
8	2.31291	2.30496	-1.02	2.30496	2.31387	1.15	sensor #5 - x direction
9	2.45095	2.43962	-1.46	2.43962	2.41273	-3.46	sensor #5 - y direction

b) 13 in lift thickness

Channel	Pass #1			Pass #2			Remarks
	voltage (before)	voltage (after)	rotation (degree)	voltage (before)	voltage (after)	rotation (degree)	
0	2.49741	2.49136	-0.78	2.49136	2.50068	1.20	sensor #1 - x direction
1	2.39584	2.40396	1.04	2.40396	2.40377	-0.02	sensor #1 - y direction
2	3.11312	3.12931	2.08	3.12931	3.12121	-1.04	sensor #2 - x direction
3	2.31553	2.34011	3.16	2.34011	2.34815	1.03	sensor #2 - y direction
4	3.10639	3.08483	-2.77	3.08483	3.09331	1.09	sensor #3 - x direction
5	2.50623	2.48475	-2.76	2.48475	2.47334	-1.47	sensor #3 - y direction
6	1.78219	1.76386	-2.36	1.76386	1.76723	0.43	sensor #4 - x direction
7	2.42267	2.42881	0.79	2.42881	2.43411	0.68	sensor #4 - y direction

Channel	Pass #3			Pass #4			Remarks
	voltage (before)	voltage (after)	rotation (degree)	voltage (before)	voltage (after)	rotation (degree)	
0	2.50044	2.49274	-0.99	2.49274	2.50160	1.14	sensor #1 - x direction
1	2.40363	2.40710	0.45	2.40710	2.40694	-0.02	sensor #1 - y direction
2	3.12223	3.12928	0.91	3.12928	3.12282	-0.83	sensor #2 - x direction
3	2.34783	2.35256	0.61	2.35256	2.35958	0.90	sensor #2 - y direction
4	3.09363	3.08874	-0.63	3.08874	3.09507	0.82	sensor #3 - x direction
5	2.47313	2.46878	-0.56	2.46878	2.46743	-0.17	sensor #3 - y direction
6	1.76636	1.76337	-0.38	1.76337	1.76770	0.56	sensor #4 - x direction
7	2.43389	2.42715	-0.87	2.42715	2.42897	0.23	sensor #4 - y direction

Channel	Pass #5			Pass #6			Remarks
	voltage (before)	voltage (after)	rotation (degree)	voltage (before)	voltage (after)	rotation (degree)	
0	2.49996	2.49381	-0.79	2.49381	2.50273	1.15	sensor #1 - x direction
1	2.40662	2.40917	0.33	2.40917	2.40882	-0.04	sensor #1 - y direction
2	3.12332	3.12698	0.47	3.12698	3.12470	-0.29	sensor #2 - x direction
3	2.35976	2.36357	0.49	2.36357	2.36788	0.55	sensor #2 - y direction
4	3.09378	3.08698	-0.87	3.08698	3.09579	1.13	sensor #3 - x direction
5	2.46674	2.46462	-0.27	2.46462	2.46571	0.14	sensor #3 - y direction
6	1.76757	1.76574	-0.24	1.76574	1.76861	0.37	sensor #4 - x direction
7	2.42855	2.42384	-0.61	2.42384	2.42861	0.61	sensor #4 - y direction

c) 20 in lift thickness

Channel	Pass #1			Pass #2			Remarks
	voltage (before)	voltage (after)	rotation (degree)	voltage (before)	voltage (after)	rotation (degree)	
0	2.98313	2.96933	-1.77	2.96933	2.97471	0.69	sensor #1 - x direction
1	2.44450	2.43800	-0.84	2.43800	2.44091	0.37	sensor #1 - y direction
2	3.10634	3.11173	0.69	3.11173	3.10261	-1.17	sensor #2 - x direction
3	2.41921	2.43418	1.93	2.43418	2.43553	0.17	sensor #2 - y direction
4	3.13252	3.13639	0.50	3.13639	3.13625	-0.02	sensor #3 - x direction
5	2.36085	2.37298	1.56	2.37298	2.37661	0.47	sensor #3 - y direction
6	3.02838	3.03811	1.25	3.03811	3.04079	0.35	sensor #4 - x direction
7	2.28202	2.28559	0.46	2.28559	2.28218	-0.44	sensor #4 - y direction
8	1.90594	1.91830	1.59	1.91830	1.93005	1.51	sensor #5 - x direction
9	2.33430	2.33523	0.12	2.33523	2.33158	-0.47	sensor #5 - y direction

Channel	Pass #3			Pass #4			Remarks
	voltage (before)	voltage (after)	rotation (degree)	voltage (before)	voltage (after)	rotation (degree)	
0	2.97578	2.96966	-0.79	2.96966	2.97296	0.42	sensor #1 - x direction
1	2.44125	2.43779	-0.45	2.43779	2.44180	0.52	sensor #1 - y direction
2	3.10369	3.11036	0.86	3.11036	3.10160	-1.13	sensor #2 - x direction
3	2.43614	2.44032	0.54	2.44032	2.44090	0.07	sensor #2 - y direction
4	3.13708	3.13656	-0.07	3.13656	3.13622	-0.04	sensor #3 - x direction
5	2.37725	2.37753	0.04	2.37753	2.38171	0.54	sensor #3 - y direction
6	3.04189	3.03306	-1.14	3.03306	3.03679	0.48	sensor #4 - x direction
7	2.28269	2.27822	-0.58	2.27822	2.27770	-0.07	sensor #4 - y direction
8	1.93039	1.91852	-1.53	1.91852	1.93310	1.87	sensor #5 - x direction
9	2.33205	2.33048	-0.20	2.33048	2.33070	0.03	sensor #5 - y direction

Channel	Pass #5			Pass #6			Remarks
	voltage (before)	voltage (after)	rotation (degree)	voltage (before)	voltage (after)	rotation (degree)	
0	2.97334	2.96946	-0.50	2.96946	2.97133	0.24	sensor #1 - x direction
1	2.44128	2.43941	-0.24	2.43941	2.44201	0.33	sensor #1 - y direction
2	3.10212	3.10758	0.70	3.10758	3.10244	-0.66	sensor #2 - x direction
3	2.44062	2.44289	0.29	2.44289	2.44265	-0.03	sensor #2 - y direction
4	3.13636	3.13723	0.11	3.13723	3.13692	-0.04	sensor #3 - x direction
5	2.38146	2.38297	0.19	2.38297	2.38345	0.06	sensor #3 - y direction
6	3.03703	3.03096	-0.78	3.03096	3.03433	0.43	sensor #4 - x direction
7	2.27755	2.27819	0.08	2.27819	2.27509	-0.40	sensor #4 - y direction
8	1.93299	1.91951	-1.73	1.91951	1.93117	1.50	sensor #5 - x direction
9	2.33061	2.33246	0.24	2.33246	2.33119	-0.16	sensor #5 - y direction

A.3.2. Rubber-tired roller

a) 13 in lift thickness

Channel	Pass #1			Pass #2			Remarks
	voltage (before)	voltage (after)	rotation (degree)	voltage (before)	voltage (after)	rotation (degree)	
0	2.81079	2.83735	3.42	2.83618	2.85118	1.93	sensor #1 - x direction
1	2.50990	2.51929	1.21	2.52225	2.51350	-1.13	sensor #1 - y direction
2	1.76386	1.76747	0.46	1.76739	1.76395	-0.44	sensor #2 - x direction
3	2.43126	2.43070	-0.07	2.43054	2.43152	0.13	sensor #2 - y direction
4	3.07894	3.08865	1.25	3.08817	3.08614	-0.26	sensor #3 - x direction
5	2.48900	2.45478	-4.40	2.45462	2.46225	0.98	sensor #3 - y direction
6	3.07584	3.06649	-1.20	3.06634	3.07248	0.79	sensor #4 - x direction
7	2.32216	2.25800	-8.25	2.25791	2.32539	8.68	sensor #4 - y direction
8	1.77661	1.78787	1.45	1.78783	1.76433	-3.02	sensor #5 - x direction
9	2.24869	2.19290	-7.17	2.19279	2.27488	10.55	sensor #5 - y direction

Channel	Pass #3			Pass #4			Remarks
	voltage (before)	voltage (after)	rotation (degree)	voltage (before)	voltage (after)	rotation (degree)	
0	2.85145	2.84648	-0.64	2.84504	2.85509	1.29	sensor #1 - x direction
1	2.51312	2.51643	0.43	2.51594	2.51135	-0.59	sensor #1 - y direction
2	1.76429	1.76518	0.11	1.76683	1.76291	-0.50	sensor #2 - x direction
3	2.43207	2.43498	0.37	2.43947	2.44069	0.16	sensor #2 - y direction
4	3.08671	3.08775	0.13	3.08752	3.08379	-0.48	sensor #3 - x direction
5	2.46269	2.47279	1.30	2.47739	2.47451	-0.37	sensor #3 - y direction
6	3.07332	3.07481	0.19	3.07803	3.07422	-0.49	sensor #4 - x direction
7	2.32579	2.32923	0.44	2.35419	2.35896	0.61	sensor #4 - y direction
8	1.76455	1.76280	-0.22	1.75423	1.75326	-0.12	sensor #5 - x direction
9	2.27568	2.27960	0.50	2.30823	2.31406	0.75	sensor #5 - y direction

Channel	Pass #5			Pass #6			Remarks
	voltage (before)	voltage (after)	rotation (degree)	voltage (before)	voltage (after)	rotation (degree)	
0	2.85576	2.85066	-0.66	2.84881	2.84705	-0.23	sensor #1 - x direction
1	2.51264	2.50946	-0.41	2.51171	2.51270	0.13	sensor #1 - y direction
2	1.76292	1.76465	0.22	1.76465	1.76483	0.02	sensor #2 - x direction
3	2.44070	2.44155	0.11	2.44136	2.43561	-0.74	sensor #2 - y direction
4	3.08383	3.08994	0.79	3.08999	3.08892	-0.14	sensor #3 - x direction
5	2.47444	2.48078	0.81	2.48069	2.47795	-0.35	sensor #3 - y direction
6	3.07420	3.07980	0.72	3.07975	3.07761	-0.27	sensor #4 - x direction
7	2.35878	2.36533	0.84	2.36539	2.35251	-1.66	sensor #4 - y direction
8	1.75345	1.74957	-0.50	1.74962	1.75176	0.28	sensor #5 - x direction
9	2.31414	2.32317	1.16	2.32299	2.31217	-1.39	sensor #5 - y direction

b) 23 in lift thickness

Channel	Pass #1			Pass #2			Remarks
	voltage (before)	voltage (after)	rotation (degree)	voltage (before)	voltage (after)	rotation (degree)	
0	1.85336	1.85847	0.66	1.85895	1.86559	0.85	sensor #1 - x direction
1	2.40376	2.40381	0.01	2.40433	2.40947	0.66	sensor #1 - y direction
2	2.91989	2.93272	1.65	2.93359	2.93988	0.81	sensor #2 - x direction
3	2.41732	2.43226	1.92	2.43281	2.43964	0.88	sensor #2 - y direction
4	3.10064	3.09342	-0.93	3.09400	3.09034	-0.47	sensor #3 - x direction
5	2.34434	2.37761	4.28	2.37815	2.42010	5.39	sensor #3 - y direction
6	2.98364	2.96969	-1.79	2.96027	2.95860	-0.22	sensor #4 - x direction
7	2.39994	2.40730	0.95	2.40037	2.41940	2.45	sensor #4 - y direction
8	2.71995	2.70583	-1.82	2.70629	2.70254	-0.48	sensor #5 - x direction
9	2.64677	2.69446	6.13	2.69515	2.67723	-2.30	sensor #5 - y direction

Channel	Pass #3			Pass #4			Remarks
	voltage (before)	voltage (after)	rotation (degree)	voltage (before)	voltage (after)	rotation (degree)	
0	1.86432	1.86193	-0.31	1.86202	1.86977	1.00	sensor #1 - x direction
1	2.40805	2.41201	0.51	2.41259	2.40278	-1.26	sensor #1 - y direction
2	2.93790	2.93780	-0.01	2.93825	2.94353	0.68	sensor #2 - x direction
3	2.43825	2.44398	0.74	2.44435	2.45173	0.95	sensor #2 - y direction
4	3.08864	3.09180	0.41	3.09227	3.08644	-0.75	sensor #3 - x direction
5	2.41875	2.42374	0.64	2.42396	2.44029	2.10	sensor #3 - y direction
6	2.95806	2.96112	0.39	2.94267	2.94973	0.91	sensor #4 - x direction
7	2.41925	2.42933	1.30	2.41507	2.45132	4.66	sensor #4 - y direction
8	2.70089	2.70383	0.38	2.70422	2.67956	-3.17	sensor #5 - x direction
9	2.67589	2.69536	2.50	2.69574	2.69255	-0.41	sensor #5 - y direction

Channel	Pass #5			Pass #6			Remarks
	voltage (before)	voltage (after)	rotation (degree)	voltage (before)	voltage (after)	rotation (degree)	
0	1.87077	1.86692	-0.50	1.86679	1.86879	0.26	sensor #1 - x direction
1	2.40436	2.40373	-0.08	2.40553	2.40337	-0.28	sensor #1 - y direction
2	2.94600	2.94256	-0.44	2.94280	2.94616	0.43	sensor #2 - x direction
3	2.45367	2.45015	-0.45	2.45035	2.45664	0.81	sensor #2 - y direction
4	3.08910	3.09146	0.30	3.09148	3.08941	-0.27	sensor #3 - x direction
5	2.44245	2.42648	-2.05	2.42684	2.44311	2.09	sensor #3 - y direction
6	2.95312	2.95589	0.36	2.95590	2.95112	-0.62	sensor #4 - x direction
7	2.45383	2.44548	-1.07	2.44569	2.46244	2.15	sensor #4 - y direction
8	2.68177	2.68266	0.11	2.68284	2.67475	-1.04	sensor #5 - x direction
9	2.69489	2.70282	1.02	2.70283	2.70083	-0.26	sensor #5 - y direction

APPENDIX B: MEMS ACCELEROMETER ROTATION MEASUREMENTS

B.1. MEMS rotation angle measurement in the fine-grained soil (natural moisture)

B.1.1. Smooth-drum vibratory roller

a) 12 in lift thickness

depth (in)	rotation: pass 1		rotation: pass 2		rotation: pass 3		rotation: pass 4		rotation: pass 5		rotation: pass 6	
	x (deg)	y (deg)										
6.0	-0.83	-0.03	1.69	-1.10	0.03	0.10	-0.22	0.47	-2.16	1.17	3.38	-2.52
8.0	-0.59	-0.71	1.53	-0.39	0.02	0.03	-0.28	-0.25	-2.52	-0.26	3.58	-0.13
8.0	-0.67	-0.62	0.74	-0.83	0.02	0.10	-0.15	-1.24	-1.29	1.21	1.42	0.22
10.0	0.67	-0.72	-1.91	-0.71	0.11	0.06	-0.42	-0.58	3.32	0.02	-3.06	-0.23
12.0	-0.82	-0.39	-1.35	0.57	0.12	0.01	-0.29	-0.01	1.14	-0.56	-2.19	0.45

b) 17 in lift thickness

depth (in)	rotation: pass 1		rotation: pass 2		rotation: pass 3		rotation: pass 4		rotation: pass 5		rotation: pass 6	
	x (deg)	y (deg)										
9.5	-0.25	0.04	0.10	0.09	-0.56	-2.01	0.07	2.20	0.14	0.06	-0.02	0.02
11.5	0.04	-1.20	-0.05	-0.85	-0.41	-1.17	-0.17	0.50	0.19	0.20	-0.05	0.17
13.0	-0.15	-0.46	0.07	-0.25	-0.57	-0.54	0.10	0.48	0.16	0.11	0.01	0.10
15.0	-0.15	0.70	-1.22	0.87	-0.12	-0.54	-0.71	0.52	0.22	0.25	-0.10	0.06
17.0	-0.02	0.96	-0.05	1.41	-0.37	0.06	-0.07	0.75	0.17	0.13	-0.06	0.07

c) 24 in lift thickness

depth (in)	rotation: pass 1		rotation: pass 2		rotation: pass 3		rotation: pass 4		rotation: pass 5		rotation: pass 6	
	x (deg)	y (deg)										
17.8	-0.22	-0.05	0.02	0.03	0.27	-0.01	-0.25	0.03	0.02	0.02	-0.27	-0.18
19.3	-0.17	0.37	-0.09	0.14	0.07	0.52	-0.14	-0.15	0.02	0.06	-0.15	-0.04
20.8	0.08	0.00	-0.13	-0.32	0.36	0.06	-0.35	-0.09	0.17	-0.03	-0.39	-0.05
22.3	0.06	-0.01	0.14	0.08	0.20	0.00	-0.22	-0.01	0.18	-0.02	-0.18	0.04
24.0	-0.02	0.00	0.07	0.30	0.14	0.09	-0.18	0.08	0.10	0.08	-0.16	0.07

B.1.2. Rubber-tired roller

a) 11 in lift thickness

depth (in)	rotation: pass 1		rotation: pass 2		rotation: pass 3		rotation: pass 4		rotation: pass 5		rotation: pass 6	
	x (deg)	y (deg)										
6.5	-0.16	-3.65	0.07	0.37	-0.11	1.73	-0.08	0.20	-0.05	-2.92	0.18	0.20
8.0	0.16	-1.40	0.08	0.29	-0.22	1.05	0.00	0.24	0.20	-1.60	0.16	0.21
9.5	0.49	-1.69	0.09	0.16	-0.05	0.83	-0.03	0.37	0.24	-1.26	0.18	0.18
11.0	-2.75	-2.52	0.17	0.33	-0.32	-1.11	-0.24	0.53	0.21	-0.27	-0.09	0.00

b) 20 in lift thickness

depth (in)	rotation: pass 1		rotation: pass 2		rotation: pass 3		rotation: pass 4		rotation: pass 5		rotation: pass 6	
	x (deg)	y (deg)										
15.5	-0.74	8.61	-0.08	-8.87	0.23	0.23	0.16	-0.64	-0.11	-0.06	-0.44	-0.22
17.0	0.50	0.90	0.55	-4.66	0.30	0.22	-0.01	-0.86	-0.08	-0.06	-0.12	-0.37
18.5	0.06	2.04	0.03	-1.69	0.27	0.22	-0.02	-0.63	-0.09	-0.08	-0.14	0.02
20.0	-0.06	-0.18	-0.09	0.98	0.14	0.23	-0.01	0.03	-0.03	-0.07	-0.06	-0.16

B.1.3. Padfoot roller

a) 16 in lift thickness

depth (in)	rotation: pass 1		rotation: pass 2		rotation: pass 3		rotation: pass 4		rotation: pass 5		rotation: pass 6	
	x (deg)	y (deg)										
10.3	-0.04	-0.09	0.26	0.04	0.01	-0.01	-0.10	-0.10	0.30	0.28	-0.80	-0.11
11.8	-0.03	-0.06	0.35	0.12	0.02	0.01	-0.10	-0.10	0.26	0.27	-0.62	-0.32
13.3	-0.03	-0.10	0.31	0.03	-0.01	0.02	0.08	-0.17	0.31	0.30	1.37	-0.01
14.5	-0.06	-0.07	-0.09	-0.08	0.01	-0.01	-0.24	-0.27	0.24	0.31	-0.11	0.27
16.0	-0.04	-0.05	0.00	0.31	-0.01	-0.01	-0.74	-0.02	0.28	0.20	0.00	1.01

b) 24 in lift thickness

depth (in)	rotation: pass 1		rotation: pass 2		rotation: pass 3		rotation: pass 4		rotation: pass 5		rotation: pass 6	
	x (deg)	y (deg)										
18.0	0.02	0.20	0.43	0.09	-0.02	0.03	0.00	-0.02	0.11	-0.01	-0.01	-0.01
19.5	0.19	0.18	-0.29	0.25	0.12	-0.01	0.10	0.00	-0.33	0.09	0.05	-0.03
21.0	0.33	0.18	-0.20	0.21	0.09	0.01	0.13	-0.04	-0.39	0.26	0.09	-0.03
22.5	0.13	0.24	0.57	0.35	-0.08	-0.03	0.20	0.02	0.51	0.35	-0.08	-0.06
24.0	0.46	-0.08	-0.06	-0.29	0.05	0.00	0.22	0.02	-0.13	-0.49	0.04	0.09

B.1.4. Scraper

a) 20 in lift thickness

depth (in)	rotation: pass 1		rotation: pass 2		rotation: pass 3		rotation: pass 4		rotation: pass 5		rotation: pass 6	
	x (deg)	y (deg)										
15.5	-0.96	2.44	0.19	-0.28	-0.36	-0.22	-0.58	-1.46				
17.0	-0.42	0.27	0.14	-0.19	-0.38	-0.22	-0.11	-1.73				
18.5	-0.04	1.39	0.12	-0.90	-0.37	-0.22	0.03	-0.58				
20.0	-0.32	-0.54	0.08	0.05	-0.18	-0.18	-0.03	0.10				

b) 24 in lift thickness

depth (in)	rotation: pass 1		rotation: pass 2		rotation: pass 3		rotation: pass 4		rotation: pass 5		rotation: pass 6	
	x (deg)	y (deg)										
17.8	-1.56	-0.90	-0.21	0.59	-0.58	-1.60						
19.3	-2.51	-0.26	0.01	0.31	-1.72	0.71						
20.8	-3.40	-3.09	0.22	0.23	-1.87	0.23						
22.3	-0.60	1.14	0.36	0.50	-0.71	-0.15						
24.0	-0.54	1.55	0.30	0.41	-0.55	-0.42						

B.2. MEMS rotation angle measurement in the coarse-grained soil (natural moisture)

B.2.1. Smooth-drum vibratory roller

a) 8 in lift thickness

depth (in)	rotation: pass 1		rotation: pass 2		rotation: pass 3		rotation: pass 4		rotation: pass 5		rotation: pass 6	
	x (deg)	y (deg)										
2.0	-12.86	1.40	0.39	11.94	0.81	-12.01	-2.70	9.24	1.51	1.36	19.59	10.46
3.5	-0.23	-0.30	-0.98	-0.18	0.45	-1.54	3.43	-0.88	0.40	-1.46	-0.27	-0.22
5.0	-3.52	1.03	-4.45	-1.70	8.31	-1.69	-2.05	-0.27	4.61	0.01	-5.90	-1.07
6.5	1.74	1.12	6.07	-0.18	-9.22	-1.30	2.83	0.60	-3.42	0.56	5.01	-0.38
8.0	2.13	0.05	-2.27	0.06	3.88	0.15	1.30	-0.88	2.18	-0.36	-2.43	-0.05

b) 13 in lift thickness

depth (in)	rotation: pass 1		rotation: pass 2		rotation: pass 3		rotation: pass 4		rotation: pass 5		rotation: pass 6	
	x (deg)	y (deg)										
7.5	-1.08	5.11	-5.31	0.75	4.21	-1.83	-2.01	1.23	2.44	0.26	-5.21	-0.28
9.5	1.14	0.38	-1.46	0.22	1.22	-1.35	-0.68	0.37	0.76	-0.10	-1.20	0.05
11.0	4.35	2.95	-4.84	0.93	4.53	-0.99	-1.53	0.30	2.74	0.10	-4.07	0.24
12.5	-0.13	5.43	-0.55	1.49	0.14	0.29	-0.24	0.41	0.20	0.12	-0.18	0.32
13.0	-2.50	0.56	7.02	1.12	-5.55	1.02	2.05	0.16	-3.23	0.29	4.19	0.12

c) 24 in lift thickness

depth (in)	rotation: pass 1		rotation: pass 2		rotation: pass 3		rotation: pass 4		rotation: pass 5		rotation: pass 6	
	x (deg)	y (deg)										
17.0			3.29	0.29	-2.15	-0.08	1.62	0.07	-1.49	0.18	1.83	0.06
18.5			-0.72	0.42	0.24	-0.07	-0.35	0.22	0.34	0.09	-0.39	0.26
20.0			2.18	0.58	-1.87	-0.41	1.22	0.19	-1.31	0.00	1.43	0.30
22.0			-1.95	0.49	1.76	-0.21	-1.30	0.05	1.60	0.09	-1.52	0.11
24.0			-1.17	0.14	1.38	-0.20	-0.96	0.00	1.30	0.05	-1.22	0.05

B.2.2. Rubber-tired roller

a) 8 in lift thickness

depth (in)	rotation: pass 1		rotation: pass 2		rotation: pass 3		rotation: pass 4		rotation: pass 5		rotation: pass 6	
	x (deg)	y (deg)										
0.3	0.89	-0.17	11.67	-2.58	0.09	0.20	-0.60	-9.45	-0.38	-0.24	-2.20	3.72
2.5	0.19	-1.56	0.20	-11.92	0.00	0.03	1.00	7.12	-0.02	-0.41	-0.20	1.45
4.5	-1.55	1.63	-0.98	-0.14	-0.01	0.04	-1.84	2.29	-0.02	-0.12	2.76	0.41
6.5	-0.56	-0.89	0.94	0.09	0.02	0.01	-0.63	4.74	0.00	-0.18	1.10	-0.35
8.0	0.46	0.04	-2.83	0.86	-0.09	0.05	0.57	0.96	-0.15	-0.05	-1.66	-0.12

b) 13 in lift thickness

depth (in)	rotation: pass 1		rotation: pass 2		rotation: pass 3		rotation: pass 4		rotation: pass 5		rotation: pass 6	
	x (deg)	y (deg)										
7.0	-0.04	-0.07	-2.44	4.22	5.10	-15.65	-1.03	-6.26	-0.35	3.62	-2.80	2.03
8.5	-0.06	-0.03	-0.96	2.81	2.29	-8.90	-0.66	-4.56	-0.22	2.19	-1.78	3.26
10.0	-0.05	-0.02	1.72	1.74	-5.42	-8.92	2.10	-1.98	0.03	1.02	1.98	3.24
11.5	-0.02	0.00	-1.62	0.70	3.33	-3.56	-1.66	-0.57	0.19	-0.13	-1.22	2.48
13.0	0.00	-0.07	2.48	-0.09	-7.44	1.03	2.55	1.27	-0.32	0.36	3.48	0.66

c) 20 in lift thickness

depth (in)	rotation: pass 1		rotation: pass 2		rotation: pass 3		rotation: pass 4		rotation: pass 5		rotation: pass 6	
	x (deg)	y (deg)										
12.5	1.24	7.03	2.42	-7.58	-0.43	1.01	1.28	-1.94	-3.03	-0.02	1.20	0.25
14.5	-0.18	3.04	0.97	-2.10	-0.03	0.02	0.32	-0.21	-0.88	0.44	0.33	0.14
16.5	-1.49	2.27	-2.32	0.81	0.43	0.55	-0.86	-0.26	3.11	-0.93	-1.39	0.90
18.0	-7.44	0.32	2.33	2.04	0.67	0.07	-0.34	0.58	2.21	-0.35	-0.54	0.34
20.0	-2.63	0.93	-0.46	1.90	0.39	0.17	-0.37	0.32	1.08	-0.75	-0.43	0.68

B.2.3. Scraper

a) 13 in lift thickness

depth (in)	rotation: pass 1		rotation: pass 2		rotation: pass 3		rotation: pass 4		rotation: pass 5		rotation: pass 6	
	x (deg)	y (deg)										
4.3	0.65	-9.34	-0.11	0.32	0.00	0.00	8.71	4.96	10.00	-34.16	-1.94	30.68
6.8	-1.90	-8.26	0.04	0.27	0.00	0.00	12.04	-41.58	0.14	1.63	-9.93	18.93
8.5	-4.73	-0.16	0.16	0.33	0.00	0.00	-2.15	-1.40	2.33	-6.79	-9.19	4.06
10.0	-5.74	2.80	0.20	0.36	0.00	0.00	-0.63	3.28	1.13	-7.23	-5.61	0.09
13.0	9.86	-2.29	-0.21	0.24	0.00	0.00	0.77	2.96	-3.74	-5.21	2.88	2.39

b) 23 in lift thickness

depth (in)	rotation: pass 1		rotation: pass 2		rotation: pass 3		rotation: pass 4		rotation: pass 5		rotation: pass 6	
	x (deg)	y (deg)										
16.8	3.97	-4.87	-0.78	3.62	1.38	-4.38			-0.15	1.14	-0.31	1.79
17.8	-5.85	3.34	0.59	2.79	-1.02	-3.55			0.11	1.06	0.06	1.42
19.5	-7.46	-3.74	-0.79	2.91	-0.99	-3.19			-0.29	0.98	-0.59	1.34
21.5	-2.95	-4.41	0.44	1.52	-0.80	-2.92			0.00	1.01	-0.36	0.90
23.0	1.18	0.37	-0.73	1.76	0.21	-1.63			-0.08	0.99	-0.25	0.86

B.3. MEMS rotation angle measurement in the coarse-grained soil (wet condition moisture)

B.3.1. Smooth-drum vibratory roller

a) 8 in lift thickness

depth (in)	rotation: pass 1		rotation: pass 2		rotation: pass 3		rotation: pass 4		rotation: pass 5		rotation: pass 6	
	x (deg)	y (deg)										
3.5	2.07	-	3.85	-2.29	-0.63	6.85	1.59	-1.27	-1.02	-1.46	1.15	-3.46
5.0	16.00	10.74	21.28	8.60	-2.26	0.23	0.82	2.82	-2.91	-2.91	2.90	1.30
6.0	3.45	3.92	21.41	-0.51	-6.57	-1.73	9.30	3.66	-3.91	-2.61	5.59	-1.80
7.0	-15.38	2.33	4.52	-2.06	5.23	1.68	-3.52	-0.22	4.33	0.78	-4.00	-1.29
8.0	0.77	2.75	8.36	-1.04	-2.78	-0.67	11.75	0.55	1.76	-0.27	9.50	-0.54

b) 13 in lift thickness

depth (in)	rotation: pass 1		rotation: pass 2		rotation: pass 3		rotation: pass 4		rotation: pass 5		rotation: pass 6	
	x (deg)	y (deg)										
8.0	0.00	0.00	0.00	0.00	0.00	0.00	0.00	0.00	0.00	0.00	0.00	0.00
9.5	-2.36	0.79	0.43	0.68	-0.38	-0.87	0.56	0.23	-0.24	-0.61	0.37	0.61
9.5	-2.77	-2.76	1.09	-1.47	-0.63	-0.56	0.82	-0.17	-0.87	-0.27	1.13	0.14
11.5	2.08	3.16	-1.04	1.03	0.91	0.61	-0.83	0.90	0.47	0.49	-0.29	0.55
13.0	-0.78	1.04	1.20	-0.02	-0.99	0.45	1.14	-0.02	-0.79	0.33	1.15	-0.04

c) 20 in lift thickness

depth (in)	rotation: pass 1		rotation: pass 2		rotation: pass 3		rotation: pass 4		rotation: pass 5		rotation: pass 6	
	x (deg)	y (deg)										
13.0	1.59	0.12	1.51	-0.47	-1.53	-0.20	1.87	0.03	-1.73	0.24	1.50	-0.16
14.0	1.25	0.46	0.35	-0.44	-1.14	-0.58	0.48	-0.07	-0.78	0.08	0.43	-0.40
16.0	0.50	1.56	-0.02	0.47	-0.07	0.04	-0.04	0.54	0.11	0.19	-0.04	0.06
18.0	0.69	1.93	-1.17	0.17	0.86	0.54	-1.13	0.07	0.70	0.29	-0.66	-0.03
20.0	-1.77	-0.84	0.69	0.37	-0.79	-0.45	0.42	0.52	-0.50	-0.24	0.24	0.33

B.3.2. Rubber-tired roller

a) 13 in lift thickness

depth (in)	rotation: pass 1		rotation: pass 2		rotation: pass 3		rotation: pass 4		rotation: pass 5	
	x (deg)	y (deg)								
5.5	1.45	-7.17	-3.02	10.55	-0.22	0.50	-0.12	0.75	-0.50	1.16
6.5	-1.20	-8.25	0.79	8.68	0.19	0.44	-0.49	0.61	0.72	0.84
9.0	1.25	-4.40	-0.26	0.98	0.13	1.30	-0.48	-0.37	0.79	0.81
11.0	0.46	-0.07	-0.44	0.13	0.11	0.37	-0.50	0.16	0.22	0.11
13.0	3.42	1.21	1.93	-1.13	-0.64	0.43	1.29	-0.59	-0.66	-0.41

b) 23 in lift thickness

depth (in)	rotation: pass 1		rotation: pass 2		rotation: pass 3		rotation: pass 4		rotation: pass 5	
	x (deg)	y (deg)								
16.0	-1.82	6.13	-0.48	-2.30	0.38	2.50	-3.17	-0.41	0.11	1.02
18.0	-1.79	0.95	-0.22	2.45	0.39	1.30	0.91	4.66	0.36	-1.07
19.5	-0.93	4.28	-0.47	5.39	0.41	0.64	-0.75	2.10	0.30	-2.05
21.0	1.65	1.92	0.81	0.88	-0.01	0.74	0.68	0.95	-0.44	-0.45
23.0	0.66	0.01	0.85	0.66	-0.31	0.51	1.00	-1.26	-0.50	-0.08

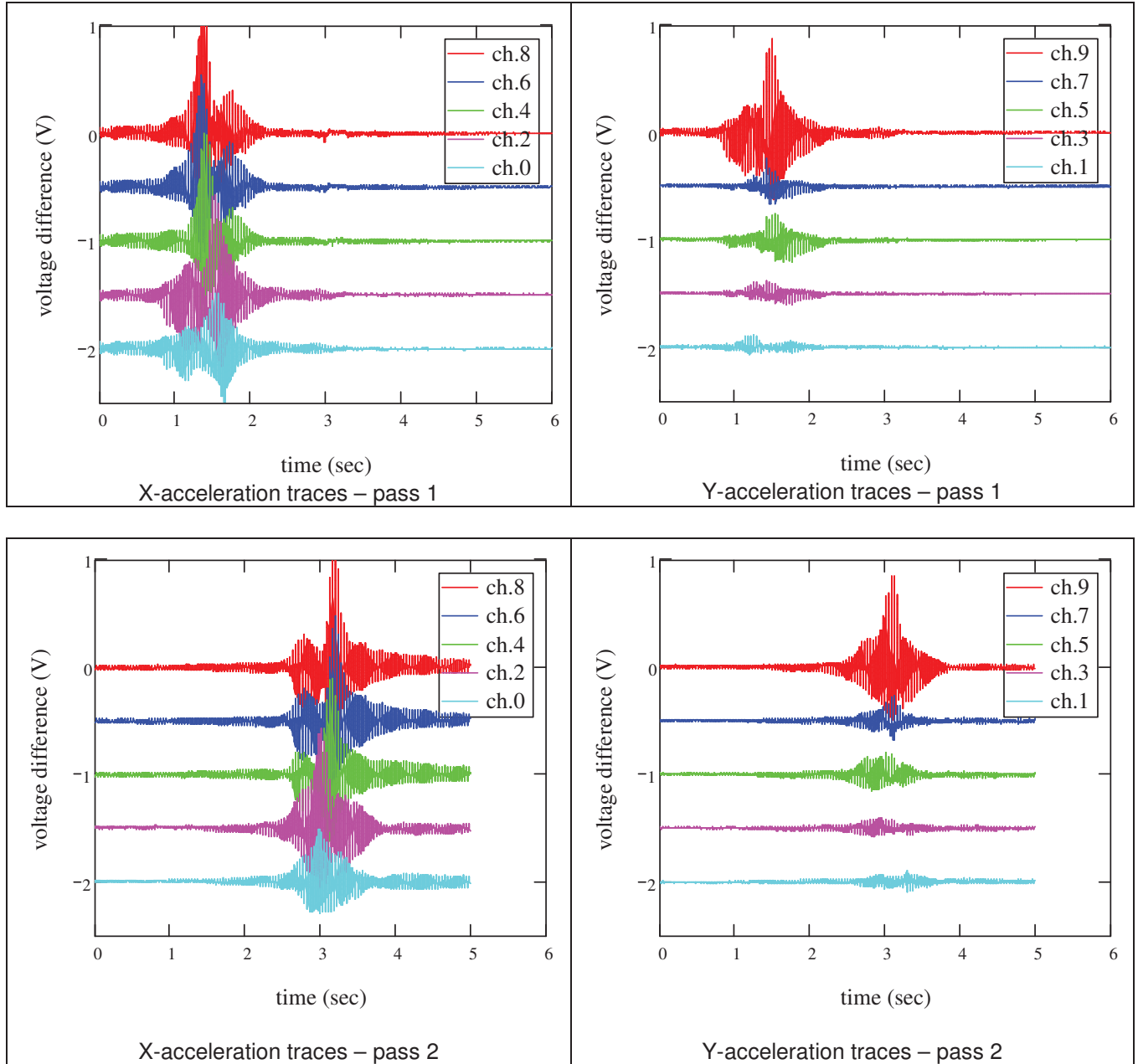
APPENDIX C: MEMS ACCELEROMETERS TIME SERIES

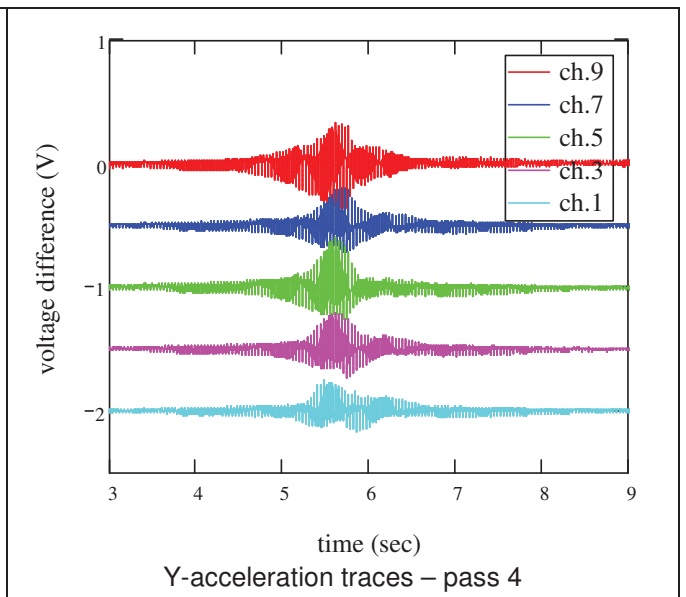
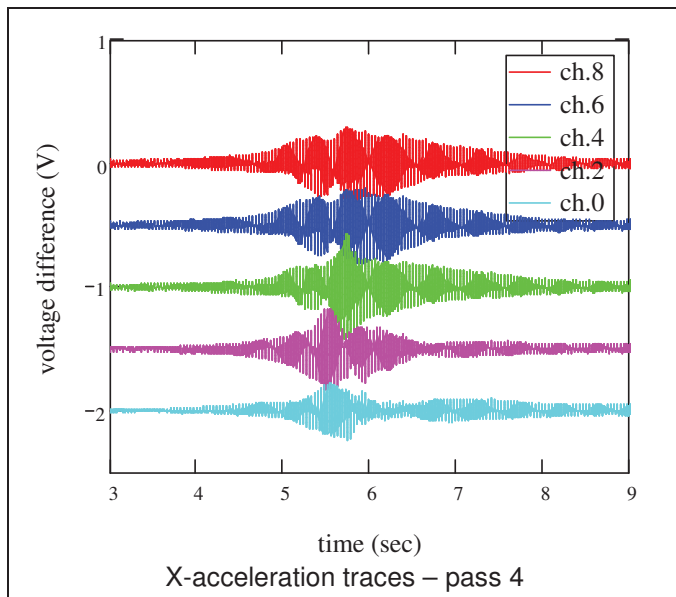
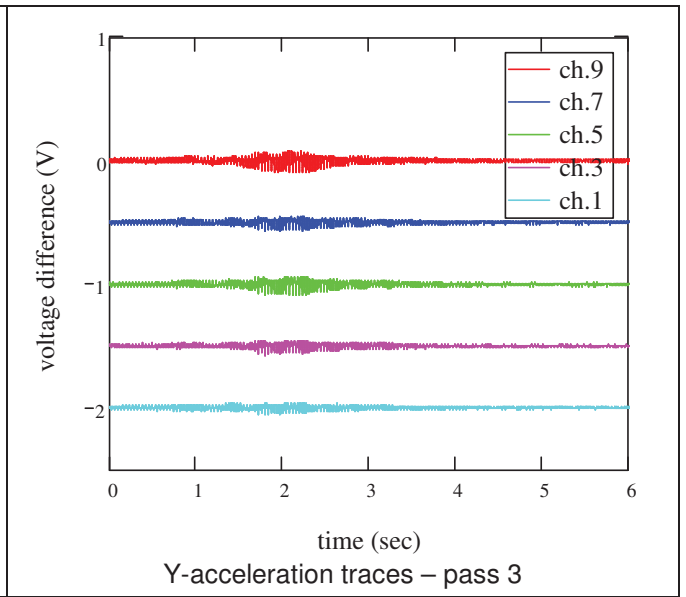
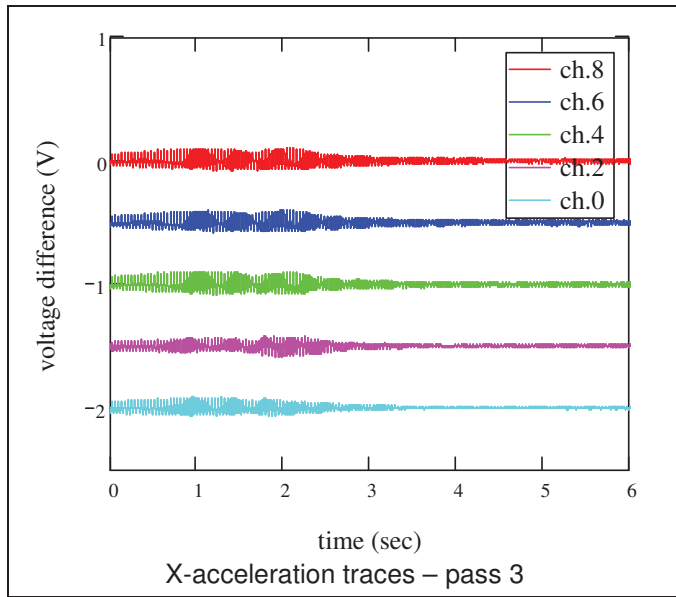
APPENDIX C.

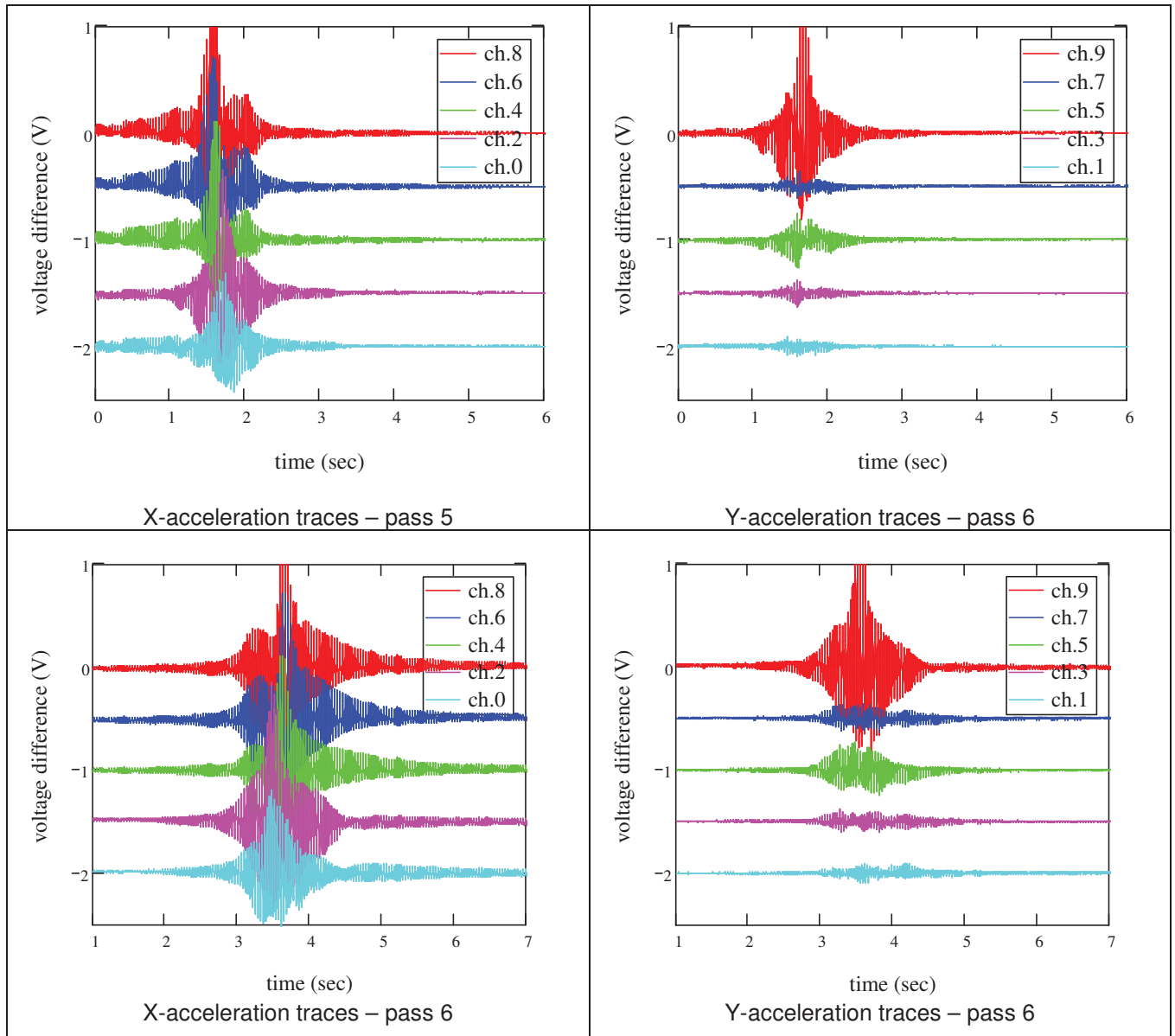
C.1. MEMS voltage differences traces

C.1.1. Smooth-drum vibratory roller

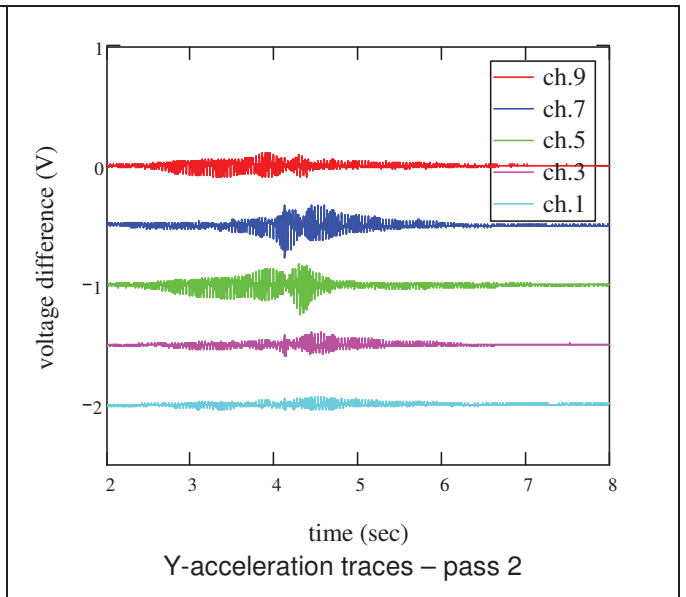
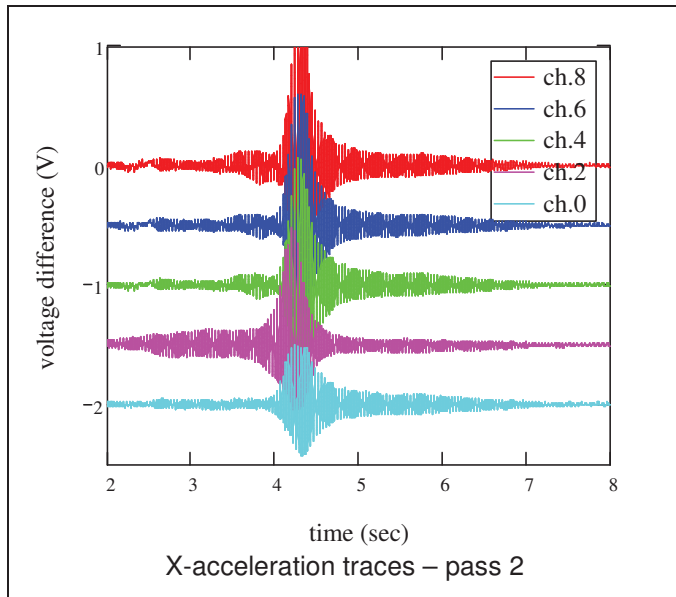
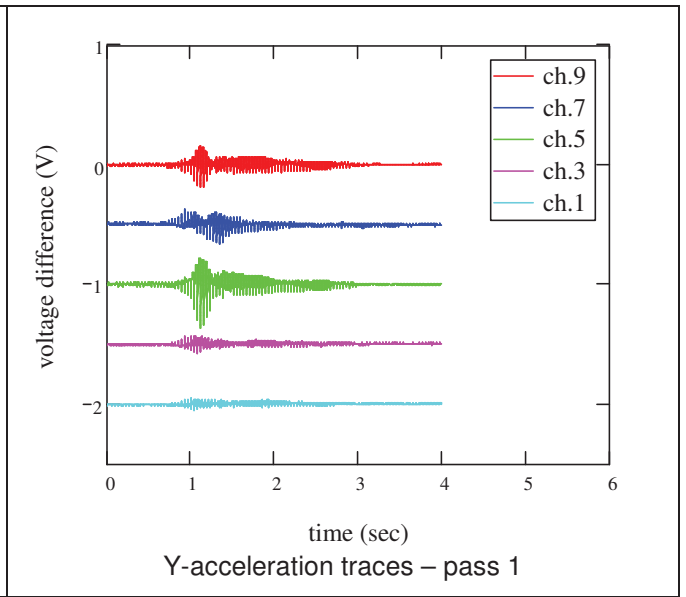
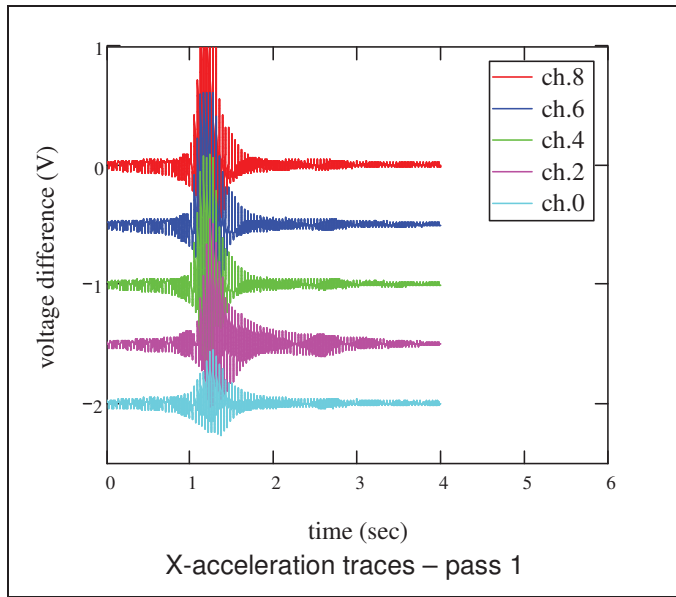
a) 12 in lift thickness

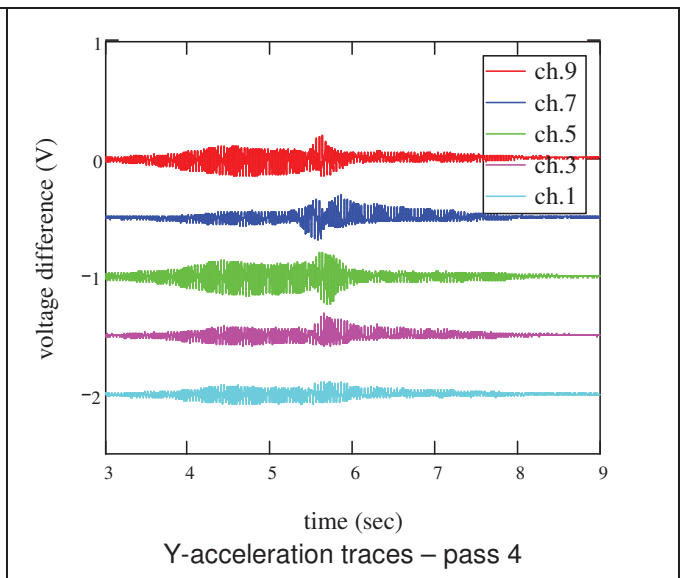
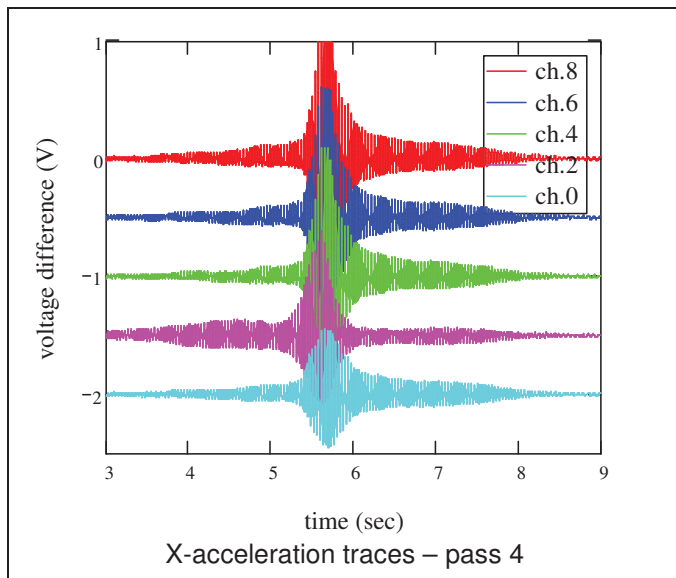
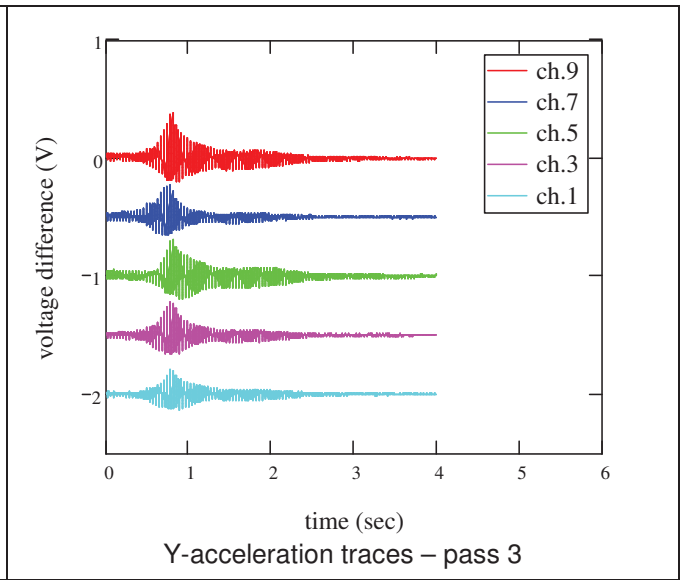
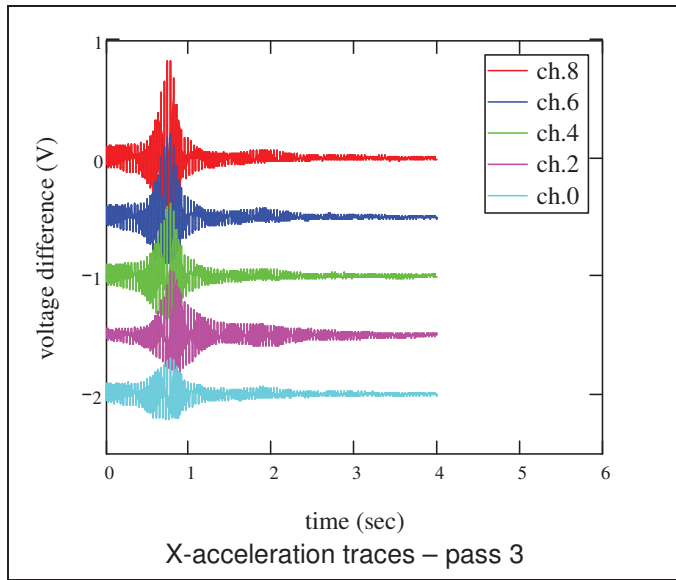


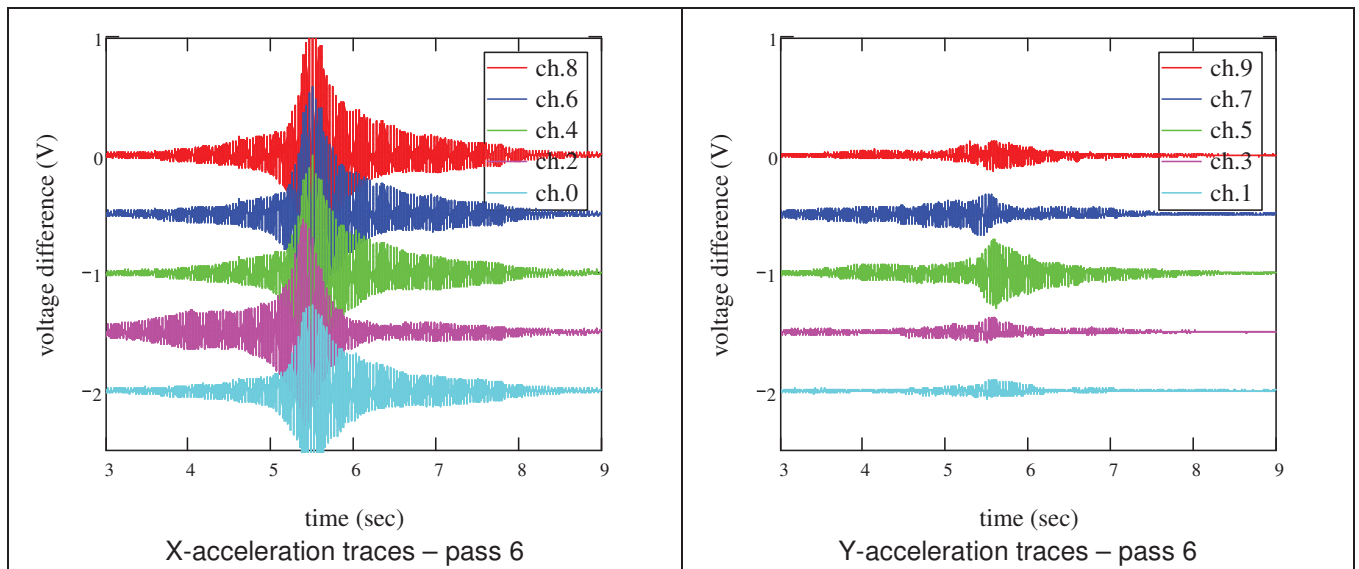
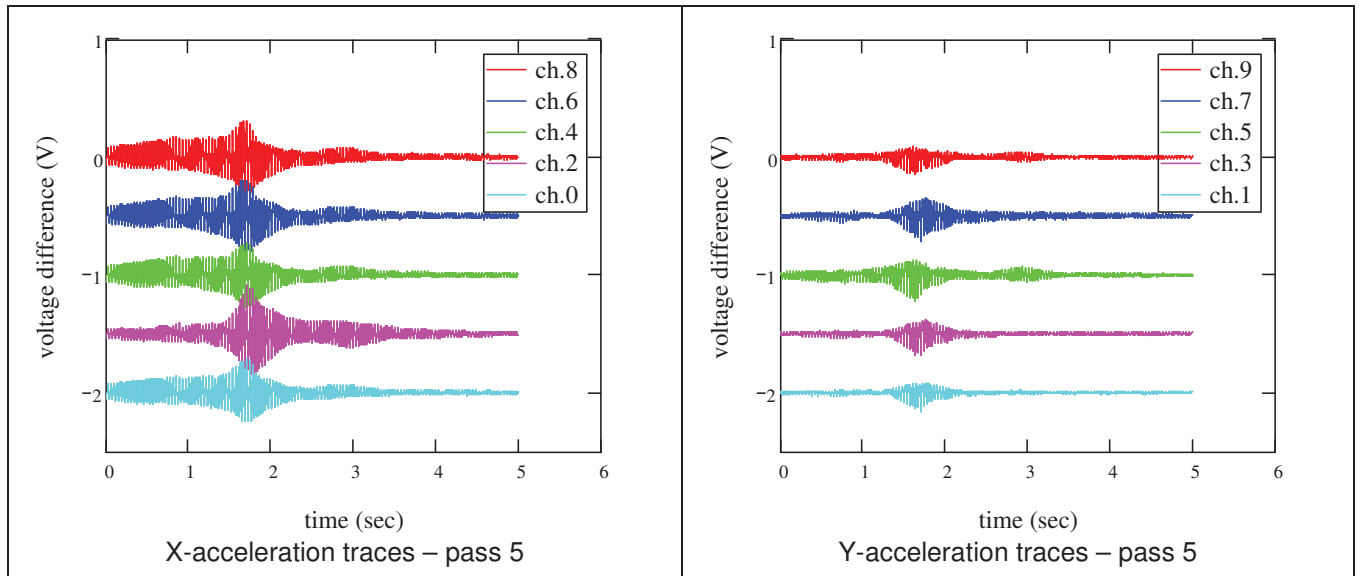




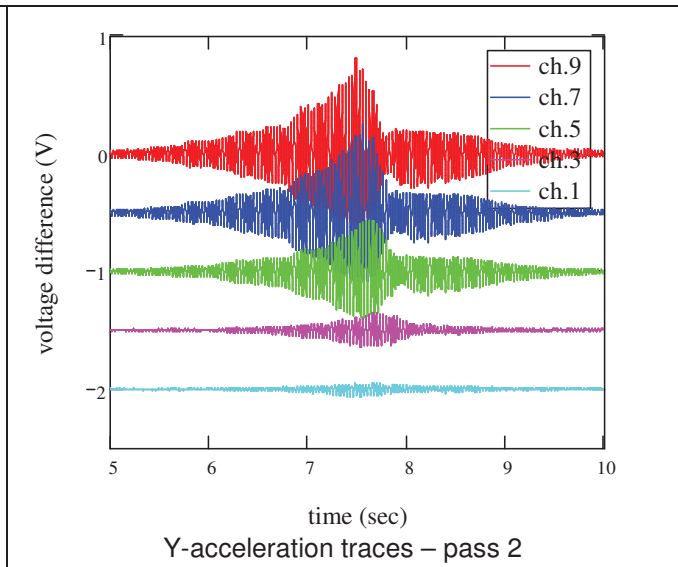
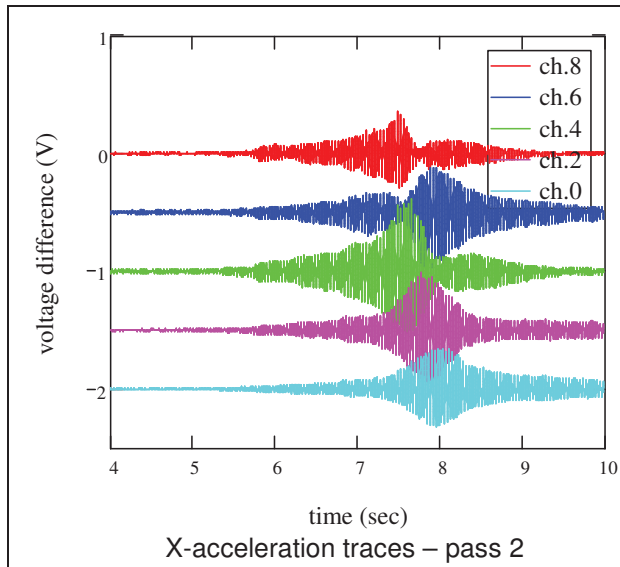
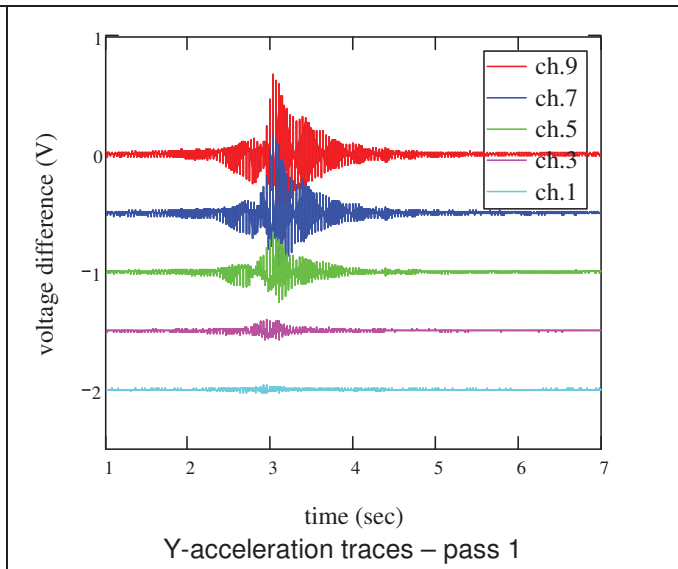
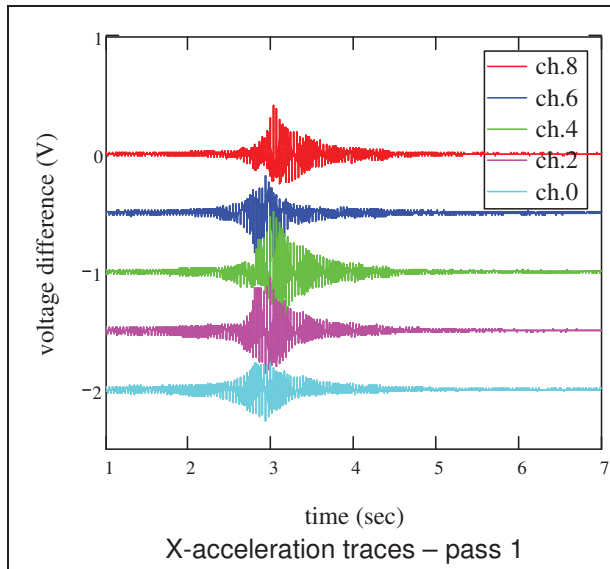
b) 17 in lift thickness

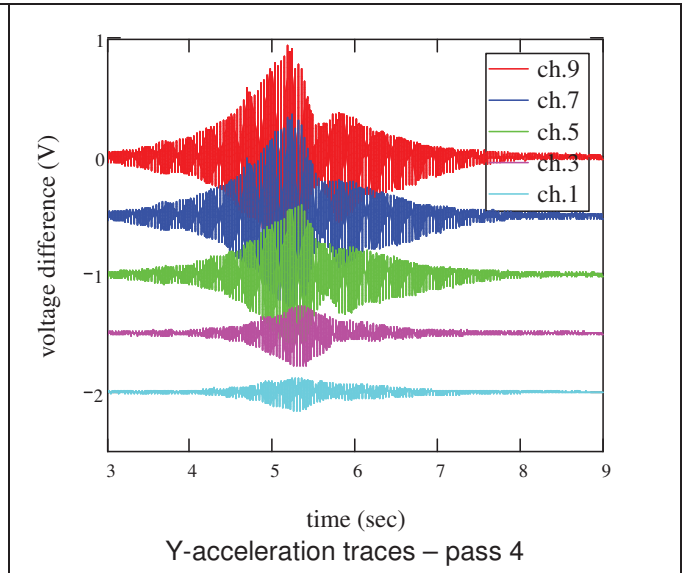
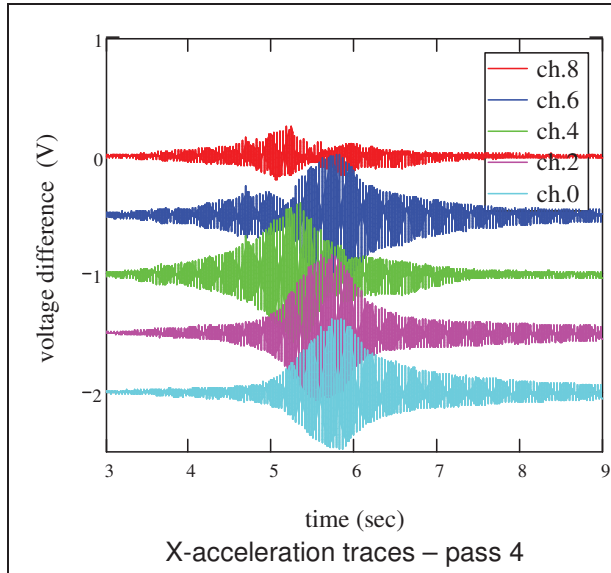
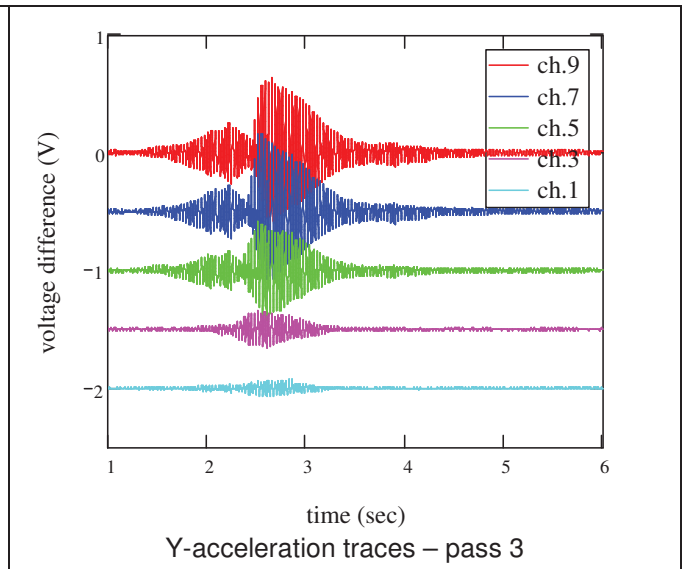
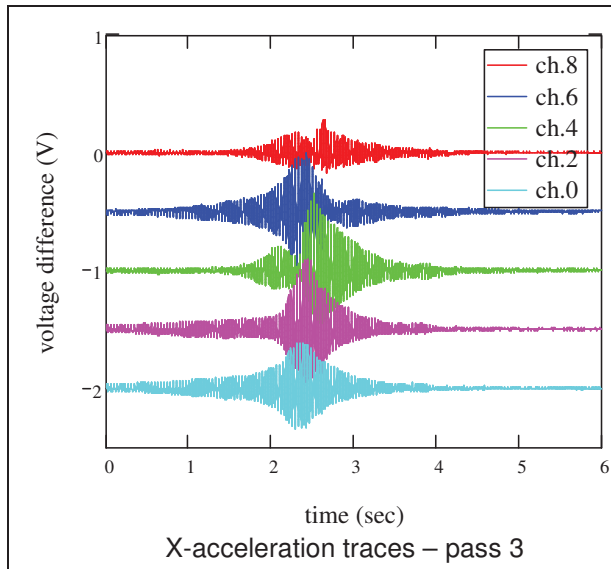


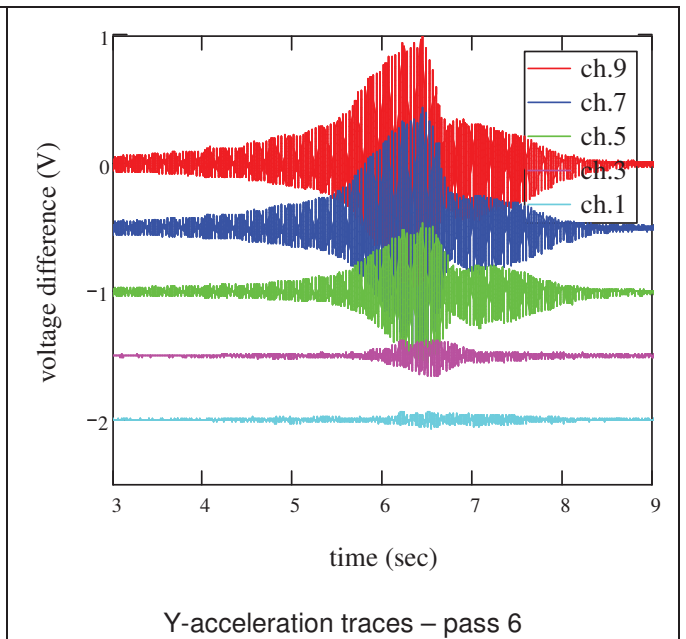
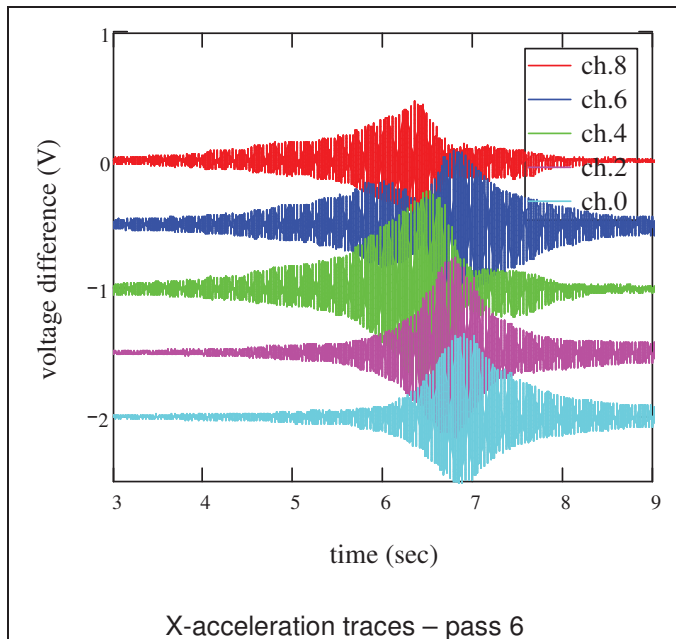
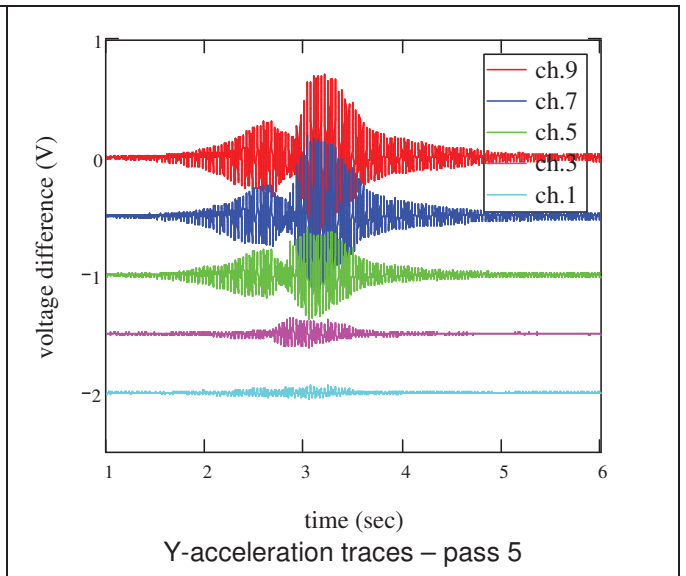
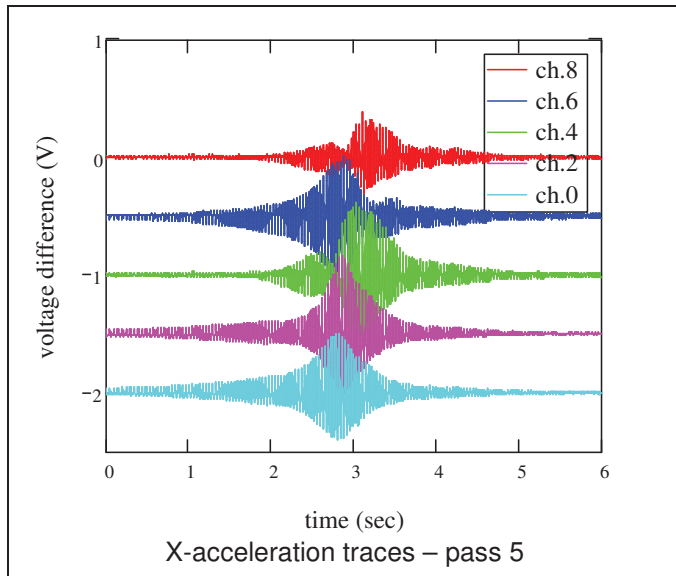




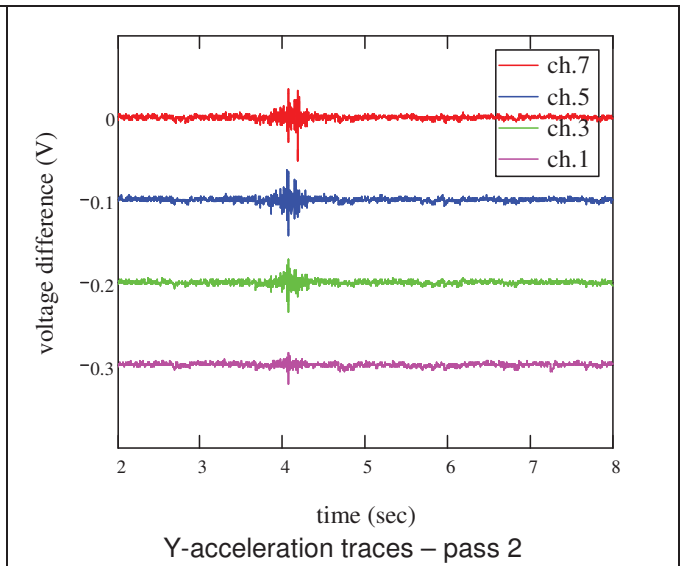
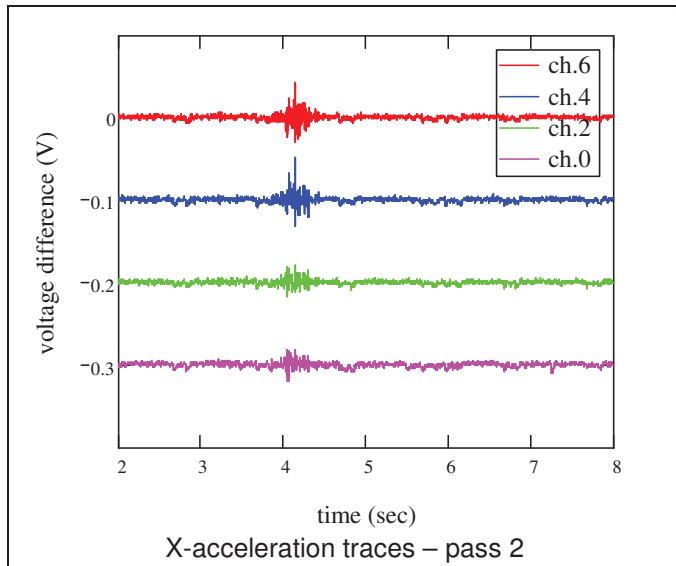
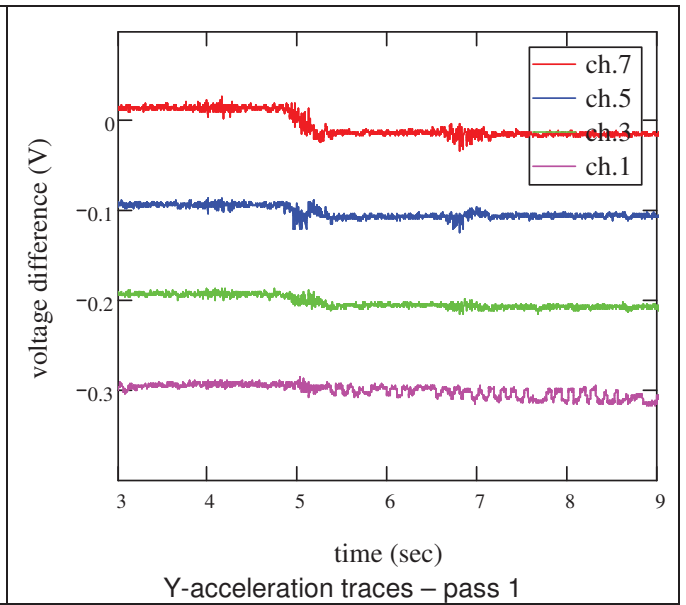
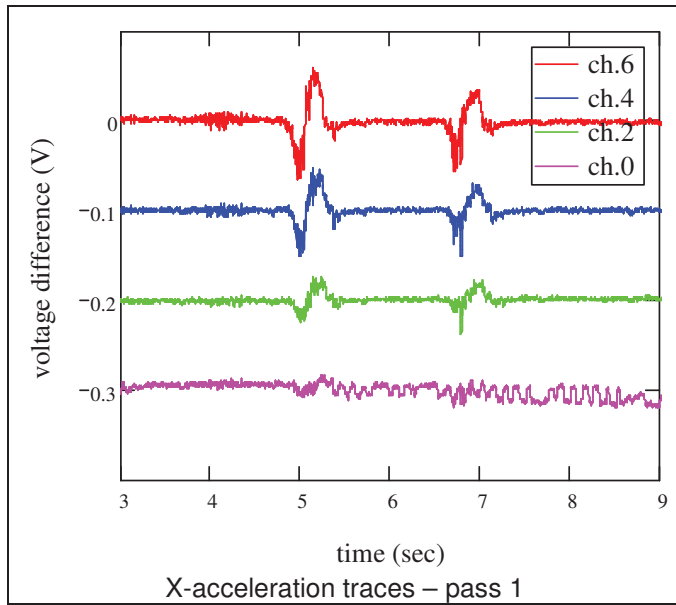
c) 24 in lift thickness

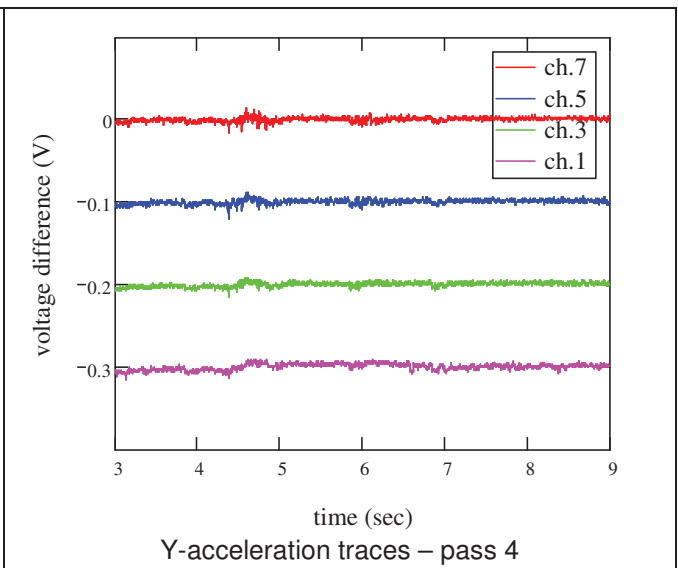
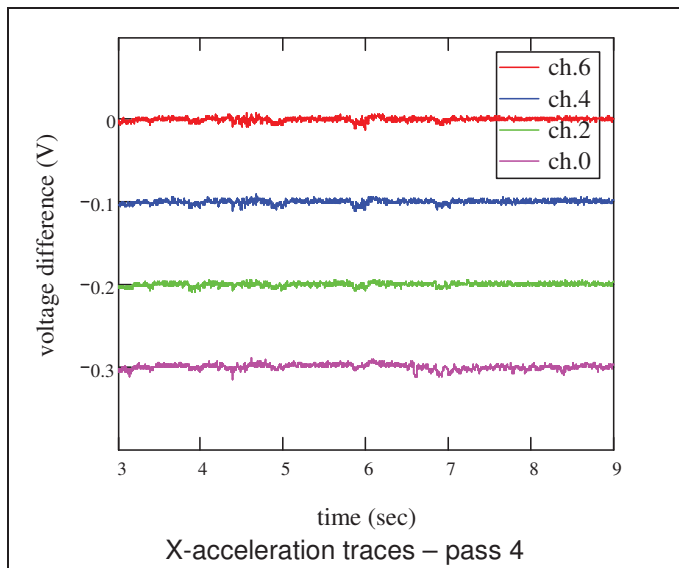
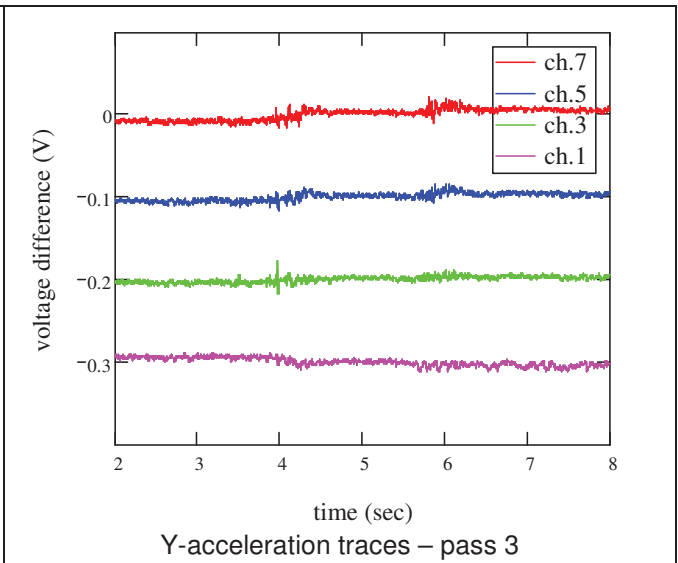
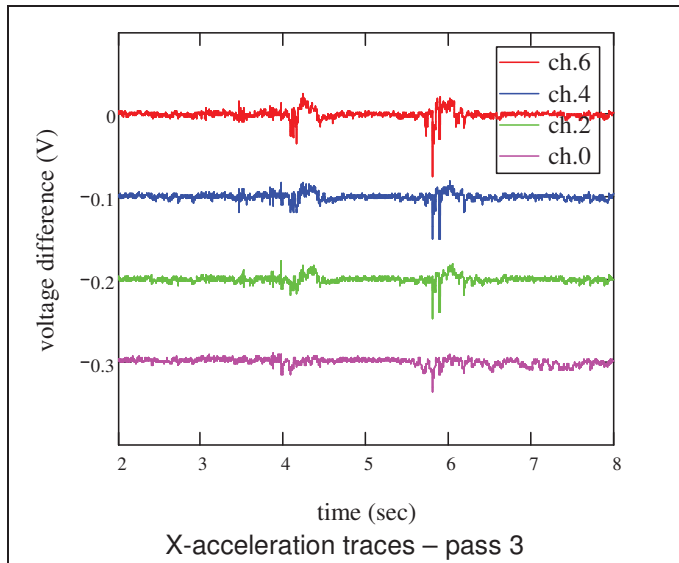


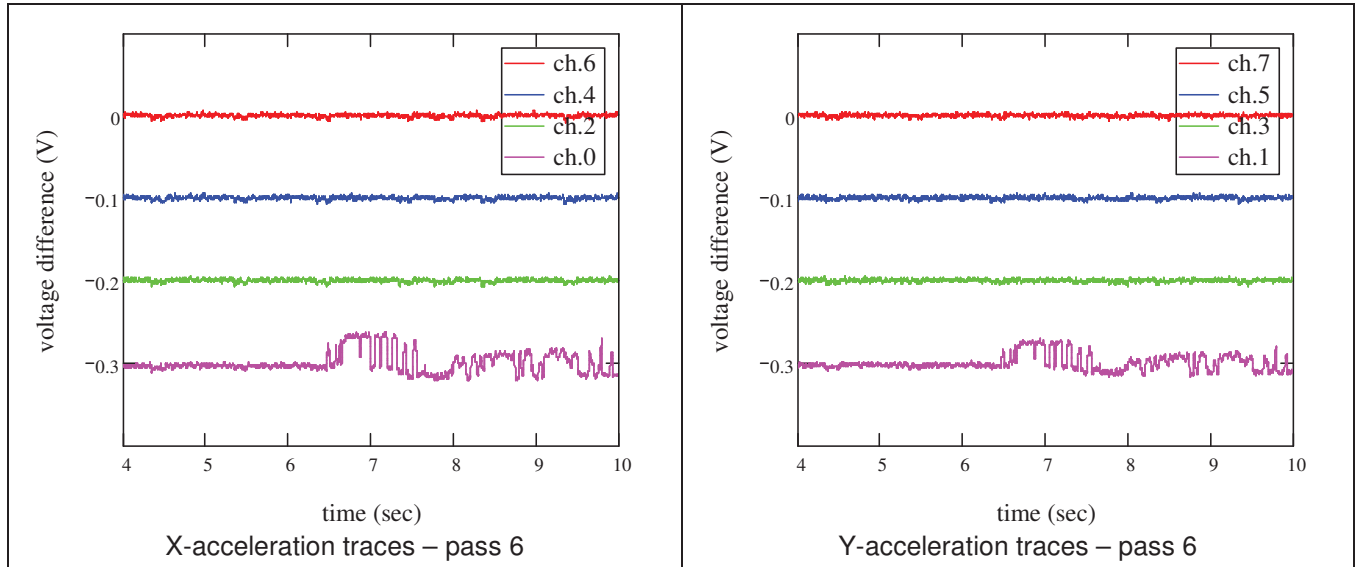
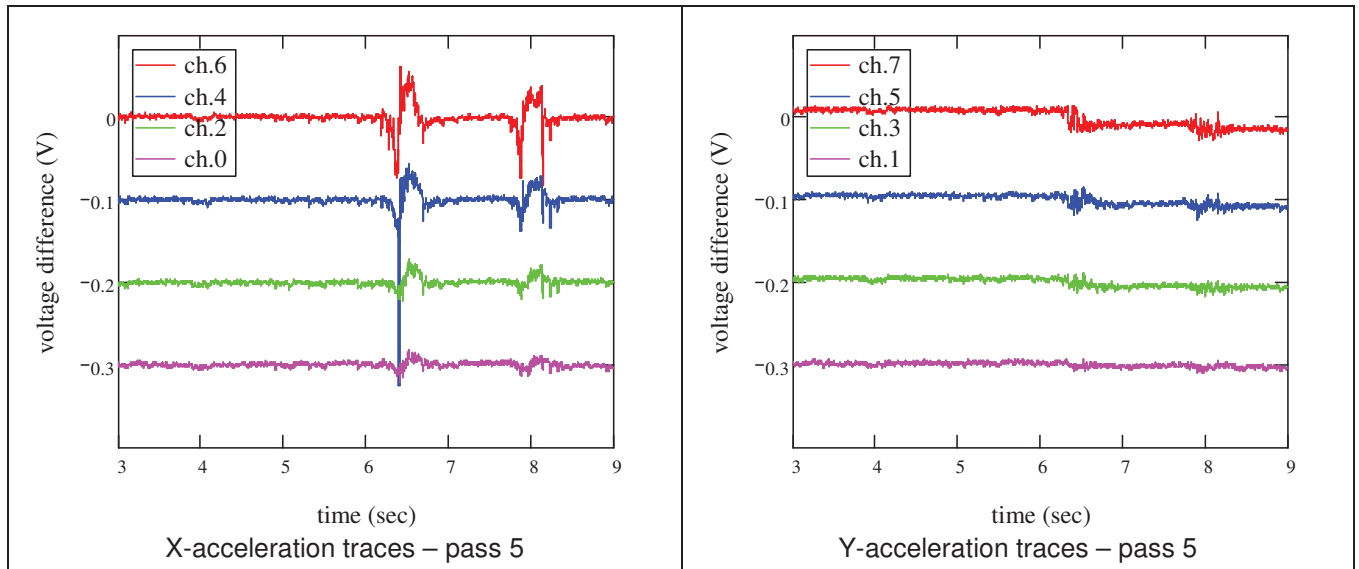




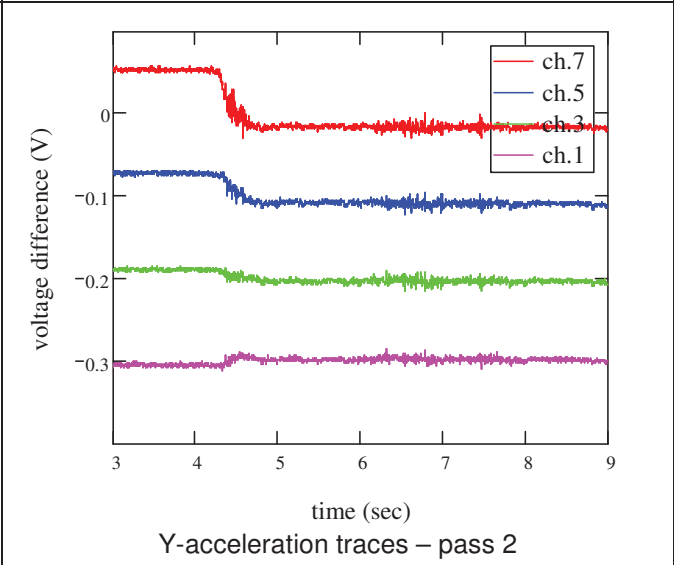
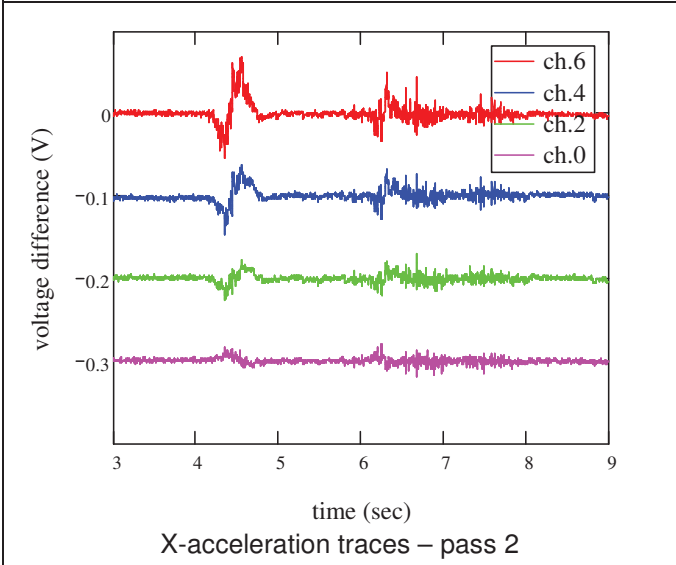
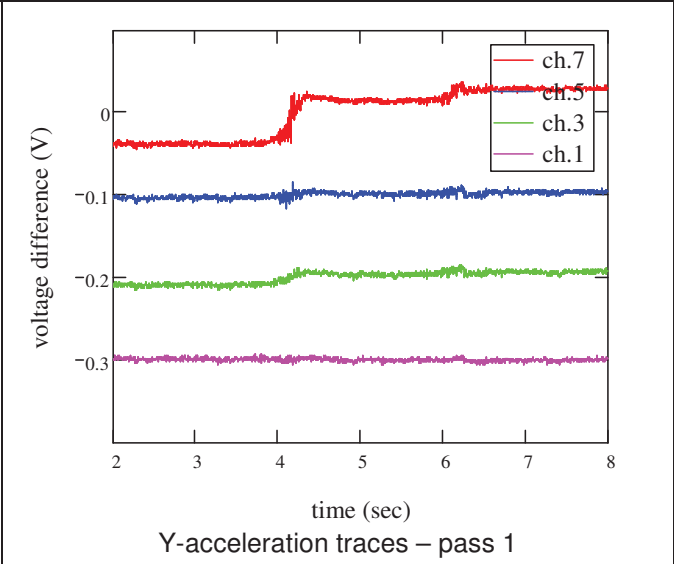
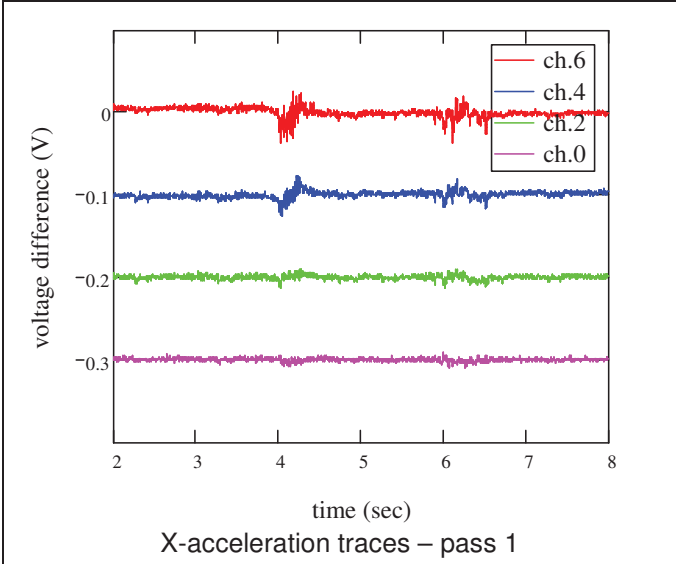
C.1.2. Rubber-tired roller
 a) 11 in lift thickness

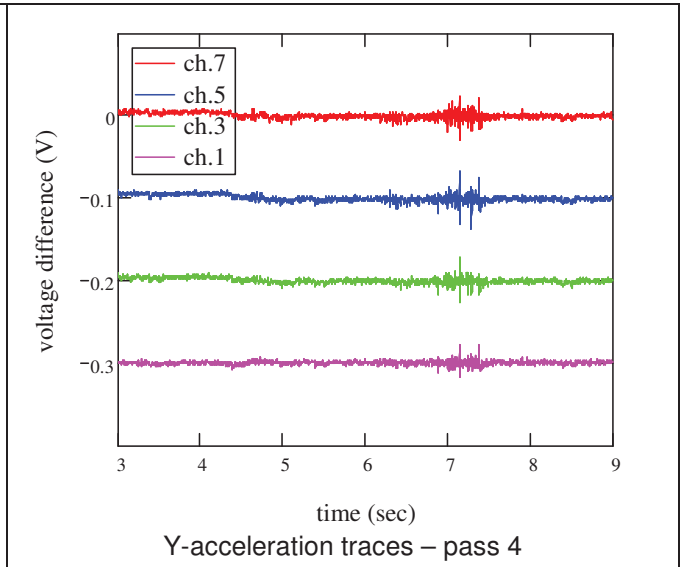
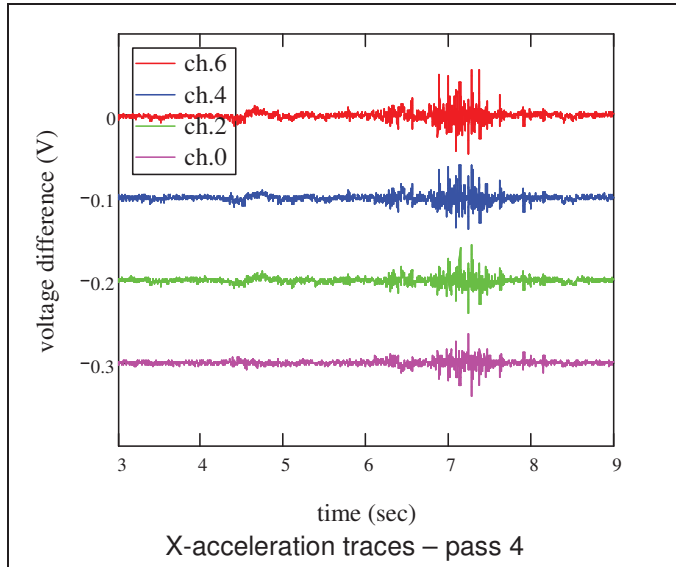
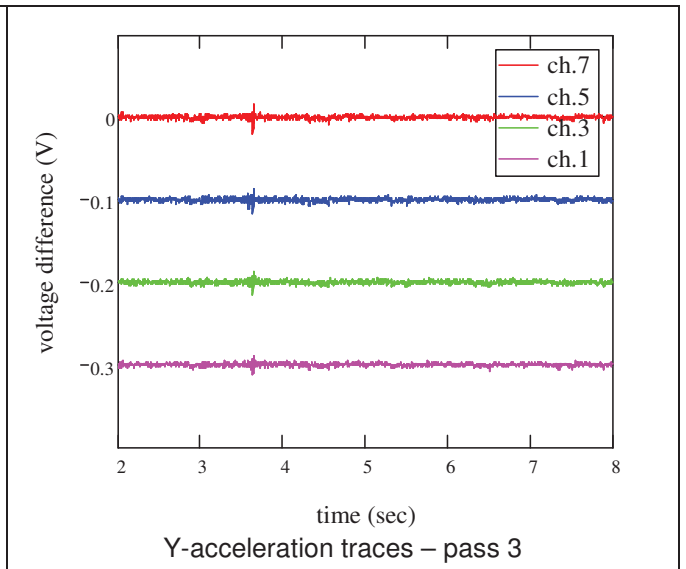
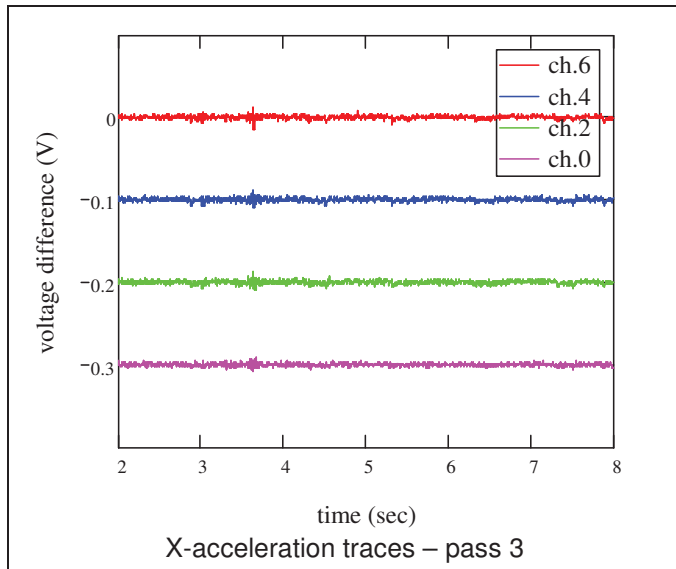


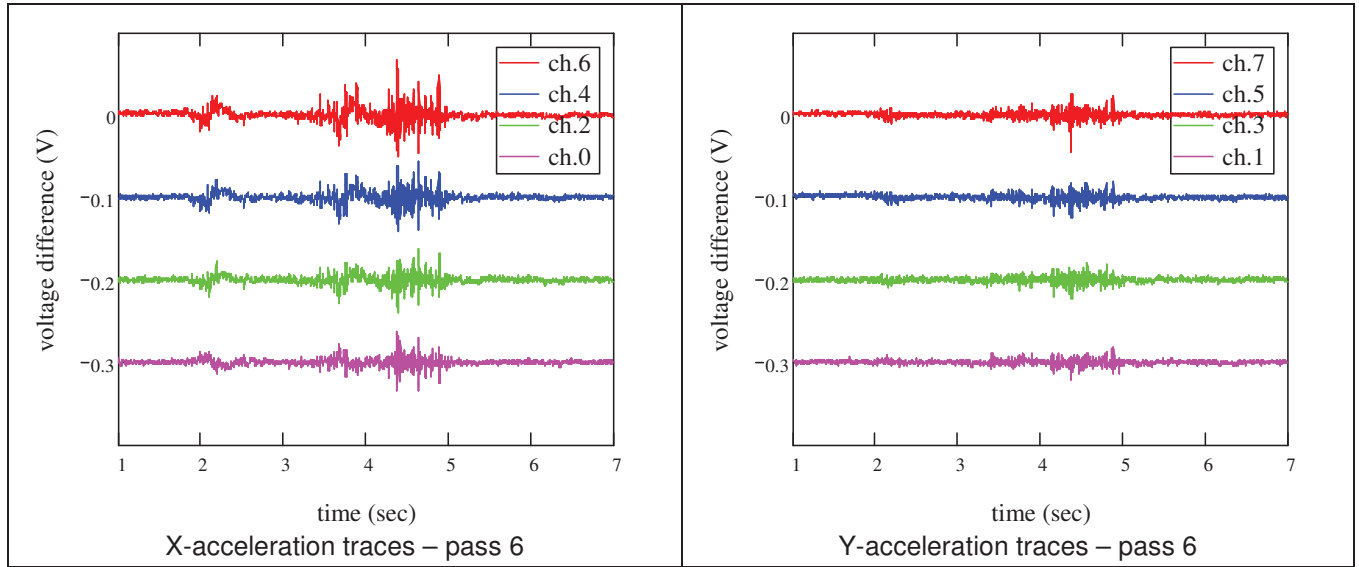
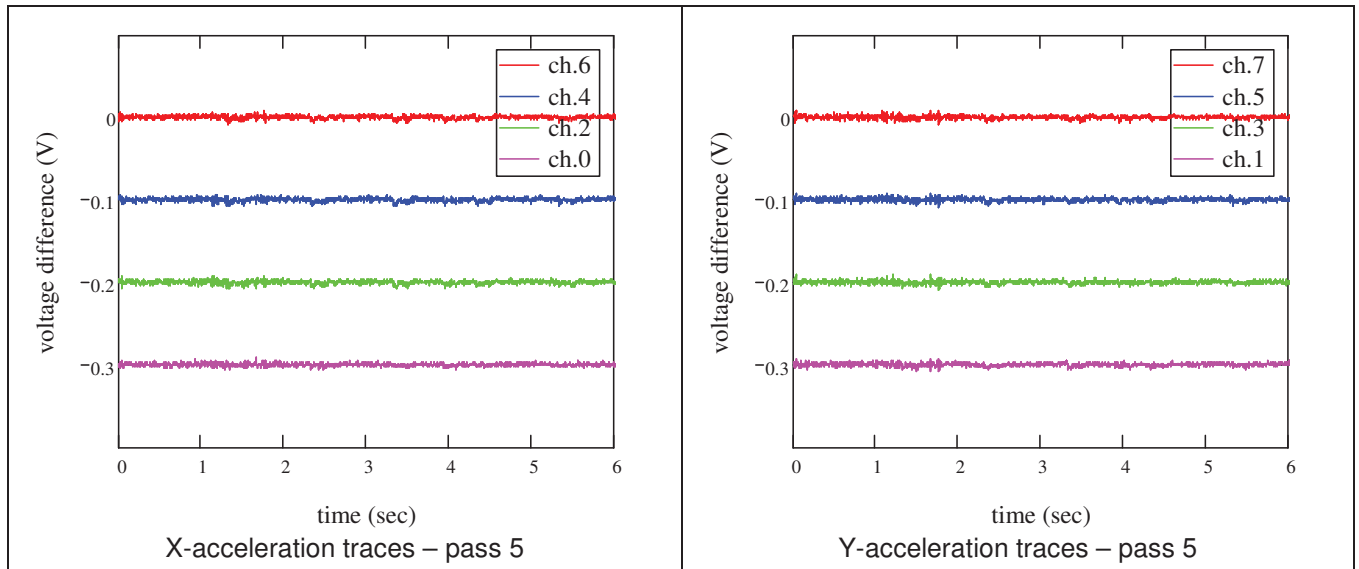




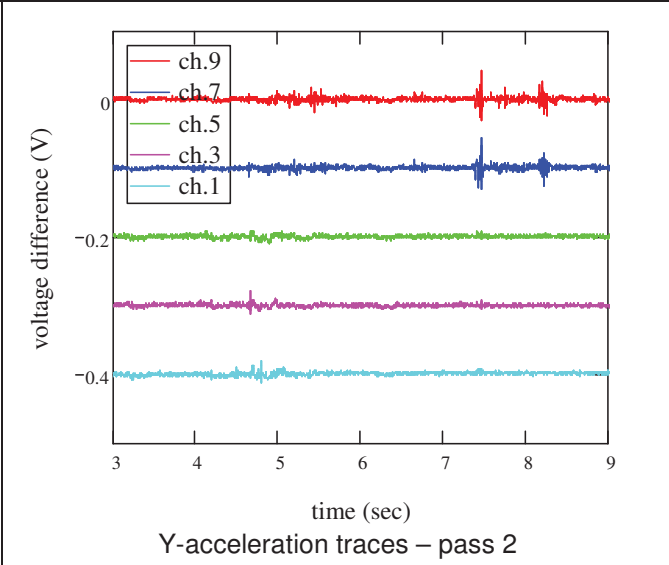
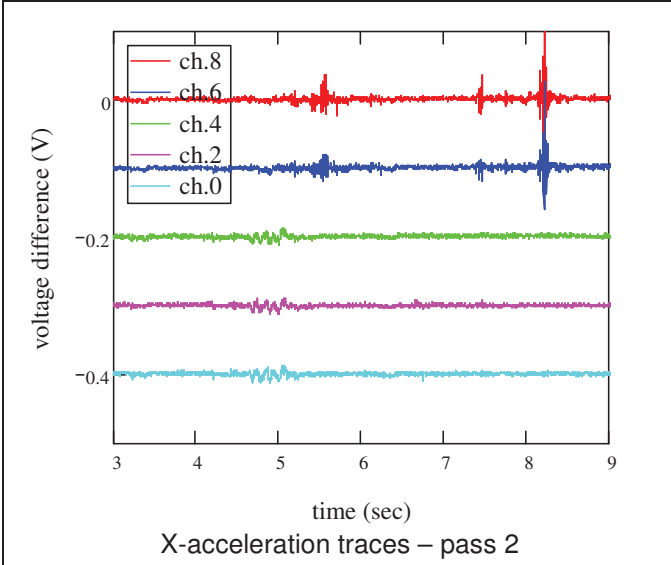
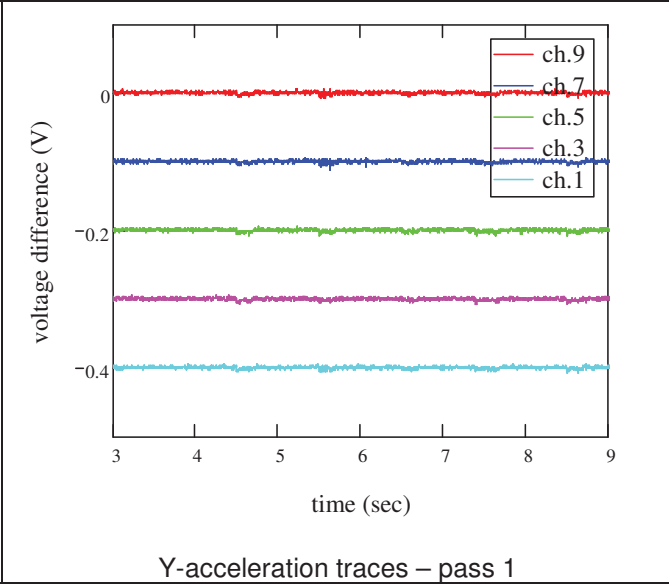
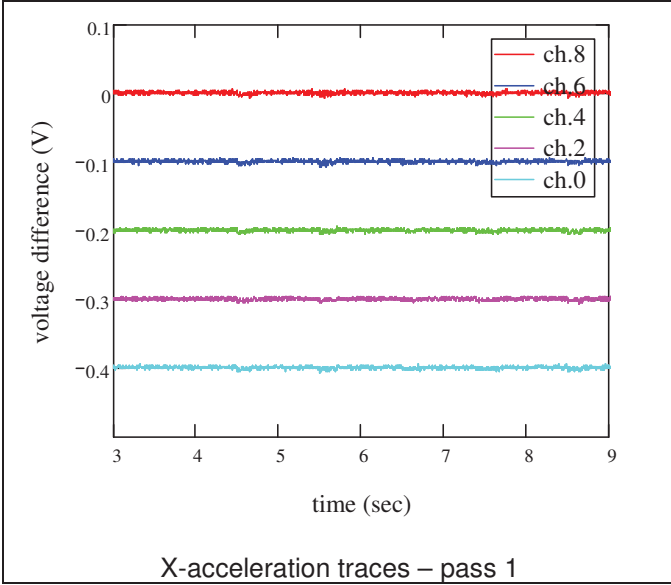
b) 20 in lift thickness

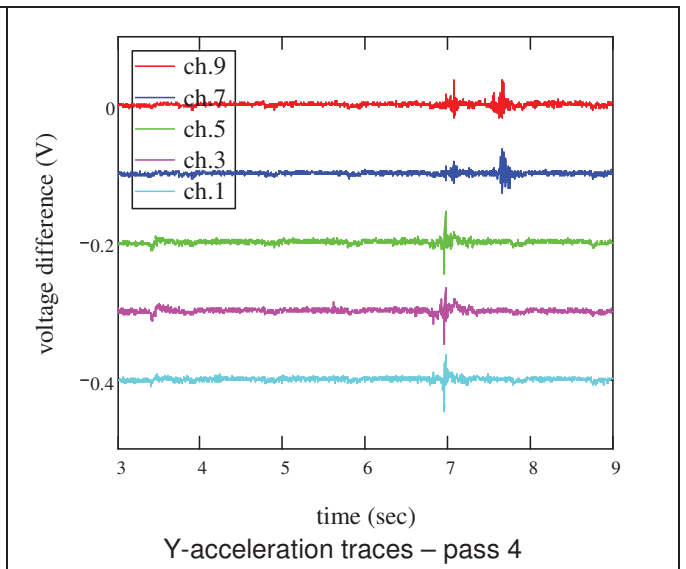
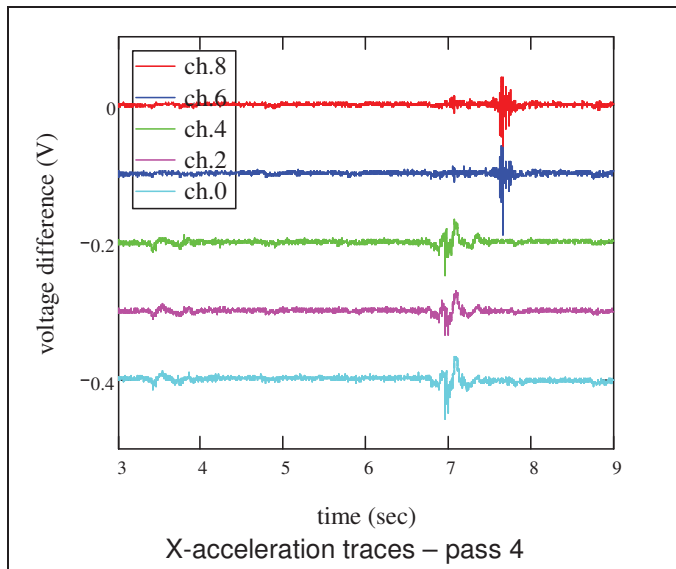
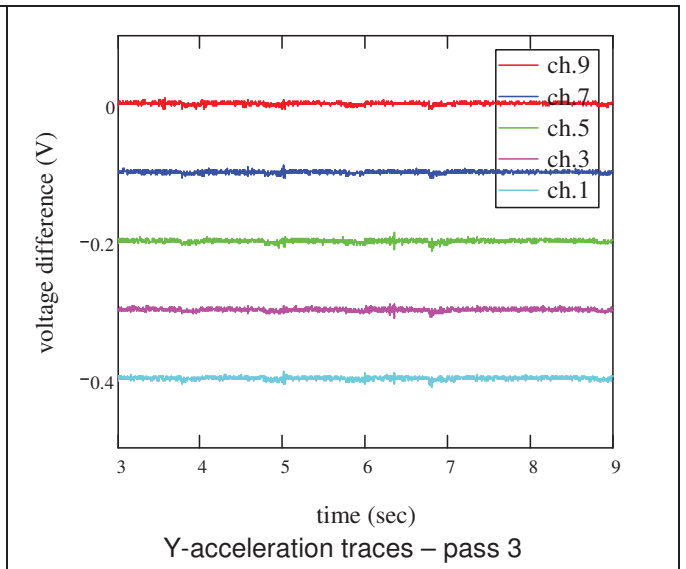
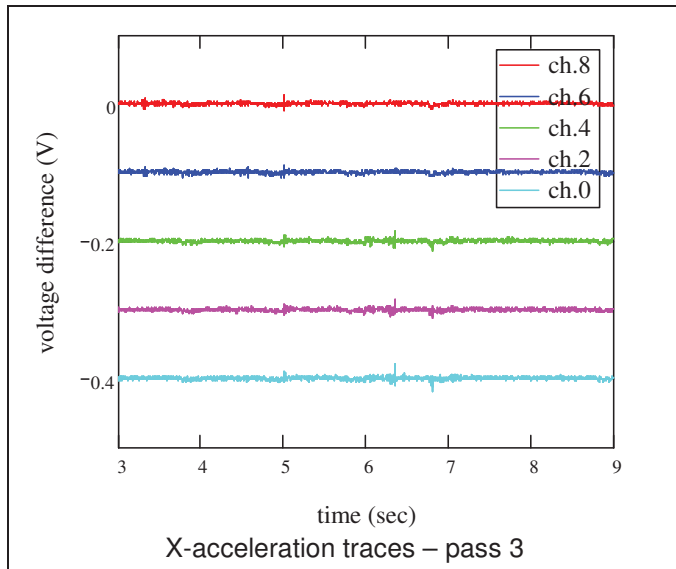


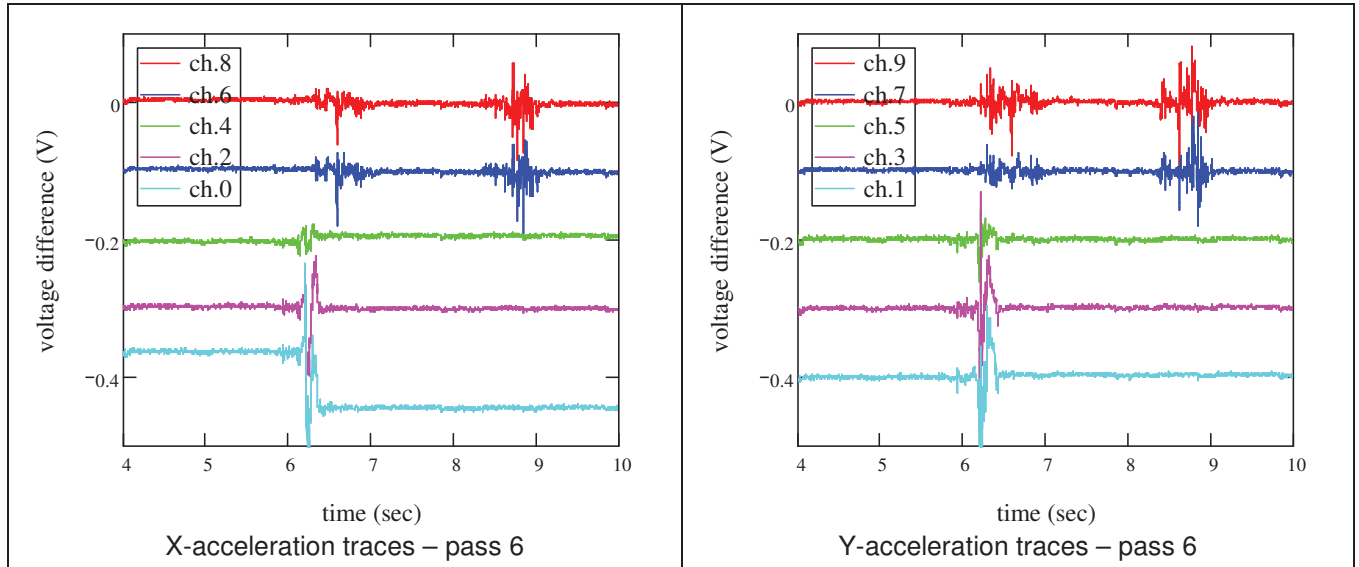
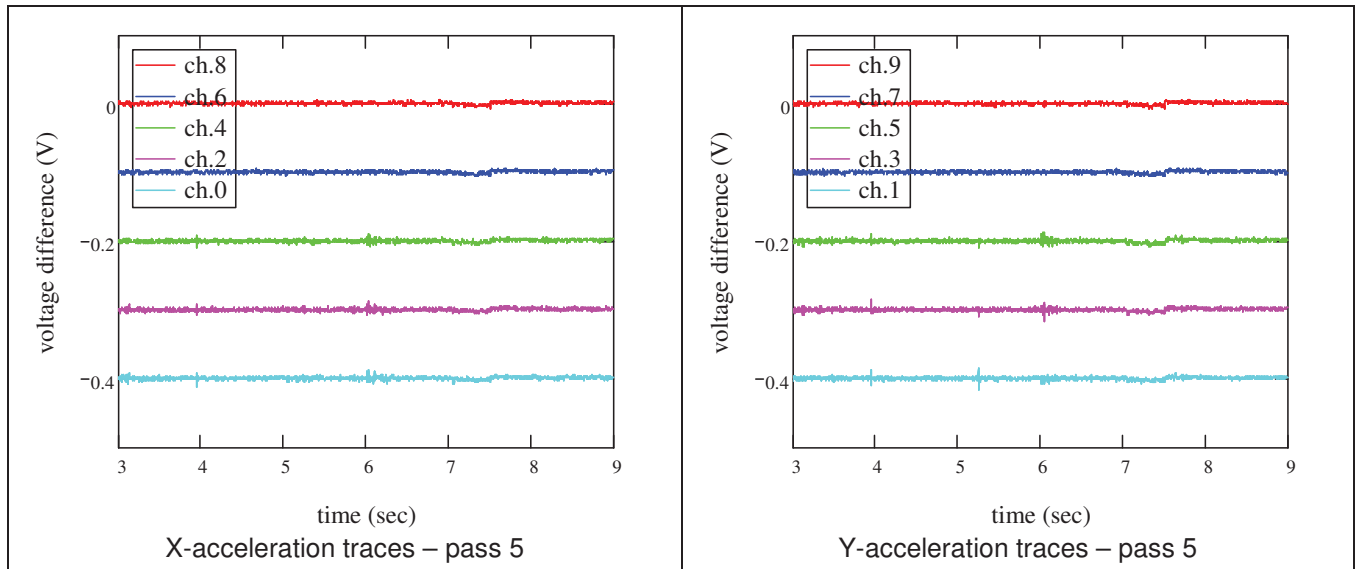




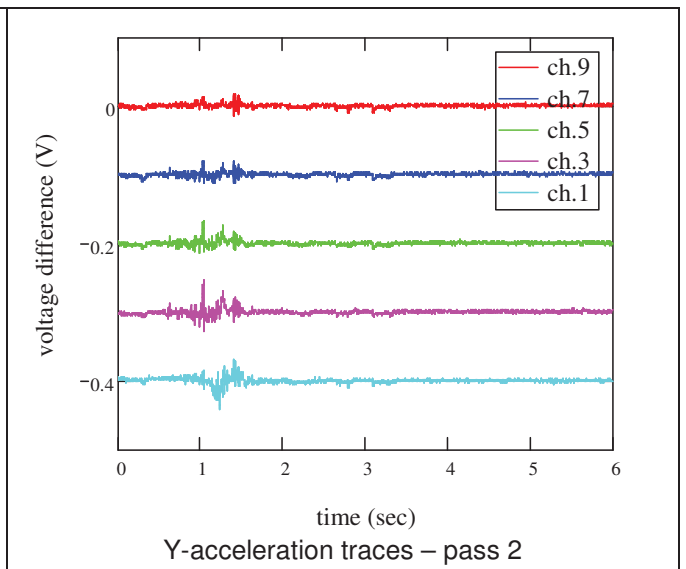
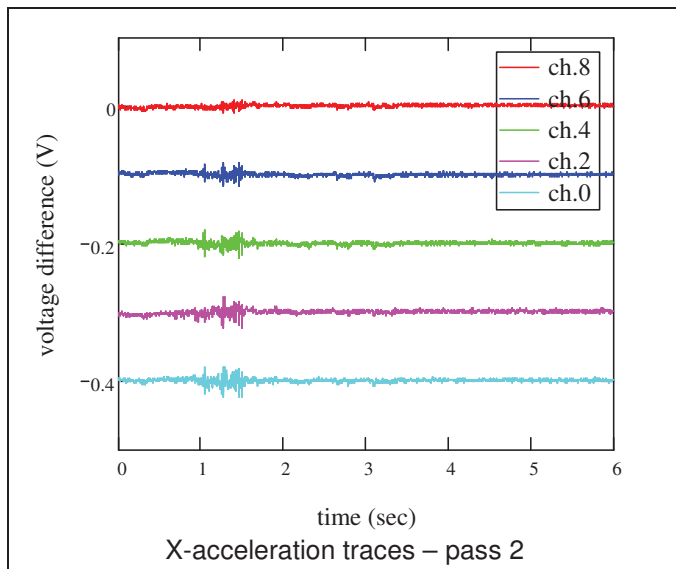
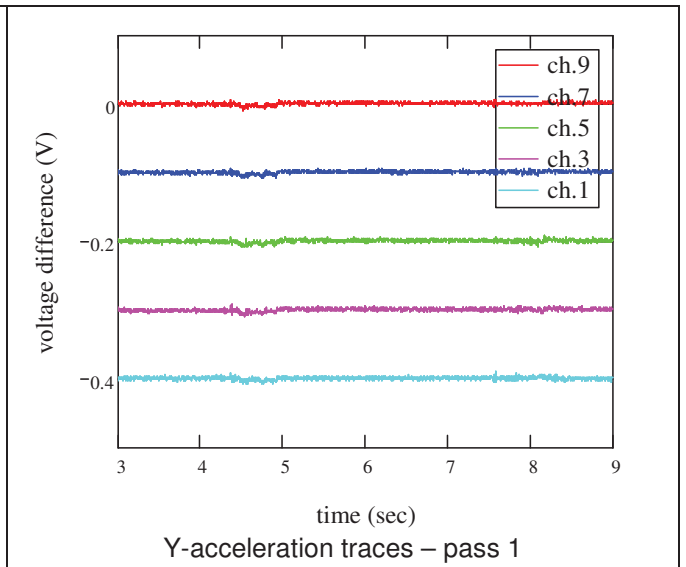
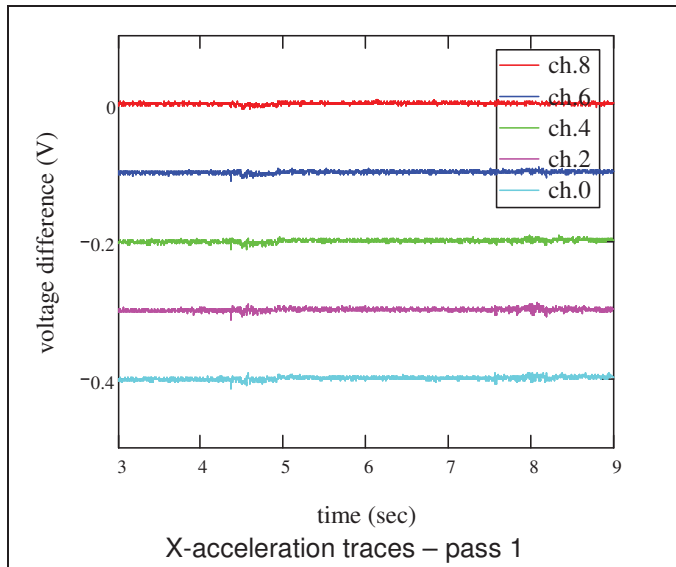
C.1.3. Padfoot roller
 a) 16 in lift thickness

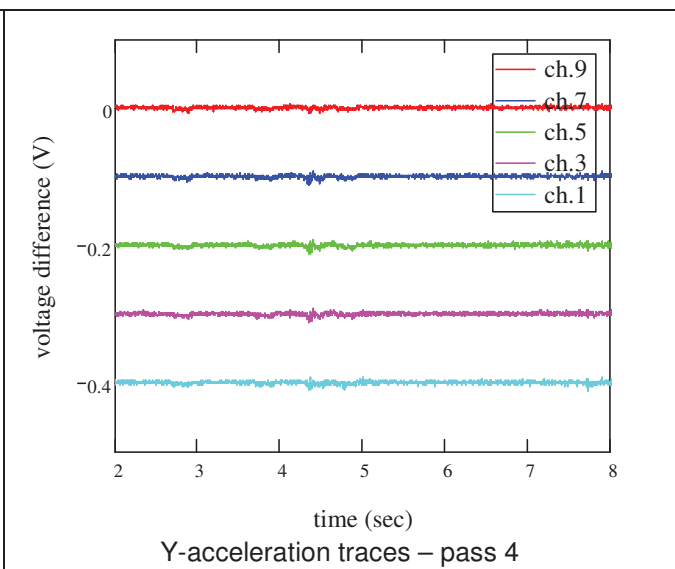
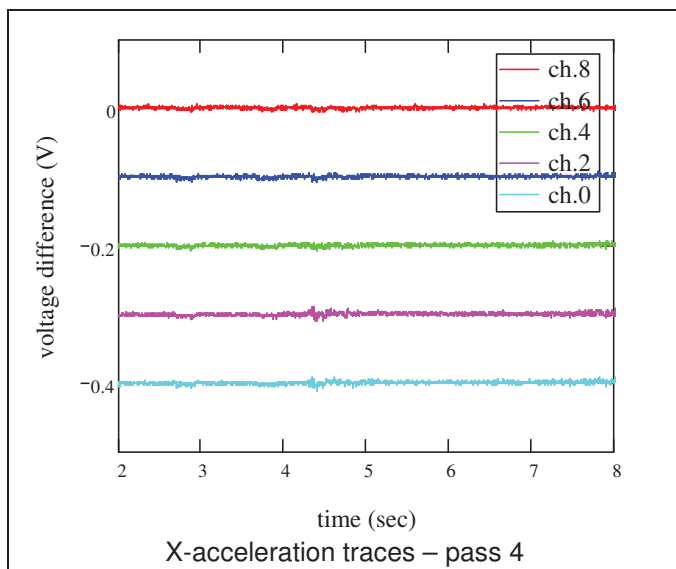
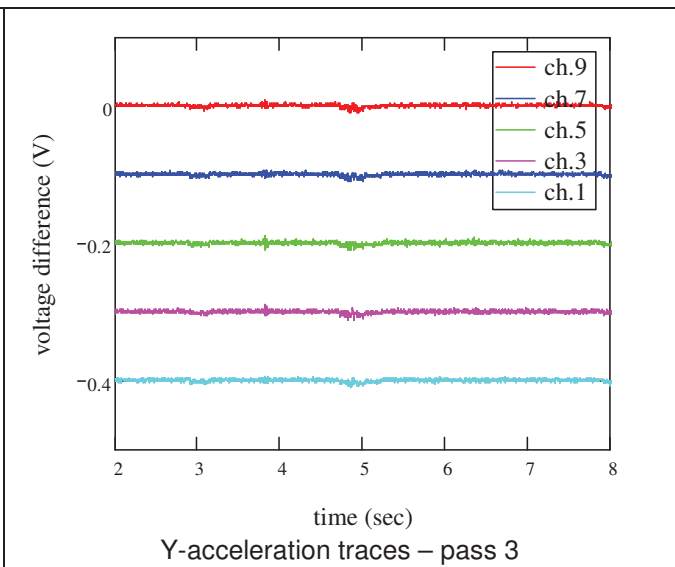
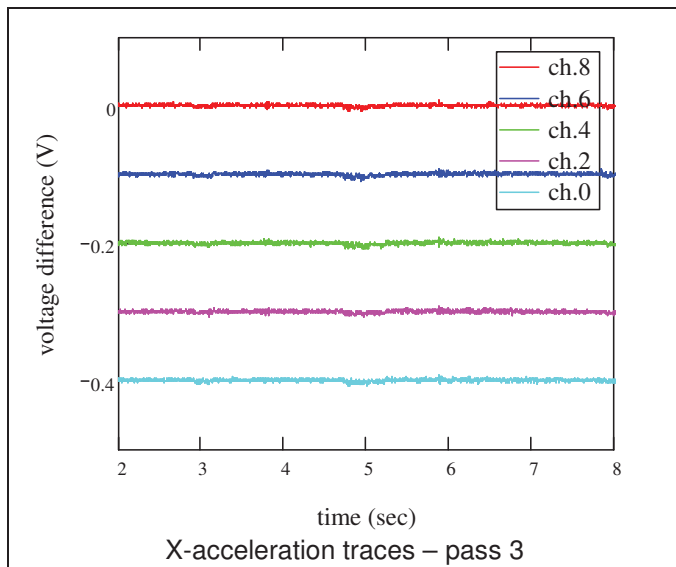


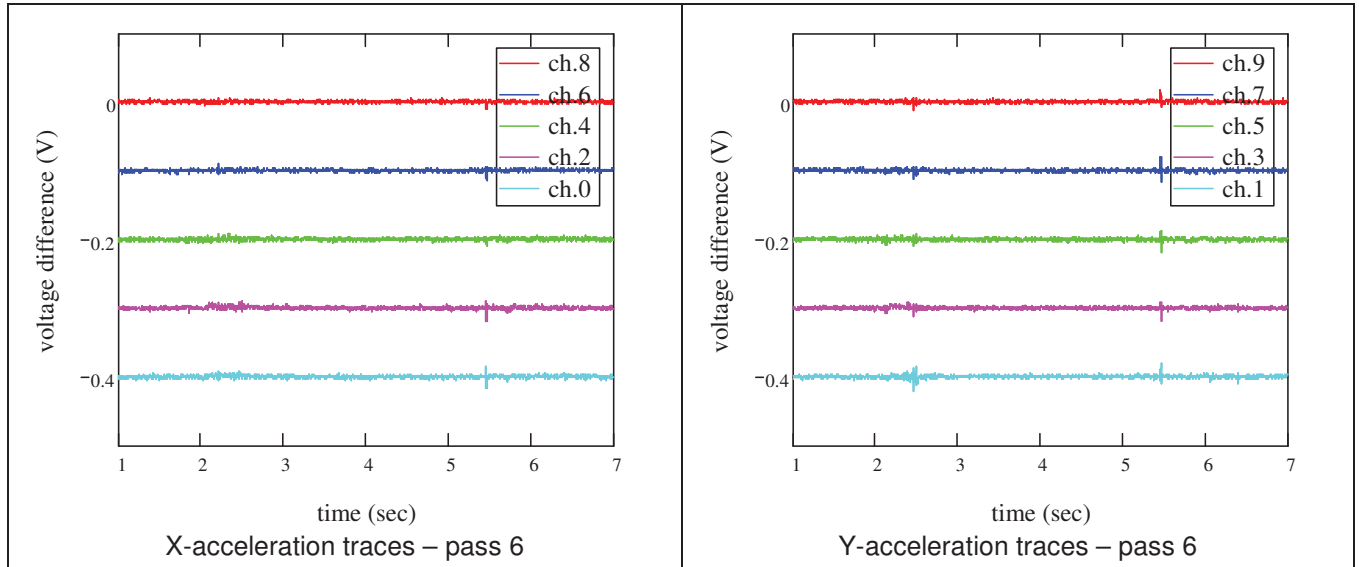
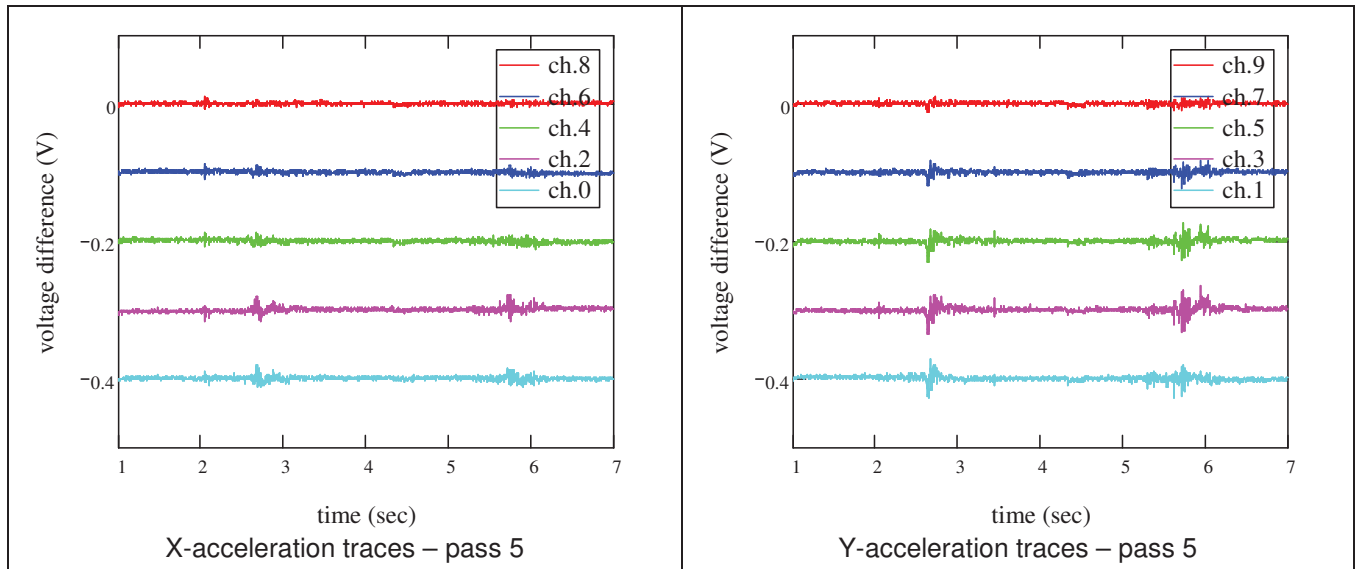




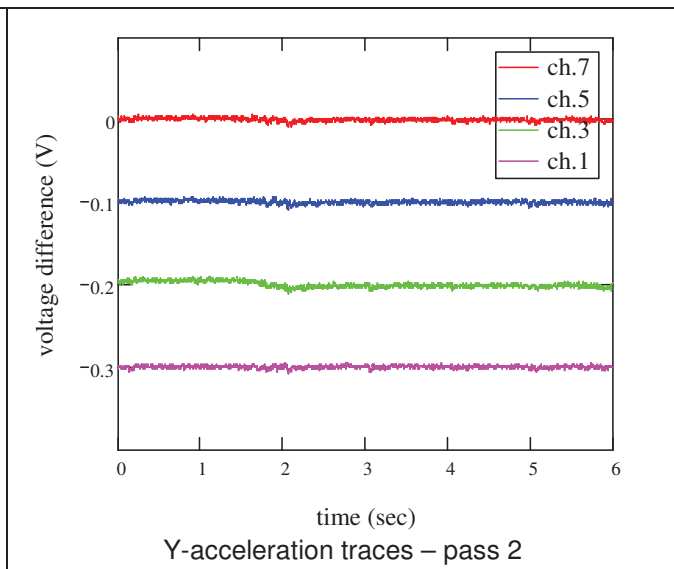
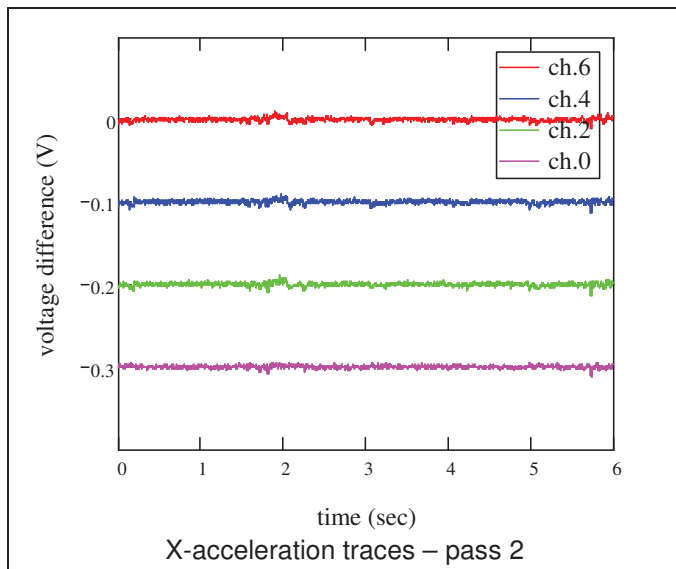
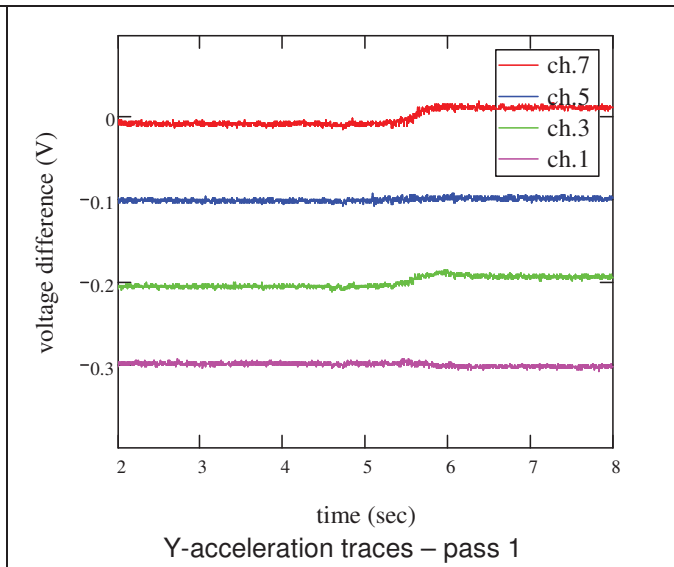
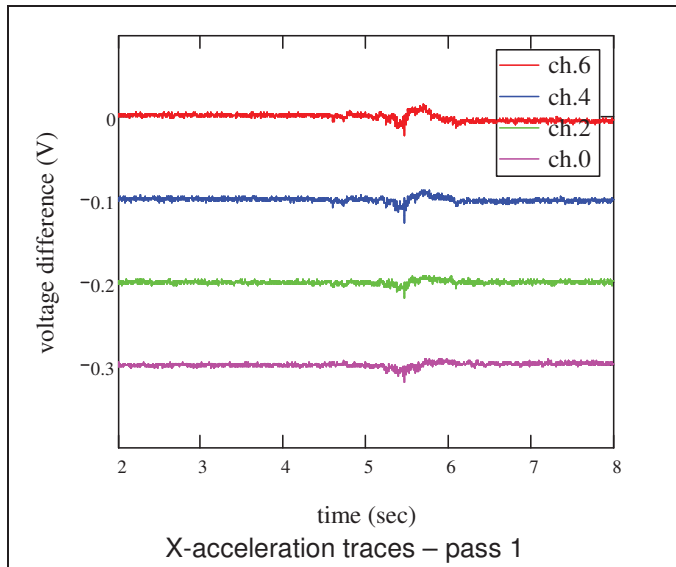
b) 24 in lift thickness

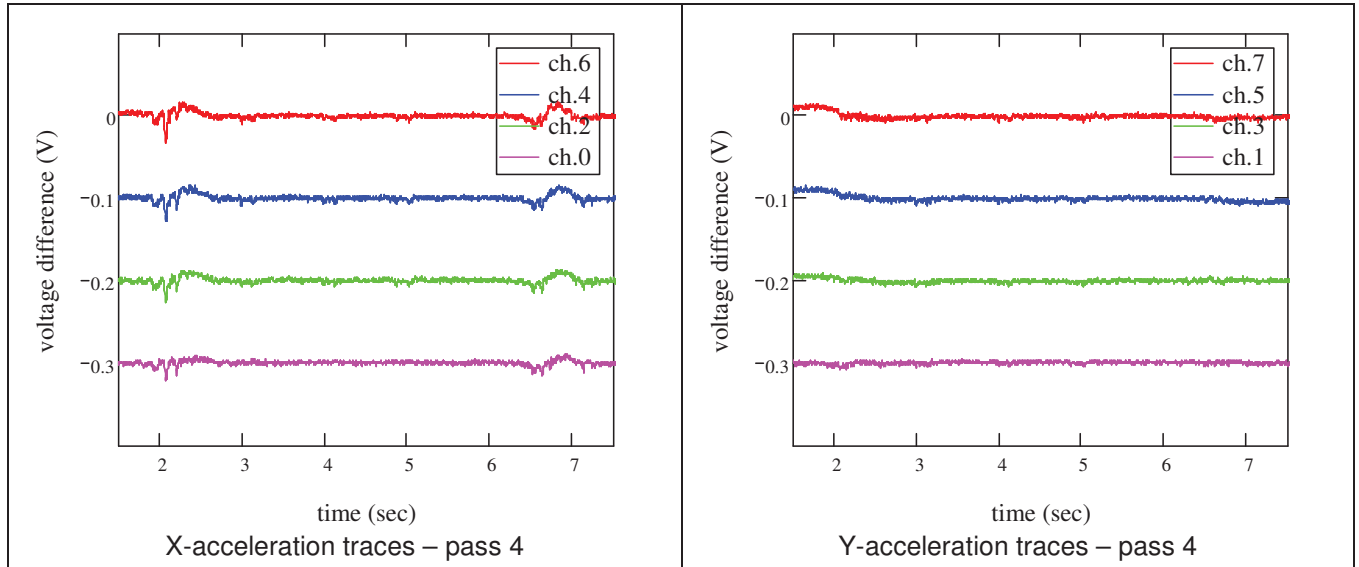
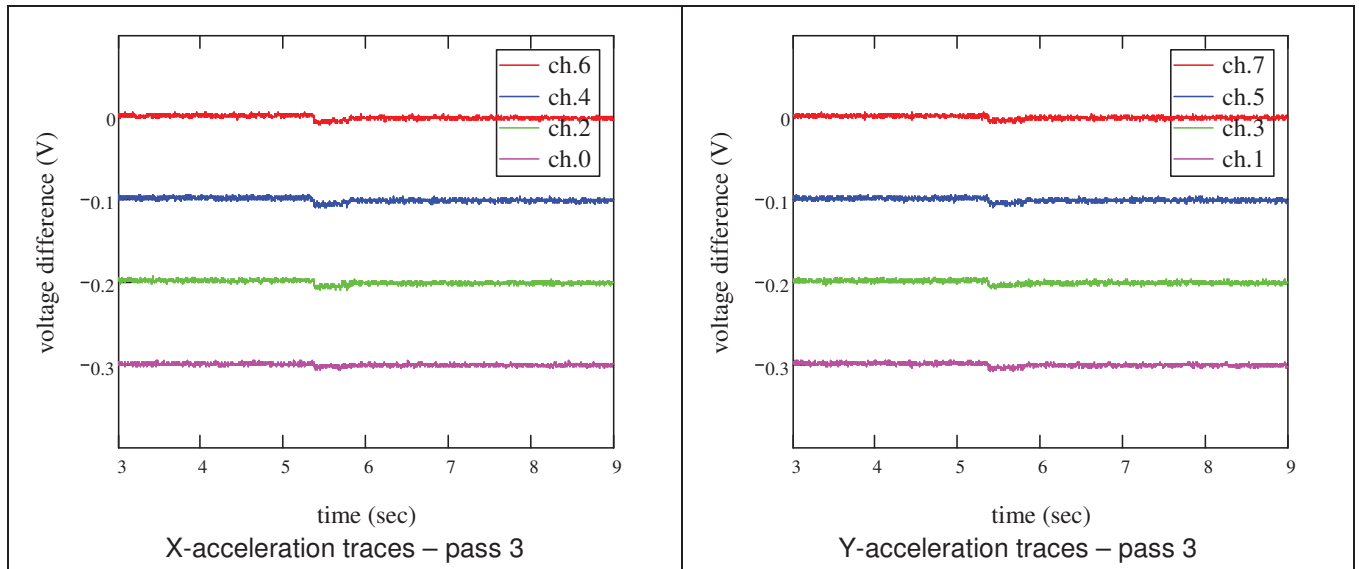




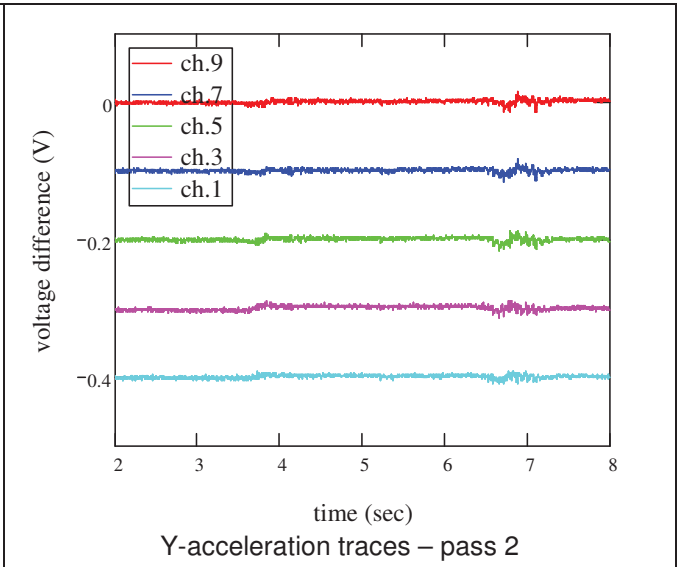
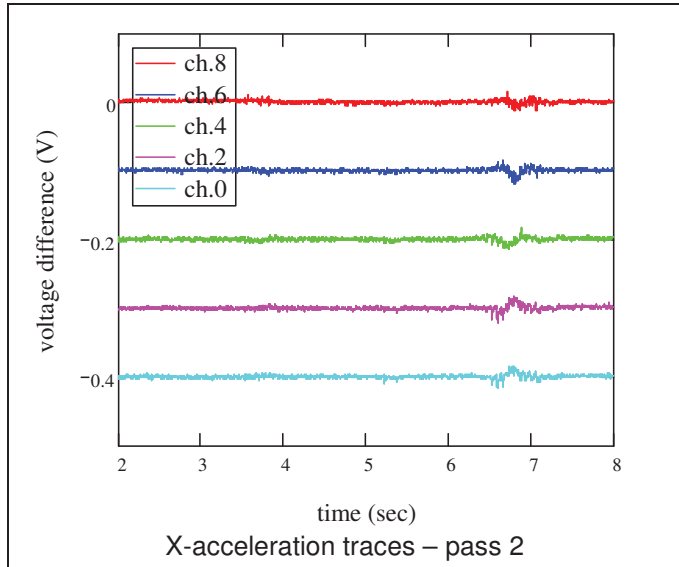
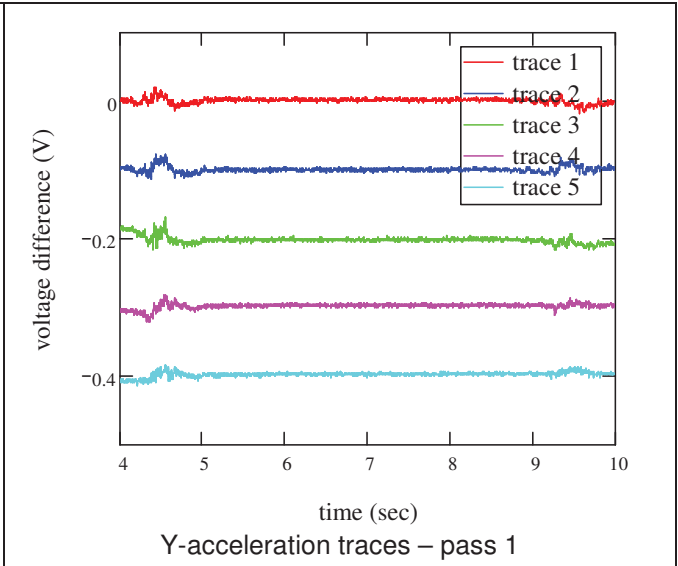
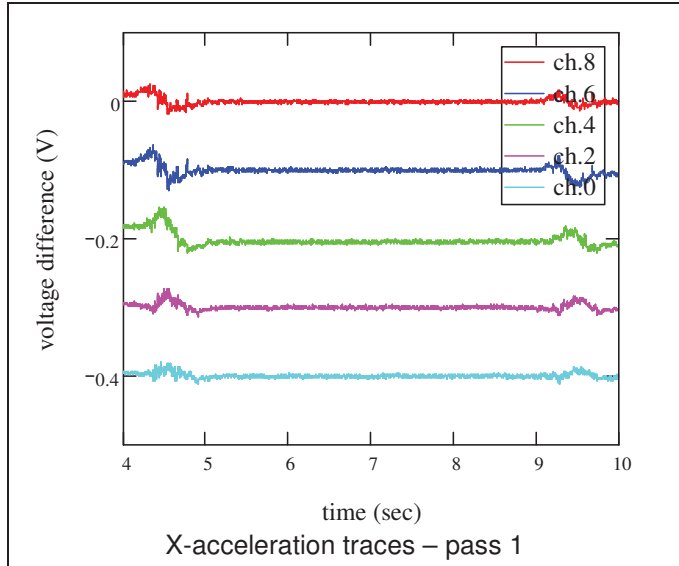


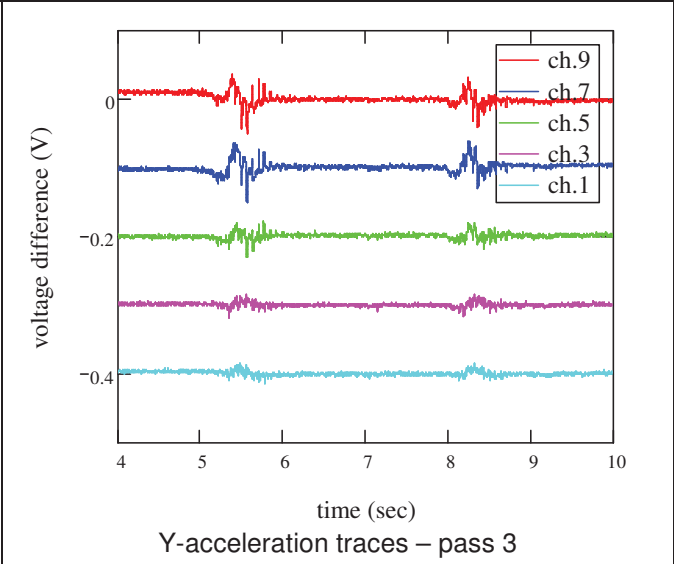
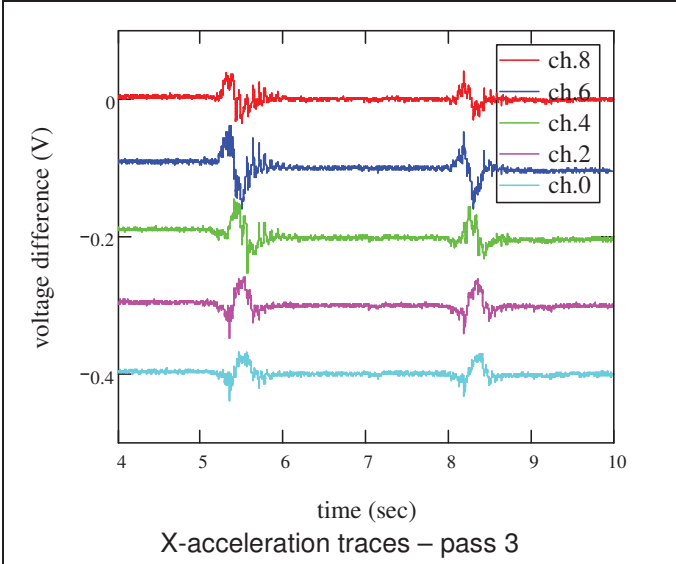
C.1.4. Scraper
a) 20 in lift thickness





b) 24 in lift thickness

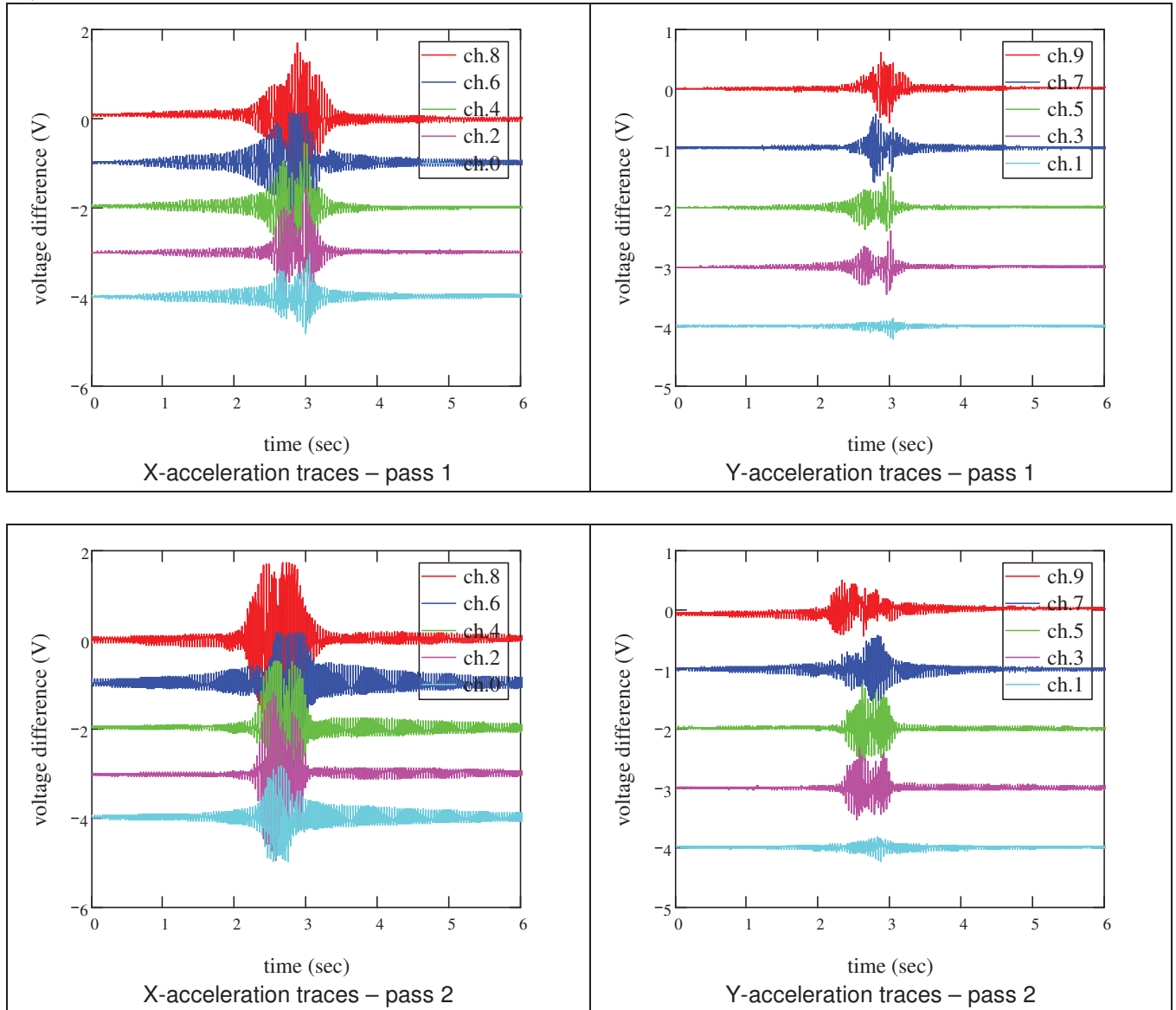


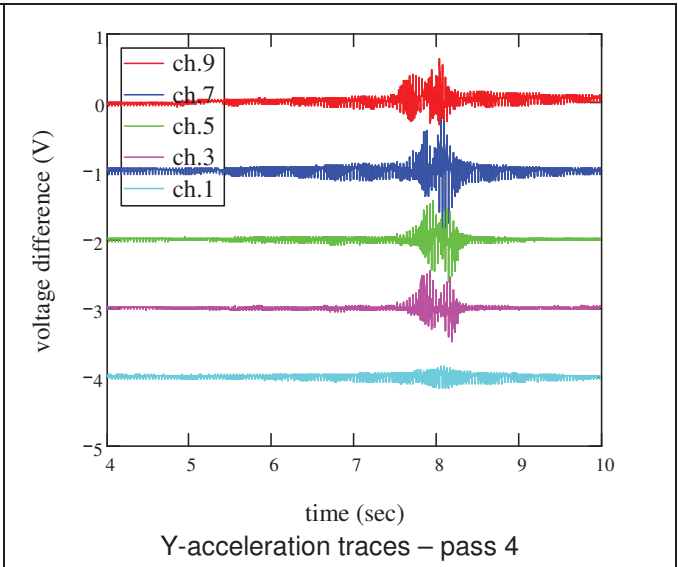
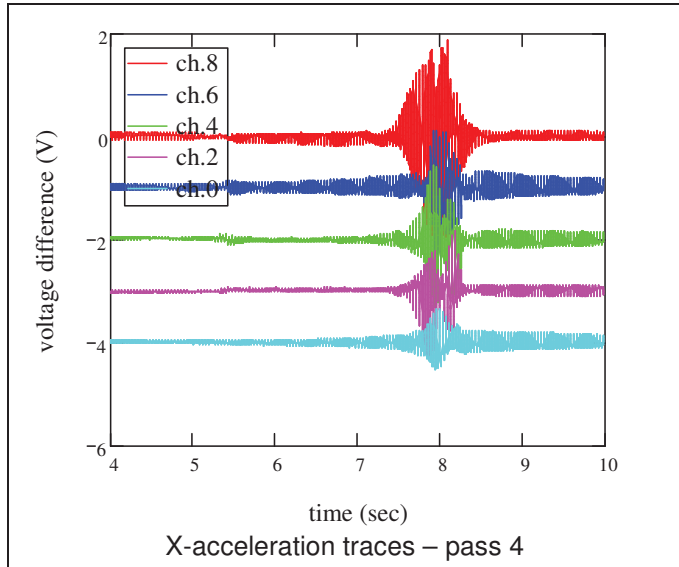
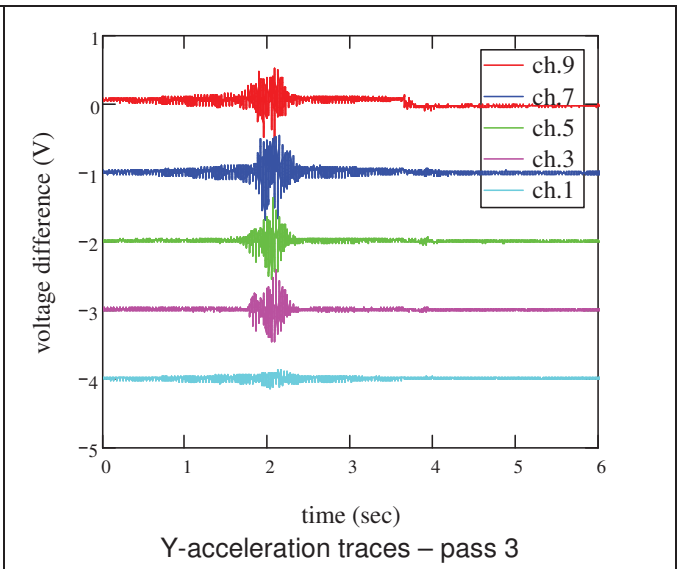
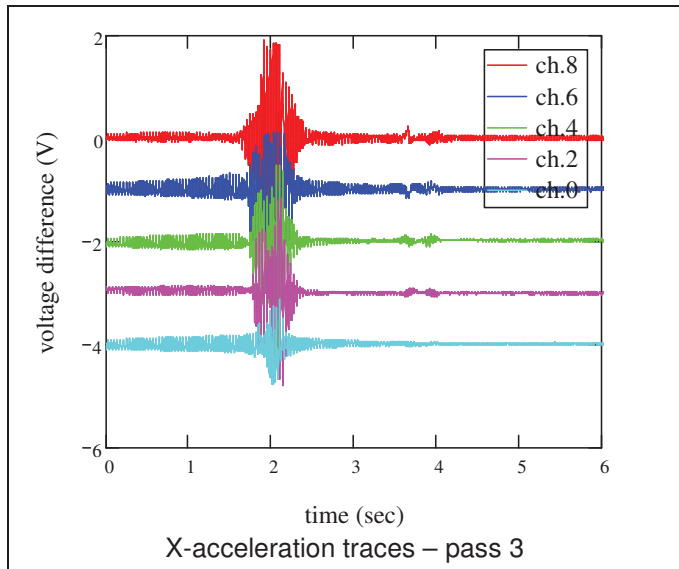


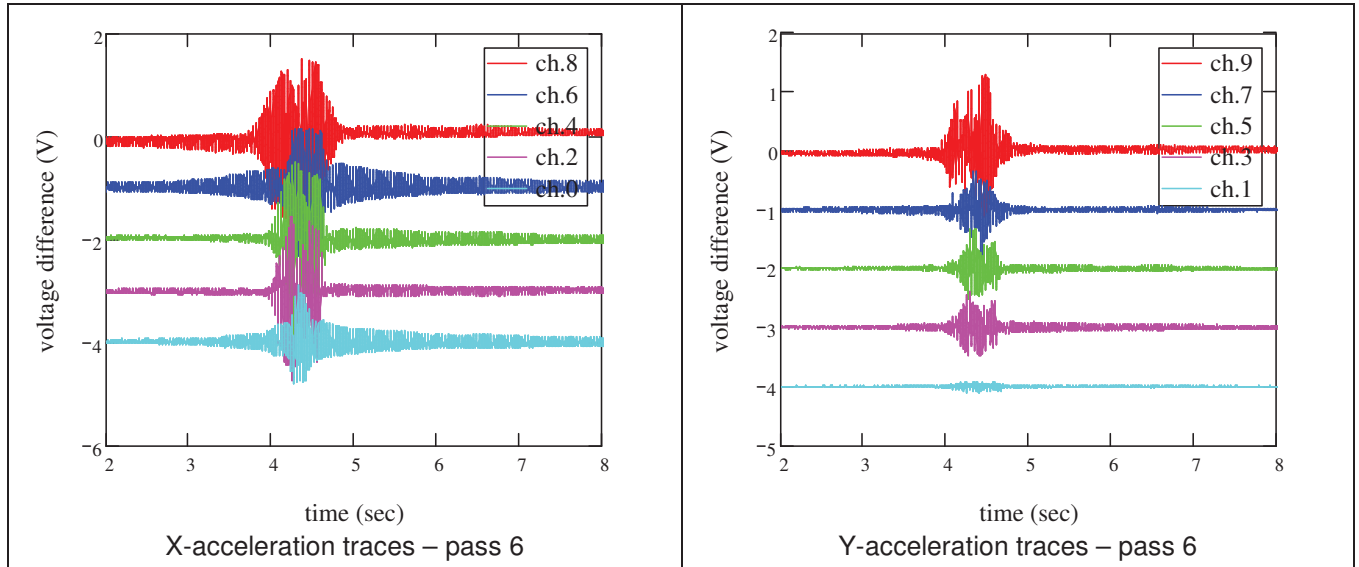
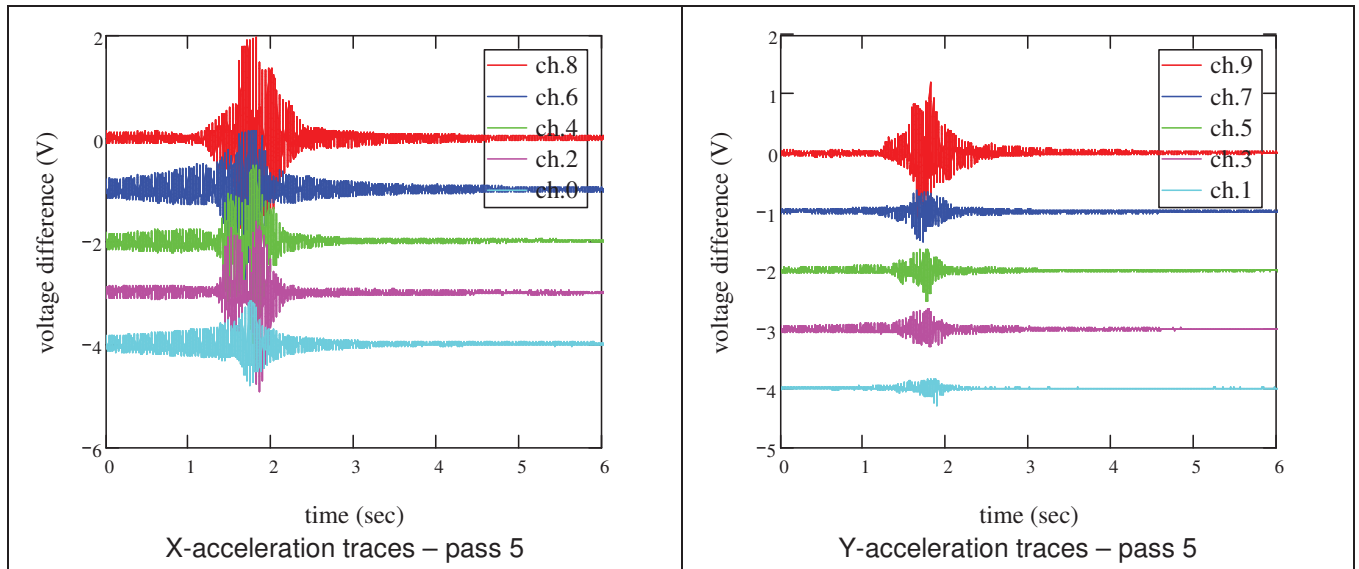
C.2. MEMS rotation angle measurement in the coarse-grained soil (natural moisture)

C.2.1. Smooth-drum vibratory roller

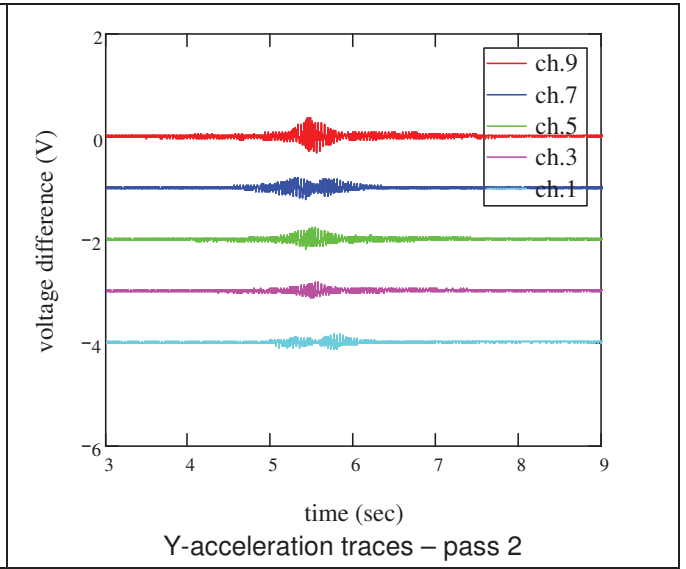
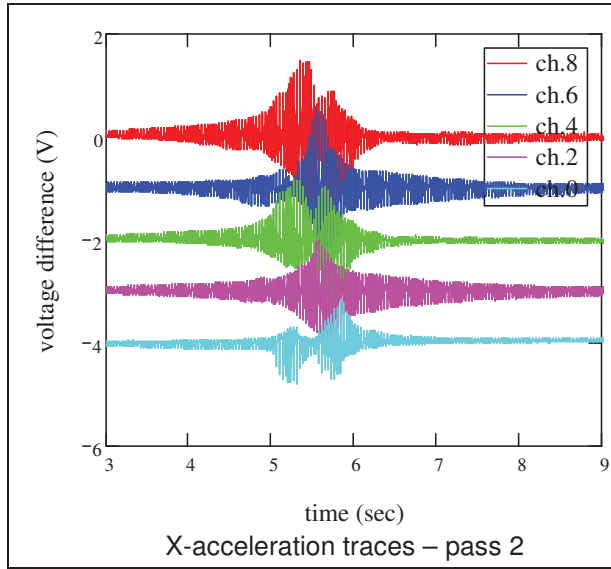
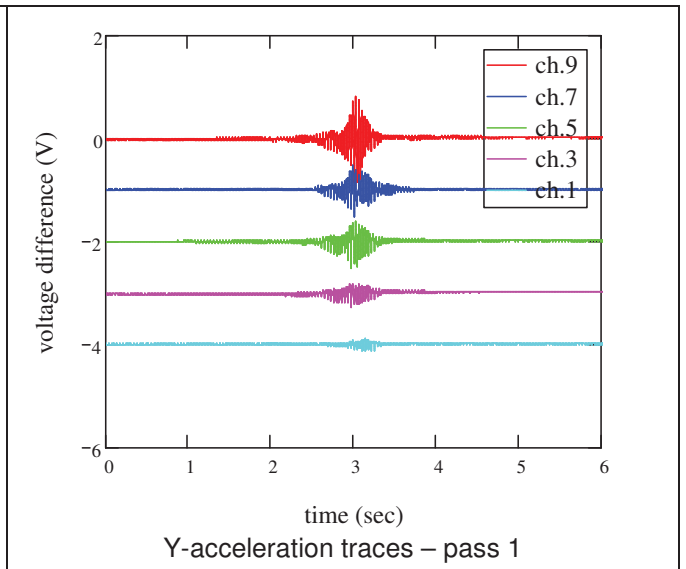
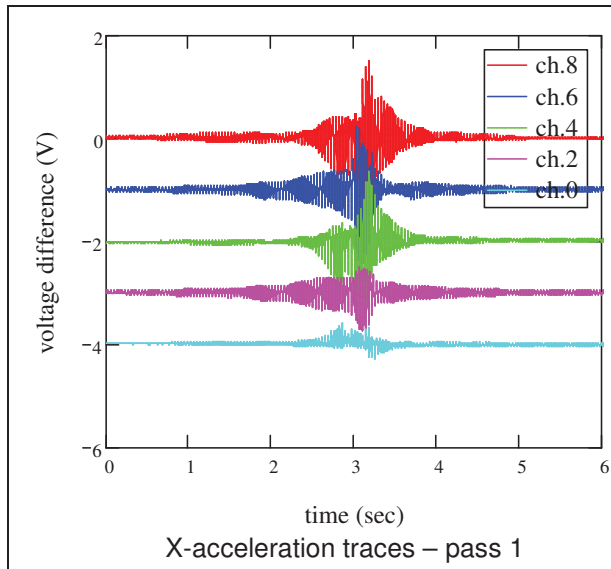
a) 8 in lift thickness

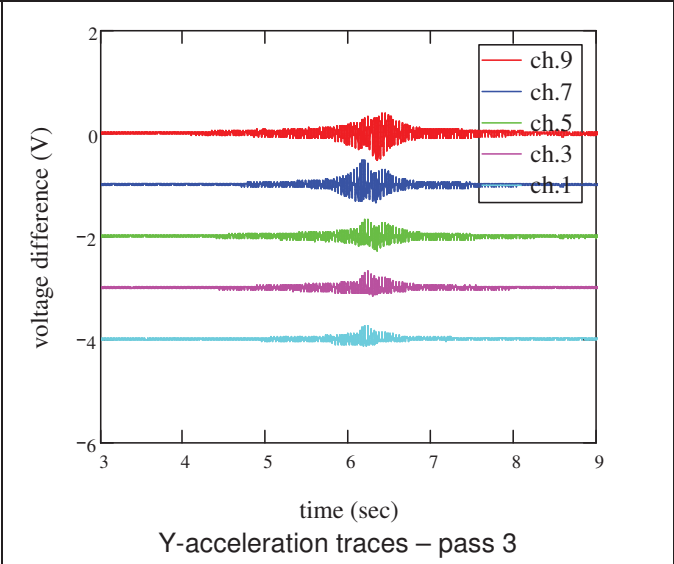
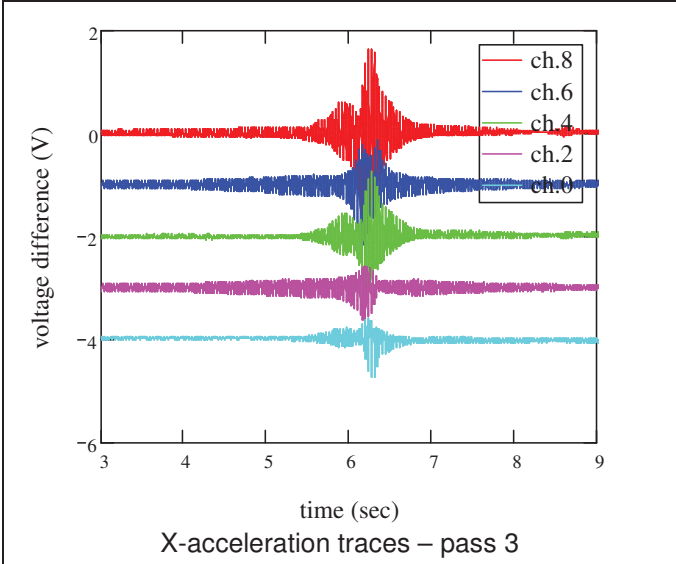


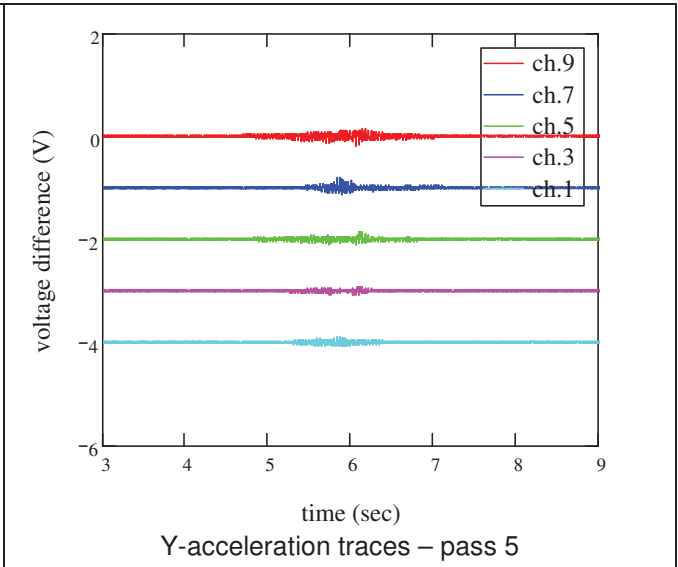
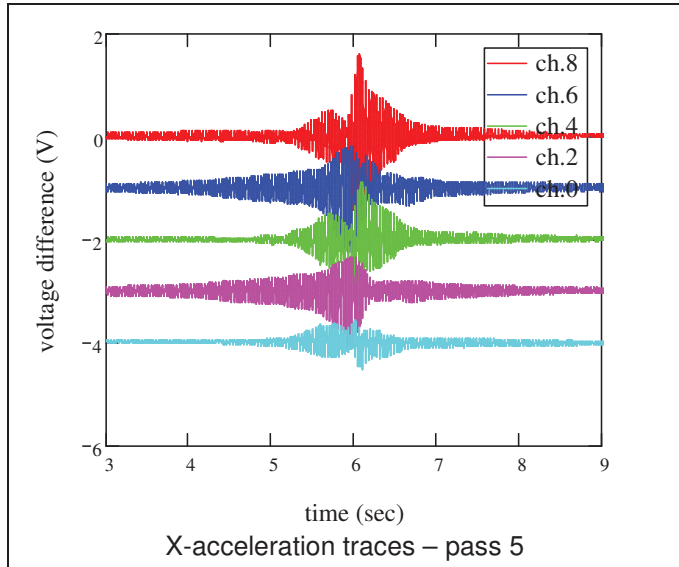
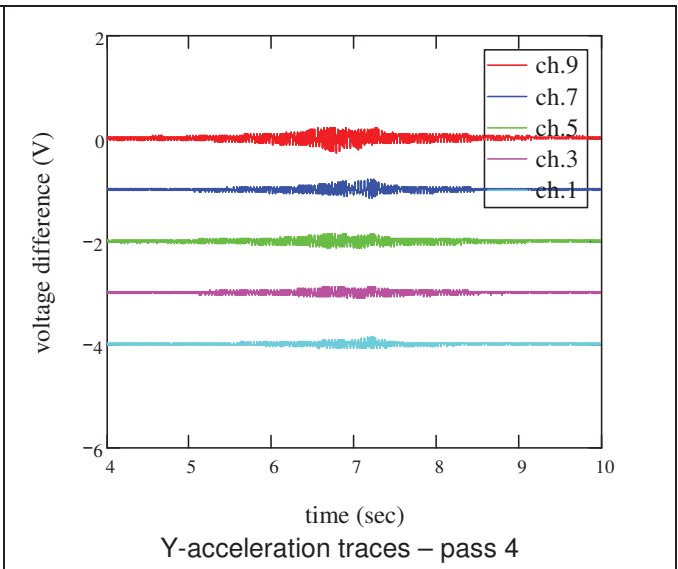
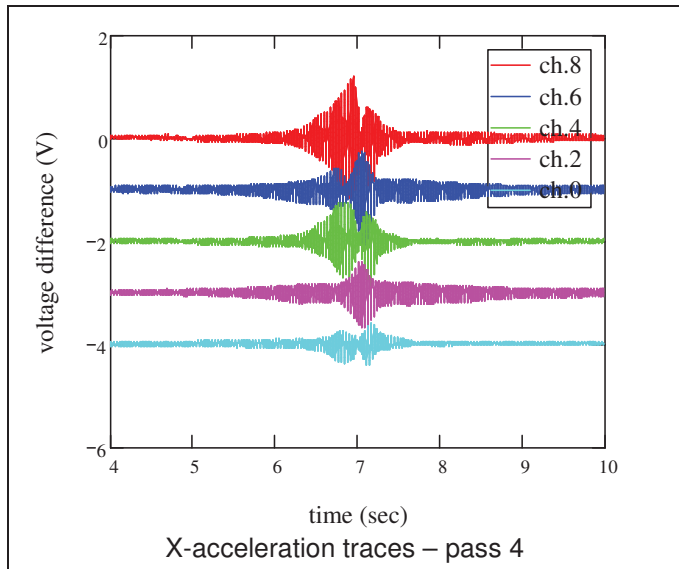


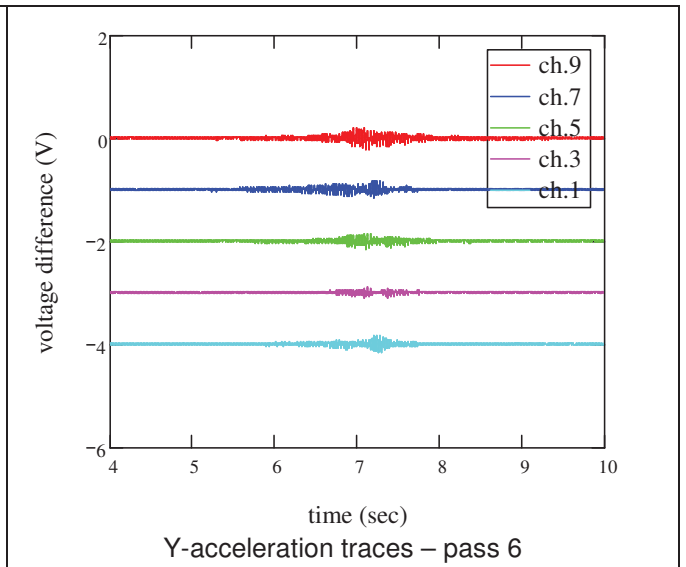
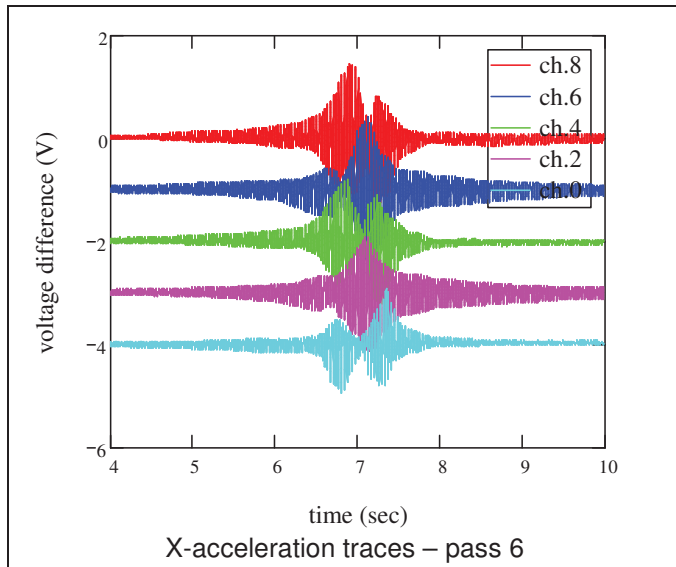


b) 13 in lift thickness

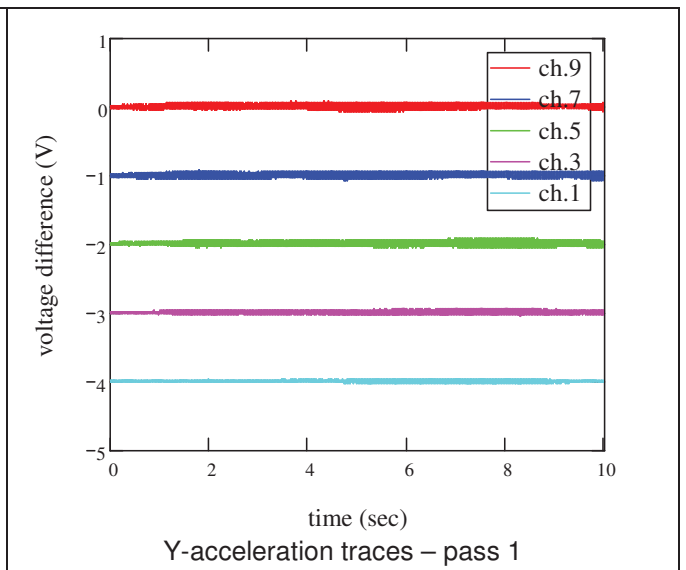
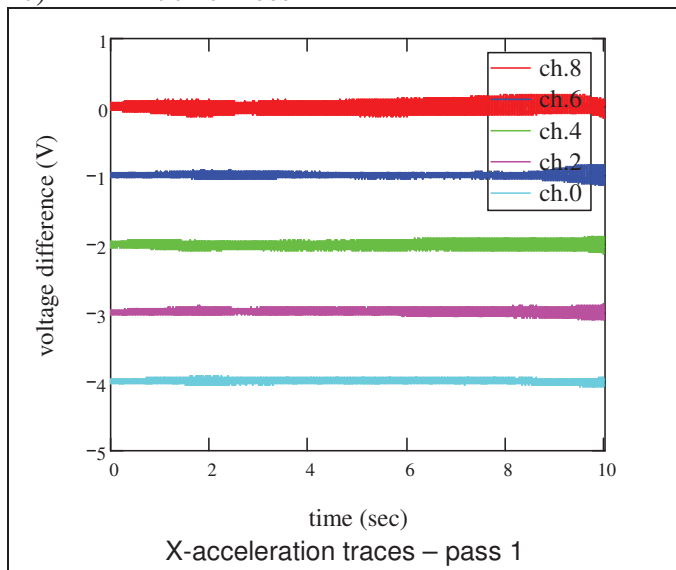


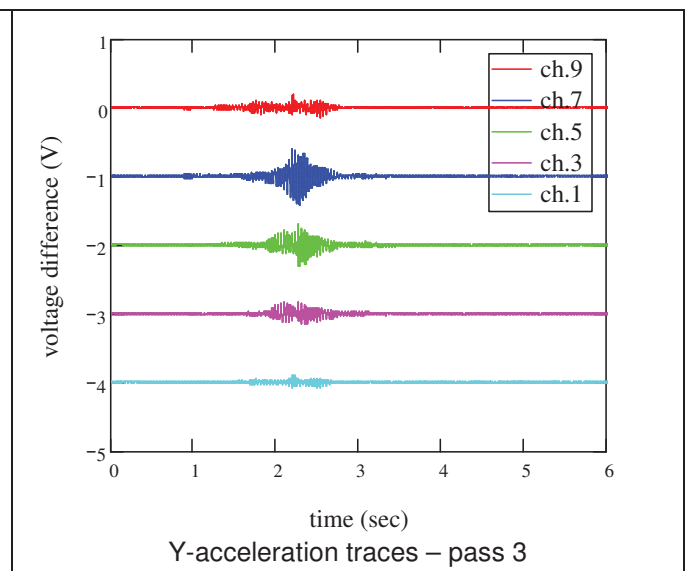
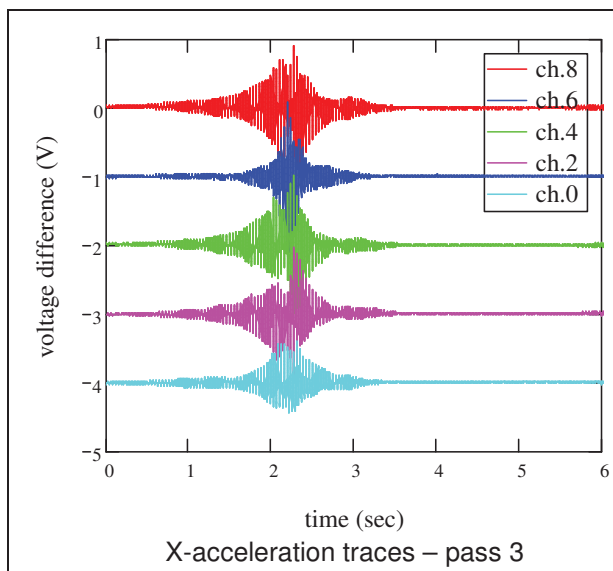
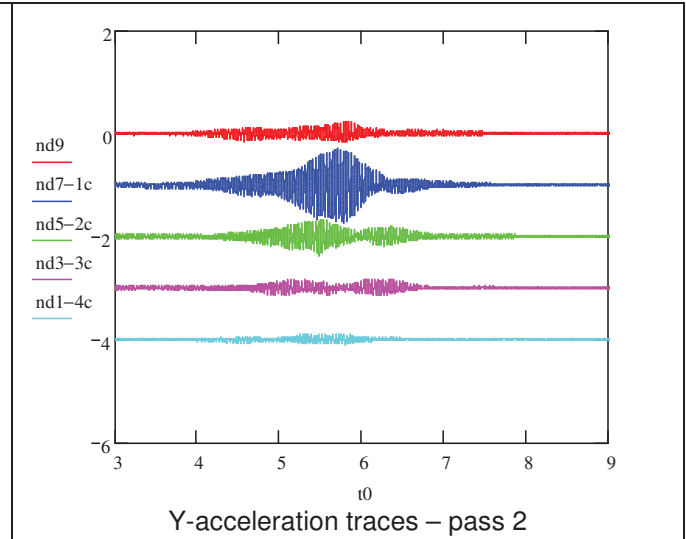
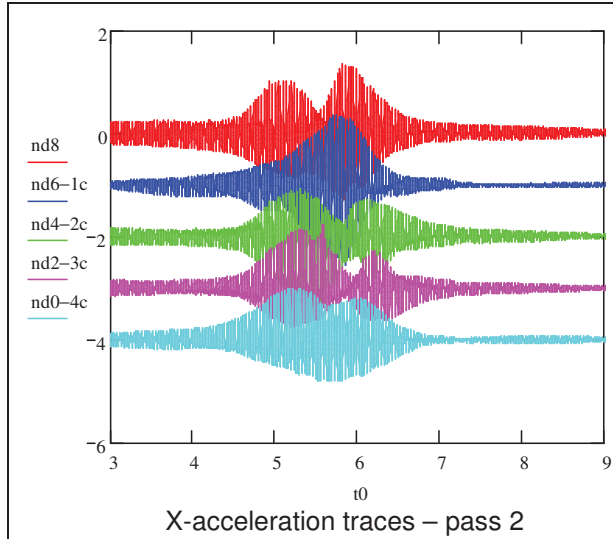


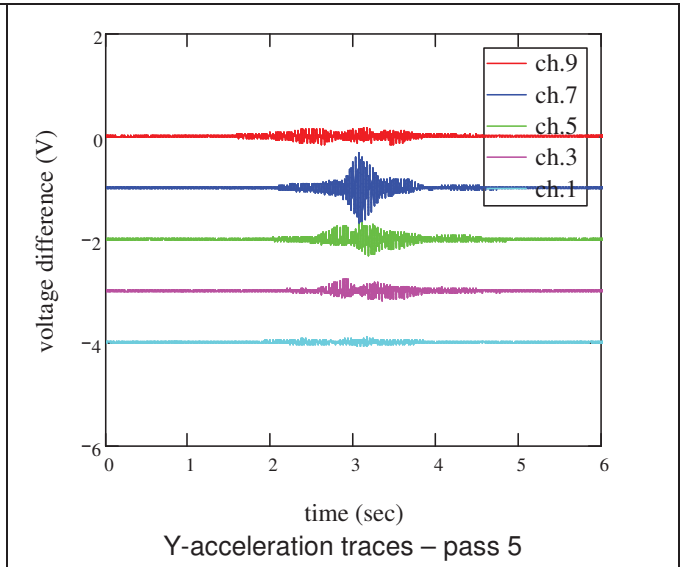
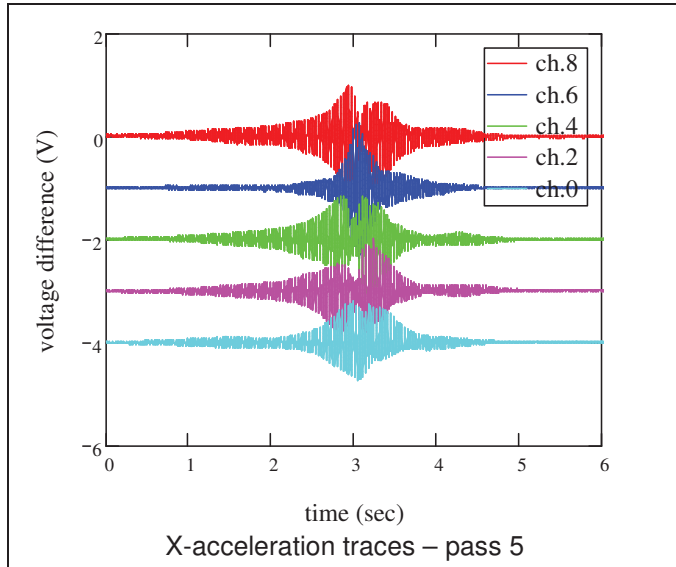
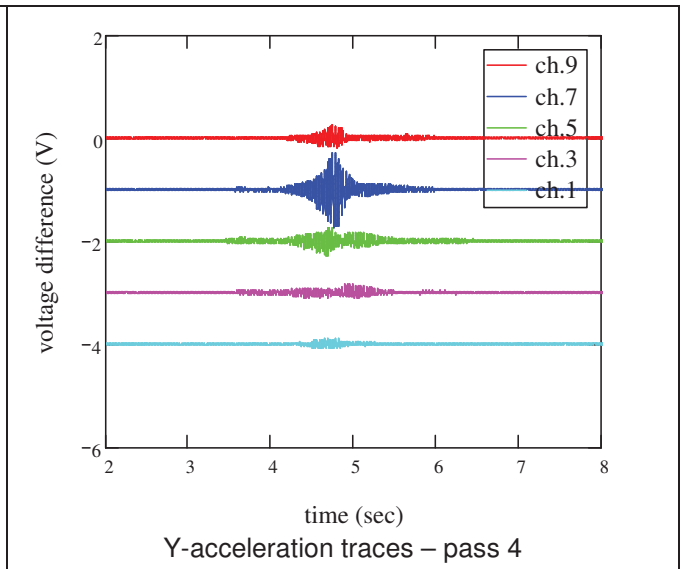
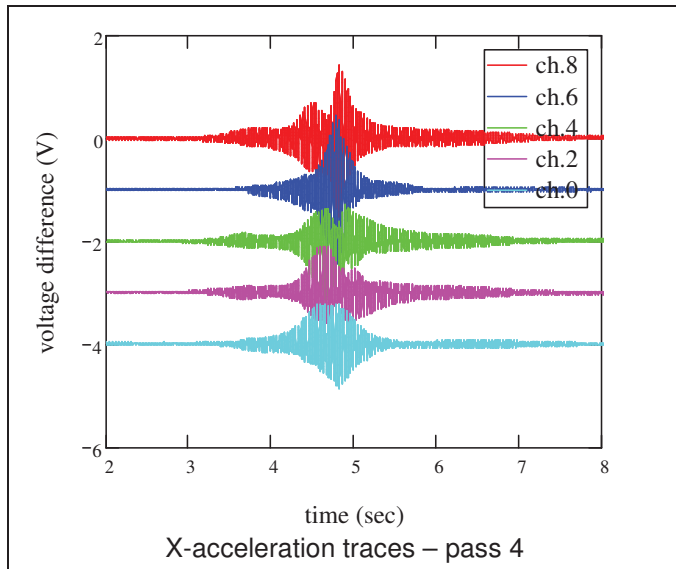


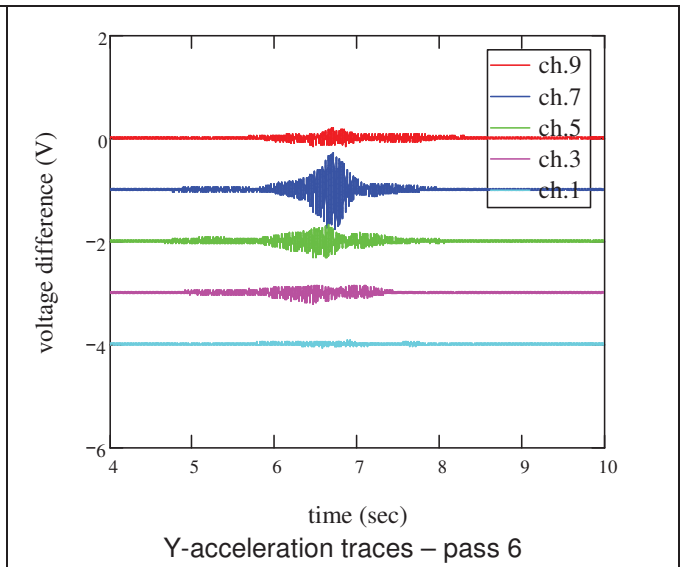
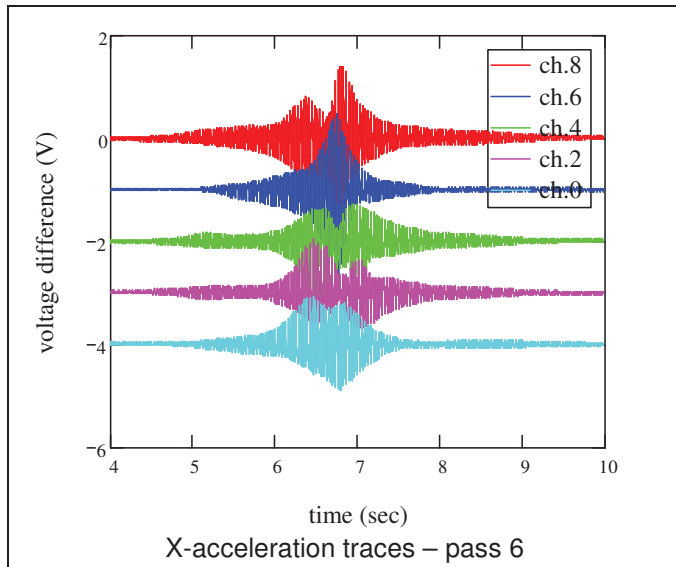


c) 24 in lift thickness

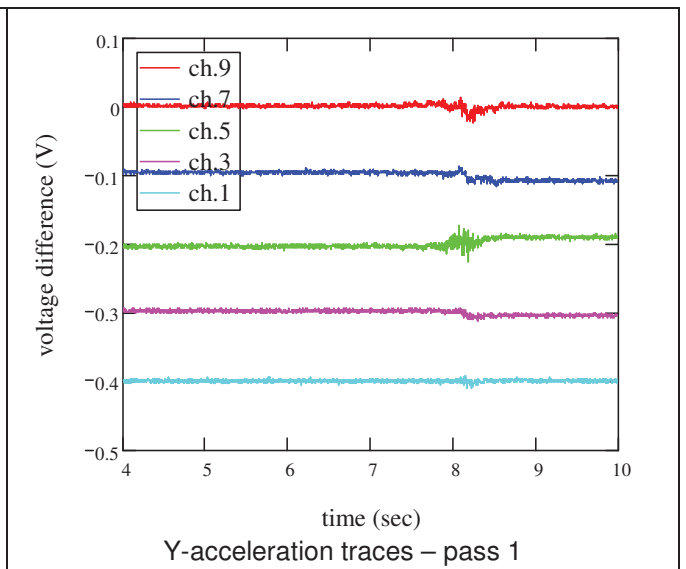
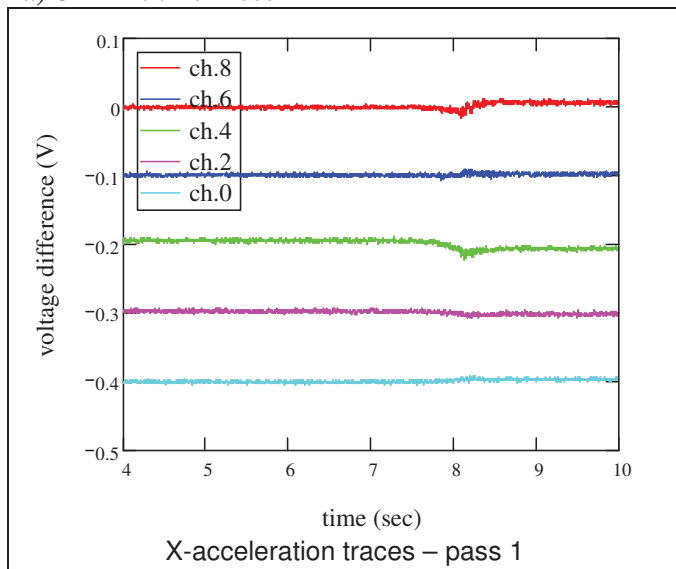


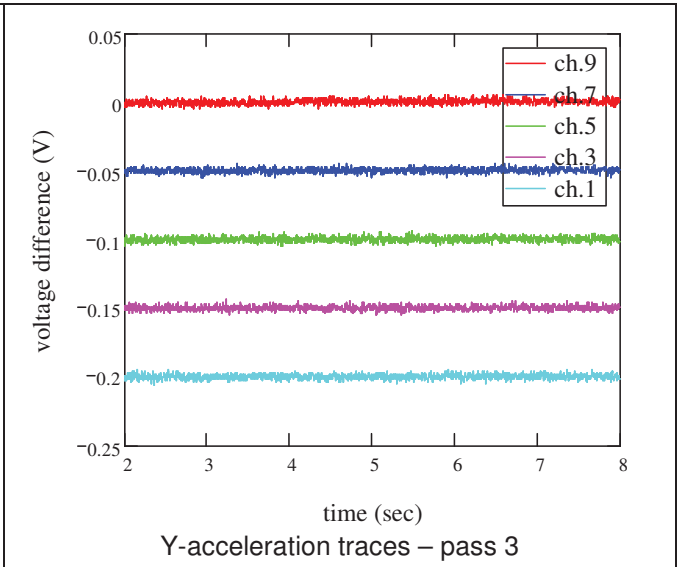
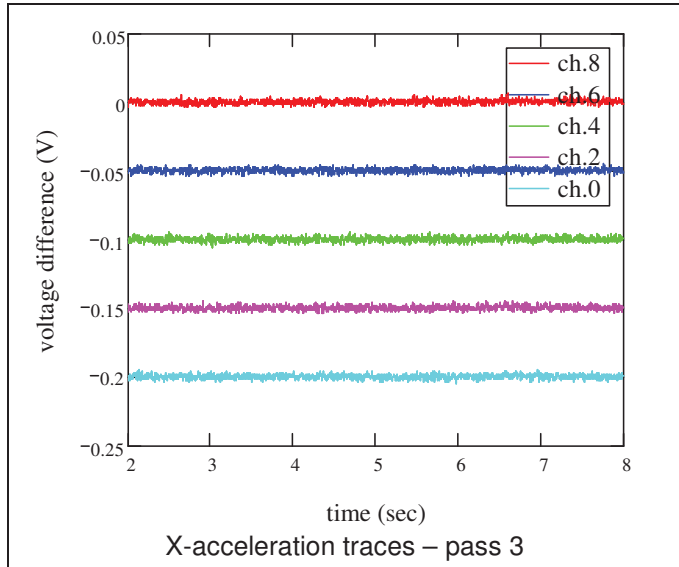
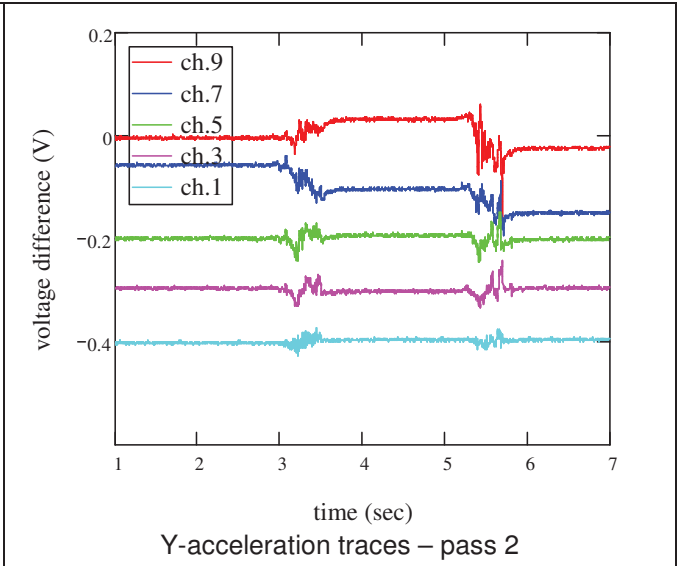
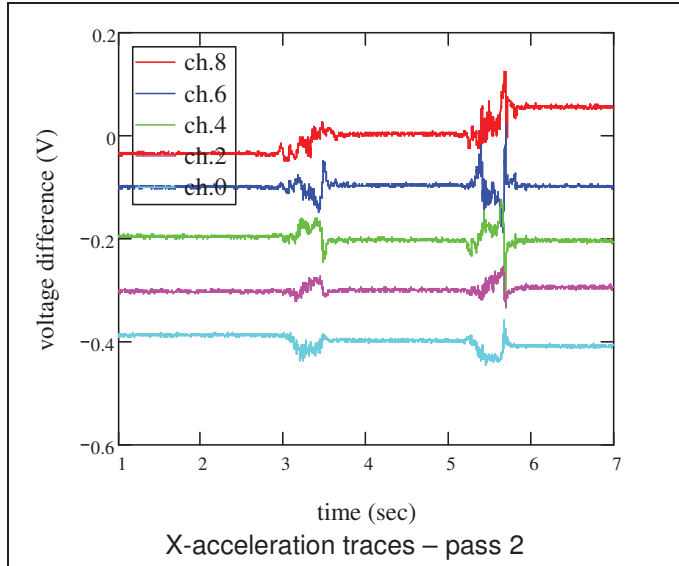


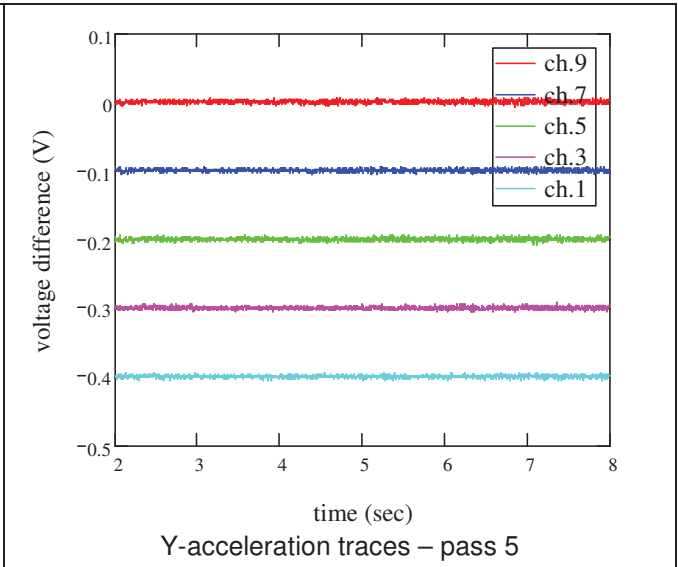
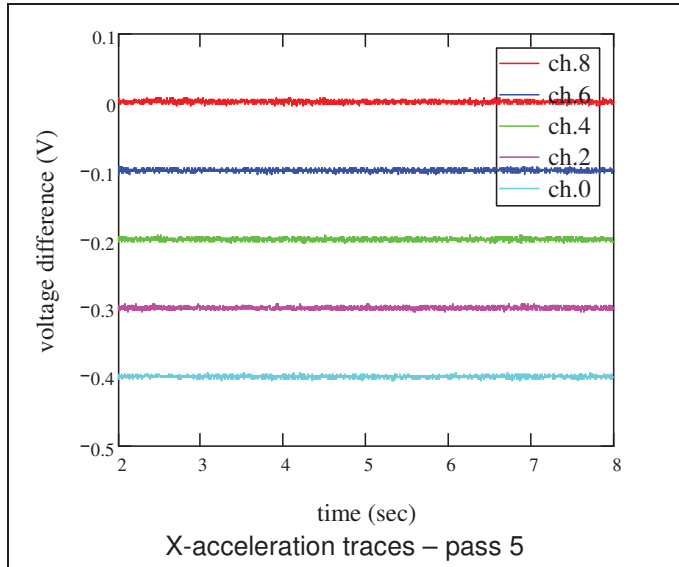
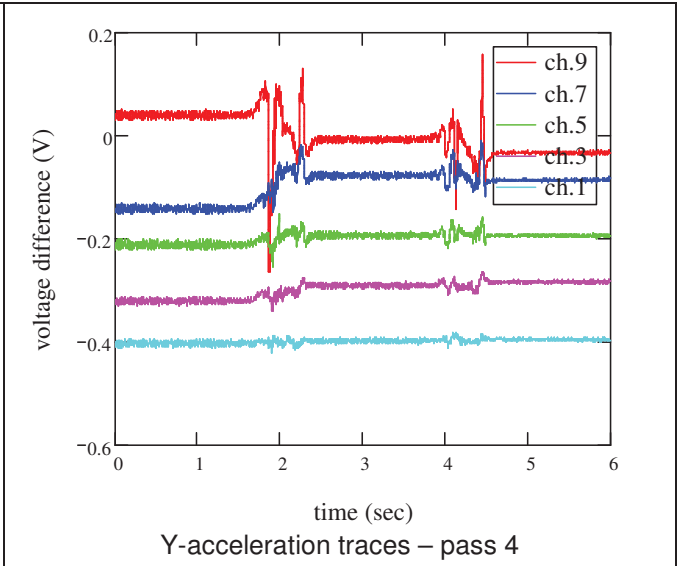
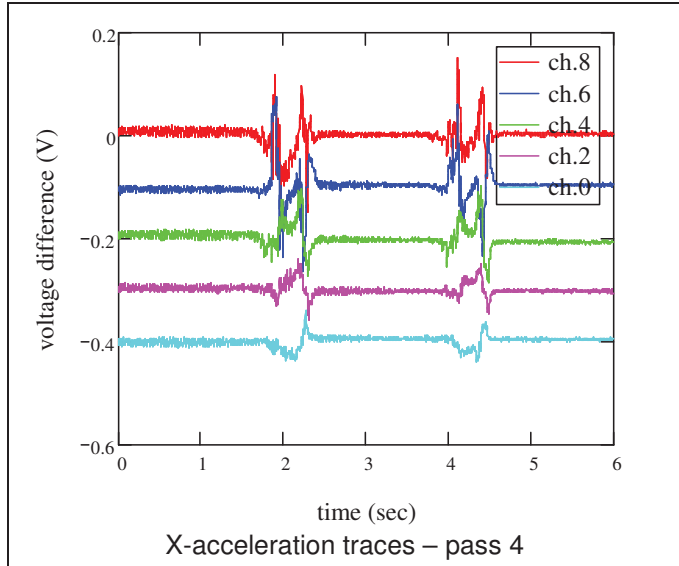


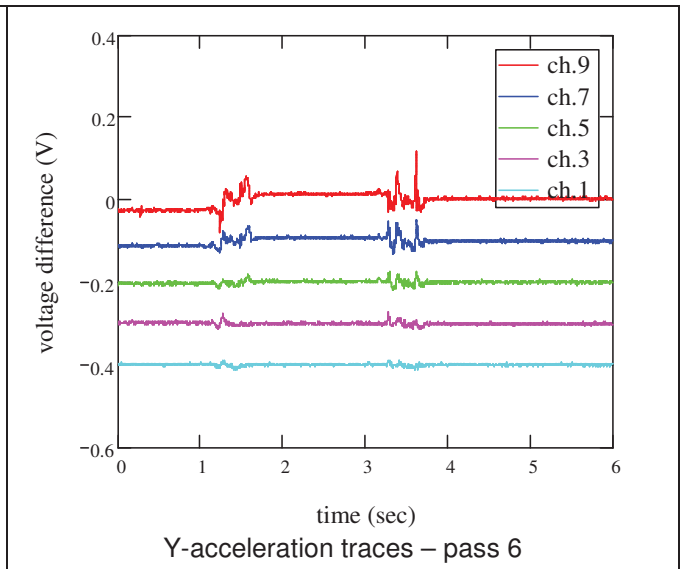
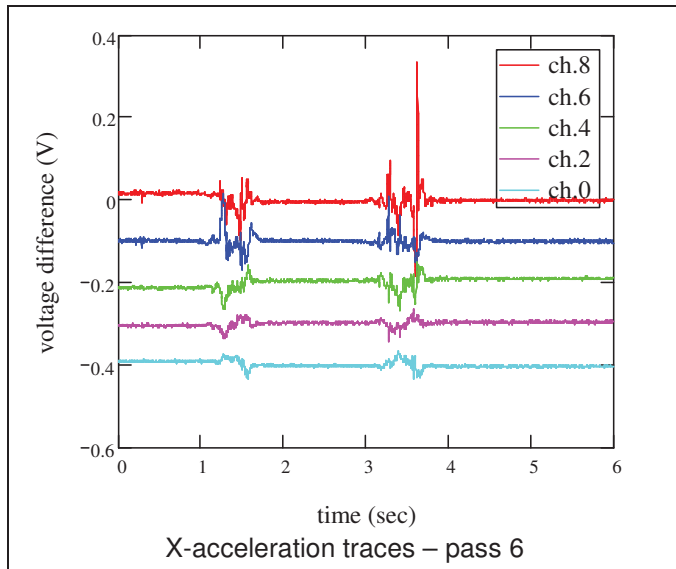


C.2.2. Rubber-tired roller
a) 8 in lift thickness

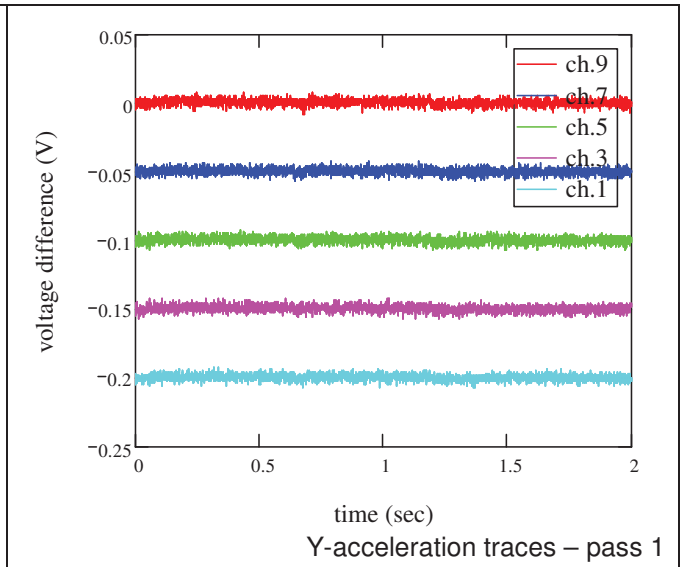
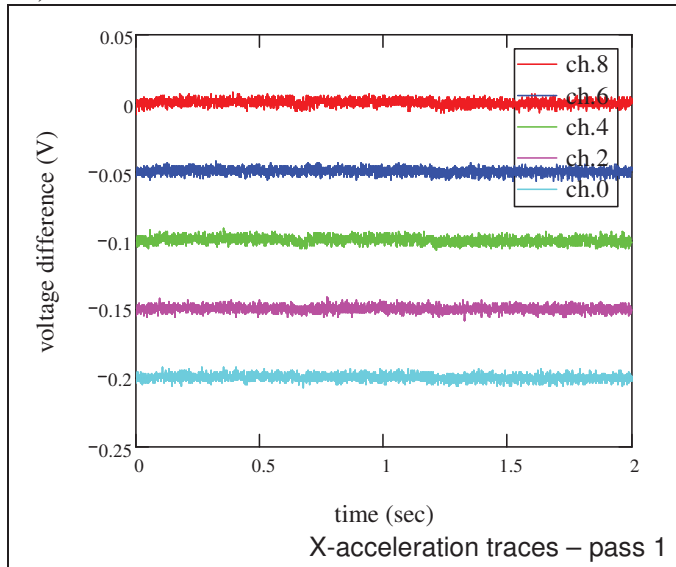


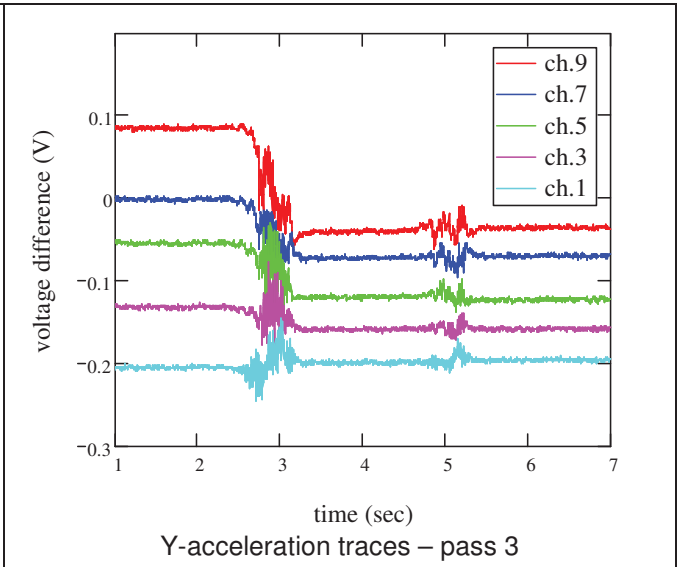
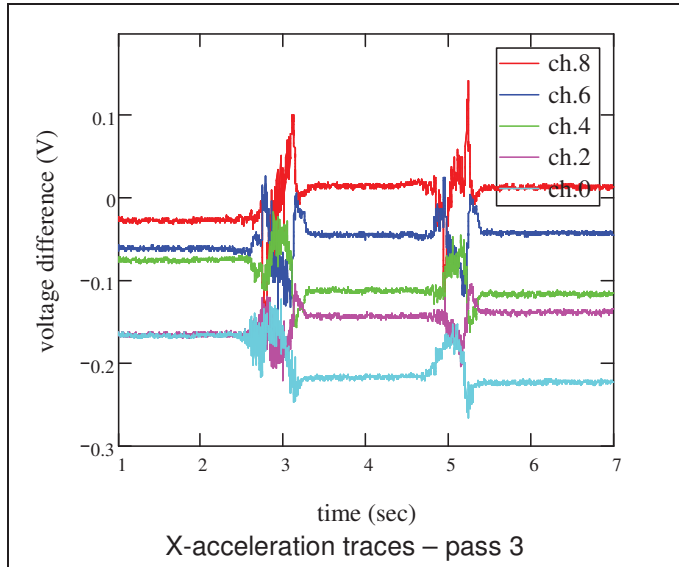
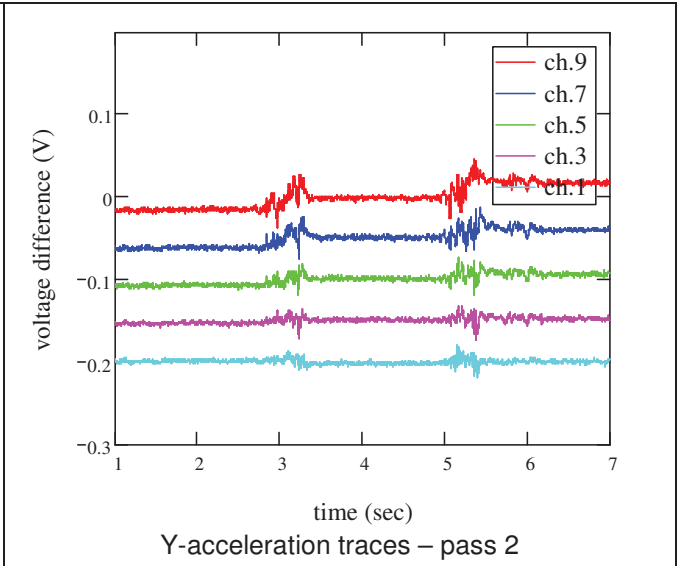
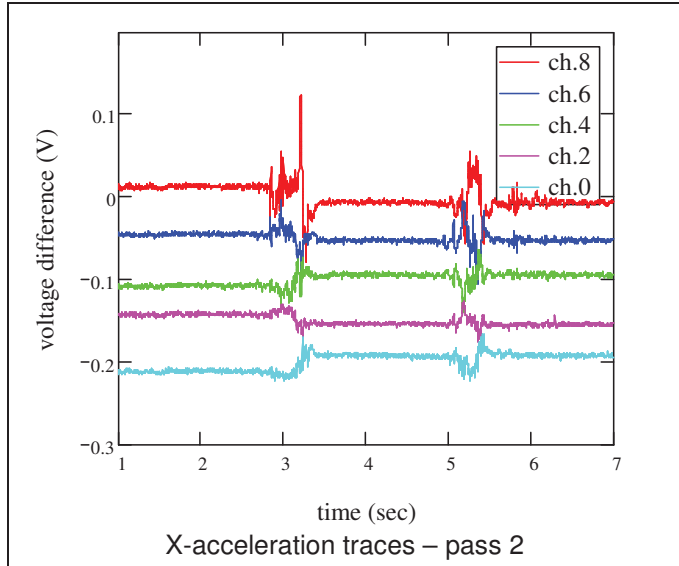


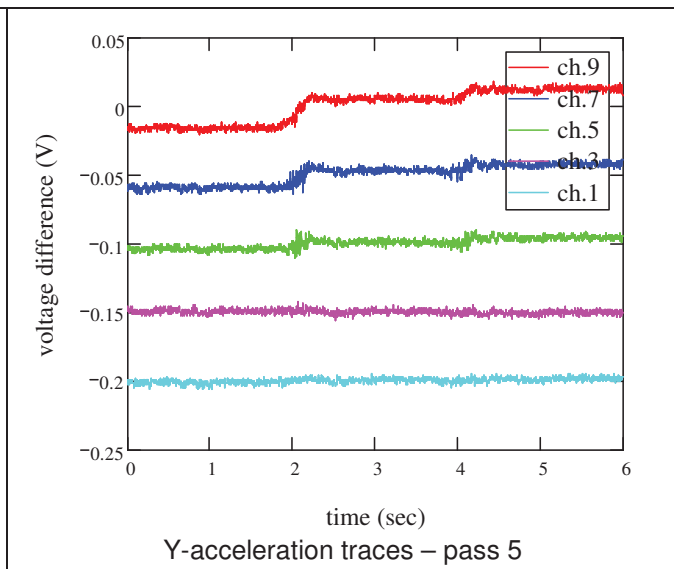
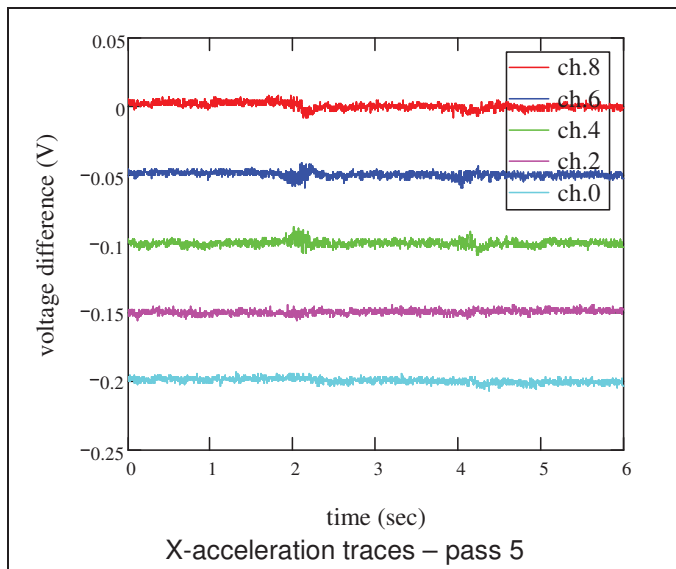
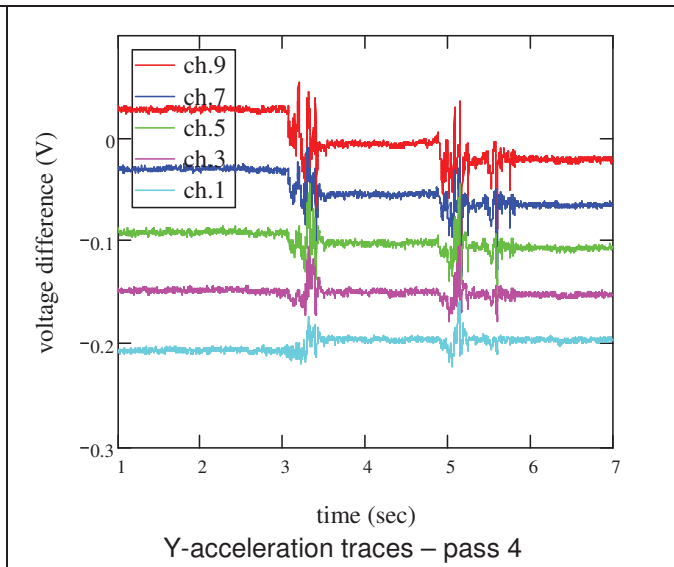
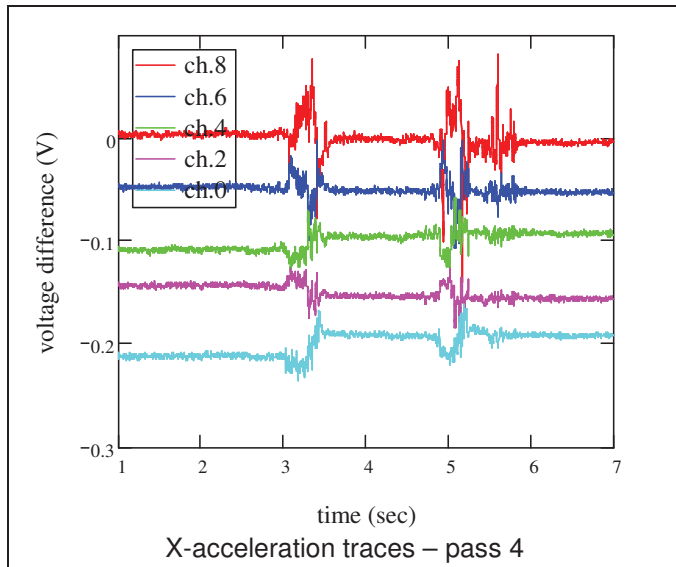


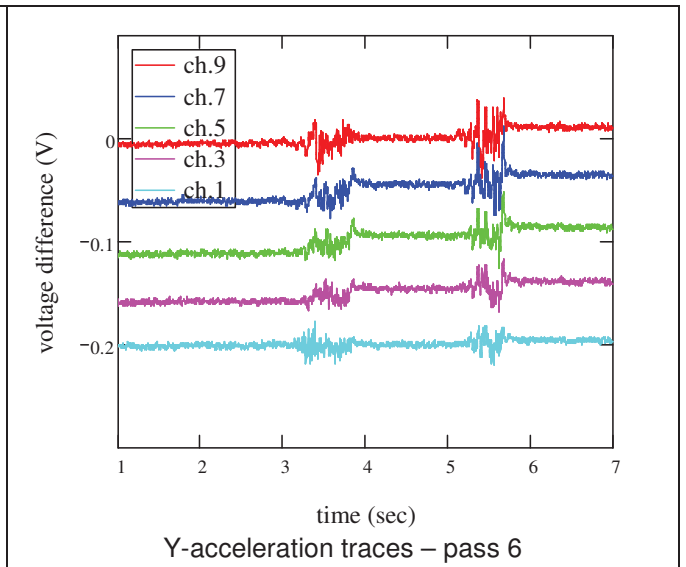
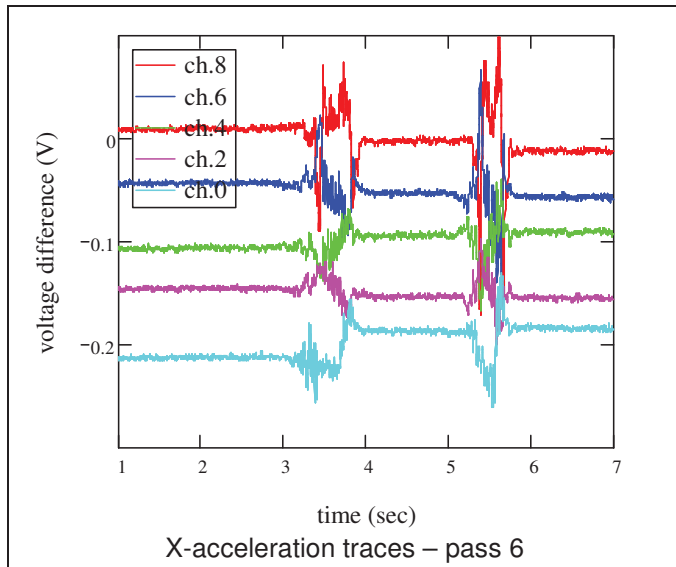


b) 13 in lift thickness

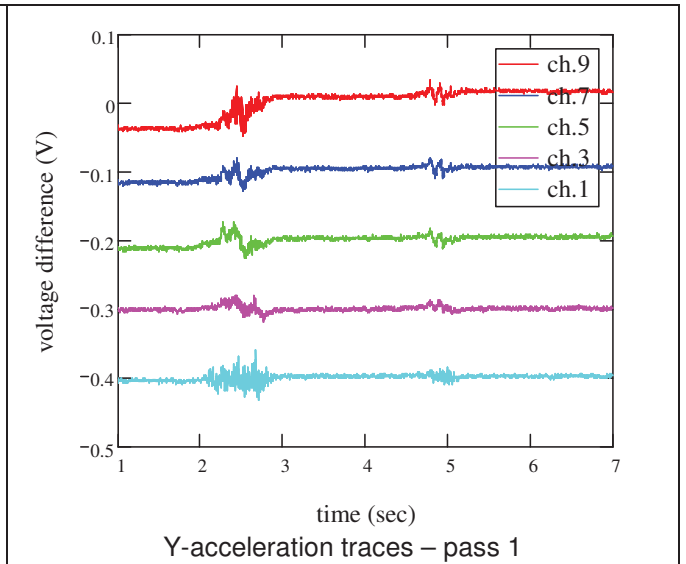
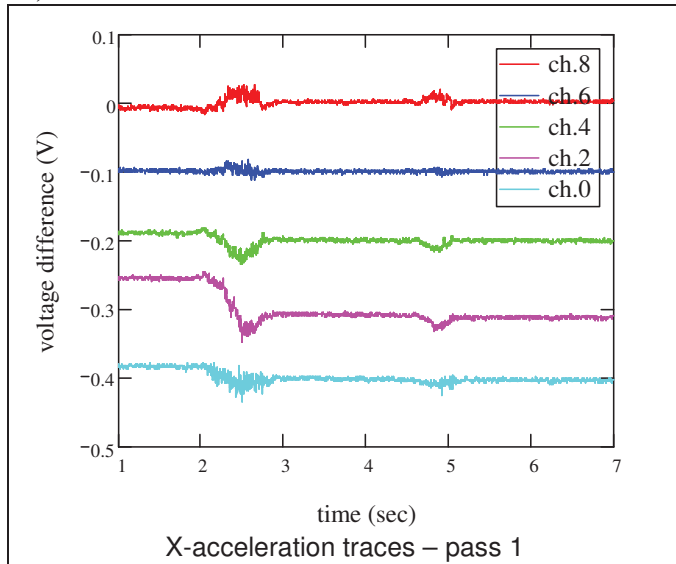


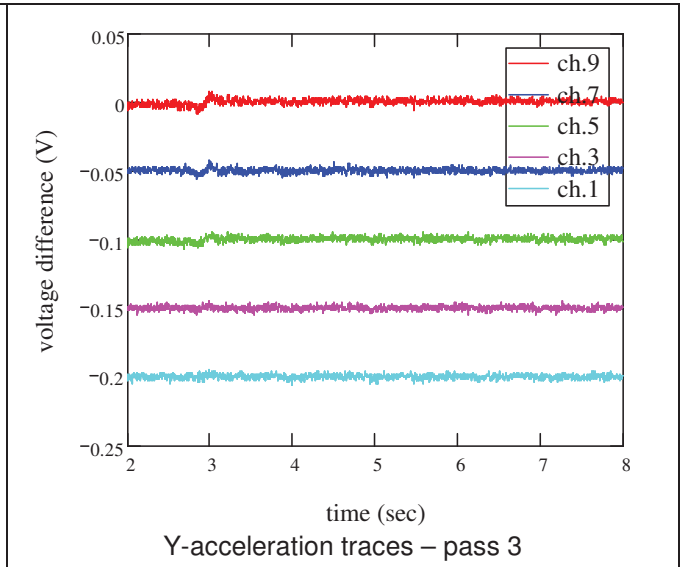
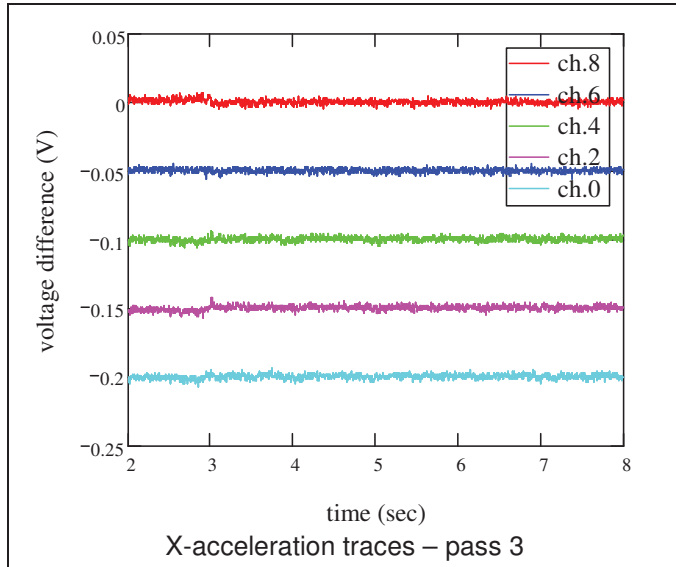
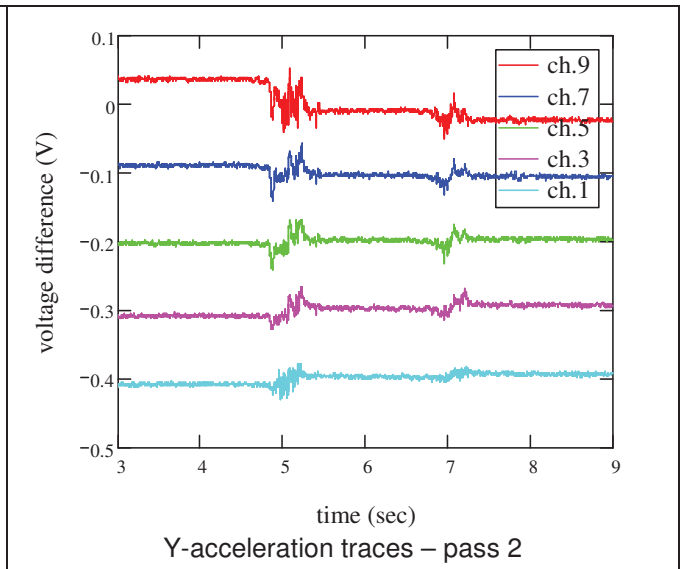
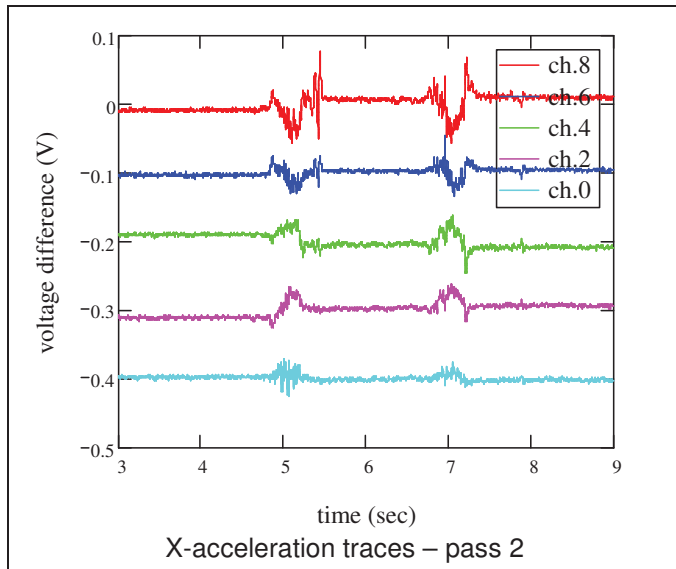


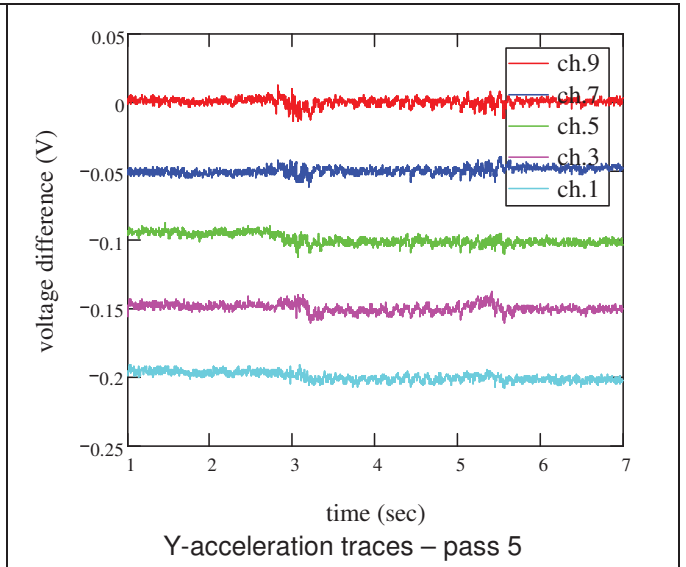
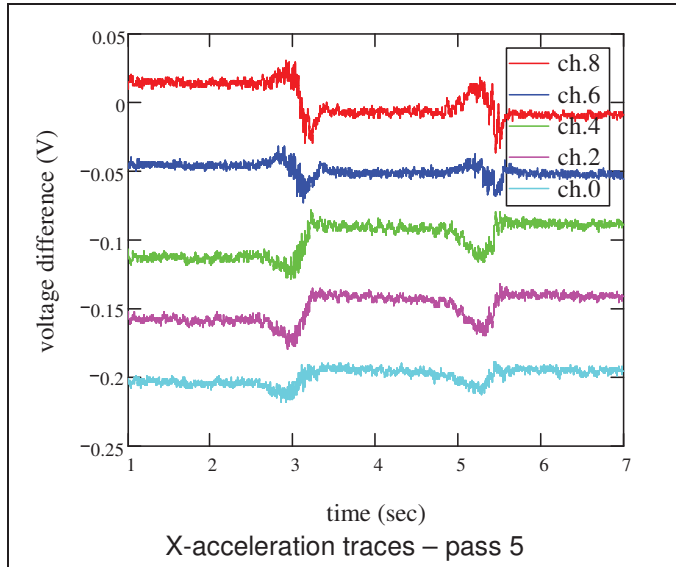
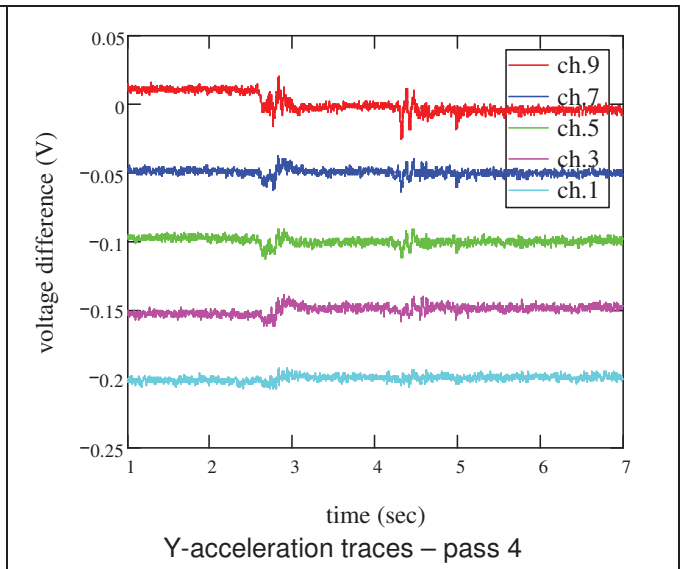
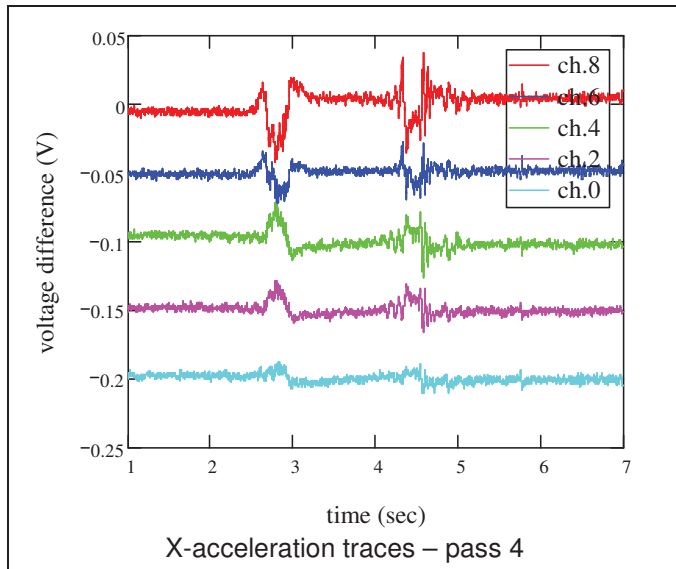


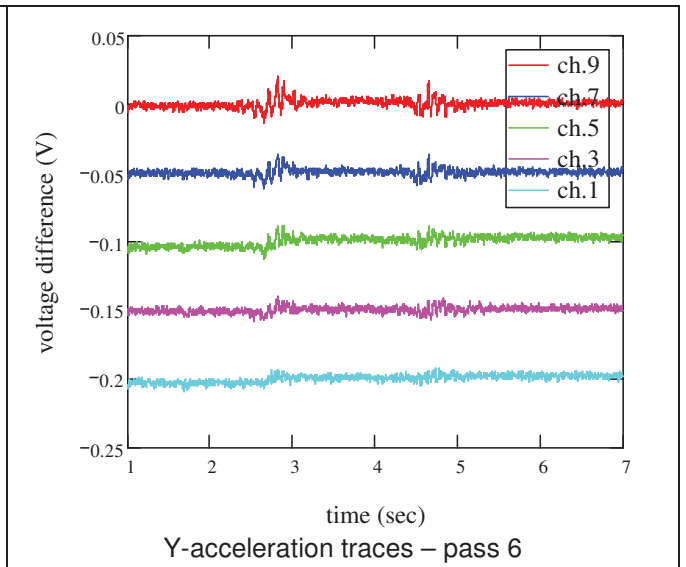
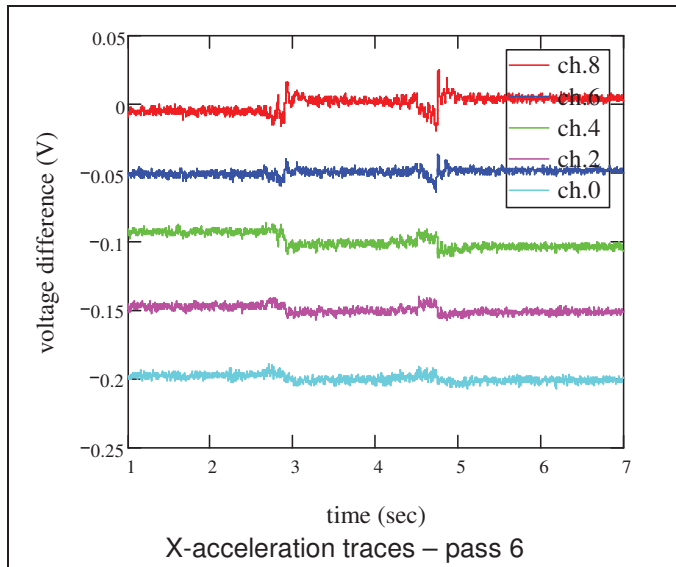


c) 20 in lift thickness



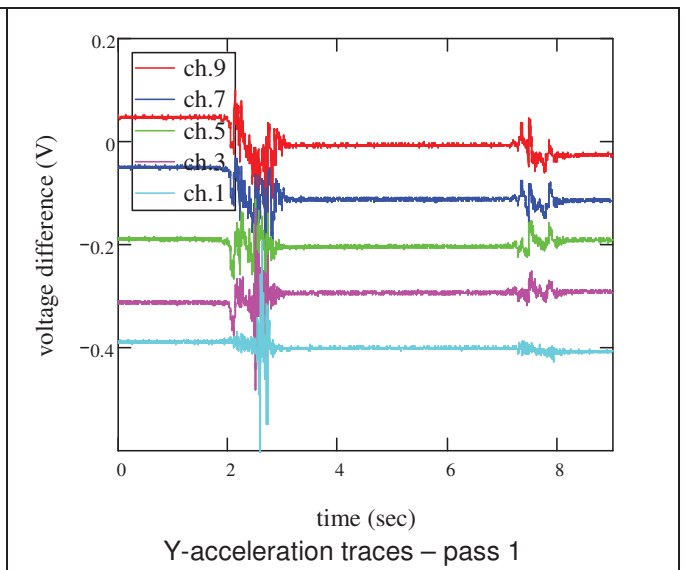
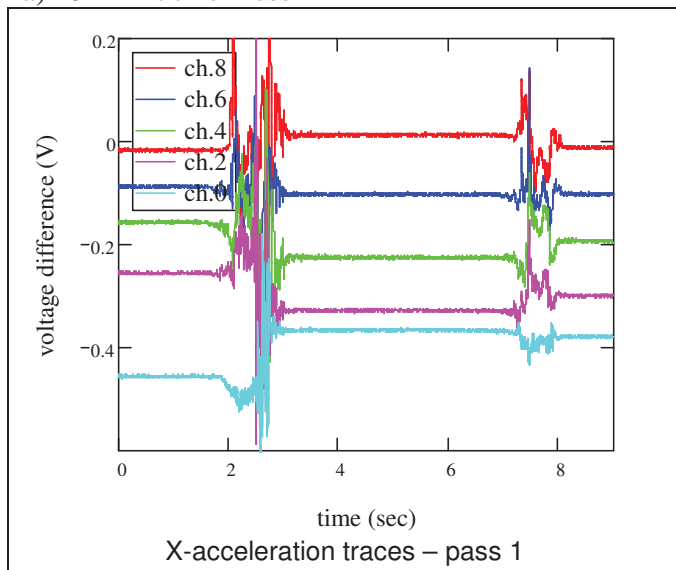


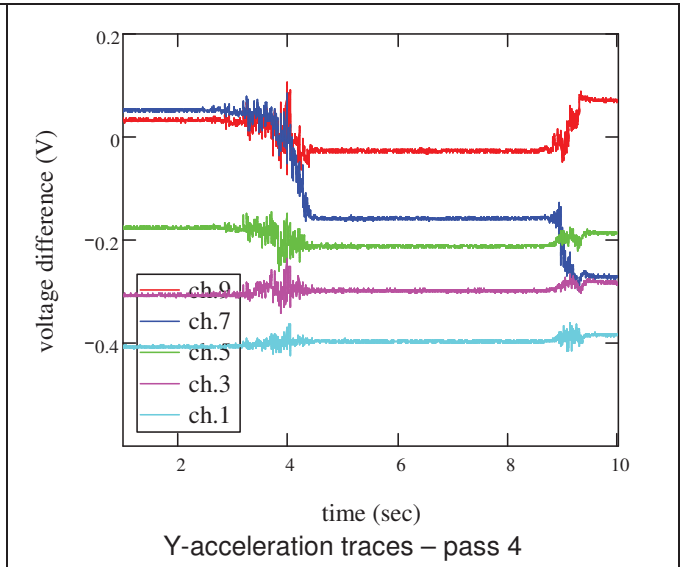
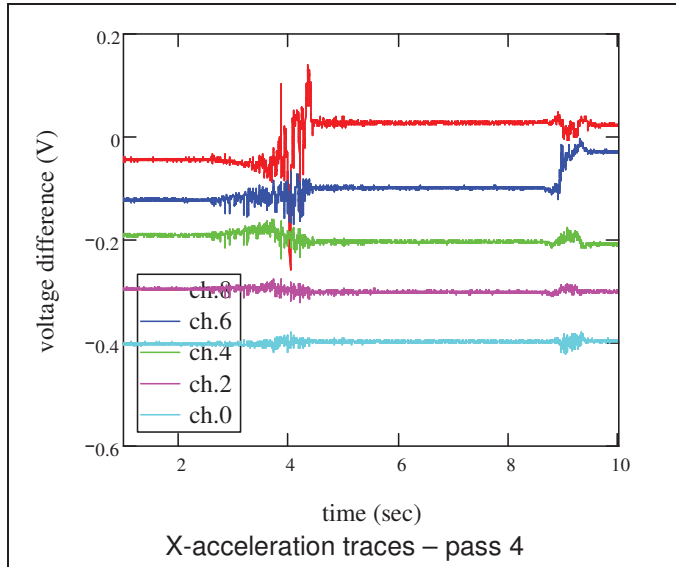
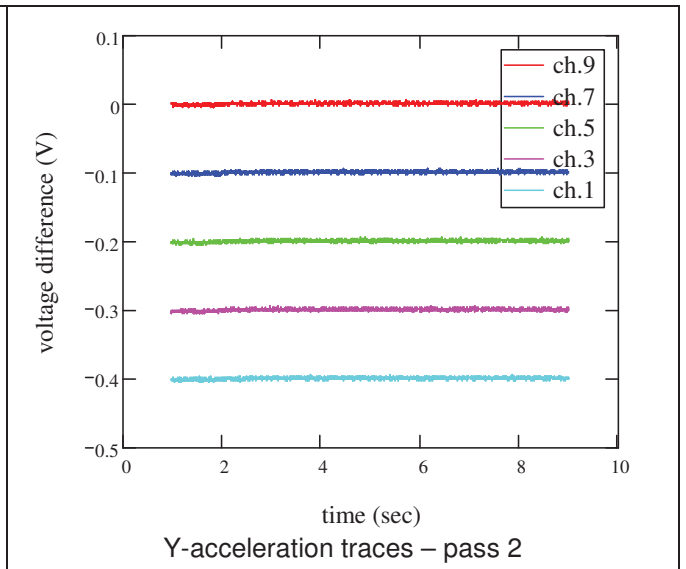
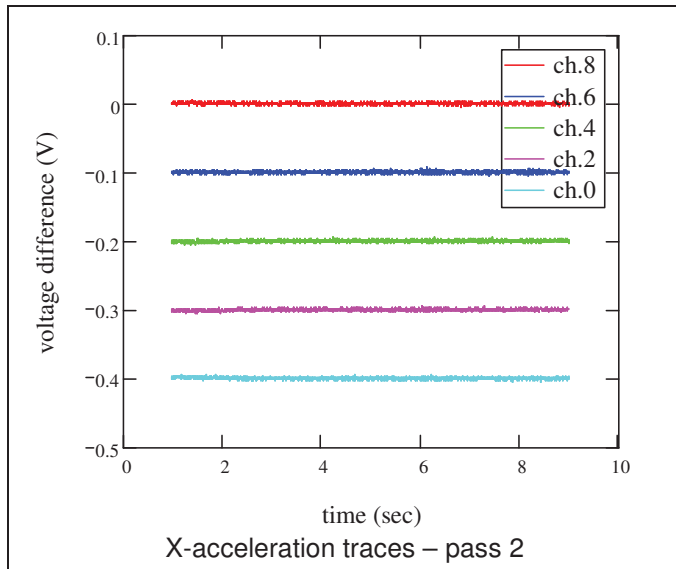


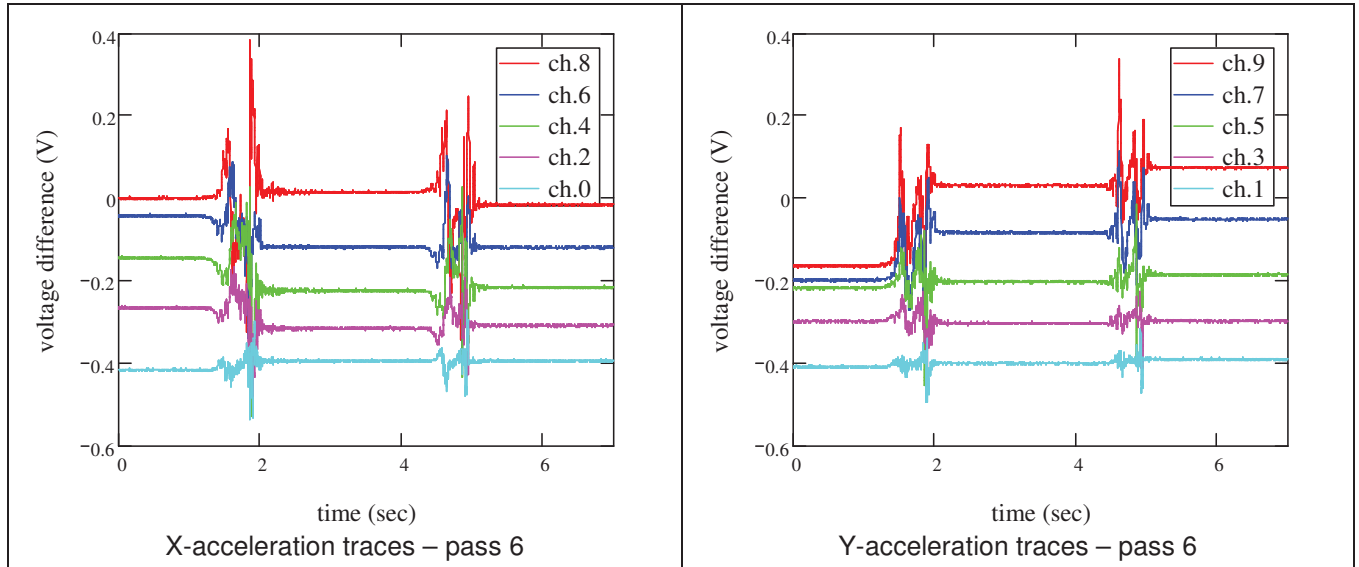
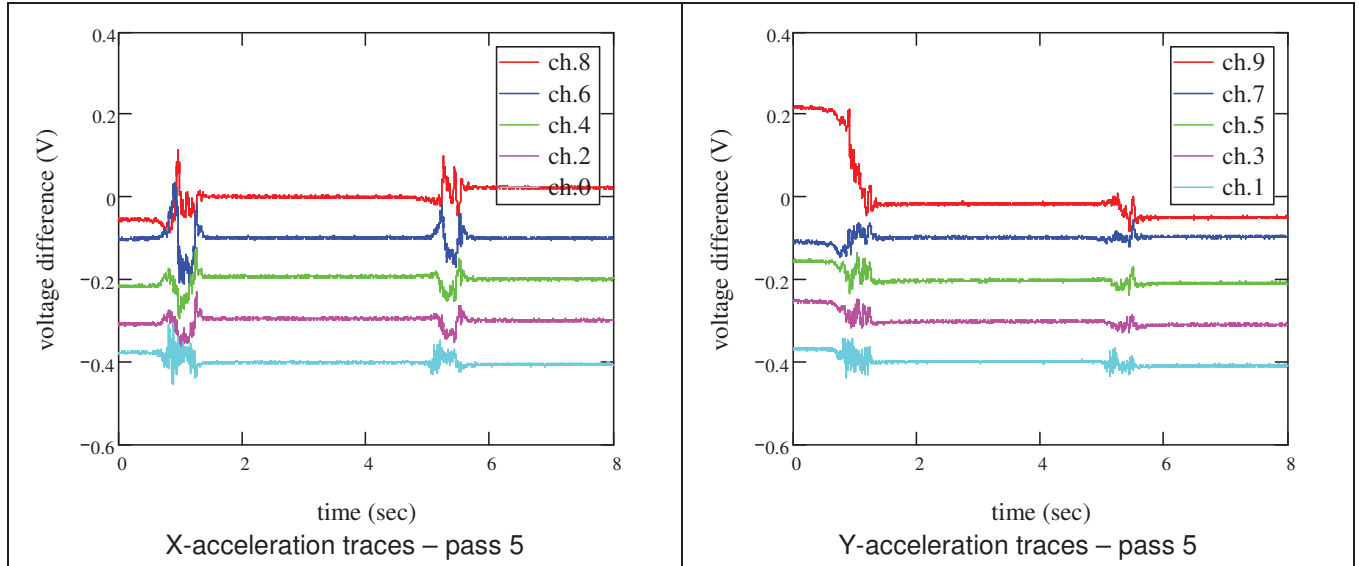


C.2.3. Scraper

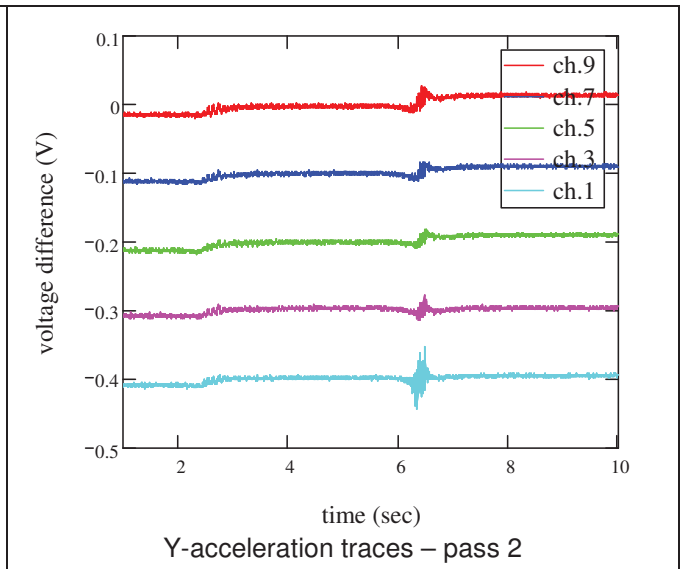
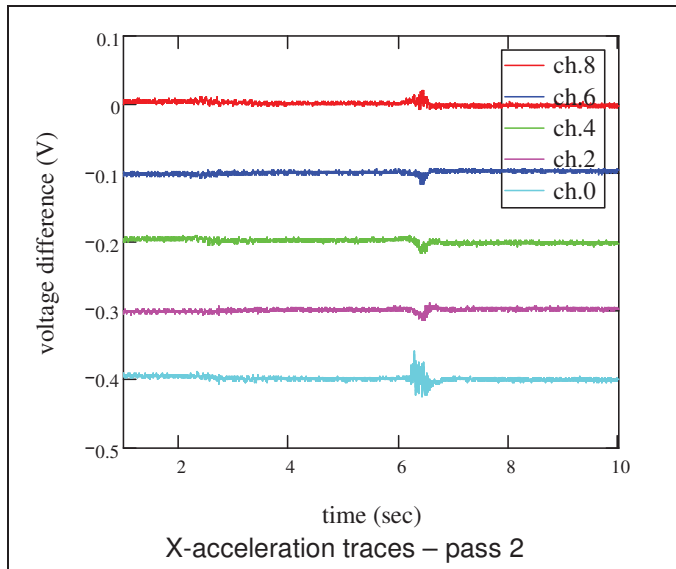
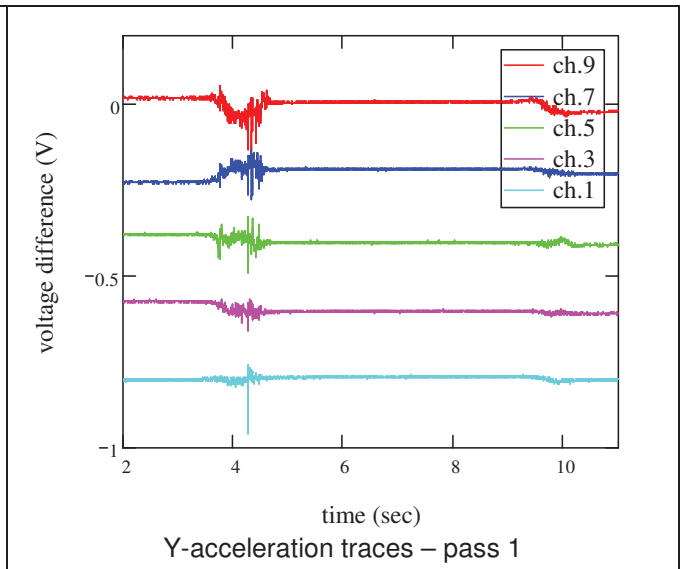
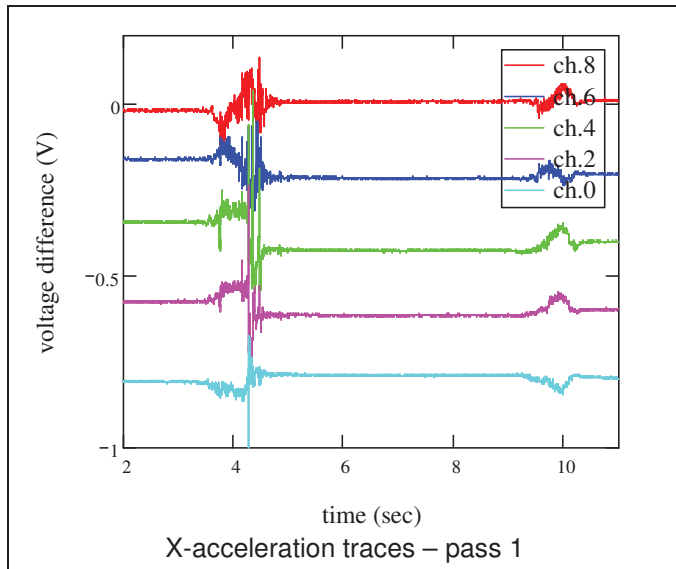
a) 13 in lift thickness

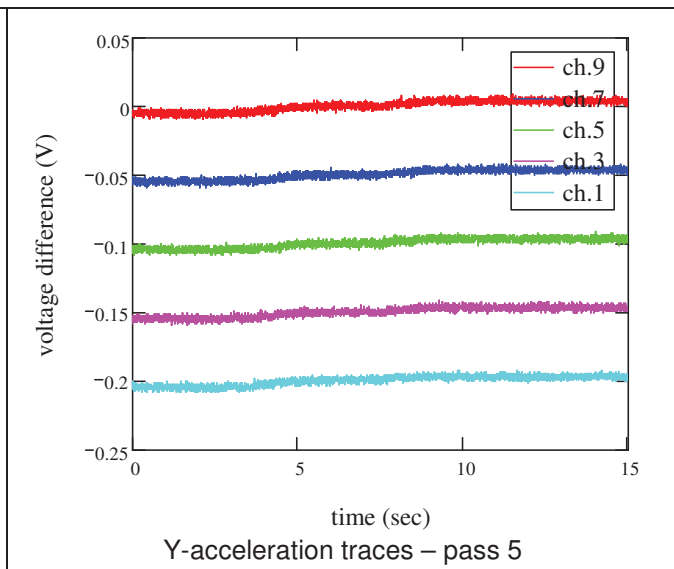
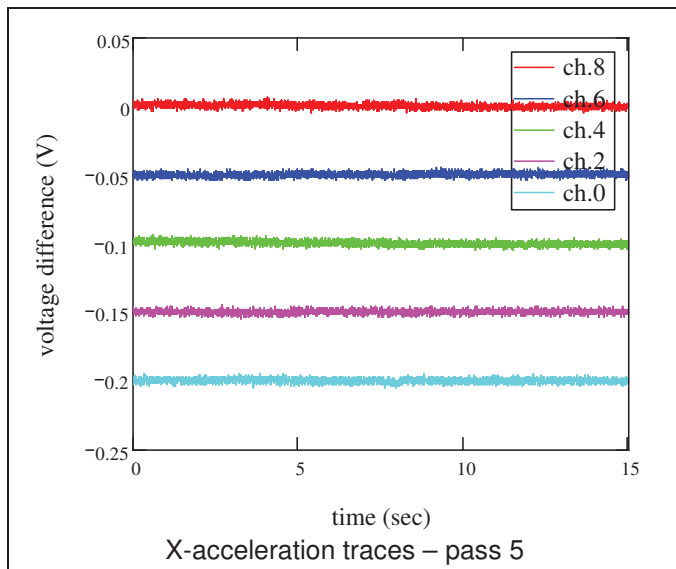
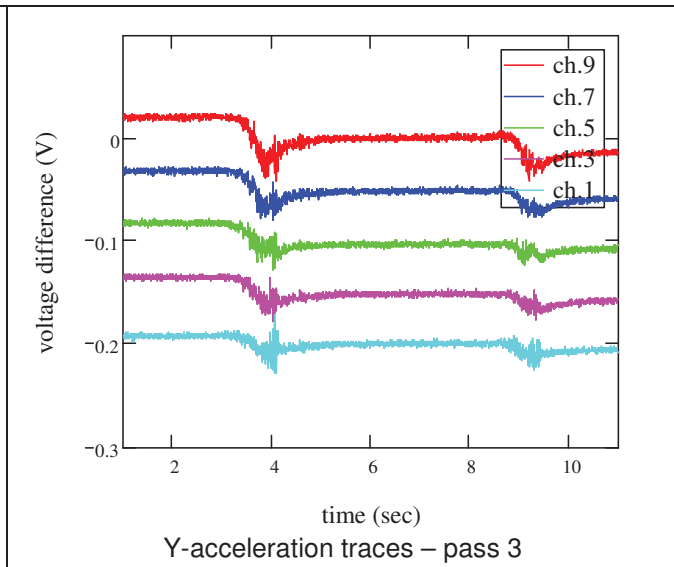
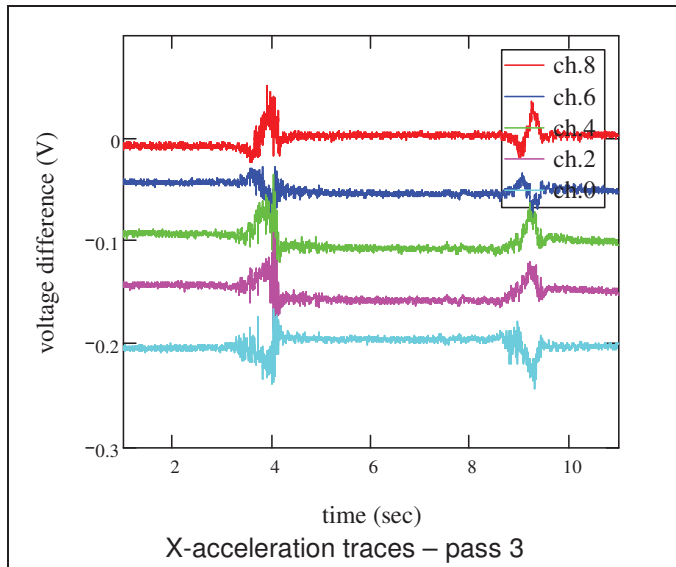


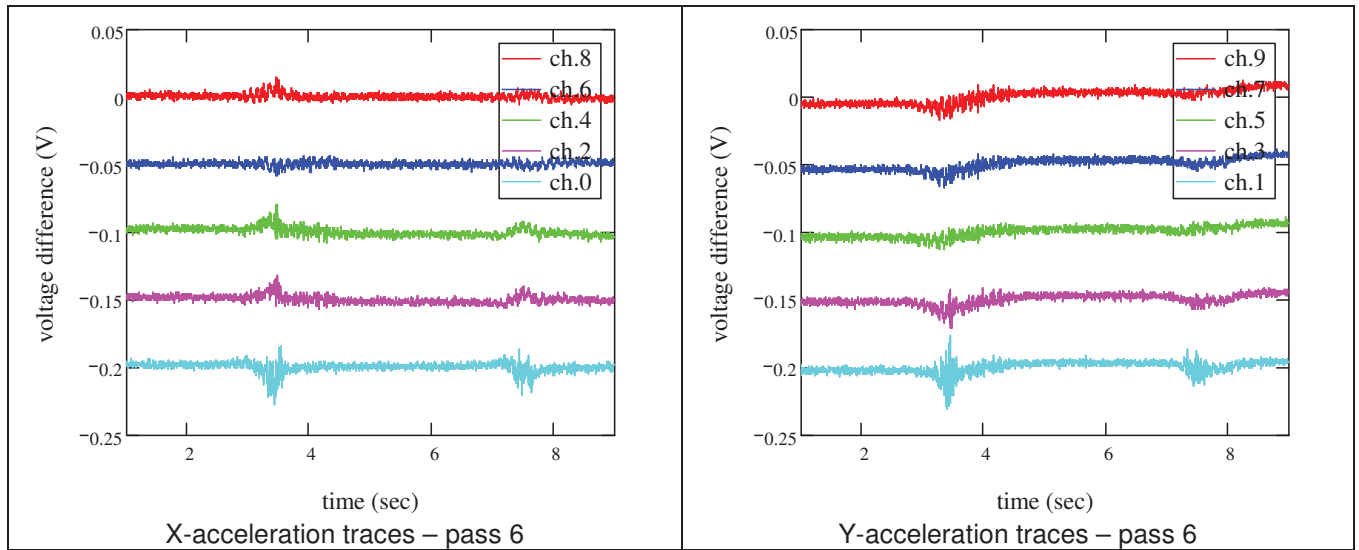




b) 23 in lift thickness



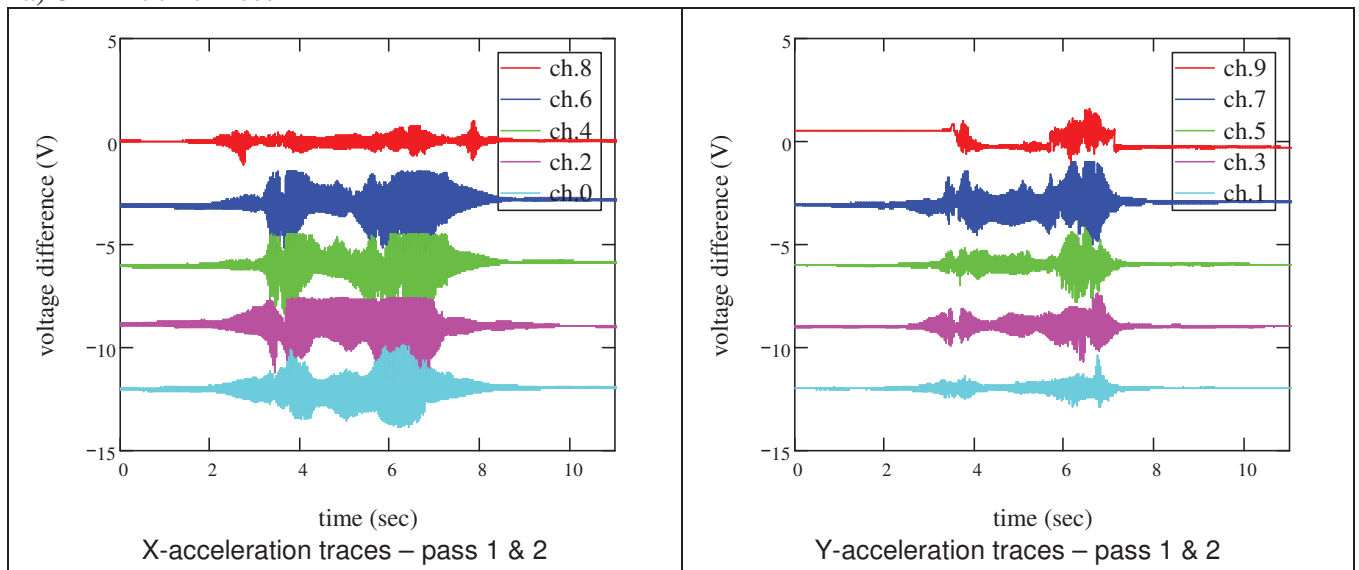


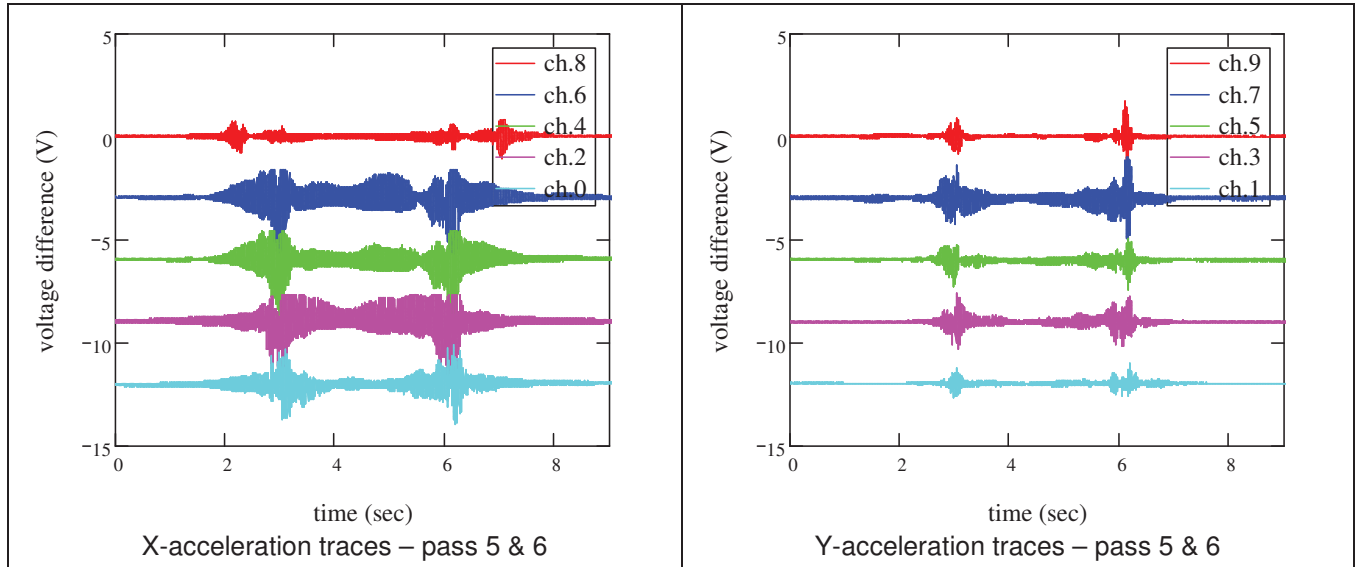
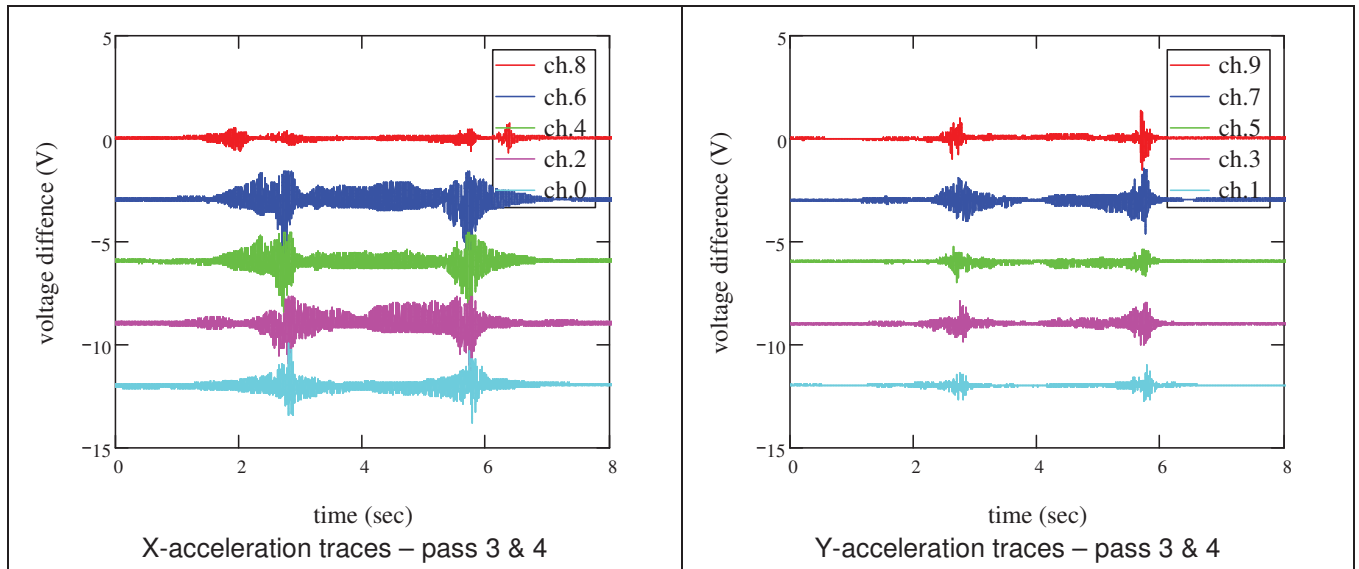


C.3. MEMS rotation angle measurement in the coarse-grained soil (wet condition moisture)

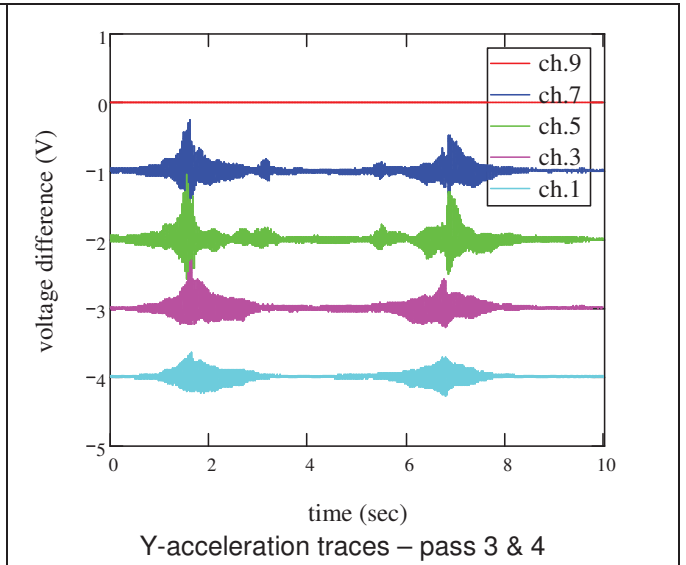
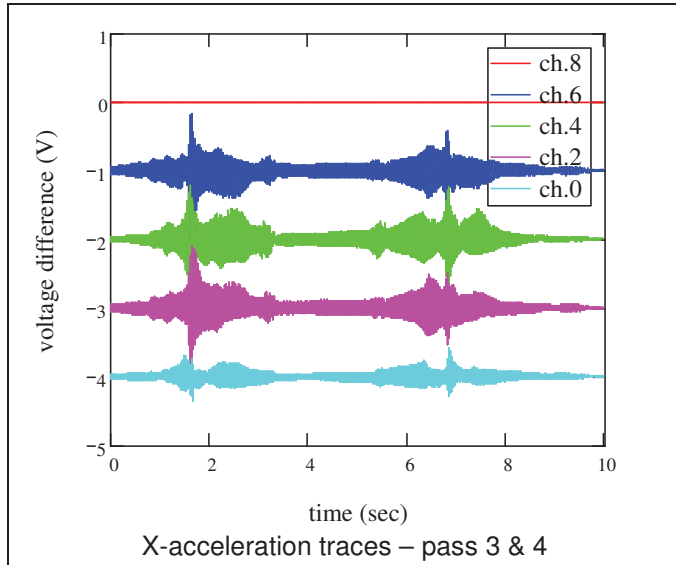
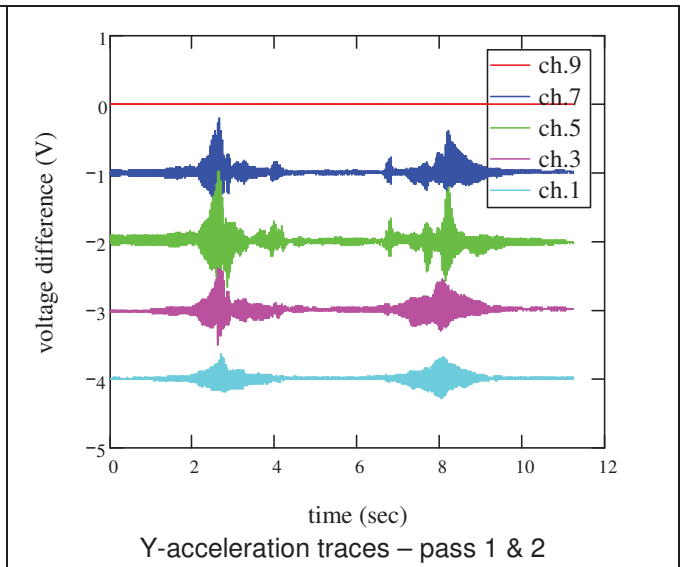
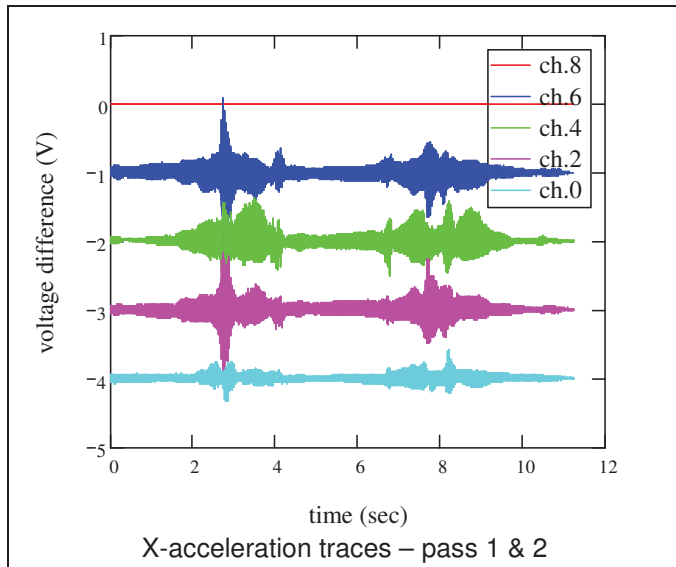
C.3.1. Smooth-drum vibratory roller

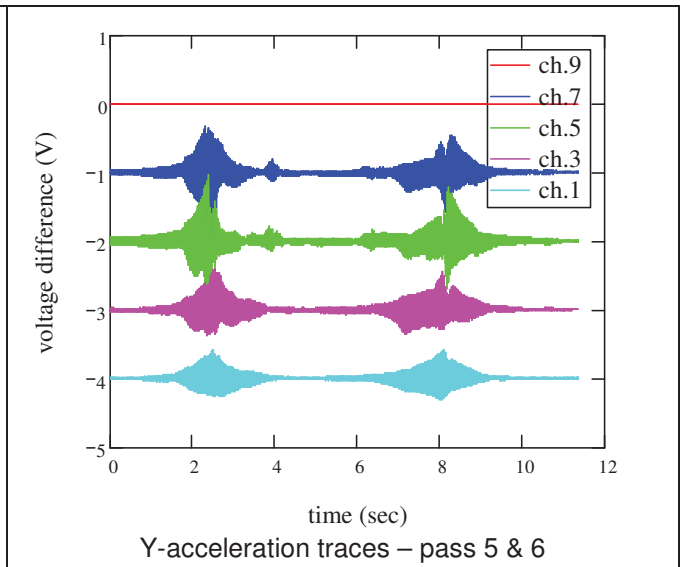
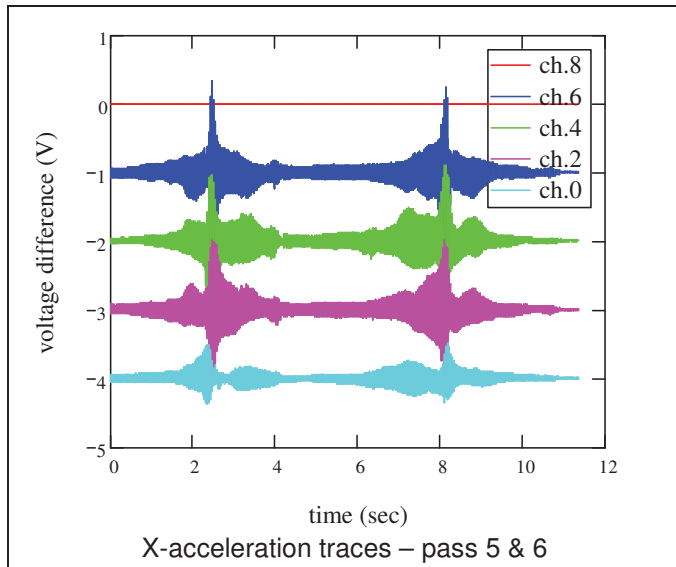
a) 8 in lift thickness



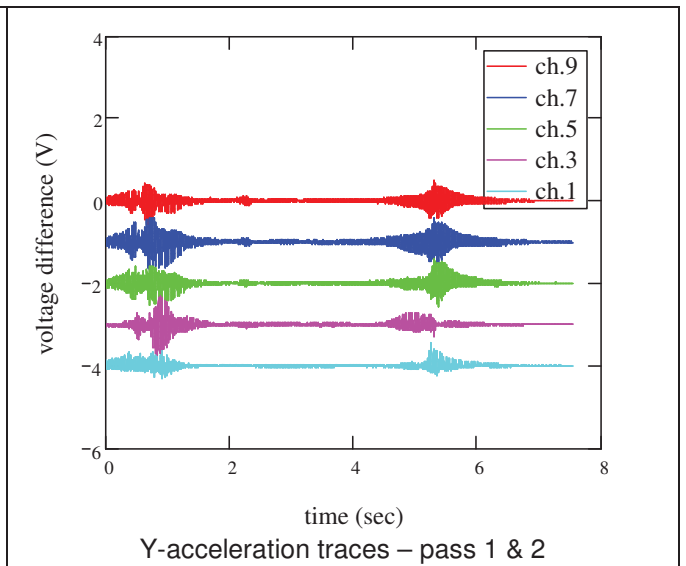
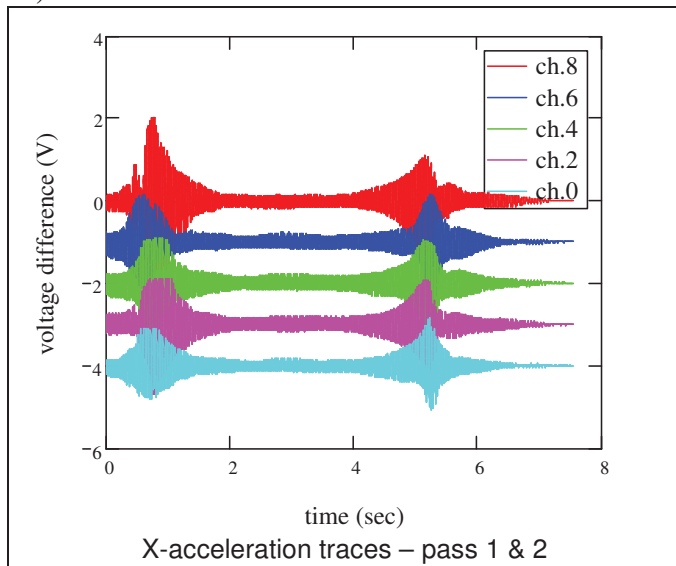


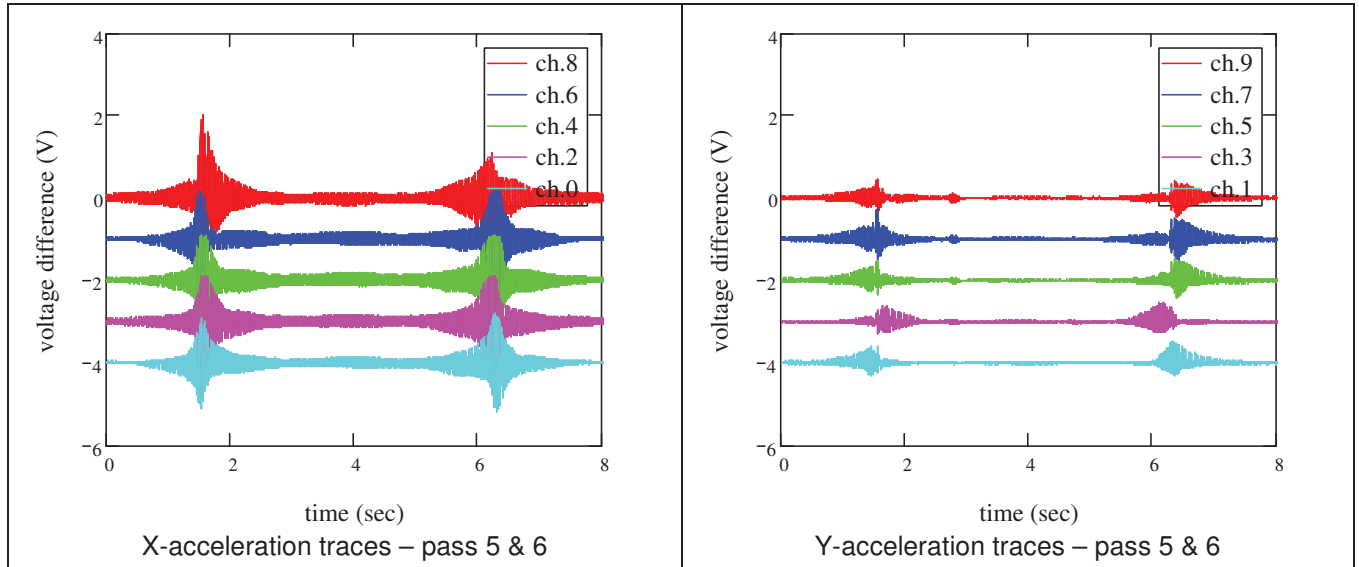
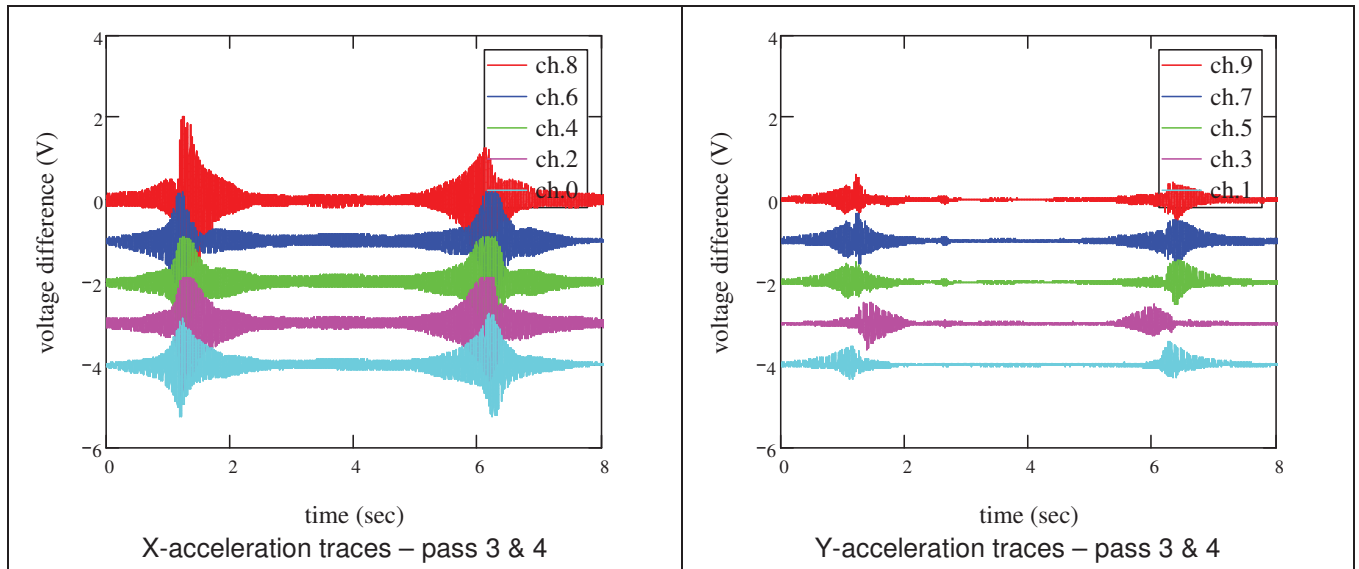
b) 13 in lift thickness



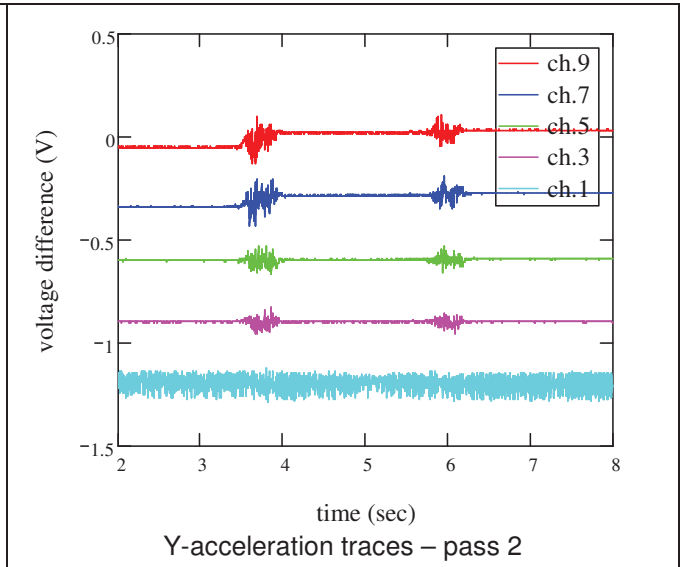
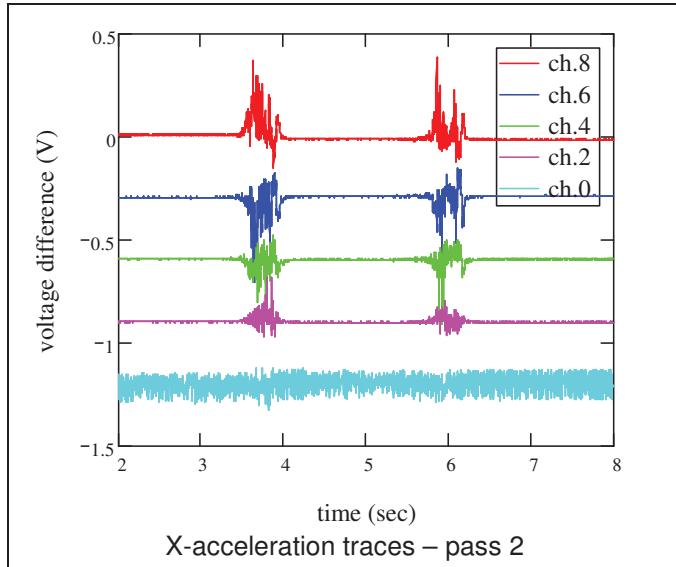
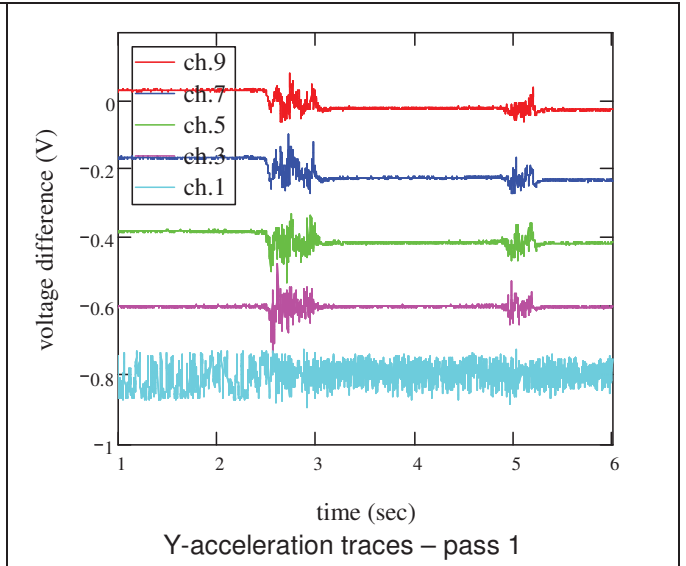
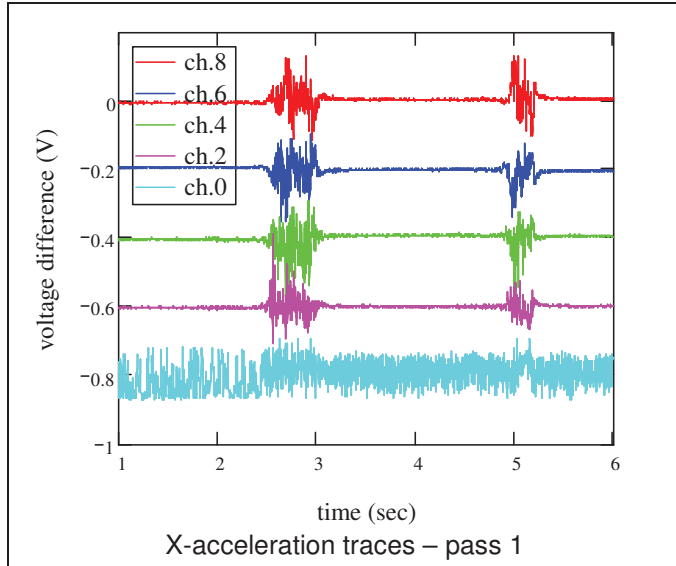


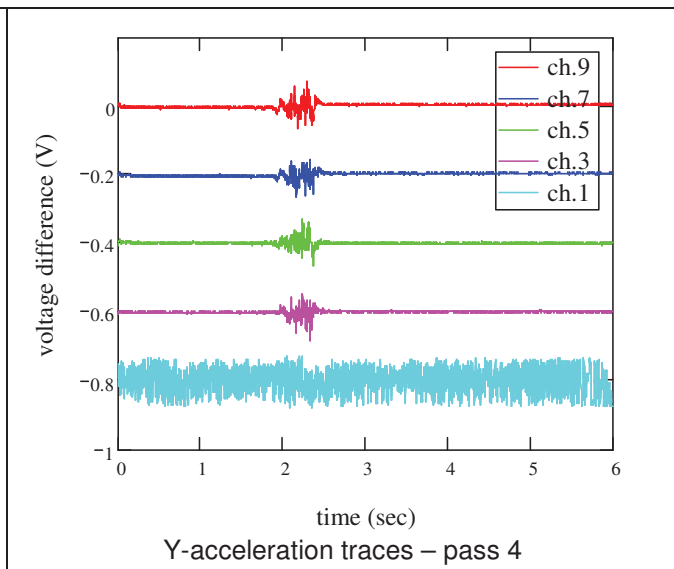
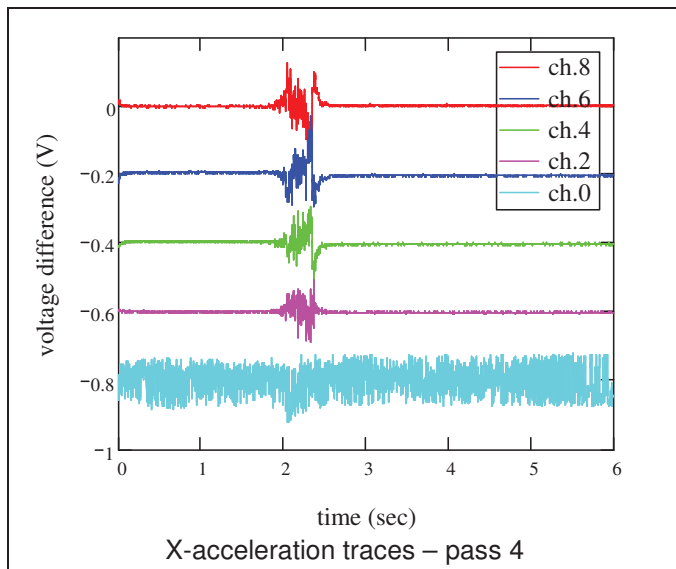
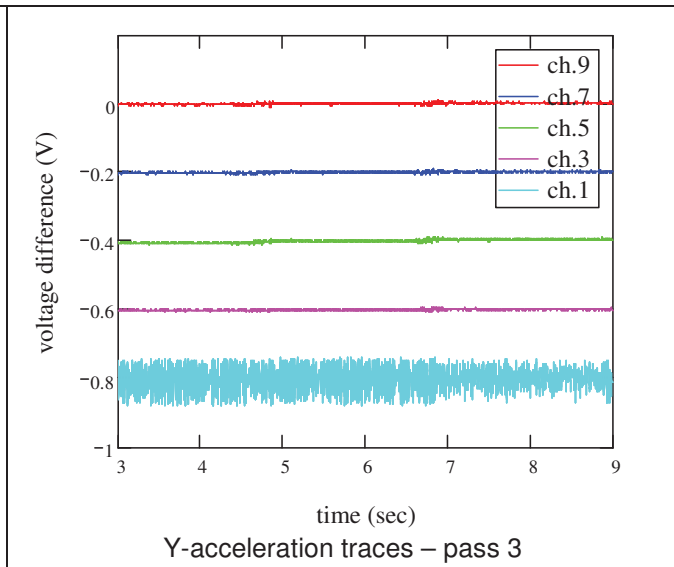
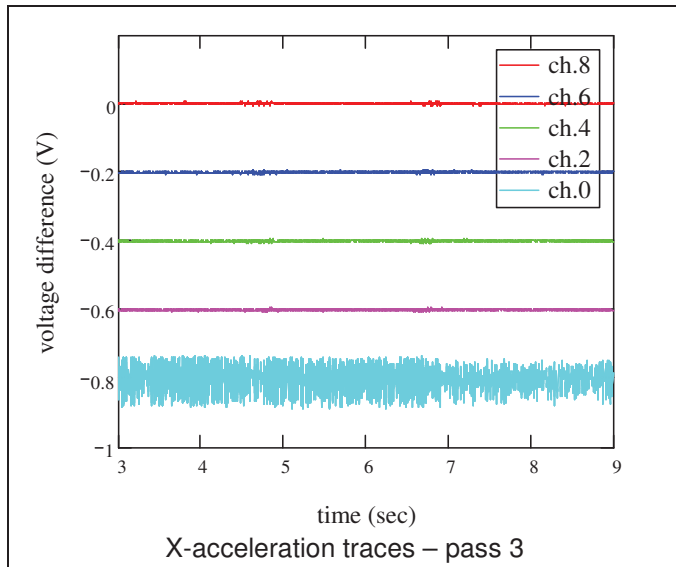
c) 20 in lift thickness

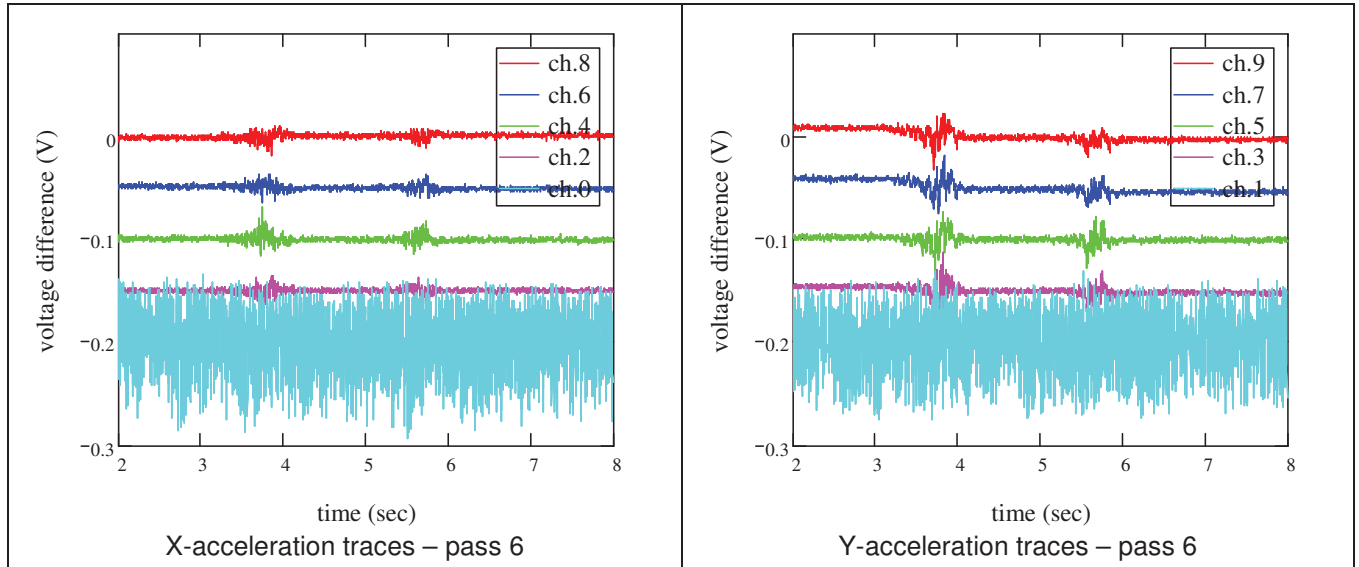
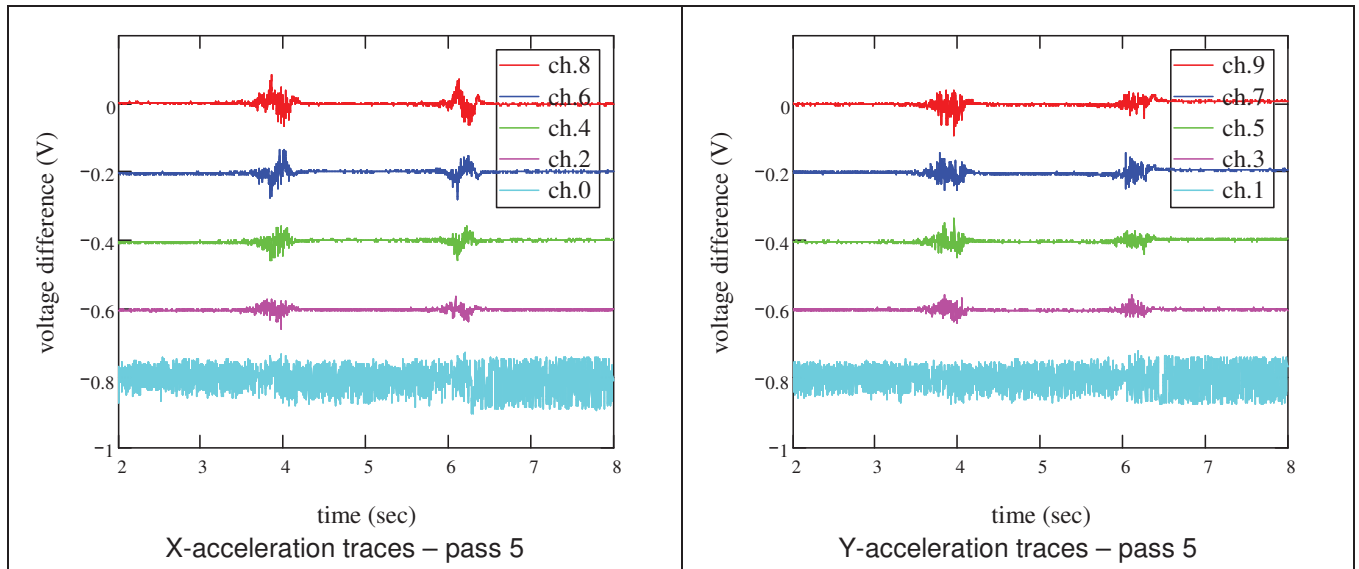




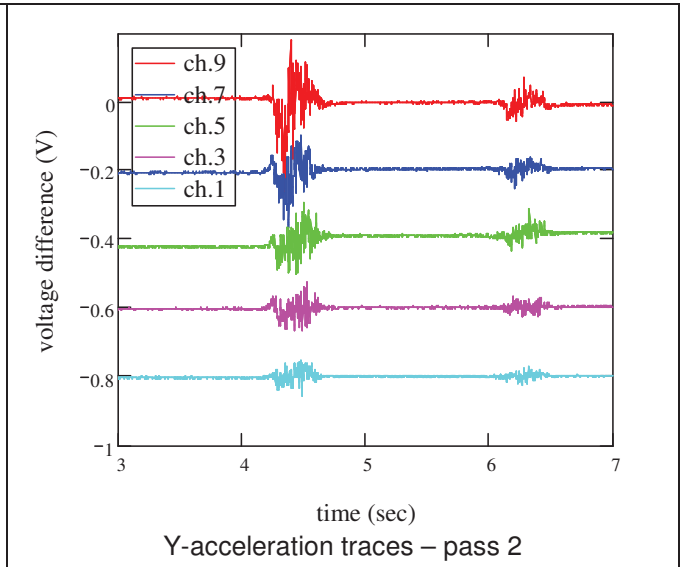
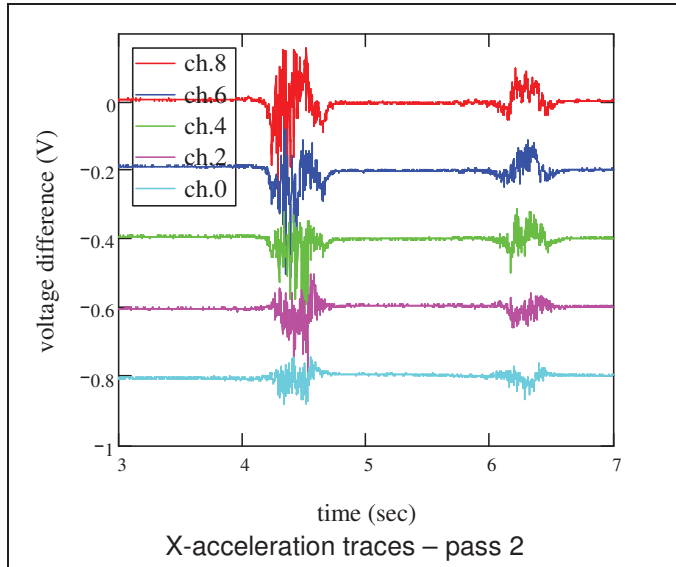
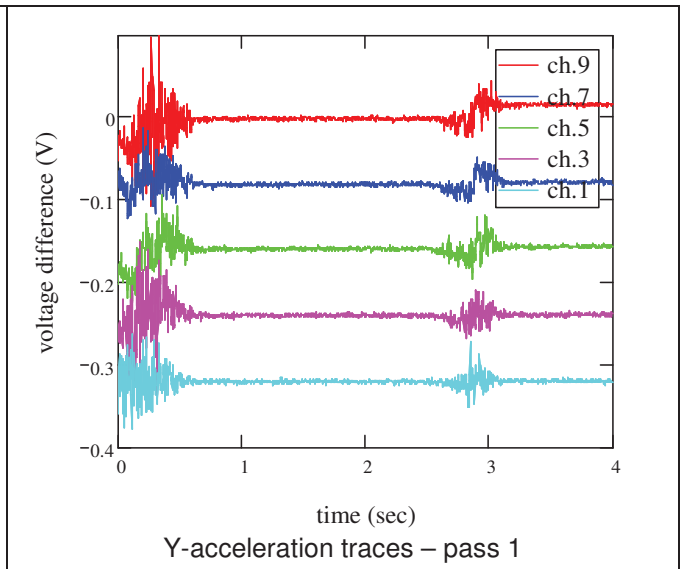
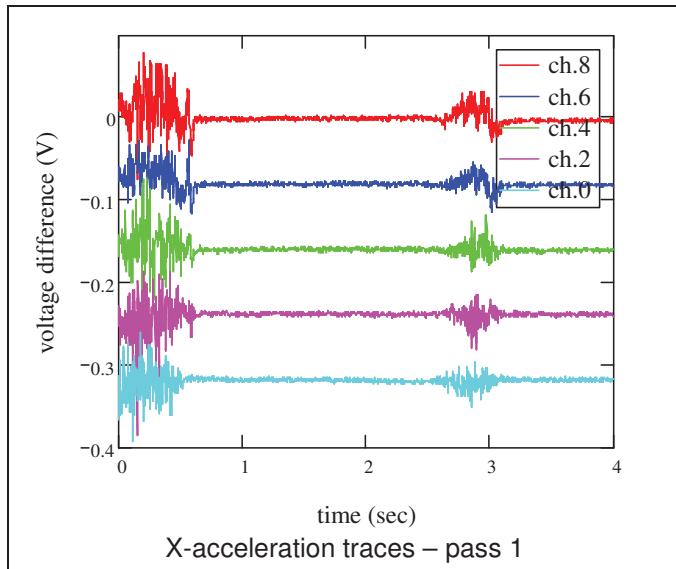
C.3.2. Rubber-tired roller
 a) 13 in lift thickness

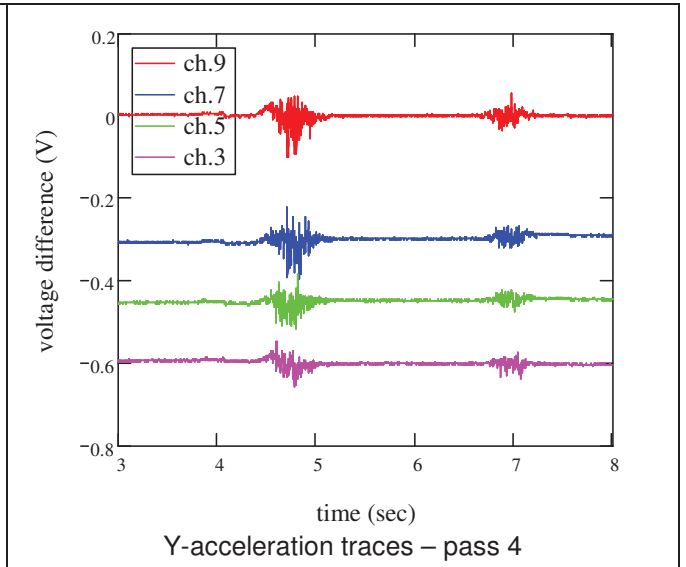
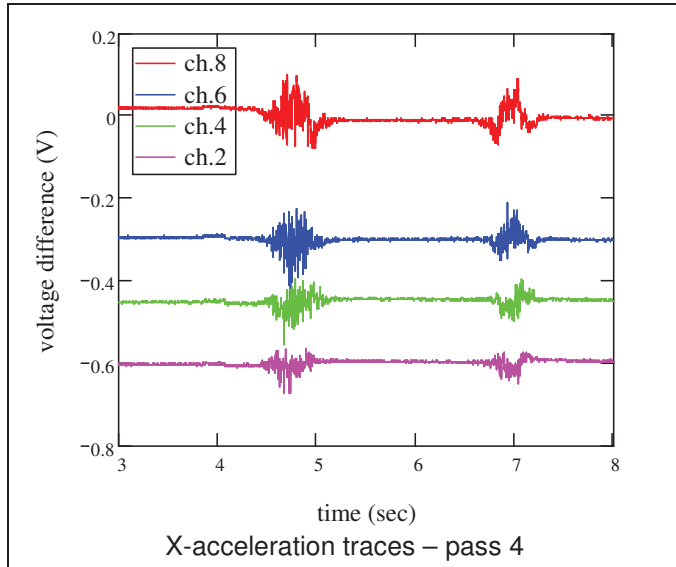
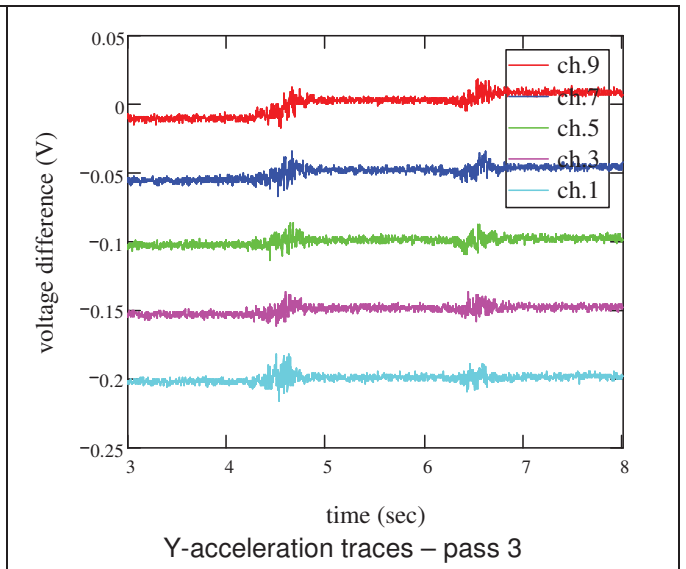
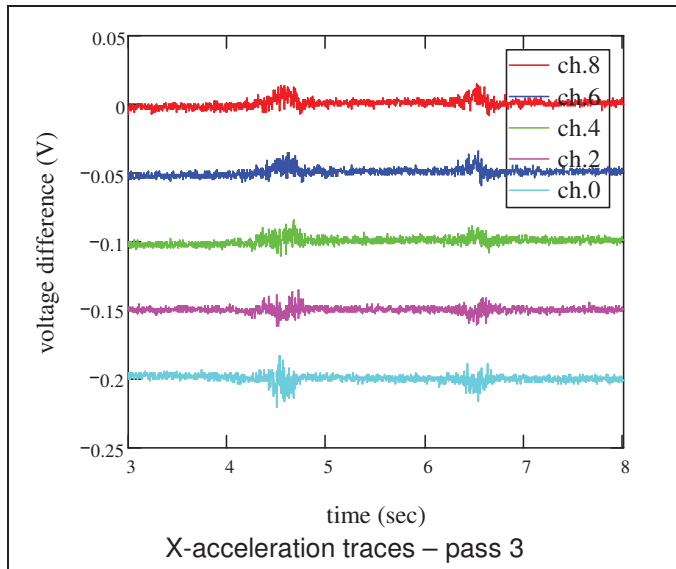


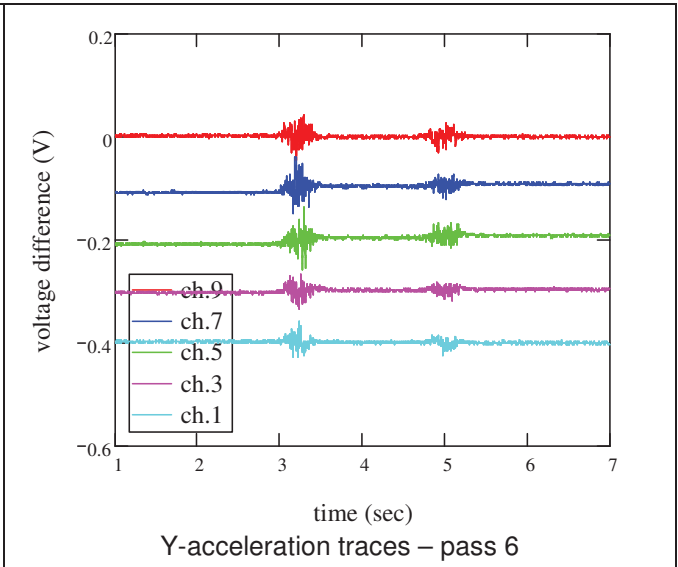
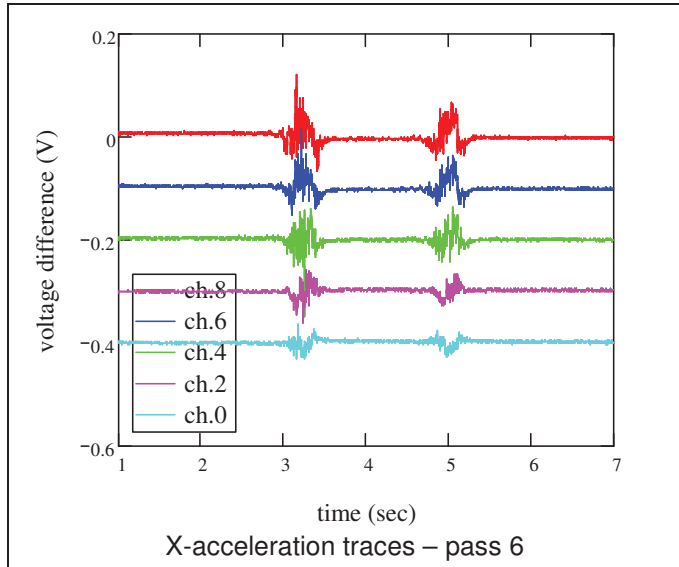
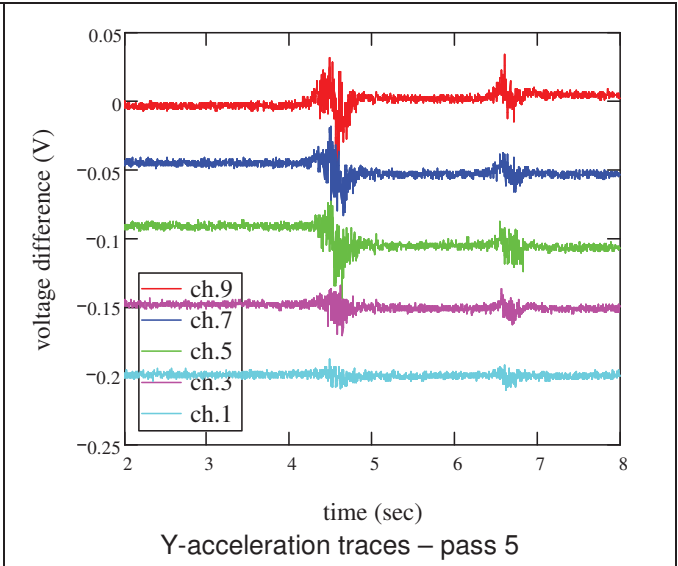
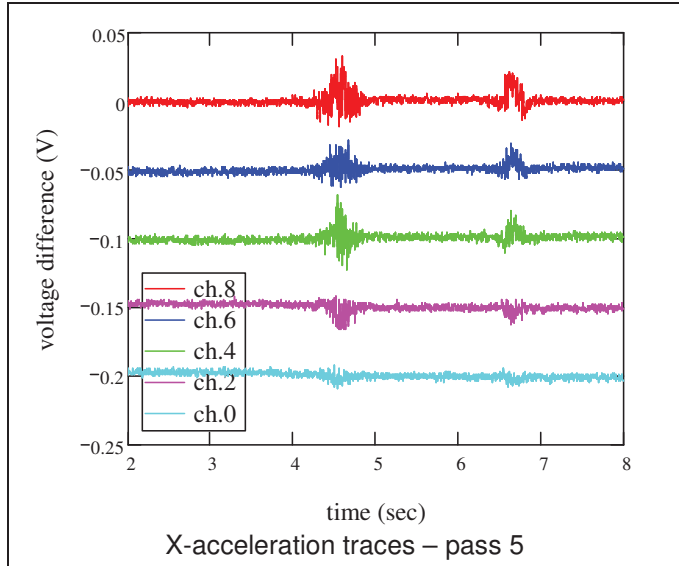




b) 23 in lift thickness







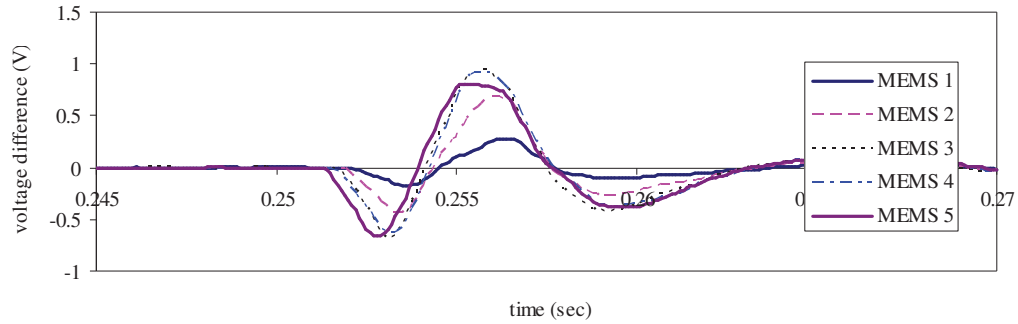
APPENDIX D: P-WAVE PROPAGATION – TRAVEL TIME EVALUATION

D.1. MEMS first arrival measurement in the fine-grained soil (natural moisture)

D.1.1. Smooth-drum vibratory roller

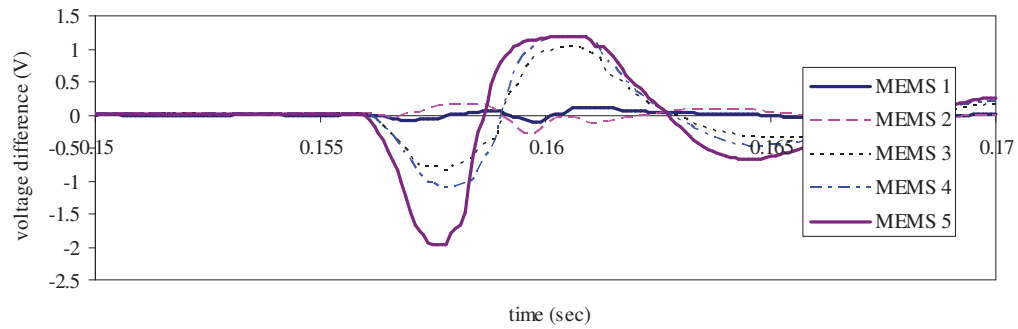
a) 12 in lift thickness

• 0 pass



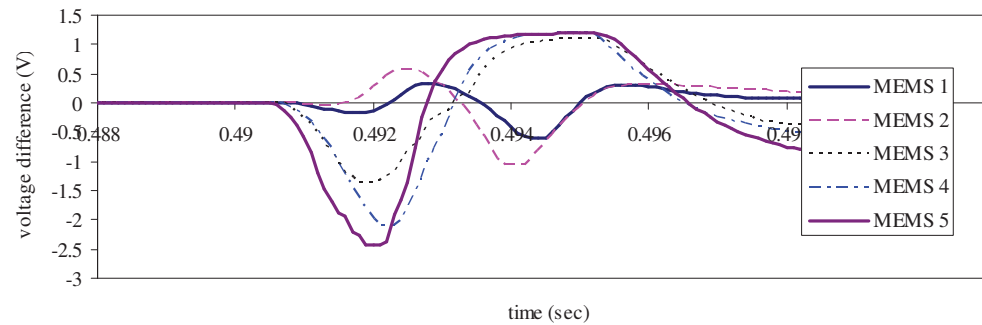
travel distance between MEMS 1 to MEMS 5	15.24 cm
measured travel time	0.00053 sec
wave velocity	287.55 m/sec

• 3 pass



travel distance between MEMS 1 to MEMS 5	15.24 cm
measured travel time	0.00048 sec
wave velocity	317.50 m/sec

• 6 pass

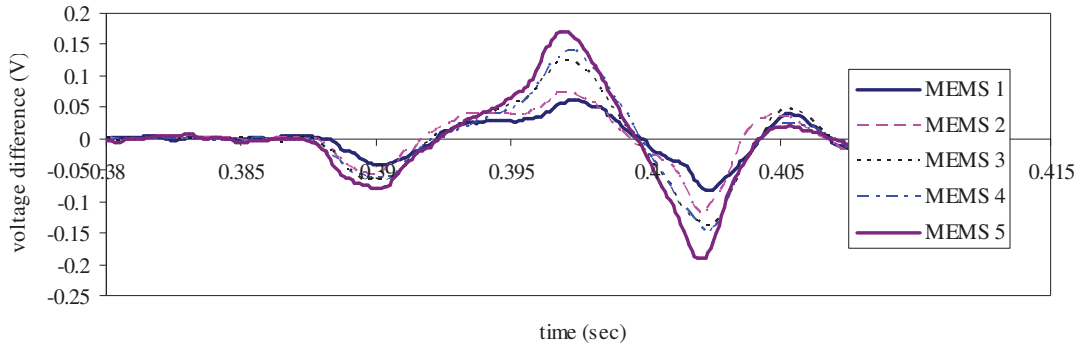


travel distance between MEMS 1 to MEMS 5	15.24 cm
measured travel time	0.00043 sec

wave velocity	354.42 m/sec
---------------	--------------

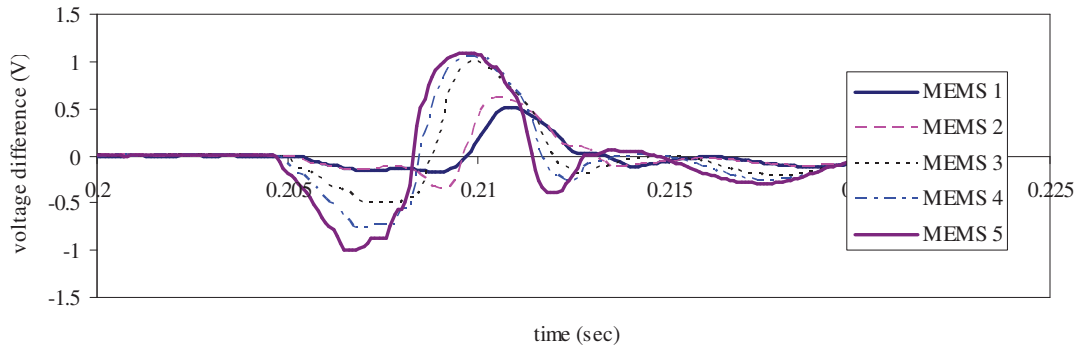
b) 17 in lift thickness

• 0 pass



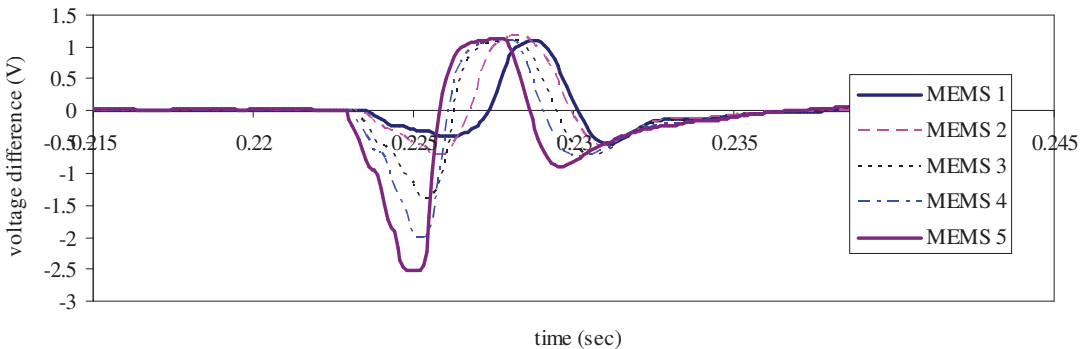
travel distance between MEMS 1 to MEMS 5	19.05 cm
measured travel time	0.00097 sec
wave velocity	196.39 m/sec

• 3 pass



travel distance between MEMS 1 to MEMS 5	19.05 cm
measured travel time	0.00078 sec
wave velocity	244.23 m/sec

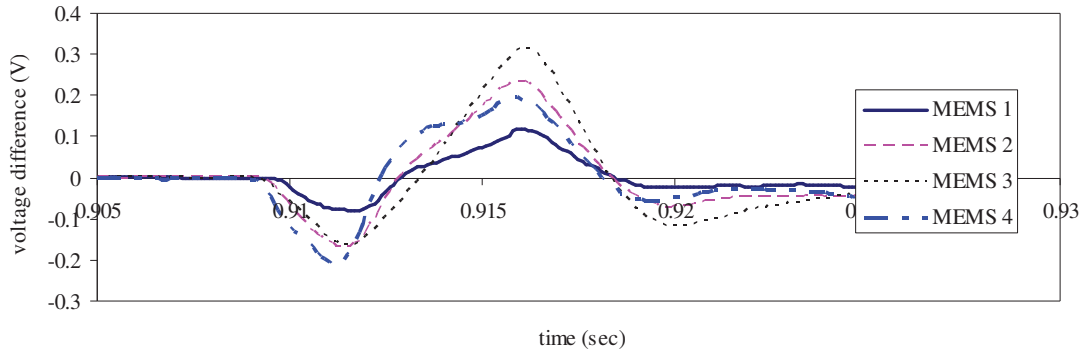
• 6 pass



travel distance between MEMS 1 to MEMS 5	19.05 cm
measured travel time	0.00072 sec
wave velocity	264.58 m/sec

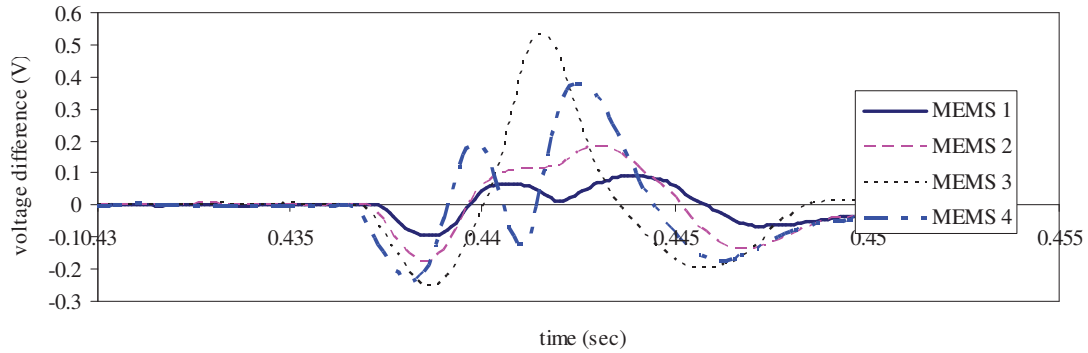
c) 24 in lift thickness

- 0 pass



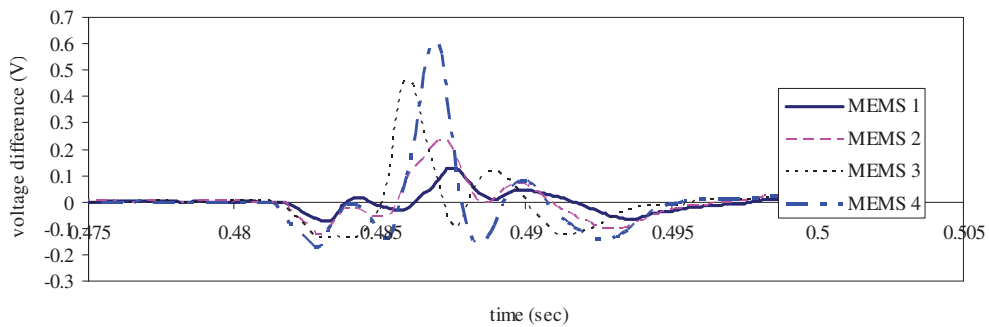
travel distance between MEMS 1 to MEMS 4	12.065 cm
measured travel time	0.00066 sec
wave velocity	182.80 m/sec

- 3 pass



travel distance between MEMS 1 to MEMS 4	12.065 cm
measured travel time	0.0006 sec
wave velocity	201.08 m/sec

- 6 pass

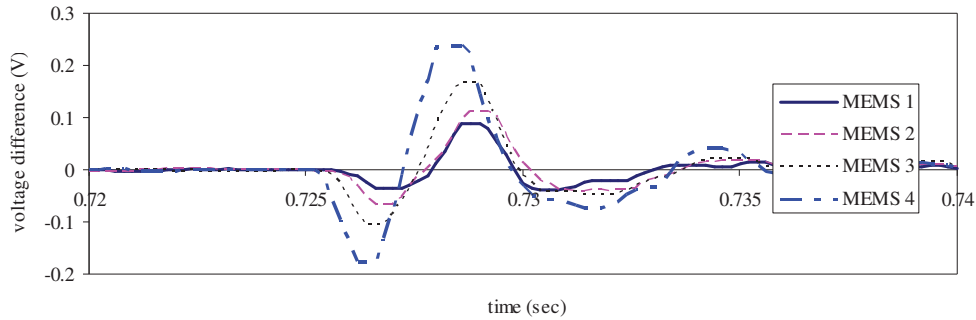


travel distance between MEMS 1 to MEMS 4	12.065 cm
measured travel time	0.00054 sec
wave velocity	223.43 m/sec

D.1.2. Rubber-tired roller

a) 11 in lift thickness

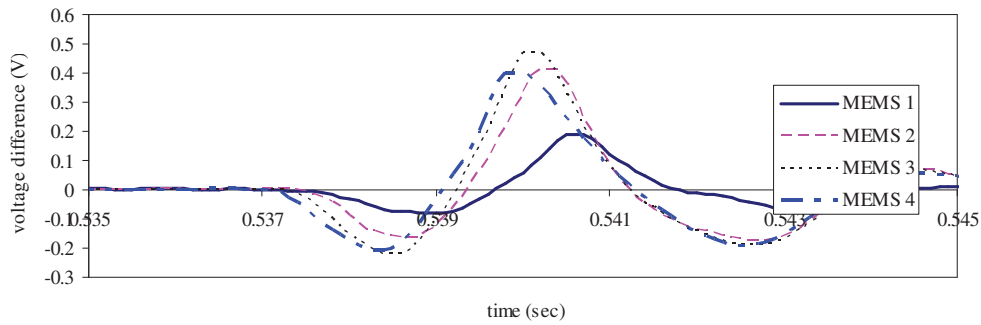
- 6 pass



travel distance between MEMS 1 to MEMS 4	11.43 cm
measured travel time	0.0005 sec
wave velocity	228.60 m/sec

b) 20 in lift thickness

- 6 pass

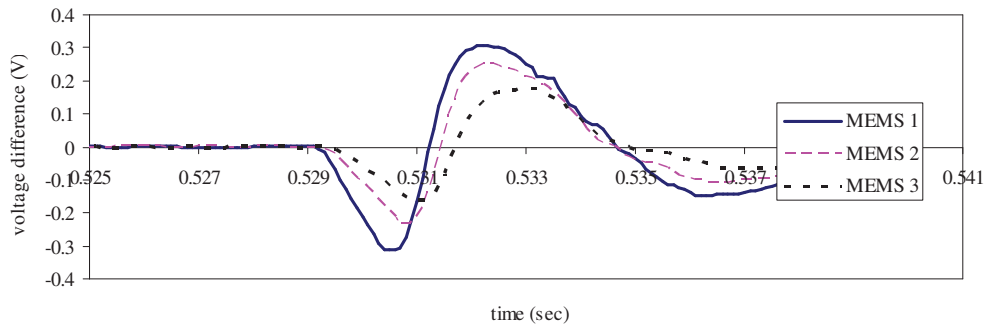


travel distance between MEMS 1 to MEMS 4	11.43 cm
measured travel time	0.00042 sec
wave velocity	272.14 m/sec

D.1.3. Padfoot roller

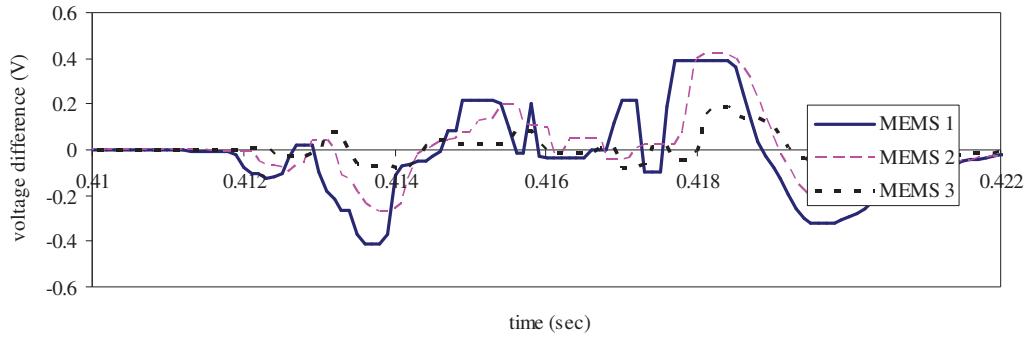
a) 10 in lift thickness

- 0 pass



travel distance between MEMS 1 to MEMS 3	7.62 cm
measured travel time	0.00028 sec
wave velocity	272.14 m/sec

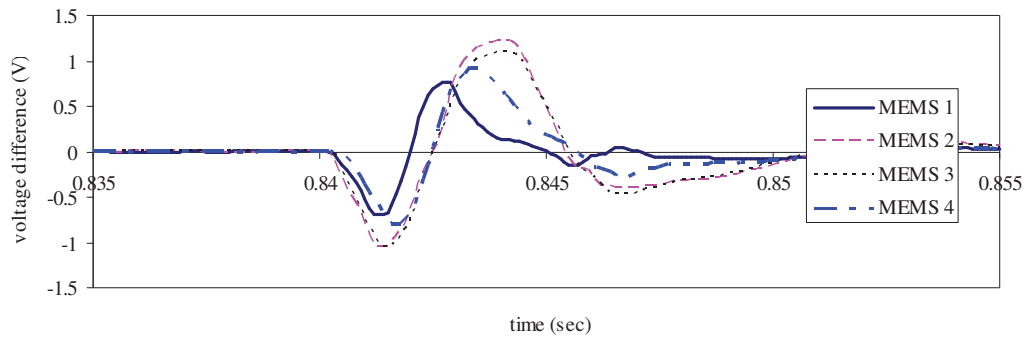
- 6 pass



travel distance between MEMS 1 to MEMS 3	7.62 cm
measured travel time	0.00026 sec
wave velocity	293.08 m/sec

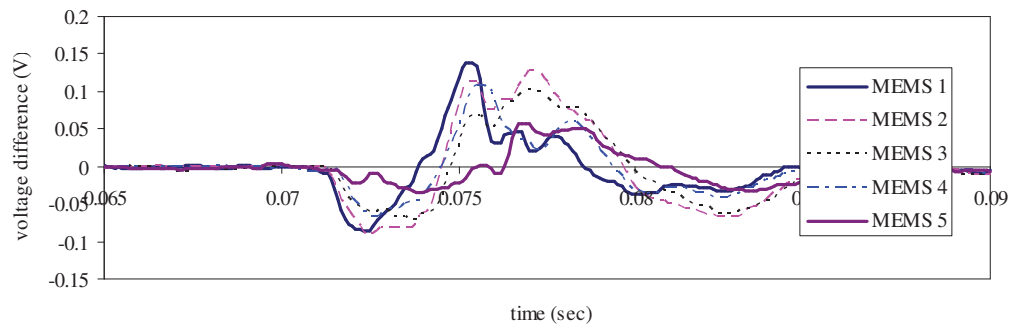
b) 16 in lift thickness

- 0 pass



travel distance between MEMS 1 to MEMS 4	10.795 cm
measured travel time	0.00039 sec
wave velocity	276.79 m/sec

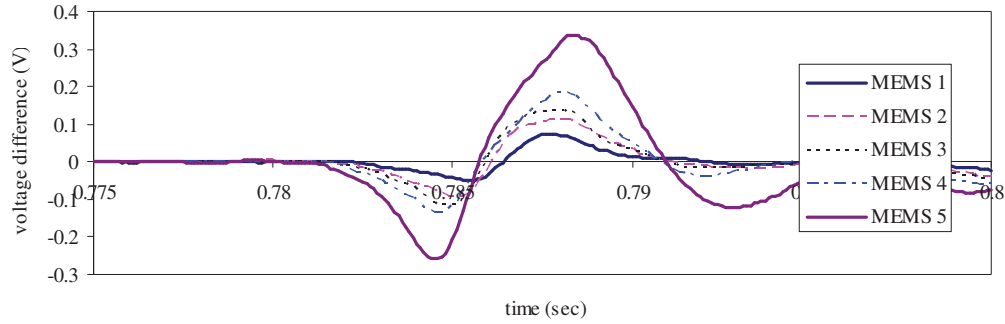
- 6 pass



travel distance between MEMS 1 to MEMS 5	10.795 cm
measured travel time	0.00038 sec
wave velocity	284.08 m/sec

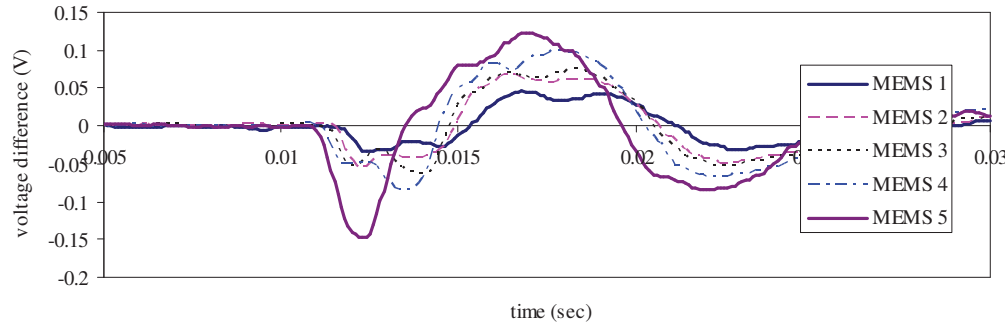
c) 24 in lift thickness

• 0 pass



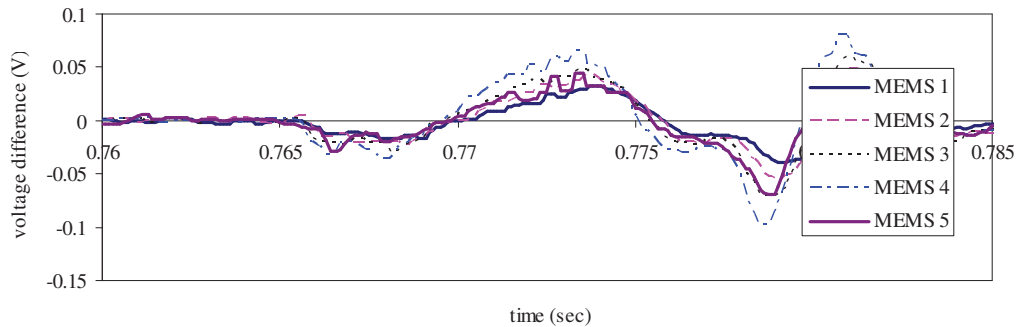
travel distance between MEMS 1 to MEMS 5	20.32 cm
measured travel time	0.0009 sec
wave velocity	225.78 m/sec

• 3 pass



travel distance between MEMS 1 to MEMS 5	20.32 cm
measured travel time	0.00085 sec
wave velocity	239.06 m/sec

• 6 pass



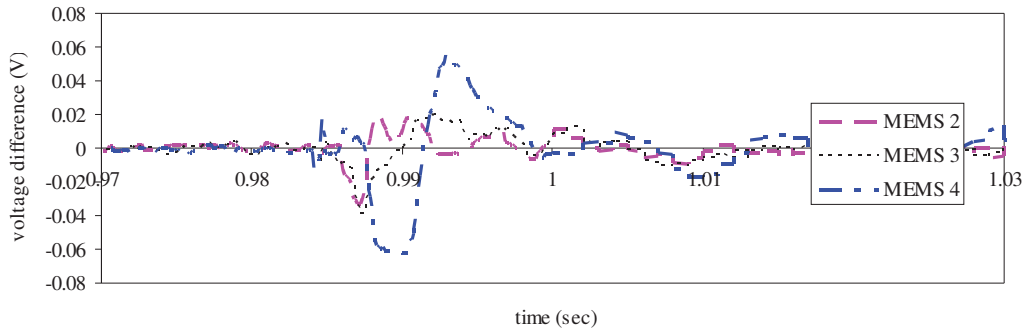
travel distance between MEMS 1 to MEMS 5	20.32 cm
measured travel time	0.00068 sec
wave velocity	298.82 m/sec

D.2. MEMS first arrival measurement in the coarse-grained soil (natural moisture)

D.2.1. Smooth-drum vibratory roller

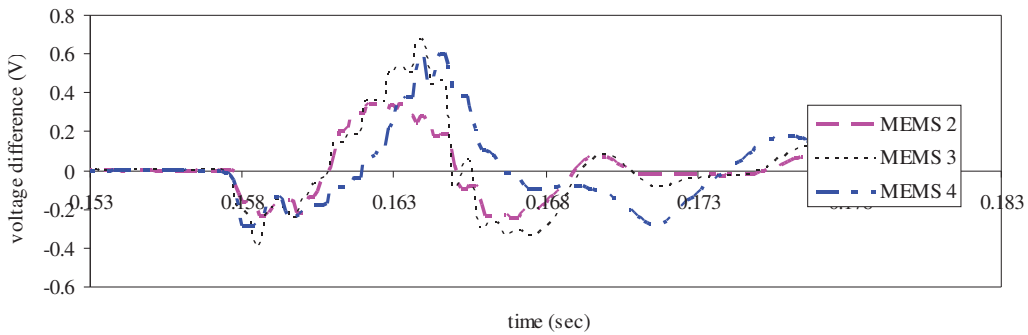
a) 8 in lift thickness

- 0 pass



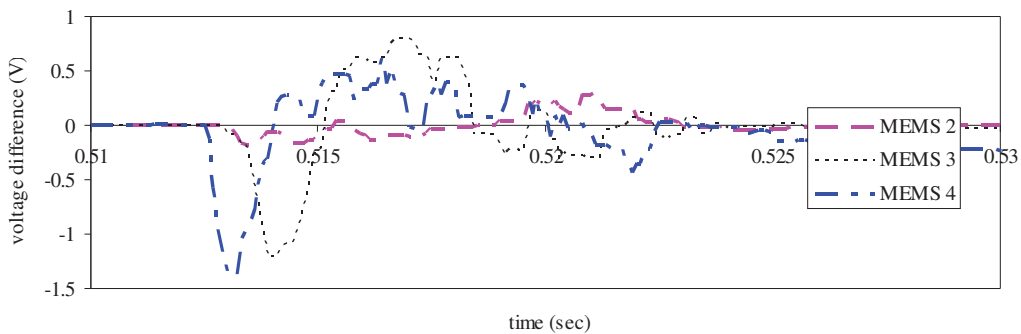
travel distance between MEMS 2 to MEMS 4	7.62 cm
measured travel time	0.00045 sec
wave velocity	169.33 m/sec

- 3 pass



travel distance between MEMS 2 to MEMS 4	7.62 cm
measured travel time	0.00036 sec
wave velocity	211.67 m/sec

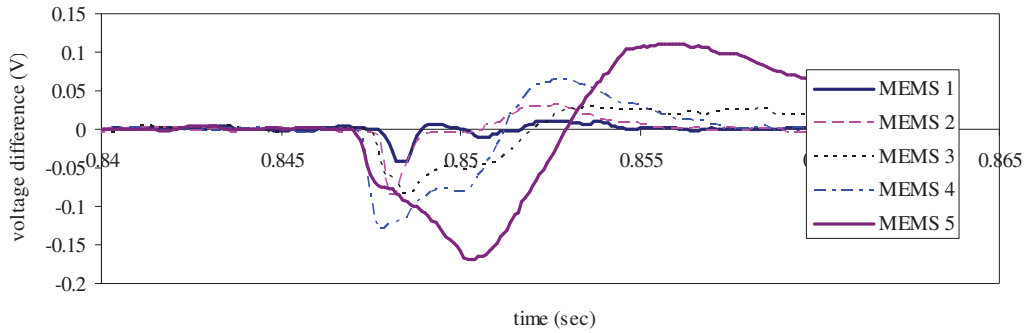
- 6 pass



travel distance between MEMS 2 to MEMS 4	7.62 cm
measured travel time	0.0004 sec
wave velocity	190.50 m/sec

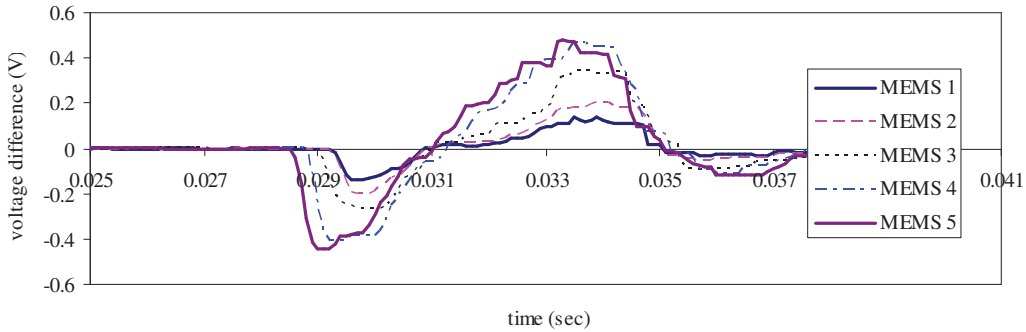
b) 13 in lift thickness

• 0 pass



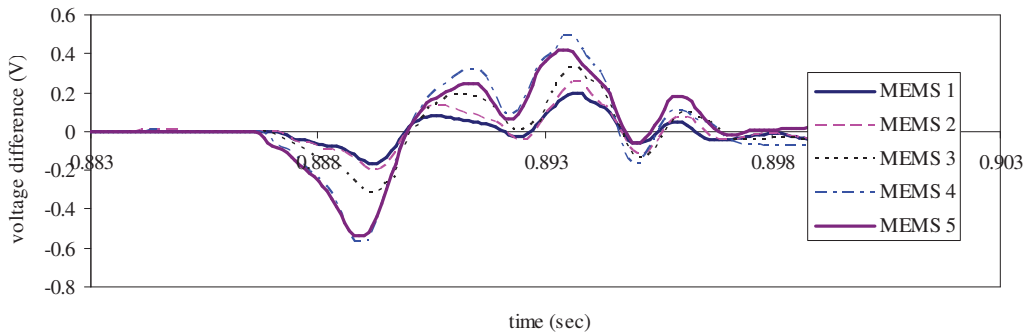
travel distance between MEMS 1 to MEMS 5	13.97 cm
measured travel time	0.00074 sec
wave velocity	188.78 m/sec

• 3 pass



travel distance between MEMS 1 to MEMS 5	13.97 cm
measured travel time	0.00071 sec
wave velocity	196.76 m/sec

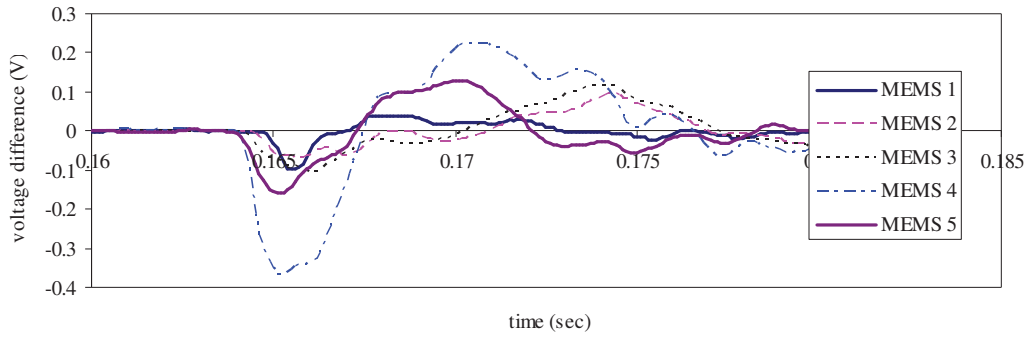
• 6 pass



travel distance between MEMS 1 to MEMS 5	13.97 cm
measured travel time	0.00062 sec
wave velocity	225.32 m/sec

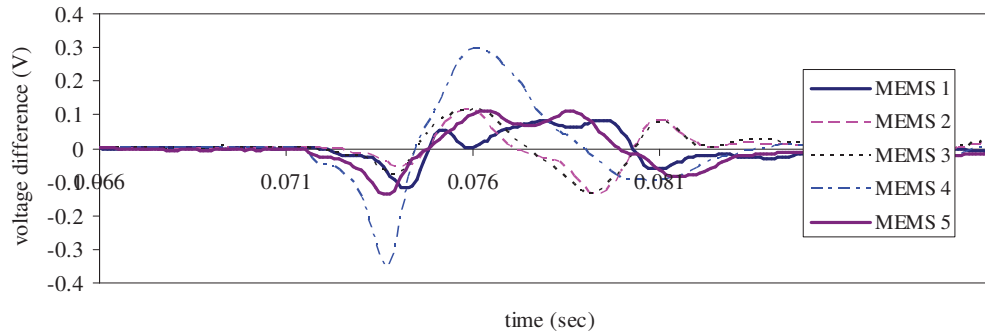
c) 24 in lift thickness

- 0 pass



travel distance between MEMS 1 to MEMS 5	13.97 cm
measured travel time	0.00075 sec
wave velocity	186.27 m/sec

- 6 pass

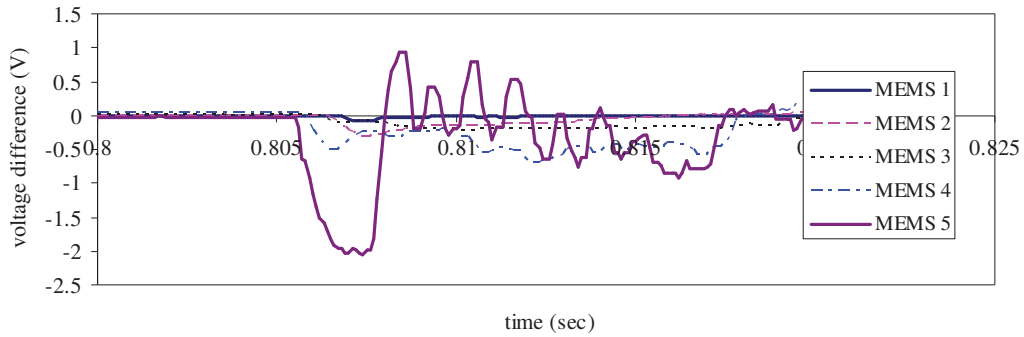


travel distance between MEMS 1 to MEMS 5	13.97 cm
measured travel time	0.00061 sec
wave velocity	229.02 m/sec

D.2.2. Rubber-tired roller

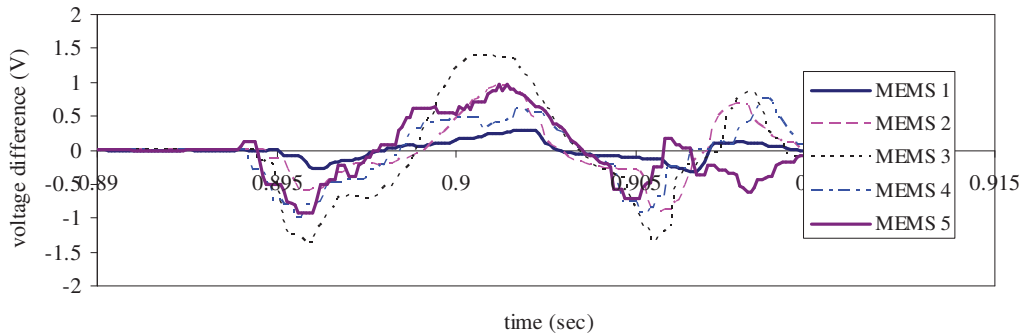
a) 8 in lift thickness

- 0 pass



travel distance between MEMS 1 to MEMS 5	19.685 cm
measured travel time	0.00121 sec
wave velocity	162.69 m/sec

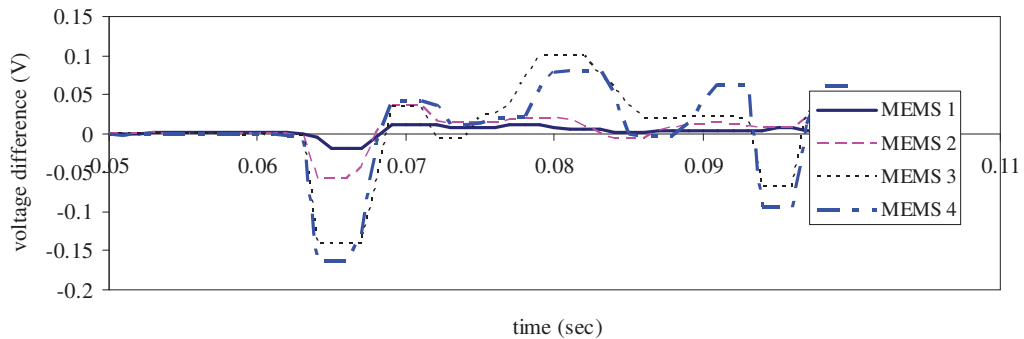
- 6 pass



travel distance between MEMS 1 to MEMS 5	19.685 cm
measured travel time	0.0011 sec
wave velocity	178.95 m/sec

b) 13 in lift thickness

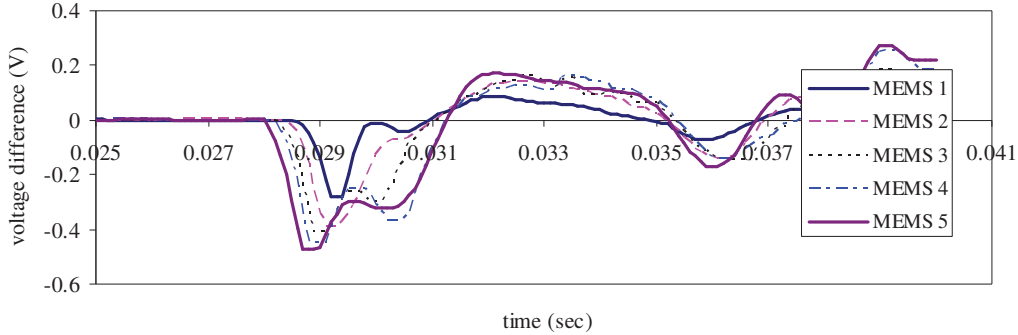
- 0 pass



travel distance between MEMS 1 to MEMS 4	11.43 cm
measured travel time	0.00085 sec

wave velocity	134.47 m/sec
---------------	--------------

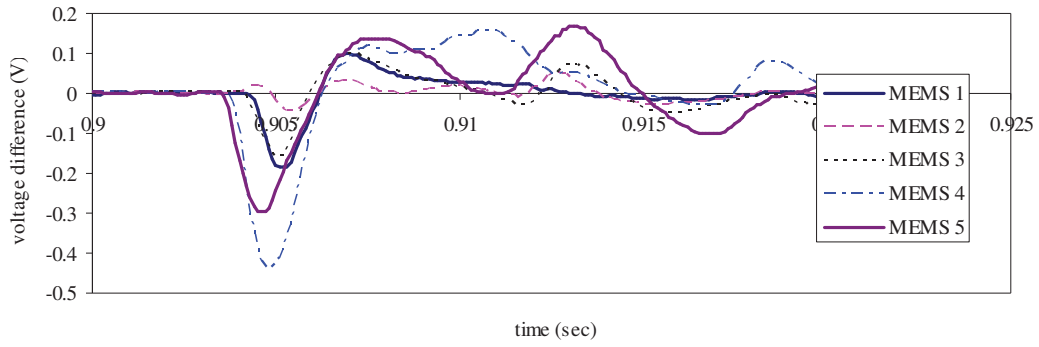
- 6 pass



travel distance between MEMS 1 to MEMS 4	15.24 cm
measured travel time	0.00068 sec
wave velocity	224.12 m/sec

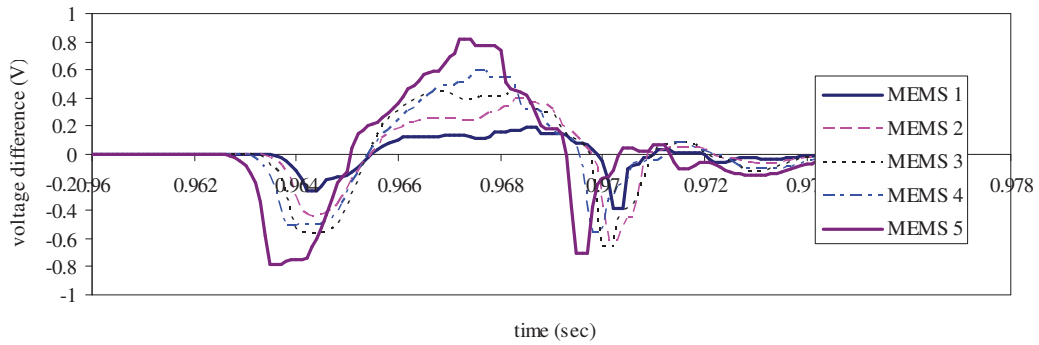
c) 20 in lift thickness

- 0 pass



travel distance between MEMS 1 to MEMS 5	19.05 cm
measured travel time	0.00083 sec
wave velocity	229.52 m/sec

- 6 pass



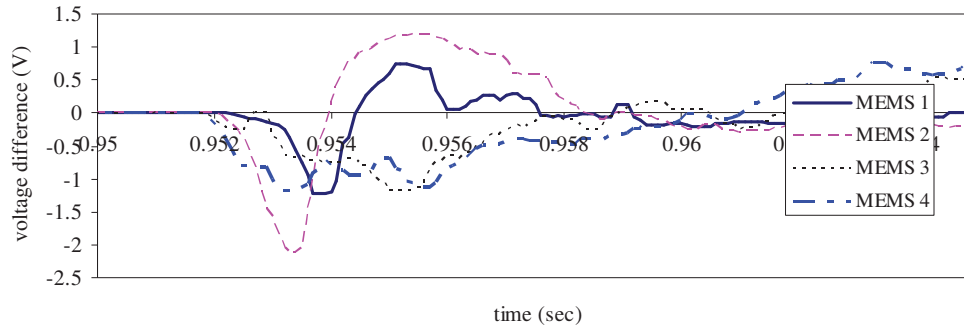
travel distance between MEMS 1 to MEMS 5	19.05 cm
measured travel time	0.00081 sec
wave velocity	235.19 m/sec

D.3. MEMS first arrival measurement in the coarse-grained soil (wet condition moisture)

D.3.1. Smooth-drum vibratory roller

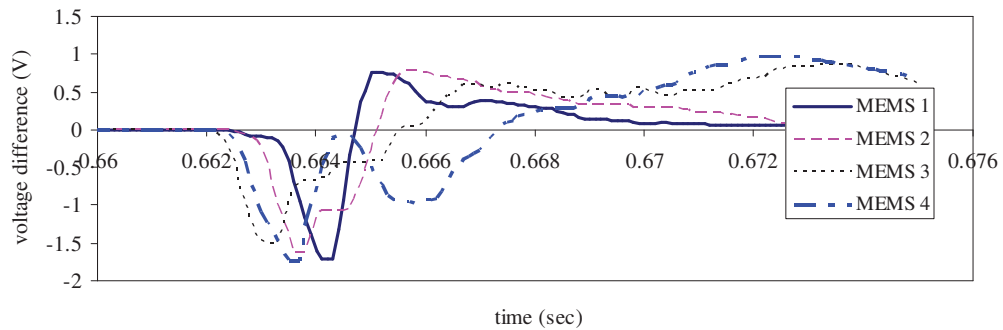
a) 8 in lift thickness

- 0 pass



travel distance between MEMS 1 to MEMS 4	7.62 cm
measured travel time	0.00049 sec
wave velocity	155.51 m/sec

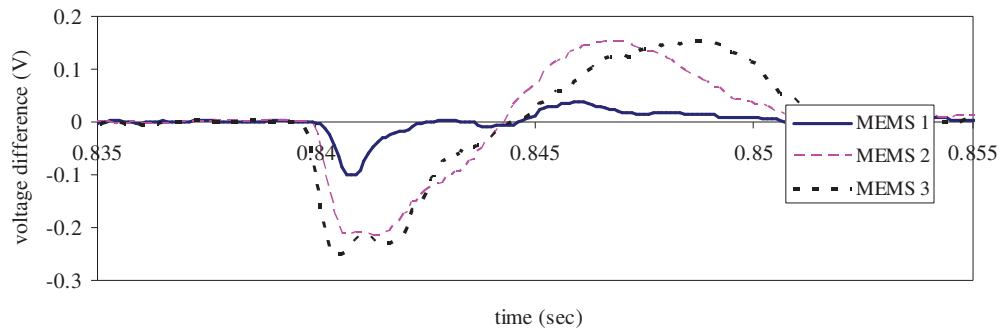
- 6 pass



travel distance between MEMS 1 to MEMS 4	7.62 cm
measured travel time	0.0003 sec
wave velocity	254.00 m/sec

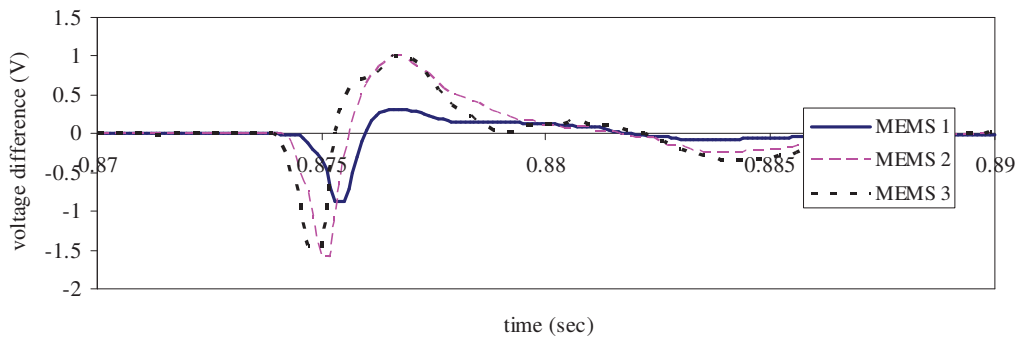
b) 13 in lift thickness

- 0 pass



travel distance between MEMS 1 to MEMS 3	8.89 cm
measured travel time	0.00045 sec
wave velocity	197.56 m/sec

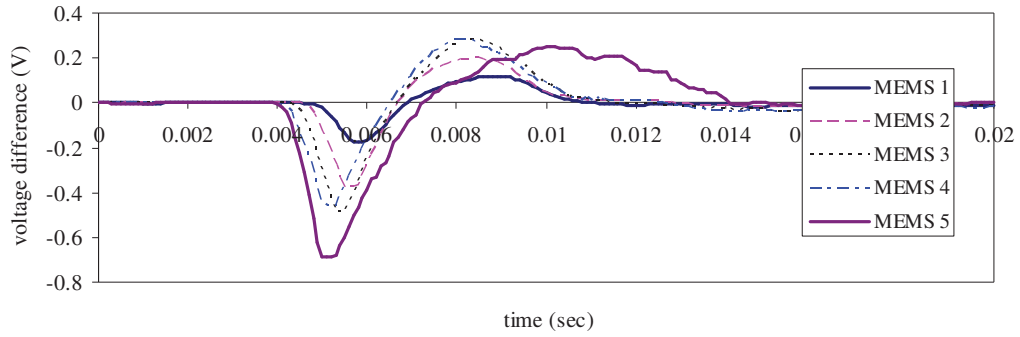
- 6 pass



travel distance between MEMS 1 to MEMS 3	8.89 cm
measured travel time	0.00047 sec
wave velocity	189.15 m/sec

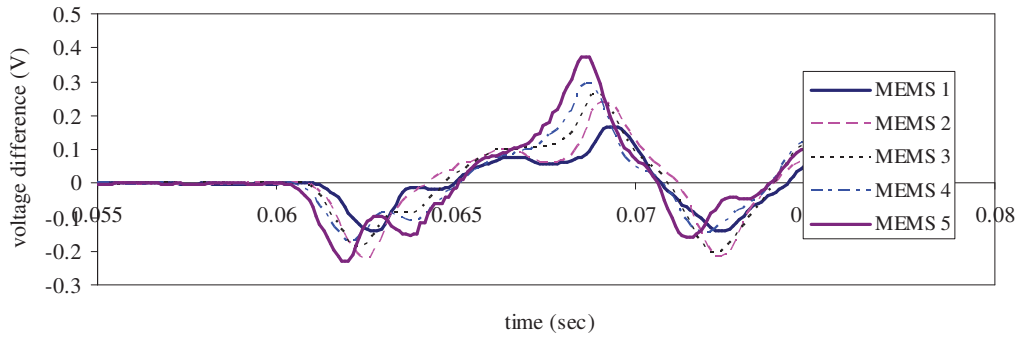
c) 20 in lift thickness

- 0 pass



travel distance between MEMS 1 to MEMS 5	17.78 cm
measured travel time	0.0009 sec
wave velocity	197.56 m/sec

- 6 pass

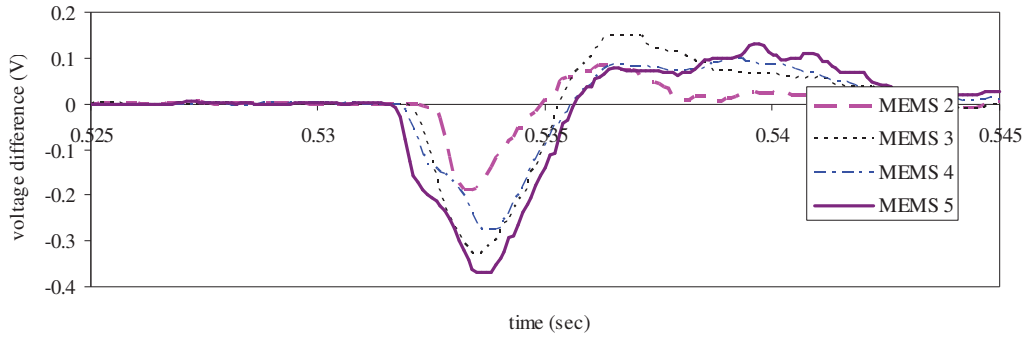


travel distance between MEMS 1 to MEMS 5	17.78 cm
measured travel time	0.00085 sec
wave velocity	209.18 m/sec

D.3.2. Rubber-tired roller

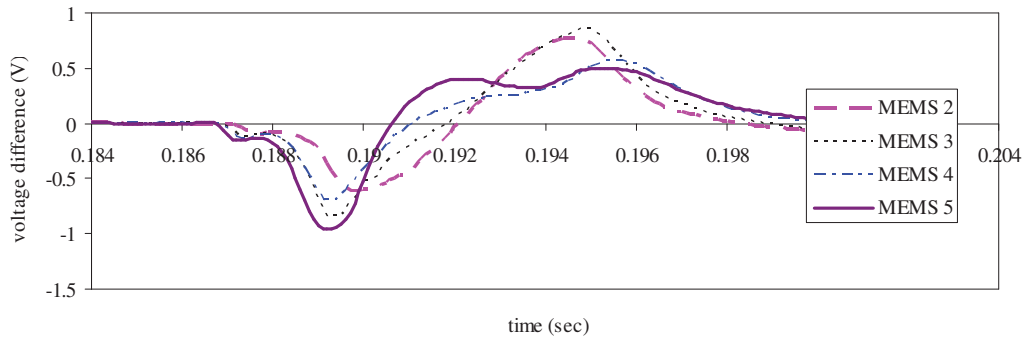
a) 13 in lift thickness

- 0 pass



travel distance between MEMS 2 to MEMS 5	13.97 cm
measured travel time	0.00075 sec
wave velocity	186.27 m/sec

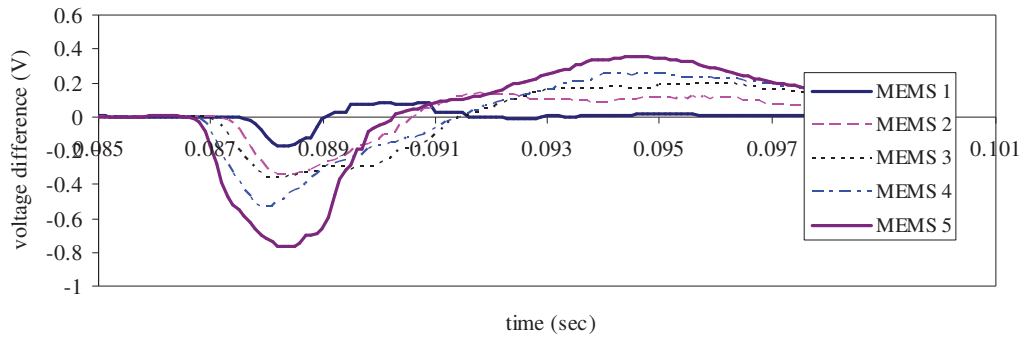
- 6 pass



travel distance between MEMS 2 to MEMS 5	13.97 cm
measured travel time	0.00054 sec
wave velocity	258.70 m/sec

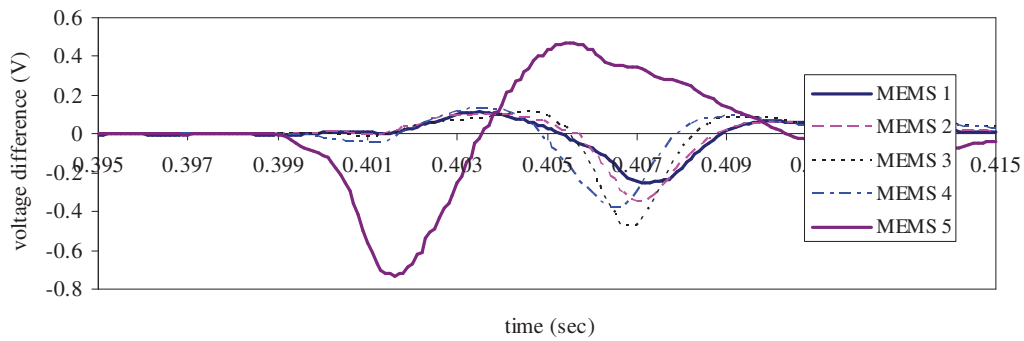
b) 23 in lift thickness

- 0 pass



travel distance between MEMS 1 to MEMS 5	17.78 cm
measured travel time	0.00085 sec
wave velocity	209.18 m/sec

- 6 pass



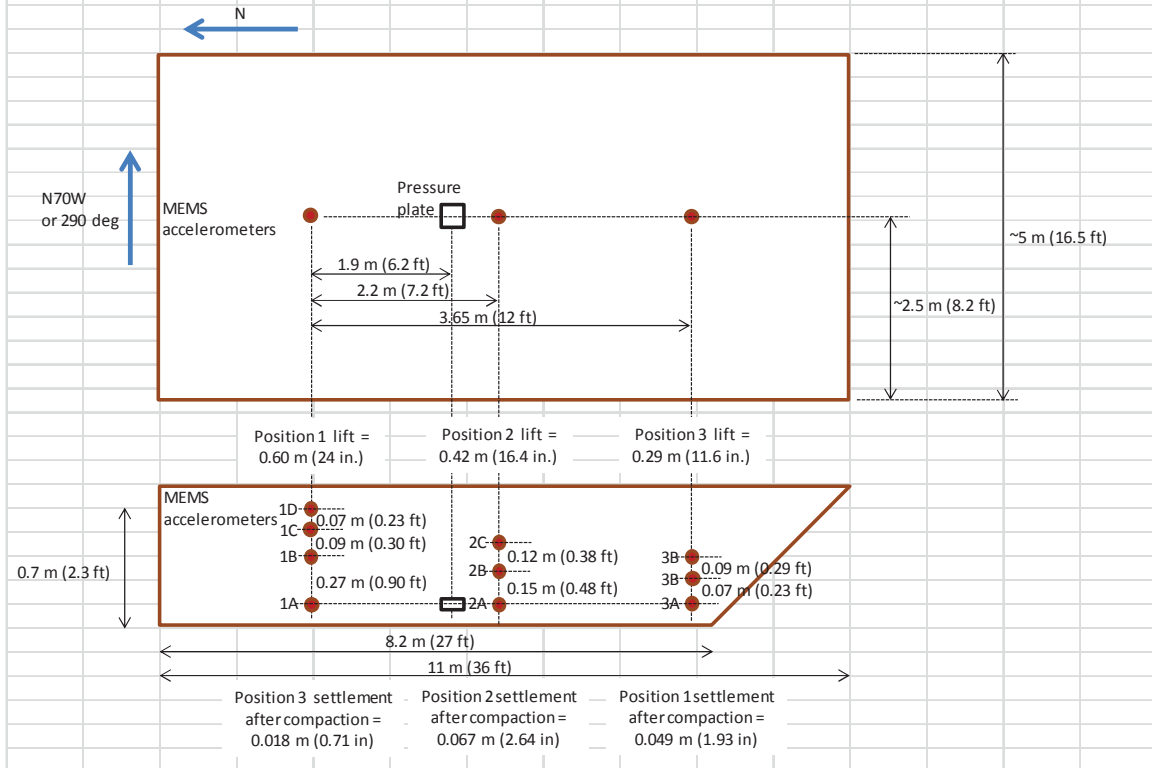
travel distance between MEMS 1 to MEMS 5	17.78 cm
measured travel time	0.0009 sec
wave velocity	197.56 m/sec

**APPENDIX E: GEOMETRY OF TESTING SETUP AT THE TOWN OF
SYLVANIA SITE**

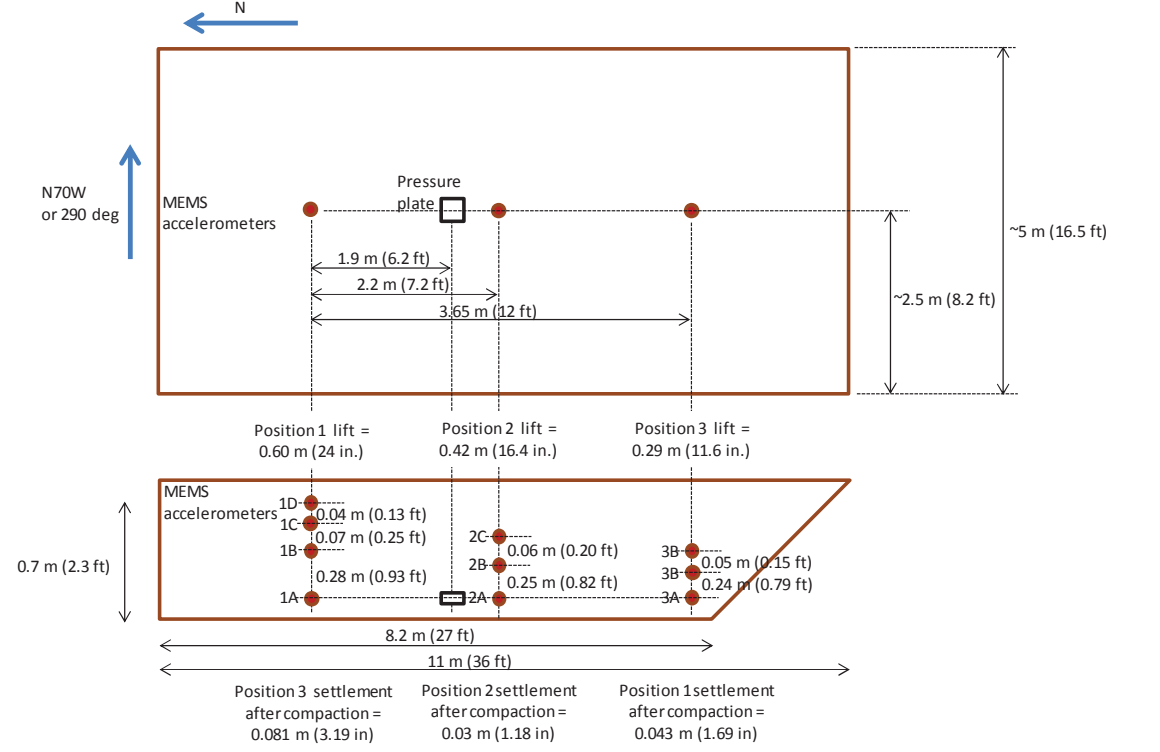
Testing Date
Tuesday October 8th 2013

Tab and fieldbook: Dry soil large compactor
 Intermediate moisture soil, large compactor

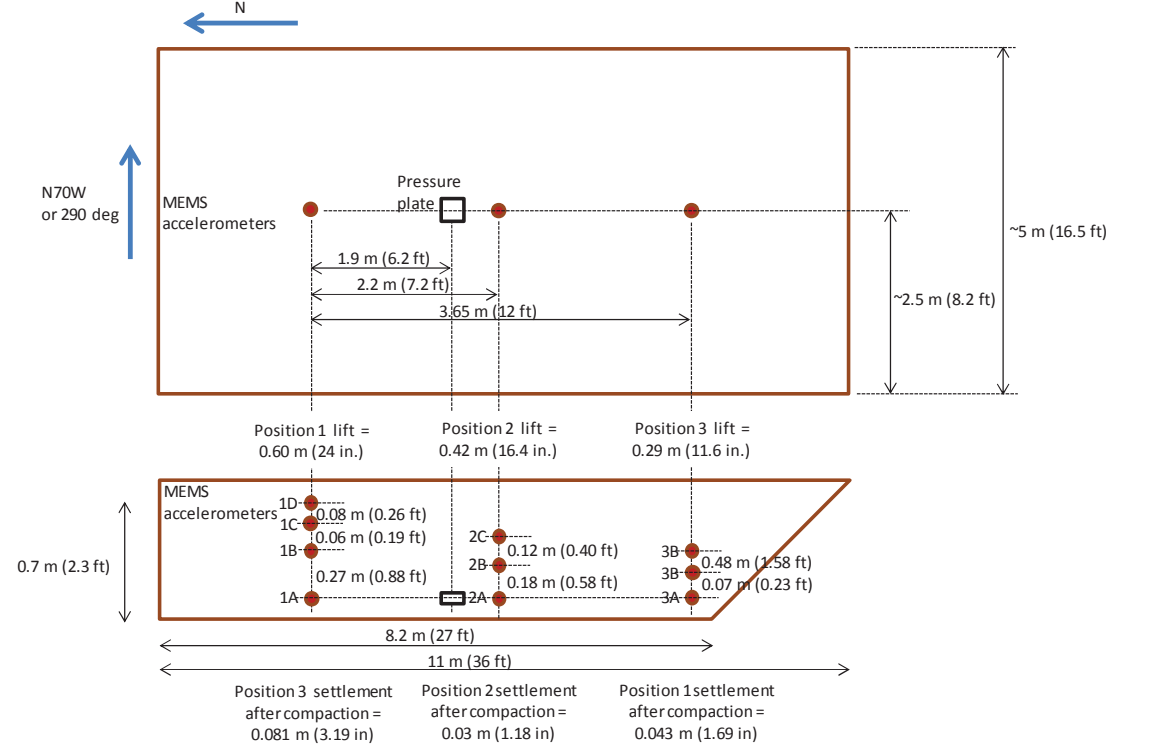
Material proctor: Max unit weight: 17.95 kN/m² 112 pcf
 Opt. moisture conte 17.2 %



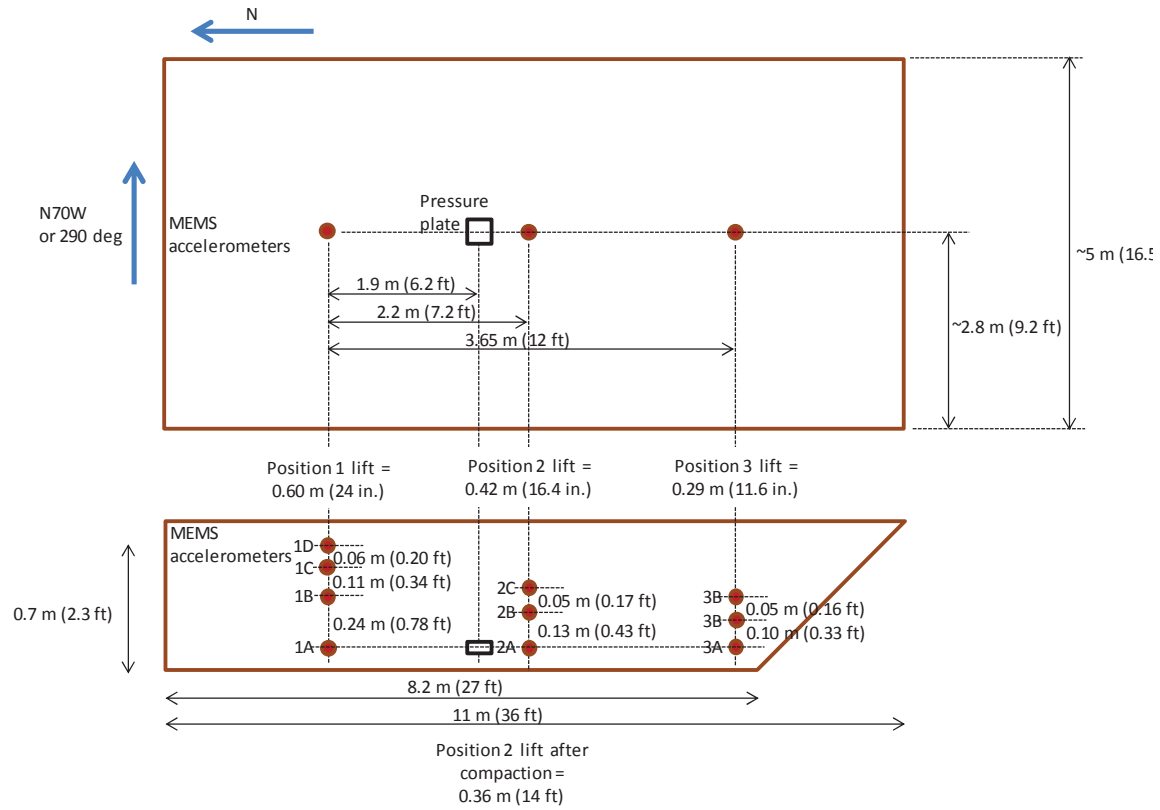
Testing Date				
Thursday October 10th 2013				
Tab and fieldbook: Wet soil large compactor		Material proctor:	Max unit weight:	17.95 kN/m ²
Wet soil, large compactor		Opt. moisture conte		112 pcf
				17.2 %



Testing Date																				
Wednesday October 9th 2013																				
Tab and fieldbook: Very dry soil small compactor				Material proctor:		Max unit weight:		17.95 kN/m ²		112 pcf										
Dry moisture soil, small compactor						Opt. moisture conte		17.2 %												



Testing Date					
Tuesday October 8th 2013					
Field book and Tab name: Dry soil small compactor		Material proctor:	Max unit weight:	17.95 kN/m ²	112 pcf
Intermediate moisture soil, small compactor			Opt. moisture conte	17.2 %	





WHRP

Wisconsin Highway Research Program
University of Wisconsin – Madison
1415 Engineering Drive
Madison, WI 53706
<http://wisdotresearch.wi.gov/whrp>